สภาพการเลือกจำเพาะของฟีนอลแอลคิเลชันโดยใช้อะลูมิเนียมพิลลาร์เบนทอไนต์ที่อิมเพรกเนตด้วยโลหะ

นางสาวภัสสรารัตน์ แก้วบัวรมย์

วิทยานิพนธ์นี้เป็นส่วนหนึ่งของการศึกษาตามหลักสูตรปริญญาวิทยาศาสตรมหาบัณฑิต
สาขาวิชาปิโตรเคมีและวิทยาศาสตร์พอลิเมอร์
คณะวิทยาศาสตร์ จุฬาลงกรณ์มหาวิทยาลัย
ปีการศึกษา 2554

REGIOSELECTIVITY OF PHENOL ALKYLATION USING METAL IMPREGNATED ALUMINIUM PILLARED BENTONITE

Miss Patsararat Kaewbuarom

A Thesis Submitted in Partial Fulfillment of the Requirements
for the Degree of Master of Science Program in Petrochemistry and Polymer Science
Faculty of Science
Chulalongkorn University
Academic Year 2011

Thesis Title	Regioselectivity of phenol alkylation using metal impregnated aluminium pillared bentonite
By	Miss Patsararat Kaewbuarom
Field of Study	Petrochemistry and Polymer Science
Thesis Advisor	Assistant Professor Warinthorn Chavasiri, Ph.D.

Accepted by the Faculty of Science, Chulalongkorn University in Partial Fulfillment of the Requirements for the Master's Degree

…… Dean of the Faculty of Science
(Professor Supot Hannongbua, Dr.rer.nat.)

THESIS COMMITTEE

…… Chairman
(Associate Professor Supawan Tantayanon, Ph.D.)

…… Thesis Advisor
(Assistant Professor Warinthorn Chavasiri, Ph.D.)

…… Examiner
(Associate Professor Voravee Hoven, Ph.D.)

…… External Examiner
(Suchada Tragoonwichian, Ph.D.)

ภัสสรารัตน์ แก้วบัวรมย์ : สภาพการเลือกจำเพาะของฟีนอลแอลคิเลชันโดยใช้อะลูมิเนียมพิลลาร์เบนทอไนต์ที่อิมเพรกเนตด้วยโลหะ. (REGIOSELECTIVITY OF PHENOL ALKYLATION USING METAL IMPREGNATED ALUMINIUM PILLARED BENTONITE) อ. ที่ปรึกษาวิทยานิพนธ์หลัก: ผศ.ดร.วรินทร ชวศิริ, 167 หน้า

ได้สังเคราะห์อะลูมิเนียมพิลลาร์เคลย์ เช่น อะลูมิเนียมพิลลาร์เบนทอไนต์ (Al-PLB) และอะลูมิเนียมพิลลาร์แทนิโอไลต์ (Al-PLT) ด้วยการแทรกสอด $AlCl_3$ เข้าไประหว่างชั้นของเคลย์และเผาที่อุณหภูมิสูง 500°C นาน 1 ชั่วโมง อิมเพรกเนตด้วยโลหะคลอไรด์ ($InCl_3$, $LaCl_3$, $CeCl_3$, $NdCl_3$ และ $GdCl_3$) และเผาที่อุณหภมิ 450°C พิสูจน์เอกลักษณ์ของตัวเร่งปฏิกิริยาด้วยเทคนิคการเลี้ยวเบนของรังสีเอ็กซ์ เทคนิคการดูดซับ-การคายแก๊สไนโตรเจน เทคนิคการคายออกของแอมโมเนียแบบโปรแกรมอุณหภูมิ และเครื่องอินดักทีฟคับเพิลพลาสมา ออฟติกเคิลอิมิชชันสเปกโทรโฟโทมิเตอร์ได้ใช้ตัวเร่งปฏิกิริยาเหล่านี้สำหรับปฏิกิริยาแอลคิเลชันของสารในกลุ่มฟีนอลที่เร่งปฏิกิริยาด้วยกรด เปรียบเทียบความสามารถในการเร่งปฏิกิริยาระหว่างชนิดของโลหะคลอไรด์ที่อิมเพรกเนตบนอะลูมิเนียมพิลลาร์เบนทอไนต์ และอุณหภูมิที่ใช้เผาเทียบกับ Al-PLT ตัวเร่งปฏิกิริยาชนิด $InCl_3$/Al-PLB ให้ผลผลิตสูงสุดสำหรับ*โอ*-แอลคิเลชัน ในขณะที่ Al-PLT ที่เผาที่อุณหภูมิ 450°C ให้ผลิตภัณฑ์ที่เลือกจำเพาะในการเกิดแบบการแทนที่ตำแหน่งเดียวที่ตำแหน่ง *ออโท* ของฟีนอล ได้พบภาวะที่เหมาะสมสำหรับปฏิกิริยาปฏิกิริยาแอลคิเลชันของฟีนอลที่ใช้กรดเป็นตัวเร่งปฏิกิริยา ให้ปริมาณผลิตภัณฑ์ในระดับดีถึงดีมากและมีความเลือกจำเพาะที่ดีเยี่ยมภายใต้ภาวะที่ไม่รุนแรง

สาขาวิชา ปิโตรเคมีและวิทยาศาสตร์พอลิเมอร์ ลายมือชื่อนิสิต .....

ปีการศึกษา 2554 ลายมือชื่อ อ. ที่ปรึกษาวิทยานิพนธ์หลัก .....

5272475923: MAJOR PETROCHEMISTRY AND POLYMER SCIENCE
KEYWORDS: PILLARED CLAY / PHENOL ALKYLATION

PATSARARAT KAEWBUAROM: REGIOSELECTIVITY OF PHENOL ALKYLATION USING METAL IMPREGNATED ALUMINIUM PILLARED BENTONITE. ADVISOR: ASSIST. PROF. WARINTHORN CHAVASIRI, Ph.D., 167 pp.

Aluminium-pillared clays such as aluminium-pillared bentonite (Al-PLB), aluminium-pillared taeniolite (Al-PLT) were synthesized by intercalation of $AlCl_3$ into clay interlayers and calcined at 500°C for 1 h. The impregnation with metal chlorides ($InCl_3$, $LaCl_3$, $CeCl_3$, $NdCl_3$, and $GdCl_3$) was carried out with calcination at 450°C. The synthesized clays and raw clays were characterized using powder X-ray diffraction, N_2 adsorption-desorption, temperature programmed desorption of ammonia and inductively coupled plasma optical emission spectrometry techniques. These synthesized catalysts were used for acid-catalyzed phenols alkylation. The catalytic activity of synthesized clays was compared with raw clays (bentonite and taeniolite), different metal chlorides on Al-PLB and calcination temperatures and with Al-PLT. $InCl_3$/Al-PLB provided significantly the highest yield for *O*-alkylation, while Al-PLT calcined at 450°C was selective for mono-substitution of *C*-alkylated product. The optimized conditions for acid-catalyzed reaction were disclosed. Those reactions could smoothly be proceeded in the presence of synthesized clays to furnish the corresponding products in good to excellent yield with excellent selectivity for *O*-alkylation under mild conditions.

Field of Study: Petrochemistry and Polymer Science Student's Signature .....

Academic Year: 2011 Advisor's Signature .....

ACKNOWLEDGEMENTS

The author would like to express her highest appreciation to her advisor, Assistant Professor Dr. Warinthorn Chavasiri for his valuable instructions, very kind assistance, generous guidance and encouragement throughout the course of this research. Furthermore sincere thanks are extended to Natural Products Research Unit, Department of Chemistry, Faculty of Science, Chulalongkorn University, for the support of chemical and laboratory facilities. I would like to thank the Graduate school, Chulalongkorn University, for financial support.

The greatest thanks are also extended to Associate Professor Dr. Supawan Tantayanon, Associate Professor Dr. Voravee Hoven and Dr. Suchada Trakoolwichain for their suggestion, comments, correction and helps as thesis examiners.

Moreover, thanks are extended to Center for Petroleum, Petrochemicals and Advanced Materials, Chulalongkorn University, Program in Petrochemistry and Polymer Science, Faculty of Science, Chulalongkorn University for granting financial support to fulfill this study and provision of experimental facilities.

Further acknowledgment is extended to her friends for friendship and helps throughout the entire of study. Especially, the author is very appreciated to her family members whose names are not mentioned for their love, assistance, understanding, encouragement and social support throughout her entire education. Without them, the author would never have been able to achieve this goal.

CONTENTS

Page

CHAPTER **Page**

CHAPTER **Page**

CHAPTER **Page**

CHAPTER **Page**

CHAPTER **Page**

LIST OF TABLES

Table **Page**

Table **Page**

Table **Page**

LIST OF FIGURES

Figure **Page**

Figure **Page**

LIST OF SHCEMES

Scheme **Page**

LIST OF ABBREVIATIONS

%	percent
BET	Brunauer-Emmett-Teller
°C	degree celsius
Å	Angstrom unit
β	beta
$CDCl_3$	deuterate chloroform
d	doublet (NMR)
dd	doublet of doublet (NMR)
eq	equivalent
Et_2O	diethyl ether
EtOAc	ethyl acetate
Fig	figure
γ	gamma
g	gram (s)
GC	Gas chromatography
Hz	hertz
h	hour (s)
ICP-OES	inductively coupled plasma-optical emission spectroscopy
J	coupling constant (NMR)
M	molar
m	multiplet (NMR)
mg	milligram (s)
min	minute (s)
mL	milliliter
mmol	millimole
MW	molecular weight
nm	nanometer
NaOH	sodium hydroxide

NMR	nuclear magnetic resonance
q	quatet (NMR)
RT	room temperature
s	singlet (NMR)
t	triplet (NMR)
TPD	Temperature Programmed Desorption
TLC	thin layer chromatography
wt	weight
XRD	X-ray diffraction
α	alpha
θ	theta
δ	chemical shift
λ	wavelength
μg	microgram (s)
μM	micromolar

CHAPTER I

INTRODUCTION

1.1 The importance of products from alkylation of phenol

Alkylated phenols are significant in fine chemicals industry and are utilized as intermediates for the production of surface-active agents, rubber chemicals, dyes, cosmetics, antioxidants, petroleum additives, ultraviolet absorbers, and heat stabilizers for polymeric materials [1-4]. The general catalyst used in alkylation including Lewis acid catalysts such as $AlCl_3$, BF_3, $FeCl_3$ and $ZnCl_2$, has many drawbacks such as corrosive, difficulty during separation, highly moisture sensitivity and toxicity, high refluxing temperature, long reaction time, and less selectivity. This research is focused on the utilization of clay catalyst in selective alkylation of phenol.

Clay minerals are crystalline hydrous aluminosilicates, classified as phylosilicate, or layered silicate structures. They are discovered plentifully in nature with various types. The particular characteristic properties of clays consist of high surface area, high swelling sorption, reversible ion exchange, and high acidity. Moreover, there is highly ability as acid catalyst exploiting in both Brønsted and Lewis types for catalytic applications. Many organic reactions use clays as efficient heterogeneous catalysts. For example, modified smectite clays could be used as highly selective catalyst in organic transformations and green chemistry with excellent yield, high regio- and stereoselectivity.[5] The advantage of clay catalysts over homogeneous catalysts can be clearly seen from the work up step by simple filtration. In addition, these heterogeneous catalysts are easy to recover and reusable, hence a large reduction in the generation of wasteful products.

The efficiency of clay catalysts in alkylation was designed by increasing of specific surface area of pillaring method prepared by exchanging the large inorganic hydroxyl cations, and hydrolyzed metal salt with the change-balancing interlayer [5]. Under the high temperature by calcination method, metal hydroxyl cations interlayer of clay was dehydrated and dehydroxylated turning into metal oxide pillared clay. The

stabilized metal oxides have structure like cluster which acted as pillared interlayer, and not to merge on the structure of clay [6]. Most examination on pillared clays created by synthetic methods has concentrated on the catalytic performance for catalytic proposes [7-10]. Extensively, the synthesis condition was explored on the temperature needed for the preparation of catalysts which has a profound effect on the structure of pillars. The high performance of clay catalyst was used in a variety of organic reaction such as acylation, isomerization and alkylation [11-13].

1.2 Literature review on the alkylation of aromatics

1.2.1 Alkylation of benzene

Catalytic alkylation of benzene is of crucial basal and pragmatic reaction, which is a basic reaction for production in petrochemical industry. Recently, mesopore catalysts were used extensively more than older homogeneous catalysts.

1.2.1.1 Alkylating agent as alcohols

In 1998, Valuerra *et al.* [14] presented the alkylation of benzene with *iso*-propanol catalyzed by MCM41/γ-Al_2O_3. At too high temperature (>350˚C), the formation of toluene and ethyl benzene was occurred, which was derived from cumene disproportionation. Moreover, polyalkylation and cracking were side reaction taking place at this higher temperature.

In 2000, Jun and Ryoo [15] reported the alkylation of benzene with benzyl alcohol using $AlCl_3$ supported molecular sieves (MCM-41). Comparing the catalytic activity of KIT-1, MCM-41, and MCM-48 on benzylation with benzyl alcohol, KIT-1 turned out to be principally higher activity than MCM catalysts and $AlCl_3$ impregnated on MCM.

1.2.1.2 Alkylating agent as halides

In 1998, He and co-workers [16] studied the benzylation of benzene with benzyl chloride over Fe-containing zeolite molecular sieve. This work investigated on the difference in the method of preparation and pore size. 100% mono-alkylated product selectivity was produced by this catalysis under optimization, which was better than previously reported Fe-pillared clays. Choudhari's redox mechanism [17] was chosen to explain the acidity of related catalysts containing reducible cation.

Catalyst had highly activity; although, lower number of Lewis acid when benzyl chloride was alkylating agent.

In 2001, Okumura and co-workers [18] reported the benzylation with benzyl chloride using Ga-MCM-41 (as synthesized) and Ga-MCM-41 (impreganated) as catalyst. The quantitative loading of Ga was increased until 0.4 mol/Kg and then decreased, which was believed to generate the agglomeration of Ga_2O_3 species and displayed as weak acid site from generated of Ga_2O_3 species evidenced by NH_3-TPD. Comparing different methods to synthesize catalysts, higher activity could be detected when using impregnated method which could form diphenylmethane. Highly calcination temperature in direct synthesis caused the formation of extra-framework aggregated.

1.2.1.3 Alkylating agent as olefin

The significantly demand of chemical industry was the alkylation of aromatic with olefin, for example in 2002, Hu and co-workers [19] presented $AlCl_3$ immobilized on MCM-41 mesoporous silica of different pore sizes to form a novel shape-selective catalyst for Friedel–Crafts alkylation of benzene with long-chain olefins. The selectivity toward the monoalkylated product was strongly influenced by the pore size of the carrier material. This demonstrated the opportunities offered by the micelle-templating method to tailor shape-selective catalysts for reactions with bigger molecules.

1.2.2 Alkylation of substituted benzene

In 2004, Singh and Samant [20] presented the different protocols for the preparation of catalysts and condions used in benzylation of benzene with benzyl chloride on metal supported bentonite. From the observation, K10-FePLS120 was the best catalyst for this reaction. 100% conversion and the selectivity of *para*-product, without dibenzylated products formation were achieved.

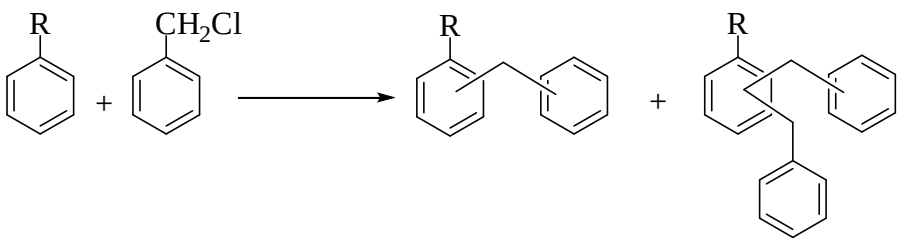

Three methods for preparing of catalysts included pillared bentonite, ion-exchange and pillared solution impregnated montmorillonite K10. The performance in catalyzing was found to be in order of pillared solution impregnated montmorillonite K10 > ion-exchange > pillared bentonite. The effectiveness of metal was discussed by reduction potential value which were found to be in order of Fe^{3+}> Zr^{4+}> Al^{3+}.

1.2.3 Alkylation of toluene

In 2000, Perego and co-workers [21] studied the effect of different catalysts for alkylating of toluene with propylene, which produced cymene as a main product. The investigation of different catalysts: amorphous mesoporous silica aluminas (MSA amd MCM-41) and amorphous microporous silica alumina (ERS-8), zeolite beta displayed different activity. The mesoporous catalyst displayed higher activity than zeolite bet and lower selectivity of cymene because the larger formation of polyalkylates, which in turn was due to the presence of larger pores and lower transalkylation activity. Likewise, MSA, MCM-41 and ERS-8 showed a larger amount of *o*-cymene causing their lower isomerization ability.

1.2.4 Alkylation of phenols using solid acid catalysts

1.2.4.1 Alkylating agent as alcohol

In 1998, Zang and co-workers [22] presented the catalytic properties of zeolite Hβ in *tert*-butylation of phenol. The medium acid sites on zeolite Hβ enhanced the formation of *p*-*tert*-butylphenol (*p*-TBP); the strong acid sites induced the production of 2,4-di-*tert*-butylphenol (2,4-DTBP), while *o*-*tert*-butylphenol (*o*-TBP) was generated at the weak acid sites. The reaction performing at 145˚C and lower reactant ratio with moderate acid sites on zeolite Hβ was recommended.

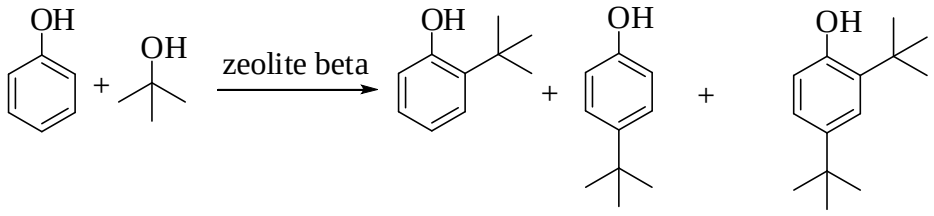

o-TBP *p*-TBP 2,4-DTBP

In 2003, Bal and Sivasanker [23] reported the selective *O*-alkyaltion of phenol over alkali loaded silica with normal alcohol such as methanol, ethanol, *n*-propanol and *n*-butanol. The activities of catalysts in this reaction were depended upon metal loading which was increased by basicity of metal ions (Cs > K > Na > Li), while using Cs loading, the conversion was the highest.

In 2004, Grabowska and co-workers [24] altered nanosized γ-Al_2O_3 catalyst by alkoxide sol-gel method. The cresol alkylation with *iso*propyl alcohol yielded *C*-alkylated product which was believed to take place *via* *O*-alkylated product rearrangement.

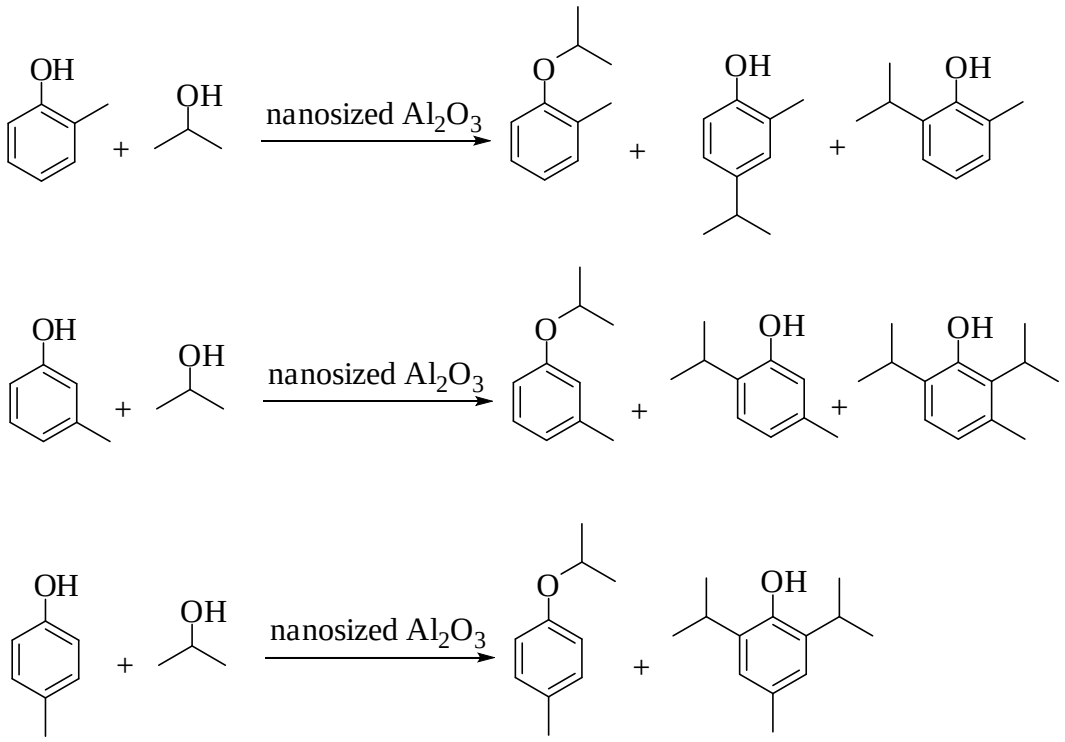

The *iso*propylation of *o*-, *m*- and *p*-cresols provided two main products depended upon reaction temperature. At higher temperature, *C*-alkylated product was predominant, while the formation of *O*-alkylated product was a minor one. The formation of *C*-alkylated product was believed to stem from ether rearrangement.

In 2005, Sarish and co-workers [25] reported the alkylation of *p*-cresol with *tert*-butanol by WO_x/ZrO_2. The amounts of WO_3 loading and calcination temperature were examined. 15 % WO_3 loading provided the highest yield. The calcination

temperature at 800°C for synthesis WO_3 loading catalyst was revealed as the most proper in *tert*-butylation. Under optimization condition, at 130°C the molar ratio of *tert*-butanol/*p*-cresol was 3 giving the highest conversion of 69.8% and selectivity of 2-*tert*-butyl-*p*-cresol as 92.4%.

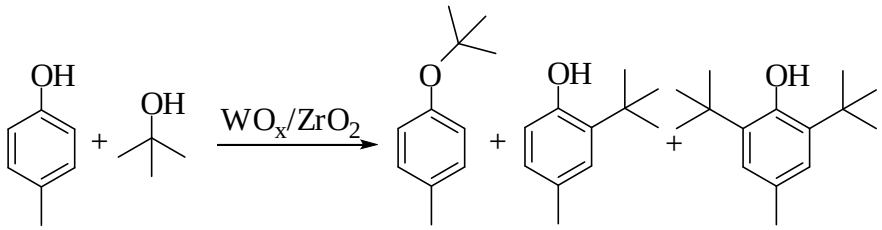

In 2006, Devassy and co-wokers [26] examined the alkylation of phenol with *tert*-butanol catalyzed by zirconia-supported 12-molybdophosphoric. Under optimization condition, the amount of MPA loading was 15%wt, and the suitable calcination temperature was 700°C. The highest conversion could be reached to 80.6%. When the reaction time was increased to 31 h, the conversion was decreased to 58.5%. The selectivity at the highest conversion was 11.5% for 2-*tert* butylphenol (2-TBP), 55.2% for 2,4-di-*tert*-butylphenol (DTBP) and 25.7% for 4-*tert*-butylphenol (4-TBP).

In 2006, Bhatt [27] presented cyclohexylation of phenol by 12-tungstosilicic acid. The conversion of cyclohexene was 100% with high selectivity giving 2-CHP of 61% for TSA/ZrO_2 and 66% for TSA/Al_2O_3.

In 2007, Reddy and co-workers [28] showed the catalytic performance of molybdate- and tungstate-promoted zirconia catalysts for *tert*-butylation of phenol. The reaction was executed at 160–220˚C in a fixed bed micro-reactor at WHSVof 5 h^{-1} under atmospheric pressure and molar ratio of *tert*-butanol to phenol was 2. The variation of temperature from 160 to 200˚C, revealed increasing conversion of phenol at 52 to 62%, respectively, with high selectivity of *para*-product.

In 2010, Kondamuni and co-workers [29] presented the Bronsted ionic liquid catalytic activity in alkylation of *p*-cresol with *tert*-butyl alcohol. Comparative studies on the catalytic properties of ionic liquid such as *N*-(4-sulfonic acid) butyl

triethylammonium hydrogen sulfate, 1-(4-sulfonic acid) butylpyridinium hydrogen sulfate, 1-(4-sulfonic acid) butyl-3-methylimidazolium hydrogen sulfate, 1-(3-sulfonic acid) propyl pyridiniumtoluenesulfonate, 1-(4-sulfonic acid) butyl pyridiniumtoluene-sulfonate were carried out under identical reaction conditions.

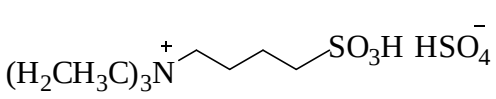

IL-1

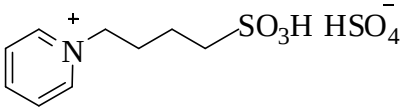

IL-2

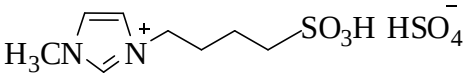

IL-3

IL-1: N-(4-sulfonic acid) butyl triethylammonium hydrogen sulfate

IL-2: 1-(4-sulfonic acid) butylpyridinium hydrogen sulfate

IL-3: 1-(4-sulfonic acid) butyl-3-methylimidazolium hydrogen sulfate

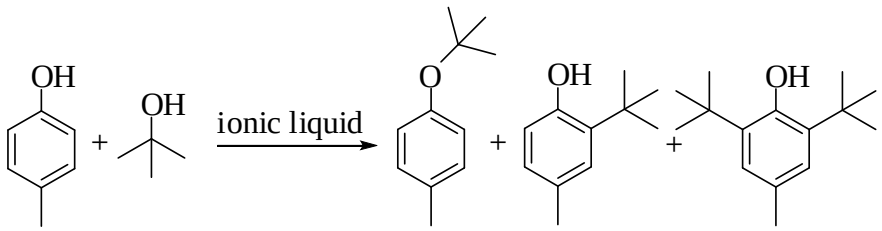

The investigation on optimizing conditions in alkylation of phenol was peroformed to reach high conversion of 90% and high selectivity of 2-*tert*-butyl-*p*-cresol.

1.2.4.2 alkylating agent as olefins

In 2000, Wilson and co-workers [29] reported mild solid acid catalysts used in both homogeneous and heterogeneous BF_3 catalysts in phenol alkylation with cyclohexene at 85-90°C for 3 h. Using homogeneous BF_3 catalysts, 30-50% conversion of phenol and *O*-alkylated product was obtained in 50-60% selectivity. In homogeneous catalyst case, the BF_3 catalyst could occur both *O*- and *C*- alkylated

product; but still, could not observe in heterogeneous catalyst to produce *C*-alkylated product. The reason was suggested to be steric restriction and lower acidity of silica support. The mechanism was involved ether rearrangement.

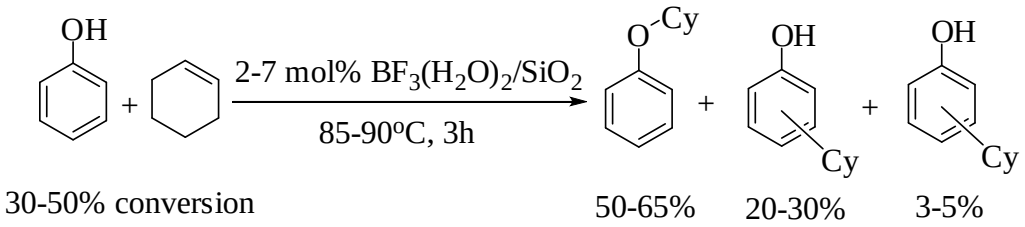

1.3 Literature reviews on clay catalysts

In 1997, Geatti and co-workers [30] presented the alkylation of benzene with propane by cation exchanged aluminium pillared clays. The aluminium pillared bentonite was exchanged by K^+, La^{3+} and Al^{3+}cation. La^{3+} and Al^{3+}acted as Lewis acid catalyst for benzylation providing high yield and only aluminium pillared bentonite gave lower activity. The result of the reactivity from Lewis acid center was strong while the amount of Brønsted acid site was not found. The function of Lewis acid and Brønsted acid was confirmed by IR spectroscopy of adsorbed pyridine.

In 2002, Singh and co-workers [31] reported Friedel-Crafts alkylation of cresols with suitable alkylating agents catalyzed by montmorillonite K10 affording the corresponding three sesquiterpenes: elvirol, curcuphenol and sesquichemaenol.

In 2002, Yadav and Doshi [32] presented the alkylation of phenol with methyl *tert*-butyl ether (MTBE) and *tert*-butanol over solid acid. 20% (w/w) dodecatungstophosphoric acid (DTP)/K-10, K-10, Zr-exchanged-K-10 and Cr-exchanged K-10 were used in alkylation of phenol under optimize conditions. Comparative studies were investigated for 20% (w/w) DTP/K-10 which found to be the most active catalyst and all of them gave only *C*-alkylated products. MTBE was found to give better results than *tert*-butanol.

Sorce of isobutylene (*in situ* generated)

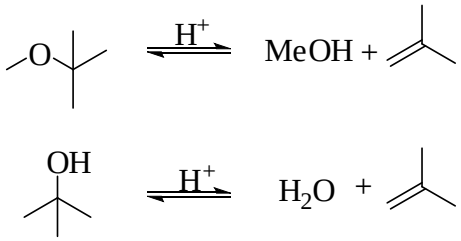

Alkyaltion of *p*-cresol with isobutylene

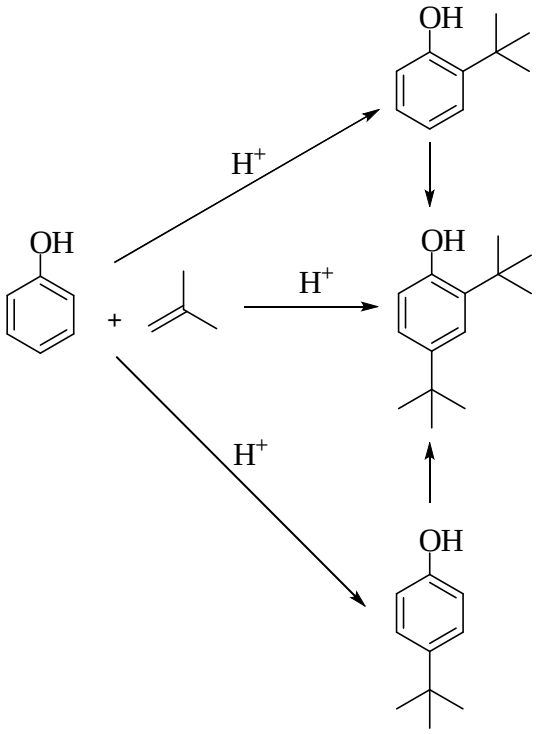

Figure 1.1 Possibility of production on alkylation of phenol

From the *in situ* generation of isobutylene there were several products to associated with such as dimer and trimer of isobutylene depending on reaction conditions, especially loading temperature and mole ratio.

In 2006, Kurain and Sugunan [33] reported phenol alkylation with *tert*-butanol by metal exchanged iron pillared montmorillonites. The catalytic activities were found to depend on the acid sites on the catalyst surface and selectivity of products

depended on amount of strong acid sites. Under optimized reaction conditions, Ni/FePM provided the highest conversion of 58%. The investigation of 2,4-di-*tert*-butylphenol selectivity was characterized by temperature program desorption (TPD) which revealed the better with strong acid sites.

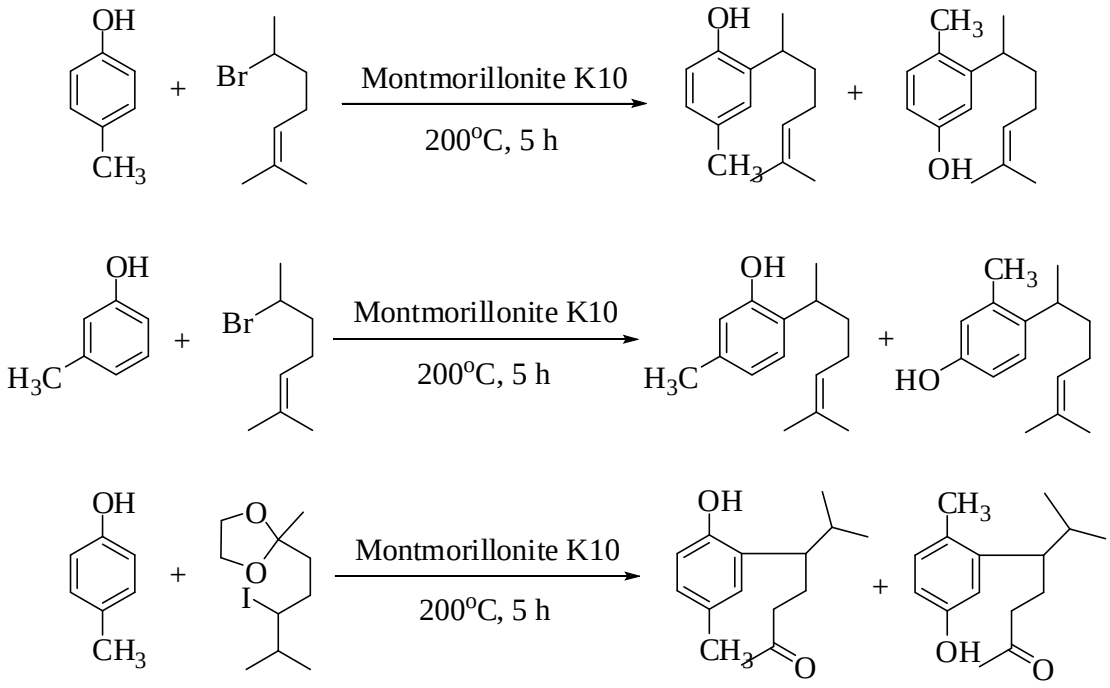

1.4 Literature review of clay catalysts on other reactions

Clay catalysis as solid acid has been extensively investigated in organic reaction under mild conditions. Several examples could be reviewed in literatures.

1.4.1 Formylation of phenols [35]

Phenols could be formylated using clay catalyst with formaldehyde and R_3N.

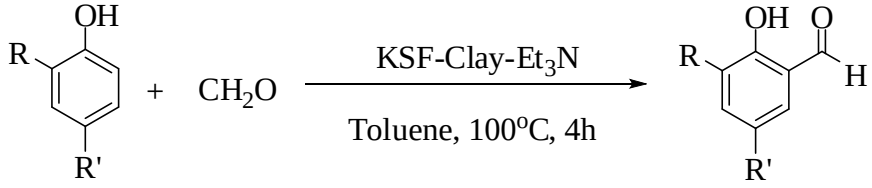

1.4.2 **Ether formation** [36]

Unsymmetrical ethers were efficiently prepared by refluxing a solution of alcohol and olefin in *n*-hexane using Al^{3+}-exchanged montmorillonite. The yields were good in the case of primary alcohols. Secondary alcohols gave low yields, while tertiary alcohols did not yield the desired ethers, generally dehydration was taken place instead.

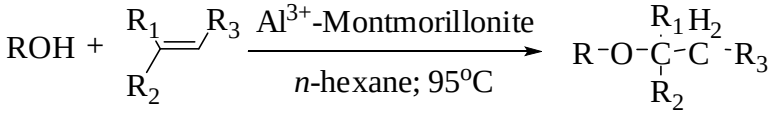

1.4.3 **Anhydride formation** [36]

Formation of cyclic anhydrides from 5-and 6-carbon dicarboxylic acid was observed by dehydration reaction using acid clay.

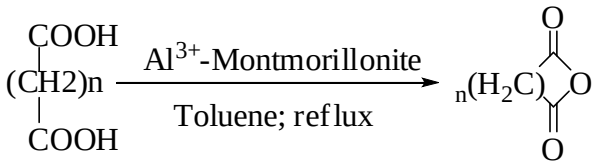

1.4.4 **Addition reaction** [37]

In 2010, Motokura reported high performance of proton montmorillonite catalysis in allylsilylation, arylsilylation and silylation of alkynes. The catalytic pathway of allylsilation [A] and alkyne catalyzed are shown in Scheme 1.2.

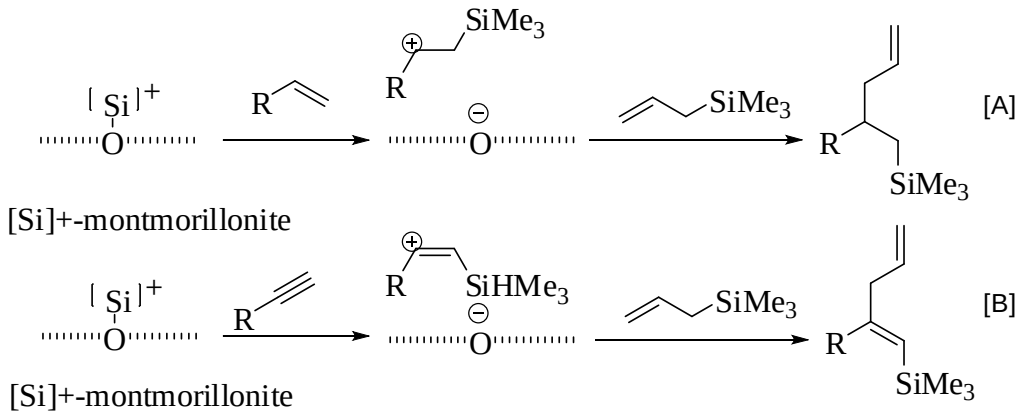

1.4.5 Oligomerization reaction [36]

The polymerization of styrene has been catalyzed by acid-treated montmorillonites.

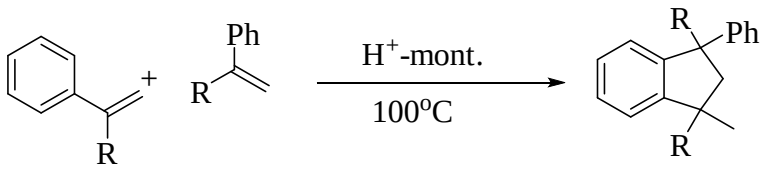

1.4.6 Oxidation-reduction reaction [35]

Clay catalyst was selected widely in oxidation-reduction using alcohol and thio compounds acted as oxidizing agent. Clayfen and claycop were explored in oxidation reaction, which supported by K10 clay and exchanging with iron (III) nitrate and copper (II) nitrate, respectively.

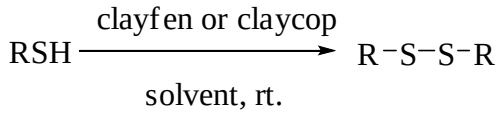

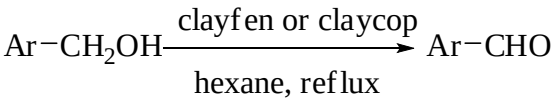

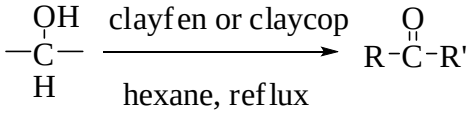

1.4.7 Esterification

Clay-catalyzed ester-forming reactions has many method are shown below.

- *Addition of olefins*

The addition of olefin with carboxylic acid to produce ester catalyzed by clay catalyst was shown below. [35]

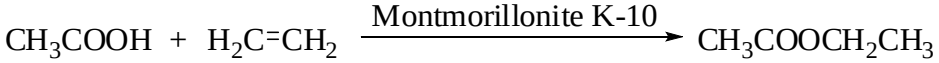

- *Synthesis of tosyl and sulpheny compound*

Another type ester such as tosyl or sulpheonyl esters were synthesized by Fe^{3+} -montmorillonite catalyst for high yield. [35]

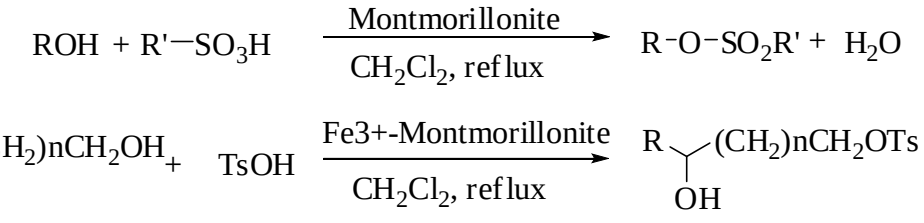

- *Production of tert-butyl acetate*

In 2001, Coundhary *et al.* [38] reported effect of clay supported on esterification of *tert*-butanol with acetic anhydride, is following: kaolite, montmorillonite-K10 and montmorillonite-KSF. After that, they was exchanged by $InCl_3$, $GaCl_3$, $FeCl_3$ and $ZnCl_2$. From investigation, $InCl_3$/mont-K10 is best activity, selectivity and significant of reusability.

1.4.8 Diel-Alder reaction [39]

The Diel-Alder reaction is [4+2] cycloaddition using clay acid catalyst, it is influential for accelerating in Diel-Alder reaction. The clearance space of clay such as montmorillonite, could be significant for designing endo/exo ratio for stereochemical.

In 2008, Mitsudome reported the obsearvation of the chiral organocatalyst immobilized on montmorillonite *via* a cation-exchange reaction for studying stability of heterocatalyst reusable and stereochemistry. This recommendation brought about in green chemistry and high stereoselective on silicate layer of montmorillonite, performed counter macroanion.

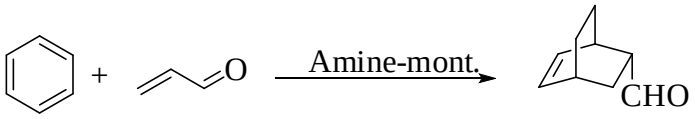

%yield = 82%

%endo ee = 92%

1.4.9 Acylation [40]

The acylation of aromatic ether with acid anhydride using metal ion exchanged montmorillonite are shown below. Metal respective were Fe^{3+}, Zn^{2+}, Cu^{2+}, Al^{3+} and Co^{2+} which Fe^{3+} and Zn^{2+} were highest activity and selective to occur 1-acyl-2-methoxynaphthalene and 4-acylanisol.

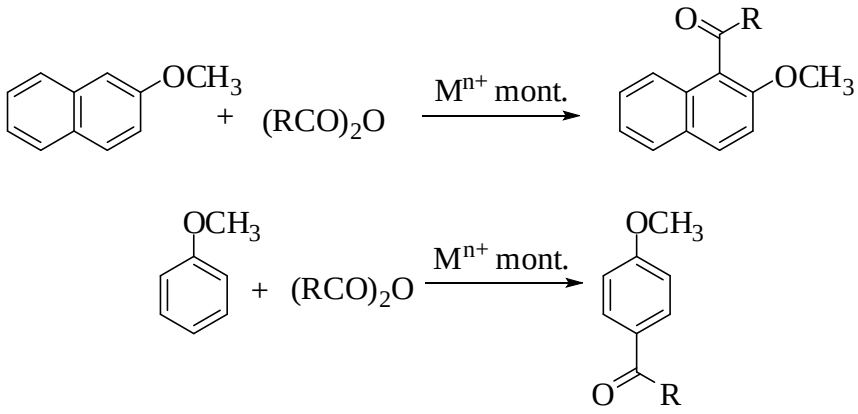

From literature reviews, clay catalysts have been reported as an efficient catalyst in acid catalyzed reactions. The importance in acid catalyzed reaction involved the use of Brønsted and Lewis acid. The development of a more efficient heterogeneous catalyst for acid catalyzed reactions is an important goal for organic synthesis and industrial point of view. Although there have been some investigations on the use of modified clays for acid catalyzed alkylation of phenol, there is no report on the utilization of $InCl_3$ impregnated Al-pillared bentonite as catalysts for phenols alkylation.

1.5 The goal of this research

The aims of this research can be summarized as follows:

1. To synthesize various efficient metal (III) chloride ($InCl_3$, $LaCl_3$, $CeCl_3$, $NdCl_3$ and $GdCl_3$) impregnated aluminium pillared bentonite for acid catalyzed reactions.
2. To synthesize the efficient aluminium pillared taeniolite and indium (III) chloride impregnated aluminium pillared taeniolite by using different calcination temperatures for acid catalyzed reactions.
3. To study the optimum conditions for acid catalyzed rections by selected indium (III) chloride aluminium pillared bentonite
4. To apply optimum conditions for alkylation of phenols with alkylating agent.

CHAPTER II

THEORY

2.1 Clay

Clay minerals are crystalline hydrous aluminosilicates and classified as phyllosilicated or layer silicates. They are the most common products of water-rock interaction under earth-surface conditions. Clay minerals occur abundantly in nature. The unique properties of clays include high surface area, high sorption, reversible ion-exchange and high acidity. Containing both Brønsted and Lewis acid types, clays have been able to exploit for various catalytic applications. Many organic reactions have been addressed employing clay as an efficient heterogeneous catalysts [41].

2.2 The structure of clay mineral

Clay minerals possess a layered structure. Their suspension in aqueous solution contains particles with average diameter of about 2 μm [42]. Each clay layer is constructed from the combination of two basic types: a sheet of corner-linked tetrahedral and a sheet of edge-linked octahedral. Normally, they are aluminum octahedral and silica tetrahedral sheets held together by sharing apical oxygen [43].

2.2.1 Basic unit

2.2.1.1 Tetrahedral sheets

Tetrahedral sheet contains tetrahedral units where Si^{4+} and Fe^{3+} are dominant cations. Each cation is surrounded with four oxygen atoms. The three corners of each tetrahedral share oxygen atoms with three other tetrahedral units to form hexagonal network. The apical oxygen points upward in the direction normal to the base of the sheet.

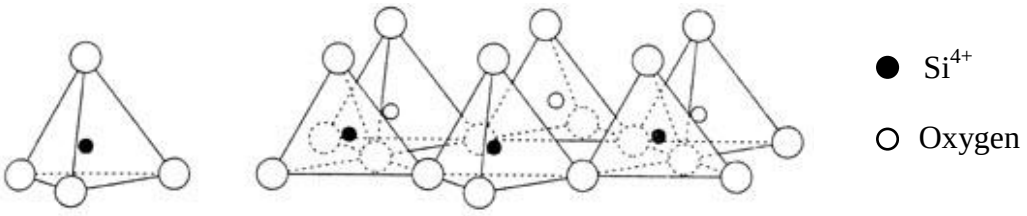

(a) (b)

Figure 2.1 A single tetrahedral silica (a), and a sheet structure of silica tetrahedral arranged in a hexagonal network (b).

2.2.1.2 Octahedral sheets

Octahedral sheet is constructed from octahedral units similar to tetrahedral sheet. Each unit contains cation such as Al^{3+} or Mg^{2+} at the center surrounded with six oxygen atoms. The neighboring octahedral units are connected in the edge-linked fashion and form extended two dimensional structures.

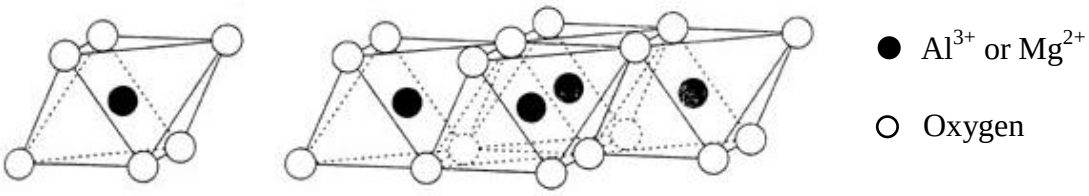

(a) (b)

Figure 2.2 A single octahedral unit (a) and a sheet structure of octahedral unit arranged in a hexagonal network (b).

2.2.2 The combinations of basic sheets

The combination of basic sheets of clays could be divided into 2 types.

2.2.2.1 The 1:1 layer type (T : O)

Each layer of 1:1 type is consisted of one tetrahedral sheet (T) and one octahedral sheet (O). The apical oxygen atoms of a tetrahedral sheet point to the

octahedral sheet and are shared with an octahedral sheet (O), such as kaolinite group (Figure 2.1).

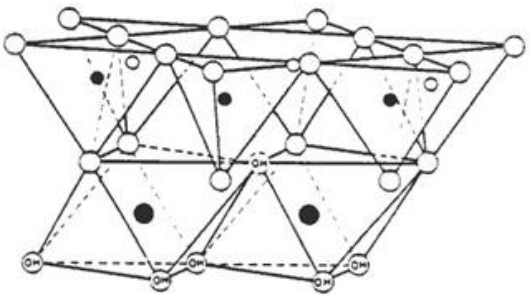

Figure 2.3 Structure of 1:1 layered type (T = tetrahedral sheet, O = octahedral sheet).

2.2.2.2 The 2:1 layer type (T:O:T)

A 2:1 layer is compound of two tetrahedral sheets and an octahedral sheet. This assembly makes a tetrahedral-octahedral-tetrahedral (T:O:T) sandwich layers such as smectite clay. Bentonite, montmorillonite and hectorite are common smectite clay (Figure 2.2).

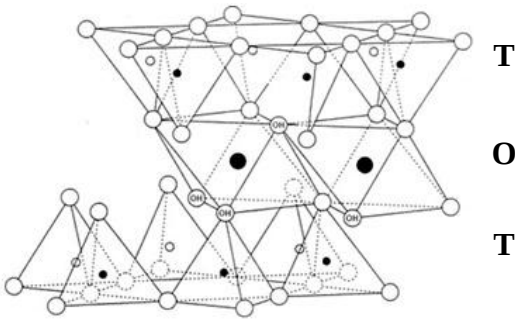

Figure 2.4 Structure of 2:1 layered type (T = Tetrahedral sheet, O = Octahedral sheet).

2.3 Types of clay

2.3.1 Smectite clay

The structures of smectite clays are derived from mineral talc and pyrophyrite, which consist of a stacking of silica tetrahedral sheet ($Al_4Si_8O_{20}(OH)_4$) and alumina octahedral sheet ($Mg_6Si_8O_{20}(OH)_4$). Clay in smectite group are

composed of layers made up of two silica tetrahedral sheets with a central alumina octahedral sheet. Substitution of cation (for example, Al^{3+} for Si^{4+} in tetrahedral sheets and Mg^{2+} for Al^{3+} in octahedral sheets) either in tetrahedral or octahedral sheet results in the formation of negative charge in the layers which are balance by additional cations located between 2:1 layers [44]. The repeating distance between the clay-layer is called the basal spacing, d_{001}. This value is easily identified by X-ray diffraction technique.

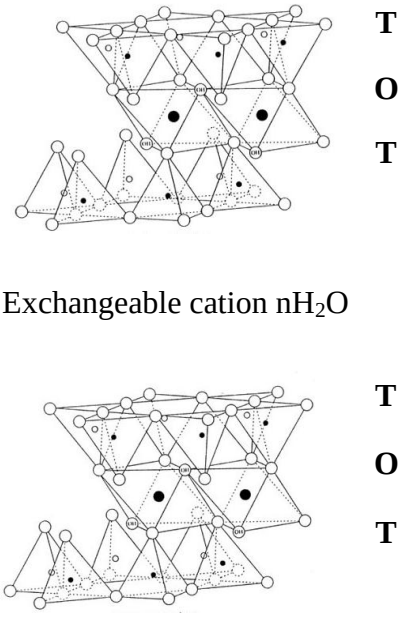

Figure 2.5 Structure of smectite clay.

2.3.1.1 Montmorillonite clay

Montmorillonite is the main constituent of bentonite (typical 80-90 %wt). The rest is a mixture of mineral impurities including quartz, crystobalite, feldspar and humic acids. Monmorillonite has an ideal formula of $(Si_8)(Al_{4-X}Mg_X)$ $O_{20}(OH)_4A_x{\cdot}nH_2O$ (where A is a monovalent or divalent cation), which Mg/Al in the octahedral sheet. Montmorillonite is the most important smectite exploited in catalytic applications [45].

2.3.1.2 Taeniolite clay

The general chemical formula of taeniolite is $(Si_8)(Mg_{6-x}Li_x)O_{20}(F)_4A_x.nH_2O$, (where A is a monovalent or divalent cation). The structure of taeniolite contains F^- which is different from bentonite and has the excess of the bivalent ions (Ca^{2+}, Mg^{2+}, Ba^{2+}, Be^{2+} and Pb^{2+} impurities). The crystal structure of taeniolite is a pack consisting of three layers of close cubic packing of F^- anion and O^{2-} anions [46].

2.4 Properties of clay

2.4.1 Ion exchange

Clay has ability to adsorb and ion exchange. In general, the ideal neutral structure of clay minerals is disrupted by the introduction of charge imbalance. Two main sources of charged imbalance are: (i) the isomorphous substitution of cations in the lactice by valent ions, such as the substitution of aluminium for silicon in the tetrahedral layer, magnesium for aluminum or sometimes lithium for magnesium in the octahedral layer, and (ii) crystal defects. Clay layers have an overall negative charge which is balanced by cations between the layers. These balance cations can be readily replaced by other cation in aqueous solution. In swelling clay, such as smectite, the interlayer cations can be exchanged with cations from external solutions. It has been observed that the smaller the size and the higher the charge of the exchange cation, the more powerful cations at replacing the inter layer exchangeable cations. The following series can be presented as shown in Scheme 2.1 can be constructed [41]:

$$\mathbf{M^+ << M^{2+} << H_2O^+ \approx K^+ \approx NH_4^+ < M^{3+} < M^{4+}} \longrightarrow$$

increasing exchange power

(decreasing ease of exchange)

Scheme 2.1 The exchange properties of cations with clays.

The concentration of exchangeable cations (CEC) is usually measured in milliequivalents per 100 g of dried clay. Since smectites have relative high

concentration of interlayer cations, they have high cation exchange capacities (typically 50-270 meq/100 g [47]). Structural defects at layer edges give rise to an additional CEC and a small amount of anion exchange capacity.

2.4.2 Swelling

Many clay minerals adsorb water between their layers, which move the layers apart and cause the clay swelling. For efficient swelling, the released energy must be sufficient to overcome the attractive forces between the adjacent layers, such as lactice energy and hydrogen bonding from layer solvation. In aqueous solution, water forms strong hydrogen bonds with hydroxyl groups on hydrophilic octahedral layers, allowing the swelling to occur for 1:1 clay minerals (kaolinite).

Similarly, the 2:1 clay minerals (smectite) have the swelling ability, which depends on the solvation of interlayer cation and the layer charge. Clays with 2:1 structures and low layer change have very low concentration of interlayer cation, therefore do not swell readily. At the other extreme, those with very high layers charges have strong electrostatic forces holding alternate anionic layers and the interlayer cation together, thus prevents the swelling. However, the divalent, trivalent and polyvalent cations, swelling decrease accordingly. The extent of swelling can be observed by measuring interlayer separations using powder X-ray diffraction [47].

2.4.3 Acidity of clay

Because the acidity of clay, it is widely used as catalysts in organic reactions. Their acidic properties and catalytic activity depend on the exchanged cations. Clay minerals have both Bronsted and Lewis acid sites [41]. The interlayer cations contribute to the acidity, with the Bronsted site mainly associated with the interlamellar region. Some of these cations (*e.g.* Al^{3+}) dissociation their coordinate water molecule to produce acidic proton, which gives Brønsted acidity. When the coordination of an organic compound to the cations, the cation is electron pair acceptors and can act as Lewis acid catalyst. In addition, clay minerals have surface layers and edge defects, which would result in weaker Brønsted and/or Lewis acidity, generally at low concentrations.

2.5 Intercalation

Intercalation is the insertion of a guest species into the interlayer region of clay with the preservation of layered structure. Intercalation compound is proven by the XRD pattern, which unambigouously must show an increase in the spacing between adjacent layers, *i.e.* an increase in basal spacing [48].

2.6 Pillaring

Pillaring is the process at used the intercalation procedure of compound into interlayer space, resulting in a pillared compound, which is thermally stable microporous and/or mesoporous materials with the preservation of a parent layer structure. A pillared derivative is distinguished from and ordinary intercalate by virtue of intercrystalline porosity made possible by the lateral separation of the intercalated guest [48].

2.7 Pillaring clay

Pillaring clays are materials obtained by the intercalation of guest molecules, which prepared by exchanging cation and polyoxocations into the interlayer of swellable clay leading to the intercalated clays. Then the intercalated clays are calcined, polyoxocations [49] transform into metal oxide pillars, resulting in the pillared clay. The pillared clay which have large specific surface are, acidic and have good thermal stability which is of great interest because of its potential application as catalysts and adsorbents in various fields. Scheme 2.2 diagram for the preparation of pillared clay compounds (cross section) [50].

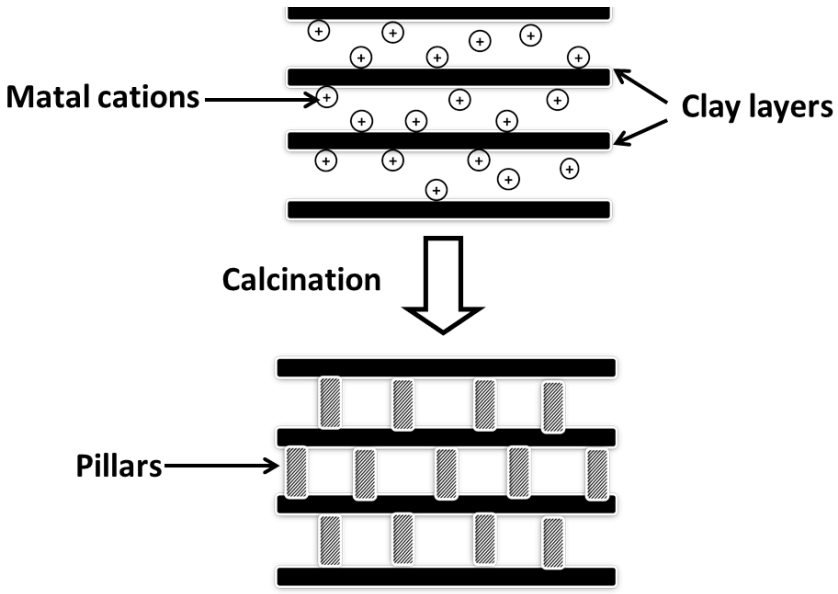

Scheme 2.2 Diagram for the preparation of pillared clay compounds (cross section)

2.8 **Impregnation** [41]

Impregnation is the method for making a heterogeneous catalyst. Generally, a support of carrier which is a porous material, it was contacted with a solution of compound that little group are held onto the support. The impregnation method requires less equipment since the forming steps, filtering and washing are needless. Scheme 2.3 shows the example of impregnation onto pillared clay.

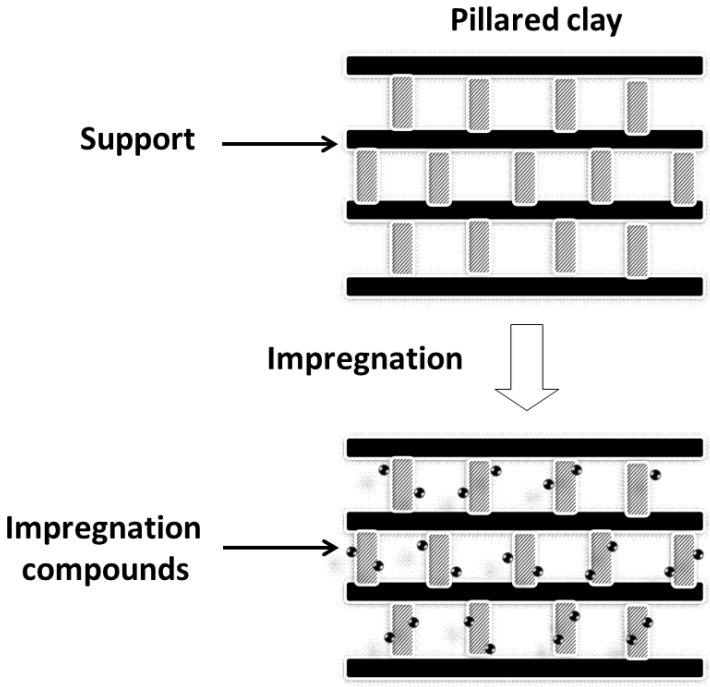

Scheme 2.3 Diagram for the preparation of impregnated pillared clay (cross section).

2.9 Characterization of clays and clay catalysts

2.9.1 Powder X-ray diffraction (XRD) [43]

X-ray diffraction (XRD) is an instrumental technique for identification and characterization of crystalline materials. XRD is a technique which a collimated beam of monochromatic X-rays is directed onto the flat surface of thin layer of finely ground material causing the X-rays is diffracted to specific angles. Figure 2.6 shows a monochromatic beam of X-ray incident on the surface of crystal at and angel θ. The scattered intensity can be measured as a function of scattering angle 2θ. An X-ray diffraction measurement the angel of incidence and detection are scanned. When the intensity of detected X-rays is plotted as a function of angle and X-ray diffraction pattern is obtained, which is characteristic for the sample material (Figure 2.6) [49].

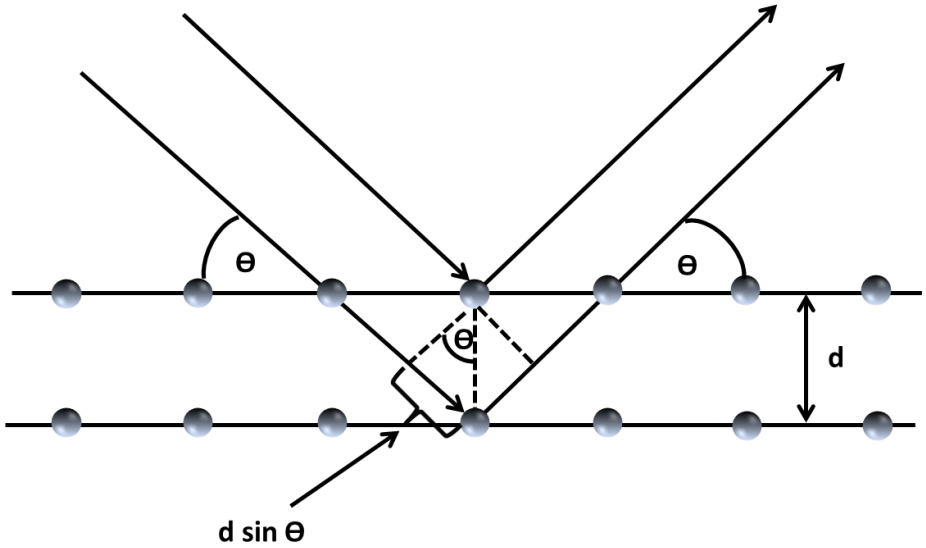

Figure 2.6 Diffraction of X-ray by regular planes of atoms.

Bragg diffraction is the general relationship between the wavelength of the incident X-rays, angel of incidence and spacing between the crystal lattice planes of atom is known as the Bragg equation.

$$n\lambda = 2d\sin\theta$$

Where n = an integer of the diffracted beam

λ = wavelength

d = a distance between adjacent planes of atoms (d-spacing)

θ = an angel between the incidence beam and the scattering plans

2.9.2 Nitrogen adsorption-desorption isotherm [52]

The N_2 adsorption technique is used to determine the physical properties of material such as the specific surface area, pore volume, pore diameter and pore size distribution of solid catalysts.

Adsorption of gas by a porous material is described by an adsorption isotherm, the amount of adsorbed gas on the material at a constant temperature as a function of pressure. Porous materials are frequently characterized in terms of pore sizes derived from sorption data. IUPAC conventions have been proposed for classifying pore size and gas sorption isotherm that reflect the relationship between porosity and sorption. The IUPAC classifications of adsorption isotherm are illustrated in Figure 2.7.

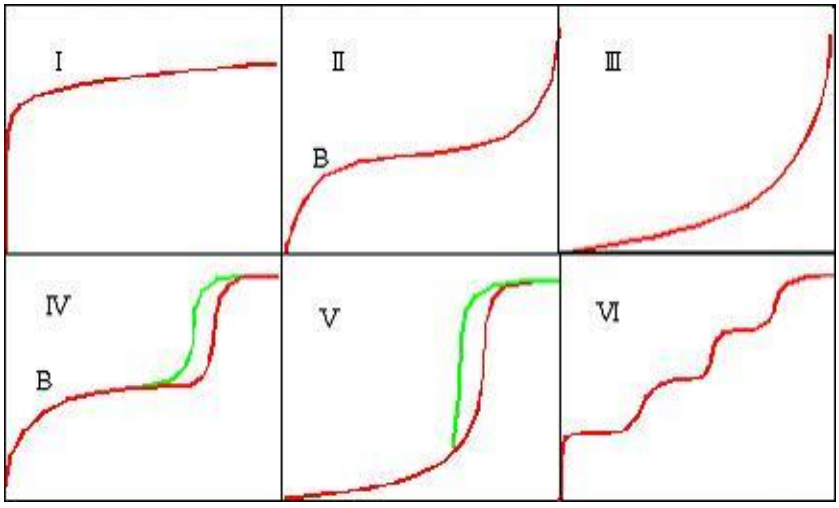

Figure 2.7 The types of adsorption isotherms.

Table 2.1 Features of adsorption isotherms

Type	**Features**	
	Interaction between sample surface and gas adsorbate	**Porosity**
I	Relatively strong	Micropore
II	Relatively strong	Nonporous
III	Weak	Nonporous
IV	Relatively strong	Mesopore
V	Weak	Mesopore
		Micropore
VI	Relatively strong Sample surface has an even distribution of energy	Nonporous

Table 2.1 shows the types and features of adsorption isotherms and describes the adsorption isotherms based on the strength of the interaction between the sample surface and gas adsorbate and the existence or absence of pores.

Table 2.2 IUPAC classification of pores

Pore type	**Pore diameter (nm)**
Micropore	Up to 2
Mesopore	2 to 50
Macropore	50 or up

Pore types are classified as shown in Table 2.2. Pore distribution is measured by the use of N_2 adsorption/desorption isotherm at liquid N_2 temperature and relative pressure (P/P_o) ranging from 0.05-0.1. The large uptake of N_2 at low P/P_o indicated filling of the micropore (< $20A^o$) in the adsorbent. The linear portion of the curve represented multilayer adsorption of nitrogen on the surface of the sample and the concave upward portion of the curve represents filling of mesopores and macropores. [53]

The multilayer Brunauer, Emmett and Teller (BET) method is commonly used to measure total surface area. The most widely used technique to measure the surface area is BET method (Brunauer, Emmett and Teller, (BET)). Thus, analogously to the Langmuir isotherm obtains the BET isotherm:

$$\frac{1}{W[(P_0/P) - 1]} = \frac{1}{W_m C} + \frac{C-1}{W_m C}\left(\frac{P}{P_0}\right)$$

Where W = weight of nitrogen adsorbed at a given P/P_0

W_m = weight of gas to give monolayer coverage

C = a constants that is related to the heat of adsorption.

P = the equilibrium pressure

P_0 = the saturation pressure

The quantity of N_2 adsorbed was obtained by a required of linear relationship between P/P_0 and $1/W[(P/P_0)-1]$. The quantity of nitrogen adsorbed in the monolayer was calculated by the slope and intercept of isotherm which was bring about to gain the surface area. The intercept was taken as zero or a small positive value for a single point method. The surface area could be calculated from the slope of BET plot [51].

2.9.3 Temperature programmed desorption (TPD) of ammonia

Temperature programmed desorption of NH_3 is the most important and widely used technique to measure acidic properties (weak acid sites and strong acid sites) of

mesoporous materials. In various solid acid catalysts, the equilibrium between the gaseous and adsorbed ammonia can control desorption of ammonia. The acid-site concentration can be given by the amount of ammonia desorbing above some characteristic temperature. The heats of adsorption can be calculated by the peak desorption temperature. The acidity of pillared interlayered clays (iron oxide-pillared clays) samples has been measured by adsorption-desorption of NH_3. It is well known that desorption temperature of NH_3 can be related to the strength of acidity of the materials tested. The bond formed between the acid site and NH_3 is broken by an energy supply. Thus, the maximum temperature in the NH_3 desorption process is a qualitative indication of the strength of the acid sites. It has been reported that in the NH_3-TPD one or more broad peaks of desorption at 150-400°C can be observed [52].

Principle of the measurement

TPD is the method to measure the status of physical adsorption and chemisorptions. It can be obtained by measuring desorption of the decomposition of adsorption molecules from the surface while continually heated. TPD can determine the number of desorption peaks (type of adsorption active sites) from the spectrum of desorbed molecules, desorption temperature (activation energy of desorption), and volume of desorption (number of adsorption active sites).

Method of the measurement

Adsorption of probe molecules to the sample is generally done by pulse injection method, volumetric method under the vacuum, or flow method. For the probe molecules, NH_3 can be used to measure the volume and distribution of acidic points. In order to measure basic points, CO_2 can be used. Also, chemisorptions gases (CO, H_2, hydrocarbon, *etc*.) can be used to obtain the information about the characteristics of adsorption during the reaction.

Although the condition of measurement varies by the ambient pressure, desorption measurement can be basically done by heating under the carrier gas flow. Desorbed gas can be detected by Thermal Conductivity Detector (TCD) or mass analyzer (Q-mass) [54].

2.9.4 Inductively coupled plasma-optical emission spectroscopy (ICP-OES)

The ICP is a type of plasma source. The energy of plasma source is supplied by electromagnetic induction as shown in Fig 2.8. The plasma can be created by the argon gas. The sample is nebulized within the nebulizer. The nebulizer is introduced directly inside the plasma flame and break up into their several atoms. The plasma torch is composed of a coil of the RF (radio frequency) generator (essentially 1-5 kW at 27 MHz) and three concentric quartz tubes. An extreme magnetic field from the radio frequency generator is turned on when the plasma torch is turned on. The plasma can be created by the argon gas which it flowing through is ignited (a Tesla unit) and ionized in those fields. The stable high temperature plasma can be generated by the results of the inelastic collisions of create ions, the argon atoms and free electrons [55].

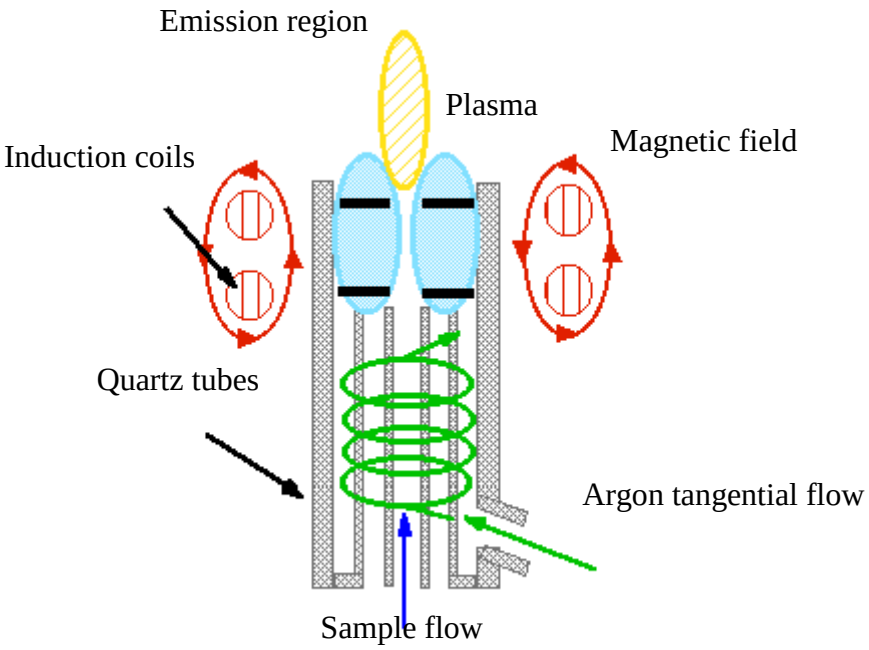

Figure 2.8 A typical plasma source [56].

ICP-OES is an emission spectroscopy (emission spectrophotometric) technique to select a single wavelength specific light for elemental analysis. ICP-OES spectroscopy used an ICP to produce excited atoms. When electrons of element are

excited, they adsorb energy then when they return to ground state, each electrons of element will emit electromagnetic radiation energy at multiple wavelength characteristic of a particular element. The concentration of the element within the sample is obtained from the intensity of this electromagnetic radiation emission. Therefore, the analyst could compare quantify concentration and composition of the element of the sample with reference standard by determining their intensities and determining emitted electromagnetic radiation energy wavelengths of the sample.

2.9.5 Nuclear magnatic resonance spectroscopy ^{27}Al MAS NMR

Structure understanding of material it has aluminium as a basic composition, was required solid NMR to investigation powerful probe of the local structure. Complementary information of Al MNR was characterized by diffraction, microscopy and vibrational spectroscopies. Basic properties of aluminium nucleus for NMR was shown gyromaneticratio (γ = 6.9763×10^{7} $rads^{-1}T^{-1}$). ^{27}Al solid state NMR spectra suffers from additional boardening because of quadupolar nuclear I = 5/2 although its natural abundance is 100% and has a moderated quadrupolar moment (eQ) of 0.149×10^{-28} m^2. [57]

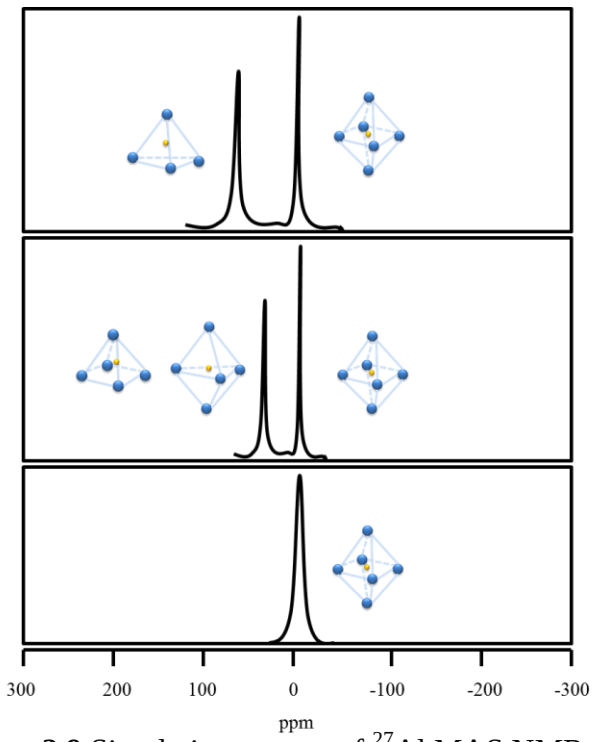

Figure2.9 Simulation spectra of ^{27}Al MAS NMR

Principally, structure of aluminium coordinated are usually formed local as tetrahedral (Al(4)), pentahedral (Al(5)) and octahedral (Al(6)), was characterized by ^{27}Al solid NMR which was shown relation of isotropic chemical shift (δ_{iso}). Table 2.3 are shown summary of significant structure models of aluminium-contaning phase.

Table 2.3 Summarization of probability structure on coordinated aluminium atom

Coordination	Assignments	Reference
Four ($\delta \approx 54$ ppm)	Grafted aluminium	[58]
	Aluminium isomorphously substituting Si^{4+} in silica	[59]
	Four-fold coodinated aluminium in (transition) aluminas	[60]
Five ($\delta \approx 30$-35 ppm)	Interface between alumina and silica or aluminosilicated	[61]
	Five-fold coordinated aluminium in transition aluminas	[60]
	Distorted tetrahedral specicies	[62]
Six ($\delta \approx 0$ ppm)	γ-Al_2O_3 after calcination	[60]
	Amorphous polymeric aluminium oxide (Boehmite) phase	[63]
	Charge-composating cation	[64]

CHAPTER III

EXPERIMENTALS

3.1 Starting materials

3.1.1 Clays

Raw bentonite was kindly supported by Ceric international Co., Ltd. The compositions of bentonite are summarized in Table 3.1

Table 3.1 Bentonite and taeniolite sample compositions

	Bentonite[a]	Taeniolite[b]
SiO_2	63.60	57.93
Al_2O_3	17.60	0.55
MgO	-	20.40
K_2O	0.50	10.61
F	-	9.00
Fe_2O_3	3.10	0.40
CaO	3.00	0.36
Na_2O	3.40	0.05
Li_2O	-	3.30
FeO	-	0.38
Rb_2O	-	0.14
MnO	-	0.11
TiO_2	-	0.11

[a] information from Cernic International Co., Ltd.

[b] Geochemistry International, **2009**, *47*, 831-834.

3.1.2 Chemicals

1) *p*-cresol (Fluka, reagent grade)

2) *p*-cumylphenol (Fluka, reagent grade)

3) thymol (Fluka, reagent grade)

4) *tert*-butanol (Fluka, reagent grade)

5) *i*-propanol (Merck, reagent grade)

6) *n*-butanol, $C_4H_{10}O$ (Merck, reagent grade)

7) biphenyl (Merck, reagent grade)

8) indium (III) chloride hexahydrate (Fluka Chemika, 39%)

9) aluminium (III) chloride hexahydrate (Fluka Chemika, 39%)

3.2 Instruments, apparatus and analytical measurements

3.2.1 Centrifuge

The purification of clays and the collection of the synthesized catalysts were processed by the centaure 2, Sanyo centrifuge. The purification of clay is aimed to remove quartz and other impurities.

3.2.2 Oven and Furnace

Raw clays and all synthesized catalysts were dried in a Memmert UM-500 oven at 100^{o}C for 24 h. The calcination was performed on a Cerbolite RHF 1600 muffle furnace in air.

3.2.2.1 Calcination of metal (III) chloride Al-pillared bentonite

Calcination of as-synthetized clay catalysts in air was performed to convert metal precursors in the interlayer of clays into metal oxide. The calcination condition

for aluminium oxide-pillared clay was heating with the rate 5°C/min and holding at 500^{o}C for 1 h.

3.2.2.2 Calcination of metal (III) chloride impregnated aluminium oxide pillared clays

Calcination of as-synthesized clay catalysts in air was conducted to convert metal chloride impregnated on the precursor of aluminium oxide pillared clay. The calcination condition for metal (III) chloride impregnated aluminium oxide pillared clay was heating with the rate 5°C/min and holding at lower temperature of 50˚C than pillaring method and using for 4 h.

3.2.3 X-ray diffractrometer (XRD)

The XRD patterns and, in consequence, the basal spacing of catalysts (raw and modified clay catalysts) were identified using a Riguka, Dmax 2200/unimaplus XRD with a monochromate and Cu K radiation (40KV, 30 mA). The 2θ angel was ranged from 2 to 30° for bentonite and from 2 to 16° for taeniolite. The scan speed was used at 3 degree/min and the scan step of 0.02 degree. The scattering slit, divergent slit and receiving slit were fixed at 0.5 degree, 0.5 degree and 0.15 mm, respectively.

3.2.4 Nitrogen adsorptometer

The BET specific surface areas of raw and synthesized catalysts were measured using the Quantachrome Autosorp-1 nitrogen ad sorptometer. The 0.04 g of clays was pretreated at 300°C for 3 h. After that, the BET specific surface areas were obtained from nitrogen adsorption at 77 K.

3.2.5 Temperature programmed desorption (TPD) of ammonia

The NH_3-TPD of raw clays and all synthesized catalysts were measured by the BEL Japan, BELCAT.

3.2.6 Inductively coupled plasma-optical emission spectroscopy (ICP-OES)

The amount of aluminium in the aluminium oxide pillared clays were analyzed using the Perkin Elmer PLASMA-1000 inductively couple plasma optical emission (ICP-OES) spectrometer at the Scientific and Technological Research Equipment Centre of Chulalongkorn University.

3.2.7 Nuclear magnetic resonance spectrometer (NMR)

The ^{1}H NMR spectra were obtained in $CDCl_3$ by Mercury plus 400 NMR spectrometer which operated at 399.84 MHz.

3.2.8 Chromatography

Thin layer chromatrography (TLC) was carried on aluminium sheets percoated with silica gel (Merck's, kieselgel 60 PF254) in order to separate mixtures by eluting with ratio of hexane to dichlomethane of 2:3.

3.2.9 ^{27}Al-Nuclear magnetic resonance spectrometer (^{27}Al NMR)

The ^{27}Al MAS NMR was measured by superconducting magnet (14.1 T, JEOL ECA-600) with ^{27}Al resonance frequency of 156.32 MHz. The sample rotor of zirconia (4 mmφ) was spun at the spinning frequency of 15 kHz. The measurement of NMR specta was performed using single-pulse method (non-decoupling) with a small flip angle of 30 degree estimated from the 90 degree pulse width for $AlCl_3$ aqueous solution, and a pulse delay of 1 to 3s. Chemical shifts were referenced to 1.0 M aqueous $AlCl_3$ as external standard (-0.1 ppm) .

3.3 Homoionic clays

Homoionic clays were prepared by purification the raw clay and ion-exchange with aqueous solution of sodium ions, following the method of Kanjanaboonmalert.[65]

3.3.1 Purification of bentonite

Bentonite was purified by fractionated sedimentation. 30 g of bentonite were dispersed in 1,000 mL of deionized water under vigorous stirring for 3 h at RT. Then, quartz sediments were separated from the suspension of bentonite by centrifugation at 4,000 rpm for 10 min. The suspension of bentonite was dried at 100°C for 48 h to obtain pure montmorillonite. Montmorillonite character was confirmed by XRD measurement.

3.3.2 Na-ion exchange

Na-montmorillonite was prepared by cation exchange. Montmorillonite from the previous step was suspended in 5 M NaOH with ratio of clay to NaOH solution of 1 g : 50 mL for 24 h at RT. The above process was repeated three times. The hydroxide ions and the excess sodium ions were removed from Na-montmorillonite using a dialysis membrane (Seamless Cellulose Tubing, small size 30, Wako chemical USA). Then the products were dried at 100°C. The Na-montmorillonite was characterized by XRD technique.

3.4 Synthesis of Al-pillared clay (Al-PLC)

2 g of Na-montmorillonite or Li- taeniolite was dispersed into 100 mL water under stirring for 48 h at RT. The Al-pillar agent was prepared by adding 0.2 M NaOH to 0.2 M $AlCl_3$ with the ratio of OH/Al 1.9 and stirring for 24 h at RT. The Al-pillar agent was then slowly added to the prepared clay suspension with the ratio of Al/clay 3.8 mol/Kg. The mixture was stirred for 24 h at RT. The precipitates were collected by centrifugation at 4,000 rpm for 10 min and washed with distilled water until free of chloride ion. The intercalated product (Al-PLC) was dried at 100°C for 24 h and calcined at 500°C at the rate of 5°C/min for 1 h.

3.5 Synthesis of indium chloride impregnated Al-pillared clay (MCl_3/Al-PLC)

Metal (III) chloride impregnated aluminium oxide pillared clay was synthesized by following the provious work of Masaleh. The aluminium oxidepillared clay was impregnated using a solution of 2% MCl_3 in EtOH. The slurry mixture was

dried at 60°C and calcined with the rate of 5°C/min and holding at lower temperature of 50˚C than pillaring method and using for 4 h. The product was desinged MCl_3/Al-PLC.

3.6 Sample preparation for ICP

The 0.0400 g of a calcined catalyst, placed in a 100 mL Teflon beaker, was soaked with 10 mL concentrated HCl and subsequently with 10 mL of 48% HF in order to remove silica in the form of volatile SiF_4 species. The mixture was heated but not boiled to dryness on a hot plate. The removal of silica was repeated three times. Then, 10 mL of 6 M HCl: 6 M HNO_3 mixtures in the ratio of 1:3 was added and further heated to dryness. 5 mL of 6 M HCl was added and the mixture was warmed for 5 min to complete dissolution. The solution was transferred to 50 mL polypropylene volumetric flask and made up its volume by adding deionized water. If the sample was not analyzed immediately, the solution was then transferred into a plastic bottle with a treated cap underlined with a polypropylene seal.

3.7 Preparation of authentic samples

3.7.1 Authentic sample of *O*-alkylation

1-isopropoxy-4-metylbenzene

Place 47 g (4 mmol) of *p*-cresol, 60.5 g (0.5 mol) of isopropyl bromide, 9.1 g (0.5 mol) of anhydrous K_2CO_3 and 100 mL of acetone in a 250-mL, two-necked round-bottomed flask fitted with a reflux condenser, and boil on oil bath for 8 h with stirring. Pour the reaction mixture into 500 mL of water, separate the organic layer and extract the aqueous layer with three 20 mL portions of Et_2O. Wash the combined organic layer and Et_2O extracts 2M sodium hydroxide solution, and dry over anhydrous K_2CO_3. Remove the Et_2O with a rotary evaporator and distil the residue under reduced pressure.

1-*tert*-butoxy-4-methylbenzene

In a two-necked flask equipped with a magnetic stirring bar and a condenser coil, $Mg(ClO_4)_2$ (0.10 mmol) and *p*-cresol (1.0 mmol) were mixed together. Then di-*tert*-butyl dicarbonate was added, and a bubbling was immediately observed. The mixture was stirred at 40 °C until the TLC analysis revealed the presence of di-*tert*-butyl dicarbonate. The crude reaction mixture was diluted with H_2O and extracted with CH_2Cl_2. The organic layer was separated, dried over anhydrous $MgSO_4$, and filtered, and the solvent was removed by rotary evaporation. The *tert*-butyl ethers were separated from the residual alcohol by silica gel flash chromatograph with a mixture of 9:1 hexane/Et_2O.

3.8 Optimum condition study on alkylation of *p*-cresol with *tert*-butanol

3.8.1 General procedure

In a two-necked flask equipped with a magnetic stirring bar and a condenser coil, catalyst (0.05 mmol) and *p*-cresol (1.0 mmol) were mixed together. The mixture was stirred at 60°C for 15 min. Then *tert*-butanol (8 mmol) was added dropwise until in the period of 30 min and stirred at 150°C for 2 h. The crude reaction mixture was filtered and then submitted to GC analysis.

3.8.2 Effect of reaction time

The alkylation of *p*-cresol was performed according to the general procedure, but varied reaction time as 0.5, 1, 1.5 and 2 h.

3.8.3 Effect of reaction temperature

The alkylation of *p*-cresol was performed according to the general procedure, but varied reaction temperature as 60, 100, 120, 160 and 180°C.

3.8.4 Effect of mole ratio

The alkylation of *p*-cresol was performed according to the general procedure, but varies mole ratio of *p*-cresol to *tert*-butanol as 1: 8, 1: 10 and 1: 30.

3.9 The screening of substrates

3.9.1 Variation of alkylating agents

The general procedure using $InCl_3$ impregnated Al-pillared clays at reflux temperature for 2 h was carried out. The *n*-butanol, *iso*-propanol, *t*-butanol and MTBE were tested.

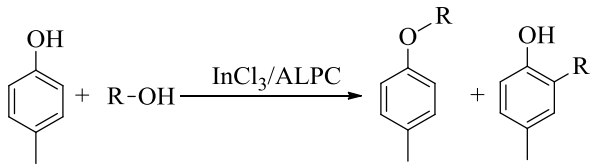

a **b**

(1) R = $(CH2)_3(CH_3)$

(2) R = $CH(CH_3)_2$

(3) R = $C(CH_3)_3$

(4) R = $CH_2CH=CH_2$

(5) R = $C(CH_3)_2CH=CH_2$

1-(*sec*-butoxy)-4-methylbenzene (1a): ^{1}H NMR ($CDCl_3$) δ (ppm): 7.11 (d, 2H, *J* = 6.0 Hz, Ar**H**), 6.83 (d, 2H, *J* = 6.0 Hz, Ar**H**), 4.20 (m, 1H, -OC**H**$(CH_3)CH_2CH_3$), 2.32(s, 3H, ArC**H**$_3$), 1.73 (m, 2H, -OCH(CH_3)C**H**$_2CH_3$), 1.41 (d, 3H, *J* = 6.0 Hz, -OCH(C**H**$_3)CH_2CH_3$) and 0.99 (t, 3H, *J* = 6.2 Hz, -OCH$(CH_3)CH_2$C**H**$_3$)

1-*iso*-propoxy-4-methylbenzene (2a): ^{1}H NMR ($CDCl_3$) δ (ppm): 7.11 (d, 2H, *J* = 6.2 Hz, Ar**H**), 6.83 (d, 2H, *J* = 6.2 Hz, Ar**H**), 3.97(m, 1H, -OC**H**$(CH_3)_2$), 2.32 (s, 3H, Ar$(CH_3)_3$ and 1.42 (d, 6H, *J* = 4.8 Hz, -OCH(C**H**$_3)_2$).

1-*tert*-butoxy-4-methylbenzene (3a): ^{1}H NMR ($CDCl_3$) δ (ppm): 7.05 (d, 2H, *J* = 6.5 Hz, Ar**H**), 6.88 (d, 2H, *J* = 6 Hz, Ar**H**), 2.31(s, 3H, ArC(C**H**$_3)_2$) and1.32 (s, 9H, -O(C**H**$_3)_3$).

1-(allyloxy)-4-methylbenzene (4a): ^{1}H NMR ($CDCl_3$) δ (ppm): 7.01 (d, 2H, *J* = 6.0 Hz, Ar**H**), 6.78 (d, 2H, *J* = 6.0 Hz, Ar**H**), 5.85(m, 1H, -OCH(C**H**$_2$CH$_2$), 5.18(m, 2H, -OCH(CH$_2$C**H**$_2$), 4.62 (d, 2H, *J* = 4.8 Hz,-OC**H**(CH$_2$CH$_2$), 2.31(s, 3H, ArC(C**H**$_3$)$_2$).

2-allyl-4-methylphenol (4b): ^{1}H NMR ($CDCl_3$) δ (ppm): 7.18 (d, 1H, *J* = 6.6 Hz, Ar**H**), 6.98 (dd, 1H, *J* = 6.6, 1.2 Hz, ArH), 6.69 (d, 1H, *J* = 6.6 Hz, ArH), 6.18 (m, 1H, -OC**H**(CH$_2$)$_2$, 5.05 (m, 2H, -OCH(CHC**H**$_2$), 3.36 (d, 2H, *J* = 4.8 Hz, -OC**H**(CH$_2$CH$_2$), and 2.31(s, 3H, ArC(C**H**$_3$)$_2$).

1-methyl-4-(2-methylbut-3-en-2-yloxy) benzene (5a): ^{1}H NMR ($CDCl_3$) δ (ppm): 7.05 (d, 2H, *J* = 6.5 Hz, Ar**H**), 6.76 (d, 2H, *J* = 6.5 Hz, Ar**H**), 5.92 (m, 1H, -O(CH$_3$)$_2$C**H**=CH$_2$), 5.22 (m, 3H, -O(CH$_3$)$_2$CH=C**H**$_2$) and 1.32 (s, 6H, -O(C**H**$_3$)$_2$CH=CH$_2$).

4-methyl-2-(3-methylbut-2-enyl) phenol (5b): ^{1}H NMR ($CDCl_3$) δ (ppm): 7.15 (d, 1H, *J* = 0.8 Hz, Ar**H**), 6.98 (dd, 1H, *J* = 6.2, 0.8 Hz, Ar**H**), 6.71 (d, 1H, *J* = 6.2 Hz, Ar**H**), 5.50 (t, 1H, *J* = 6.0 Hz, ArC(CH$_2$)C**H**=C(CH$_3$)$_2$), 3.41 (d, 2H, *J* = 1.2 Hz, ArC(C**H**$_2$)CH=C(CH$_3$)$_2$), 2.31 (s, 3H, ArC(C**H**$_3$)$_2$) and 1.57 (s, 6H, ArC(CH$_2$)CH=C(C**H**$_3$)$_2$).

3.9.2 Variation of phenols

The general procedure using $InCl_3$ impregnated aluminium oxide pillared clays at reflux temperature for 2 h was carried out. The *p*-cumylphenol, thymol, 4-hydroxybiphenyl and 2-naphthol were tested.

3.9.2.1 Alkylation of *p*-cresol

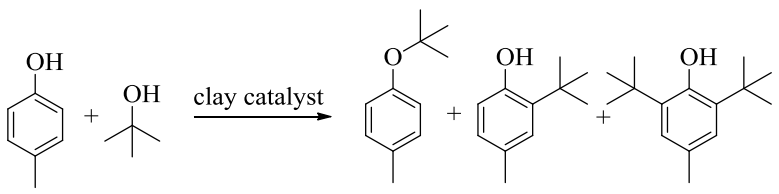

3a **3b** **3c**

1-*tert*-butoxy-4-methylbenzene (3a): ^{1}H NMR ($CDCl_3$) δ (ppm): 7.05 (d, 2H, *J* = 6.5 Hz, Ar**H**), 6.88 (d, 2H, *J* = 6.5 Hz, Ar**H**), 2.31 (s, 3H, ArC(C**H**$_3$)$_2$) and 1.32 (s, 9H, ArO(C**H**$_3$)$_3$).

2-*tert*-butyl-4-methylbenzene (3b): ^{1}H NMR ($CDCl_3$) δ (ppm): 7.04 (s, 1H, Ar**H**), 6.78 (dd, 1H, *J* = 6.6, 1.2 Hz, Ar**H**), 6.64 (d, 1H, *J* = 6.6 Hz, Ar**H**), 2.31(s, 3H, ArC(C**H**$_3$)$_2$) and 1.32 (s, 9H, ArC(C**H**$_3$)$_3$).

2,6-*ditert*-butyl-4-methylbenzene (3c): ^{1}H NMR ($CDCl_3$) δ (ppm): 7.04 (s, 2H, Ar**H**), 2.31(s, 3H, ArC(C**H**$_3$)$_2$) and 1.32 (s, 9H, ArC(C**H**$_3$)$_3$).

3.9.2.2 Alkylation of *p*-cumylphenol

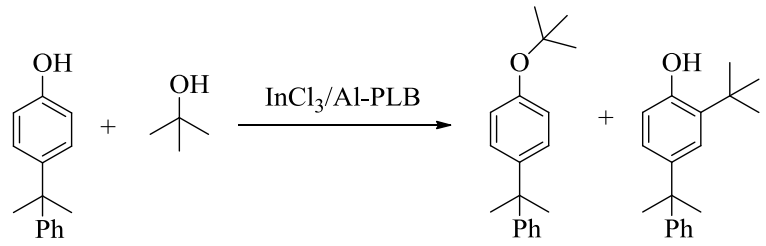

7a **7b**

1-*tert*-butoxy-4-cumylphenol (7a): ^{1}H NMR ($CDCl_3$) δ (ppm): 7.18-7.35 (m, 5H, Ar**H**), 6.93 (d, 2H, *J*=6.4 Hz, Ar**H**), 6.55 (d, 2H, *J* = 6.4 Hz, ArH), 1.71 (s, 6H, Ar(C**H**$_3$)$_2$C) and 1.41 (s, 9H, -O(C**H**$_3$)$_3$).

2-*tert*-butyl-4-cumylphenol (7b): ^{1}H NMR ($CDCl_3$) δ (ppm): 7.18-7.35 (s, 5H, Ar**H**), 7.17 (dd, 1H, *J* = 6.4, 1.2 Hz, Ar**H**), 7.09 (d, 1H, *J* = 1.2 Hz, Ar**H**), 1.71(s, 3H, ArC(C**H**$_3$)$_2$) and 1.41 (s, 9H, ArC(C**H**$_3$)$_3$).

3.9.2.3 Alkylation of thymol

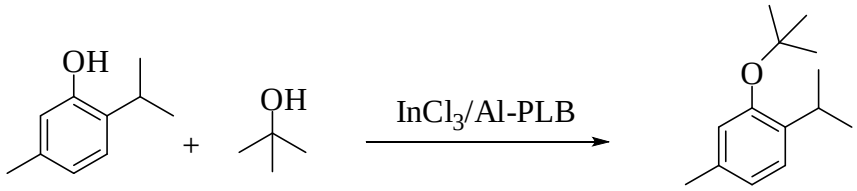

8a

1-*tert*-butoxy-2-isopropyl-5-phenol (8a): ^{1}H NMR ($CDCl_3$) δ (ppm): 7.12 (s, 1H, Ar**H**), 6.78 (d, 1H, *J* = 6.4, Ar**H**), 6.64 (s, 1H, Ar**H**) and 1.41(s, 9H, -O(C**H**$_3$)$_3$).

3.9.2.4 Alkylation of 4-hydroxybiphenyl

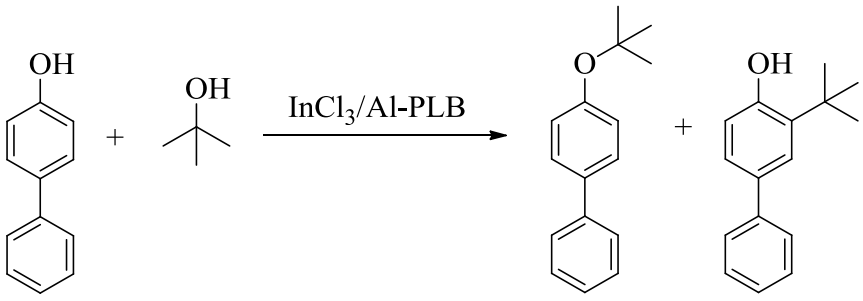

9a **9b**

1-*tert*-butoxy-4-biphenyl (9a): ^{1}H NMR ($CDCl_3$) δ (ppm): 7.18-7.35 (m, 5H, ArH), 7.06 (d, 2H, *J*=6.4 Hz, ArH), 6.95 (d, 2H, *J* = 6.4 Hz, ArH) and 1.32 (s, 9H, -O(C**H**$_3$)$_3$).

2-*tert*-butyl-4-phenylphenol (9b): ^{1}H NMR ($CDCl_3$) δ (ppm): 7.18-7.35 (s, 5H, Ar**H**), 7.17 (dd, 1H, *J* = 6.4, 1.2 Hz, Ar**H**), 7.09 (d, 1H, *J* = 1.2 Hz, Ar**H**), 6.75 (d, 1H, *J* = 1.2 Hz, Ar**H**) and 1.31 (s, 9H, ArC(C**H**$_3$)$_3$).

3.9.2.5 Alkylation of 2-naphthol

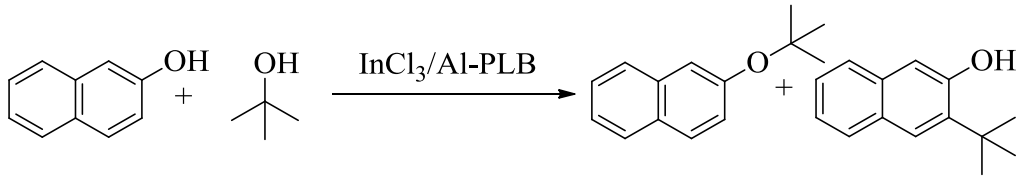

10a **10b**

2-*tert*-butoxynaphthalene (10a): ^{1}H NMR ($CDCl_3$) δ (ppm): 7.72 (m, 1H, Ar**H**), 7.69 (m, 1H, Ar**H**), 7.56 (dd, 1H, *J*=6.4, 1.2 Hz, Ar**H**), 7.38 (dd, 1H, *J*=6.4, 1.2 Hz, Ar**H**), 7.34 (m, 2H, Ar**H**), 7.05 (m, 1H, Ar**H**) and 1.49 (s, 9H, -O(C**H**$_3$)$_3$).

3-*tert*-butyl-2-naphthol (10b): ^{1}H NMR ($CDCl_3$) δ (ppm): 7.64 (m, 2H, Ar**H**), 7.32 (d, 1H, *J* = 6.4, Ar**H**), 7.25 (m, 2H, Ar**H**), 6.95 (d, 1H, *J* = 6.4 Hz, Ar**H**) and 1.45 (s, 9H, ArC(C**H**$_3$)$_3$).

3.9.2.6 Alkylation of 3-methoxyphenol

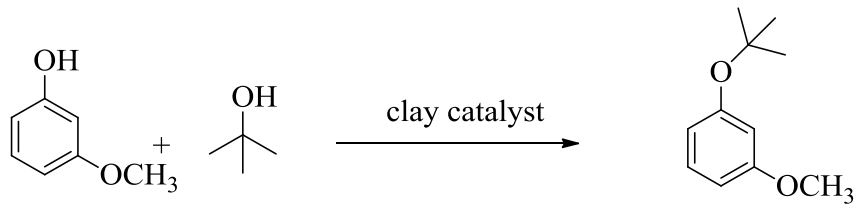

11a

1-*tert*-butoxy-3-methoxybenzene (10b): ^{1}H NMR ($CDCl_3$) δ (ppm): 7.21 (t, 5H, *J* = 6.4 Hz, Ar**H**), 6.54 (m, 3H, Ar**H**), 3.81 (s, 3H, -OC**H**$_3$), and 1.41 (s, 9H, -OC(C**H**$_3$)$_3$).

3.10 The screening of catalysts

3.10.1 Variation of clays

The metal (III) impregnated Al-pillared clays was used as a catalyst in alkylation of *p*-cresol with *tert*-butanol at reflux temperature for 2 h. Types of metal (III) chloride were varied as the followings: indium (III) chloride hexahydrate

($InCl_3.6H_2O$), lanthanum (III) chloride heptahydrate ($LaCl_3.7H_2O$), cerium (III) chloride hexahydrate ($CeCl_3 .6H_2O$), neodymium (III) chloride hexahydrate ($NdCl_3.6H_2O$), gadolinium (III) chloride hexahydrate ($GdCl_3.6H_2O$), and aluminium (III) chloride hexahydrate ($AlCl_3.6H_2O$).

3.10.2 Comparison of raw clays

The $InCl_3$ impregnated Al-pillared clays were used as a catalyst in alkylation of *p*-cresol with *tert*-butanol at reflux temperature for 2 h. Types of clay supported: bentonite and taeniolite were varied.

3.10.3 Variation of calcination temperature

The $InCl_3$impregnated Al-pillared clays were used as a catalyst in alkylation of *p*-cresol with *t*-butanol at reflux temperature for 2 h. The calcination temperature of taeniolite: 400, 450 and 500°C were varied.

3.11 The reuse of catalyst

The used $InCl_3$ impregnated Al-pillared bentonite and Al-pillared taeniolite calcined at 450˚C were generated by calcination at the similarly condition in impregnation method. The efficiency of catalyst was confirmed by X-ray powder diffraction, BET analysis and temperature programmed ammonia desorption techniques. Then, the regenerated was reuses as a catalyst in alkylation of *p*-cresol.

CHAPTER IV

RESULTS & DISCUSSION

4.1 The characterization of clays

In this research, bentonite and taeniolite (synthetic clay) were utilized as catalysts for selective organic transformation. The structures of clay were determined emphasizing on a basal spacing and the intensity of d_{001} reflection of XRD.

4.1.1 The characterization of raw bentonite

Bentonite is phyllosilicated-type clay containing montmorillonite and impurities such as calcite, quartz, feldspars, crystobalite and humic acids. Quartz is a major impurity of clays that reduced the catalytic efficiency. The characteristics of raw bentonite were analyzed by XRD as shown in Figure 4.1. The pattern shows the characteristic peaks of montmorillonite at 2θ of 7° and 19° which were related to the 001 and 100 planes of montmorillonite, respectively [65]. Its d_{001} basal spacing was 14.22 A°. The peaks at 2θ of 22°, 24° and 27° were assigned to quartz (SiO_2).

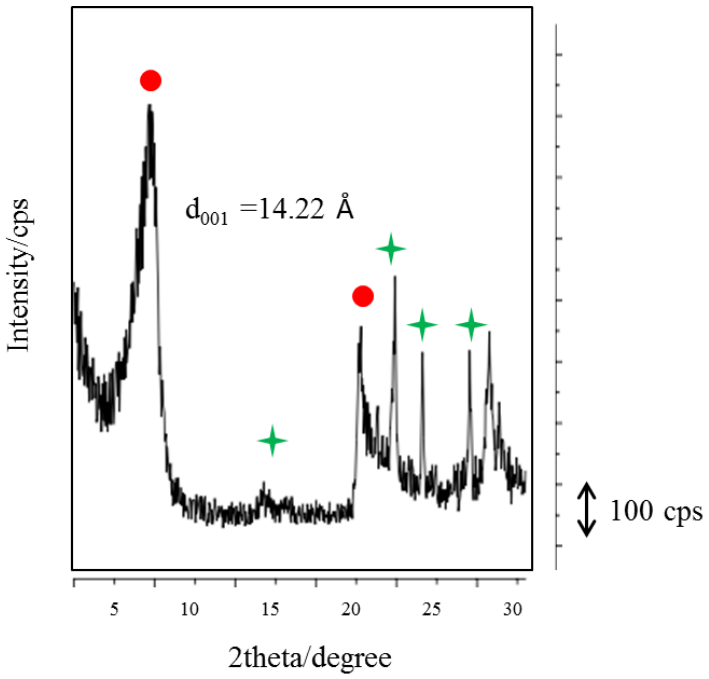

Figure 4.1 XRD patterns of raw bentonite (● represents bentonite peaks and ✦ represents impurity quartz peak).

4.1.2 The characterization of Li-taeniolite, Li-TN (synthetic clay)

In Figure 4.2, Li-TN (synthetic clay) showed the characteristic peak at 2θ of 6° corresponding to the 001 plane with the highest relative intensity. This pattern with no other crystalline phases was assigned. The d_{001} basal spacing was detected at 12.17 Å.

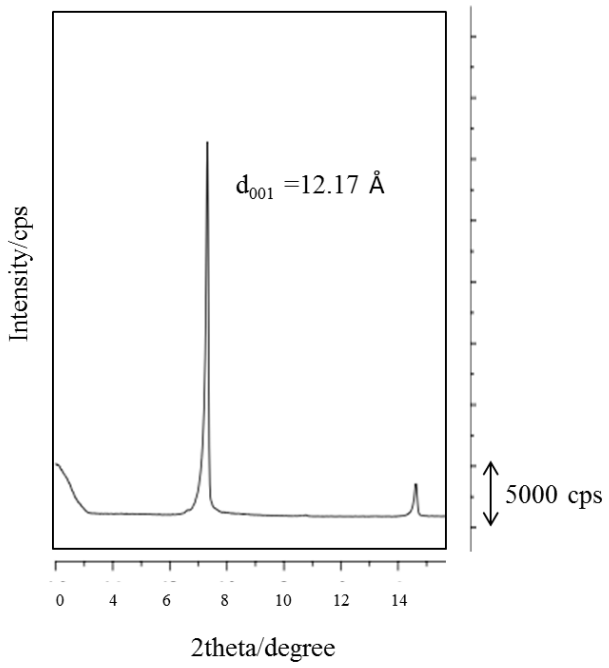

Figure 4.2 XRD patterns of Li-taeniolite.

4.2 The synthesis and characterization of homoionic clay

Homoionic clay was prepared by ion exchanging after purification. In a purification process, quartz and other impurities were removed from bentonite by dispersion and centrifugation process. Na ions were intercalated between clay layers to achieve homoionic clay which was used as starting material to synthesize clay catalysts.

4.2.1 The purification of bentonite

Generally, bentonite was purified by dispersion in deionized water and centrifuged for removing quart. After purification, montmorillonite was further dispersed in deionized water and dried up at 100°C. Ultimately, the achievement of purification of bentonite to montmorillonite was assigned by basal spacing of d_{001} reflection from the XRD.

Figure 4.3 shows the XRD of purified raw bentonite (a) and montmorillonite (b). The characteristic signals of quartz generally appeared at 22°, 24° and 27° of 2θ were absence in the XRD of montmorillonite. The characteristic peak which was still

remained on montmorillonite pattern was the 001 peak at 2θ of 7°, corresponding to the d_{001} spacing of 12.37 A˚

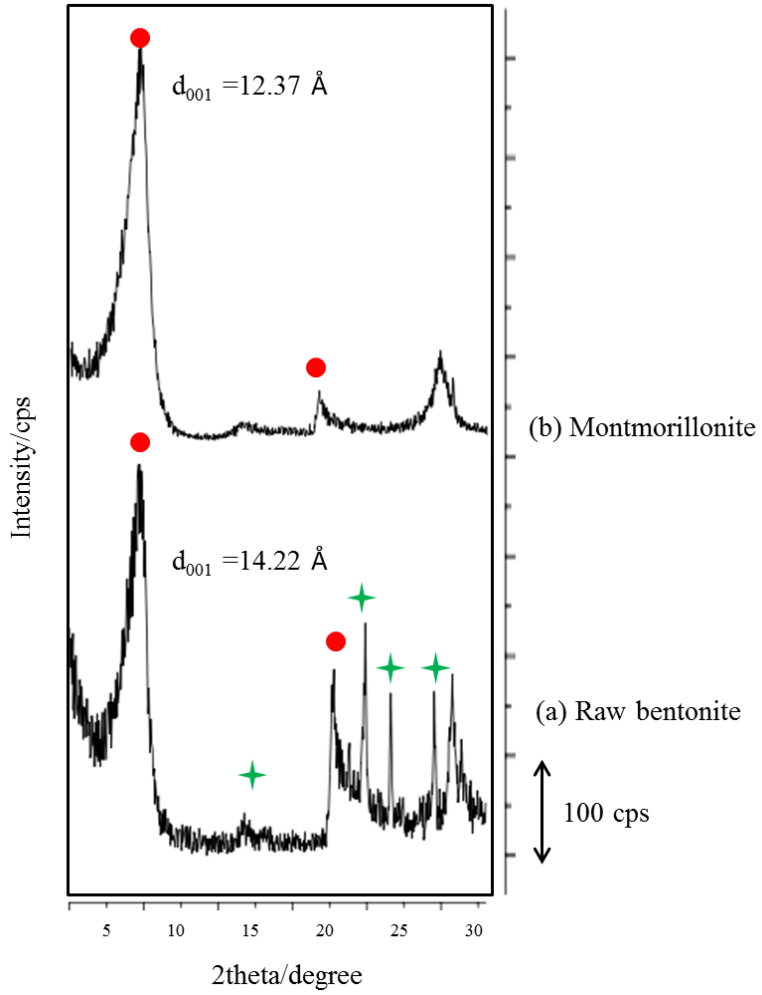

Figure 4.3 XRD patterns of (a) raw material bentonite and (b) montmorillonite (purified bentonite) obtained at the centrifugal speed of 4,000 rpm (represents ● the peaks of montmorillonite and ✦ represents impurity quartz peak).

4.2.2 Na-ion exchange of clays

Balancing charge of montmorillonite interlayer, Na cation was presented for exchanging with pasting a net negative charge layer structure of clays. From the earlier report, Na ion was presented to dominate the exchangeable cations in the clay swelling which depended on largely solvation energy (98 kcal/mol) [66] and

including to be a small electrostatic interaction between monovalent cation and negatively charged layer.

XRD of Na-montmorillonite

The intercalation of Na-ions for preparing Na-montmorillonite was exchanged by treating of 5M NaOH for three times. When a treatment process was completed, it was washed until neutral by deionized water. Figure 4.4 represents the XRD patterns of montmorillonite (a) and Na-montmorillonite (b) of 001 peak at 2θ of 6 and 7Å, respectively. The shift of peak to lower 2θ, d_{001} basal spacing became increasing of 12.37 to 15.39Å. The different clearance space of clay layers was illustrated by solvating of Na ions dispersion for balancing charge.

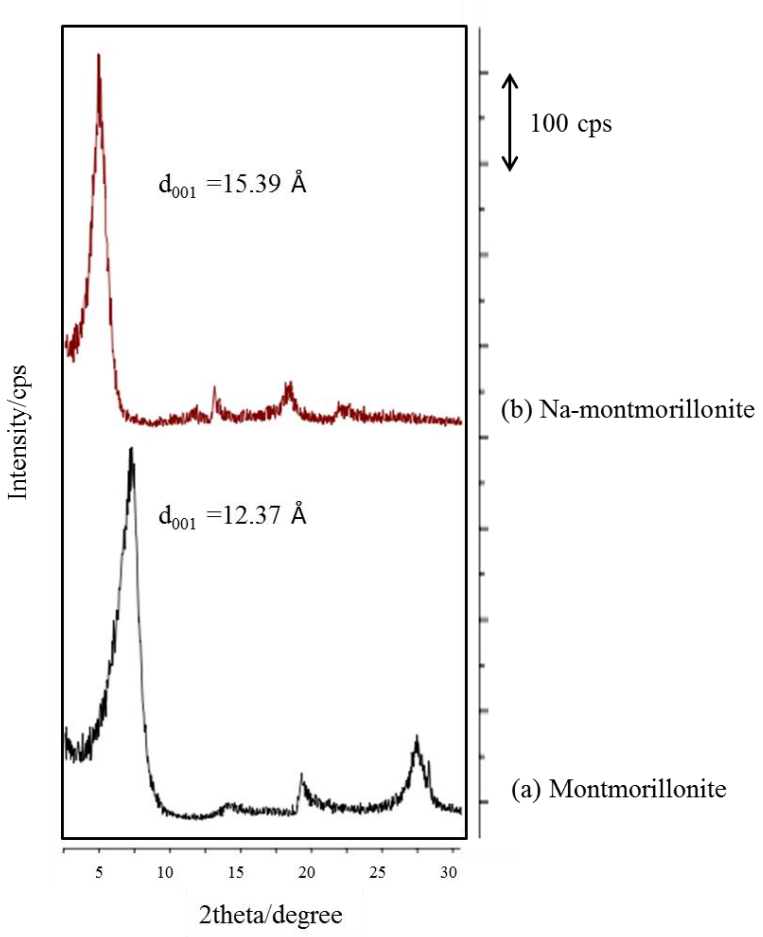

Figure 4.4 XRD patterns of a) montmorillonite and b) Na-montmorillonite

4.2.3 The synthesis and characterization of Al-pillared bentonite (Al-PLB) and Al-pillared taeniolite (Al-PLT)

Pillaring aluminium agent was applied to interlayer of montmorillonite and Li-TN for synthesis of aluminum precursors between clay layers *via* calcination processing. Formation of aluminium precursors produced better catalytic active site.

The XRD of Al-pillared bentonite, Al-PLB (a) and Na-montmorillonite (b) (Figure 4.5) show the difference of d_{001} basal spacing peak. The board peak of Al-PLB was detected at 17.51° which was shifted slightly to the larger basal spacing comparing with the d_{001} peak of Na-montmorillonite. The resulting of larger basal spacing of Al-PLB with Na ion between the layers of montmorillonite could be exchanged by aluminium polyoxocations [67]. The OH/Al was 1.9 intercalated into clay layer and converted to Al-pillars during calcination process.

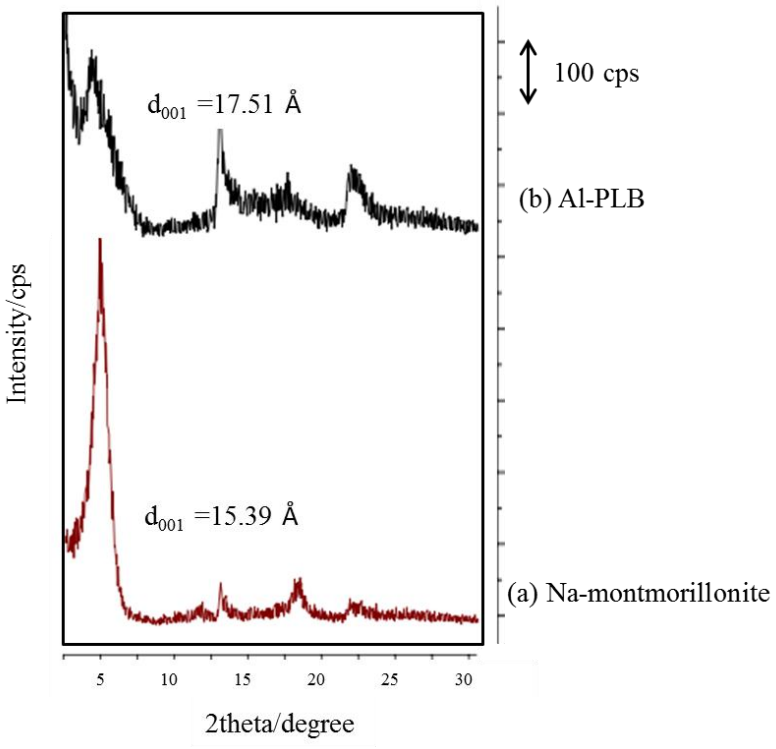

Figure 4.5 XRD patterns of (a) Na-montmorillonite and (b) Al-PLB.

The XRD of Al-PLT (a) and Li-TN (b) (Figure 4.6) show the difference of d_{001} basal spacing peak. The board peak of Al-PLB displayed at 13.20° which was

shifted slightly to the larger basal spacing comparing with the d_{001} peak of Li-TN. This result revealed the same trend as observed in montmorillonite.

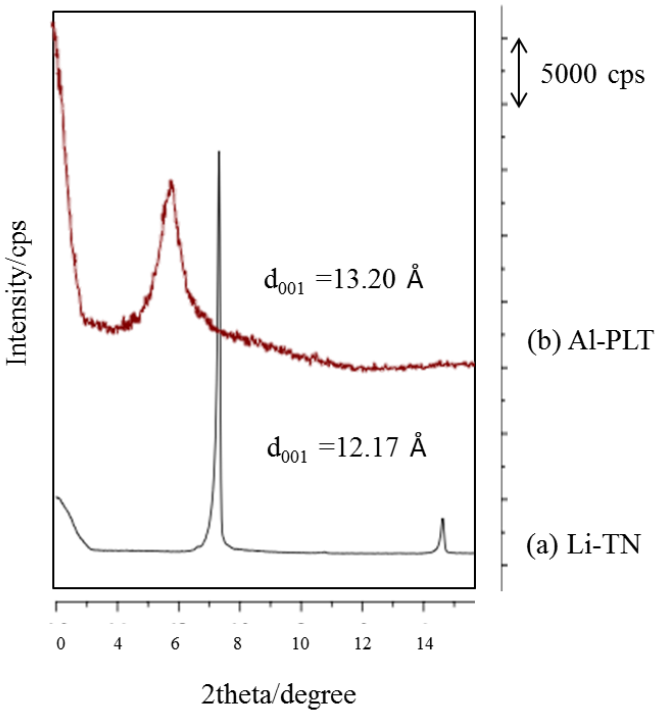

Figure 4.6 XRD patterns of (a) Li-TN and (b) Al-PLT.

4.2.4 The synthesis and characterization of MCl_3/PLB

The XRD patterns of metal (III) chloride ($InCl_3$, $LaCl_3$, $CeCl_3$, $NdCl_3$, $GdCl_3$) impregnated Al-pillared bentonite ($InCl_3$/Al-PLB, $LaCl_3$/Al-PLB, $CeCl_3$/Al-PLB, $NdCl_3$/Al-PLB and $GdCl_3$/Al-PLB) and taeniolite ($InCl_3$/Al-PLT) are compared as presented in Figures 4.7 and 4.8, respectively. The d_{001} basal spacing of metal (III) chloride impregnated Al-pillared bentonite (MCl_3/Al-PLB) were about 14-15 Å which were trivial lower than Al-PLB. The d_{001} peaks were a lot broader indicating that the re-calcination process caused the pillared structure collapse slightly and the impregnation of metal (III) chloride increased the disordering between the interlayer spacing of clay.

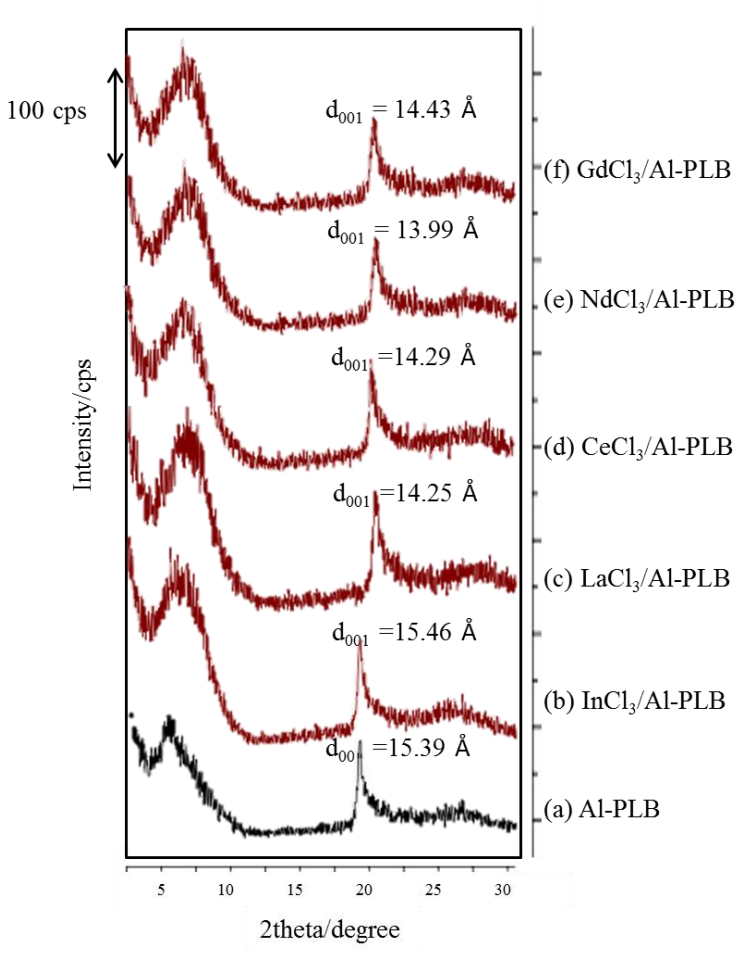

Figure 4.7 XRD patterns of (a) Al-PLB, (b) $LaCl_3$/Al-PLB, (c) $LaCl_3$/Al-PLB, (d) $CeCl_3$/Al-PLB, (e) $NdCl_3$/Al-PLB and (f) $GdCl_3$/Al-PLB.

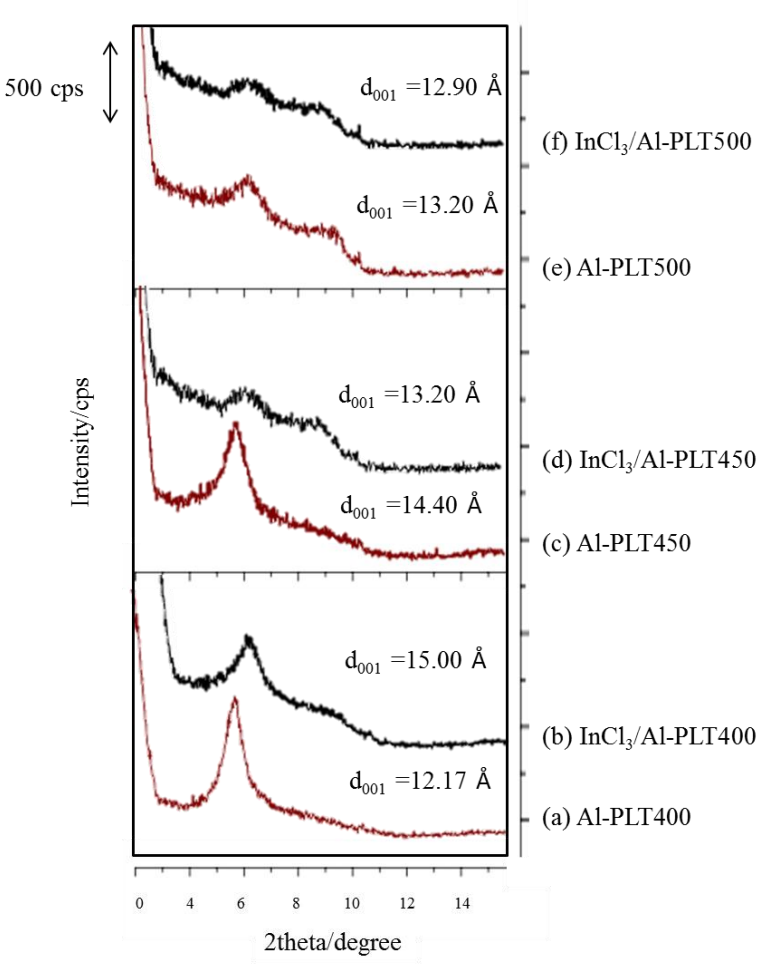

Figure 4.8 XRD patterns of (a) Al-PLT400, (b) $InCl_3$/Al-PLT400, (c) Al-PLT450, (d) $InCl_3$/Al-PLT450, (e) Al-PLB500 and (f) $InCl_3$/Al-PLT500.

4.3 Temperature Programmed Desorption (TPD)

The comparison of the acidity (mmol/g) of montmorillonite, Al-PLB, metal (III) chloride impregnated Al-pillared bentonite ($InCl_3$/Al-PLB, $LaCl_3$/Al-PLB, $CeCl_3$/Al-PLB, $NdCl_3$/Al-PLB and $GdCl_3$/Al-PLB) was investigated by NH_3-TPD acidity analysis. The acidity thermogram of derived bentonite case was shown in Figure 4.9.

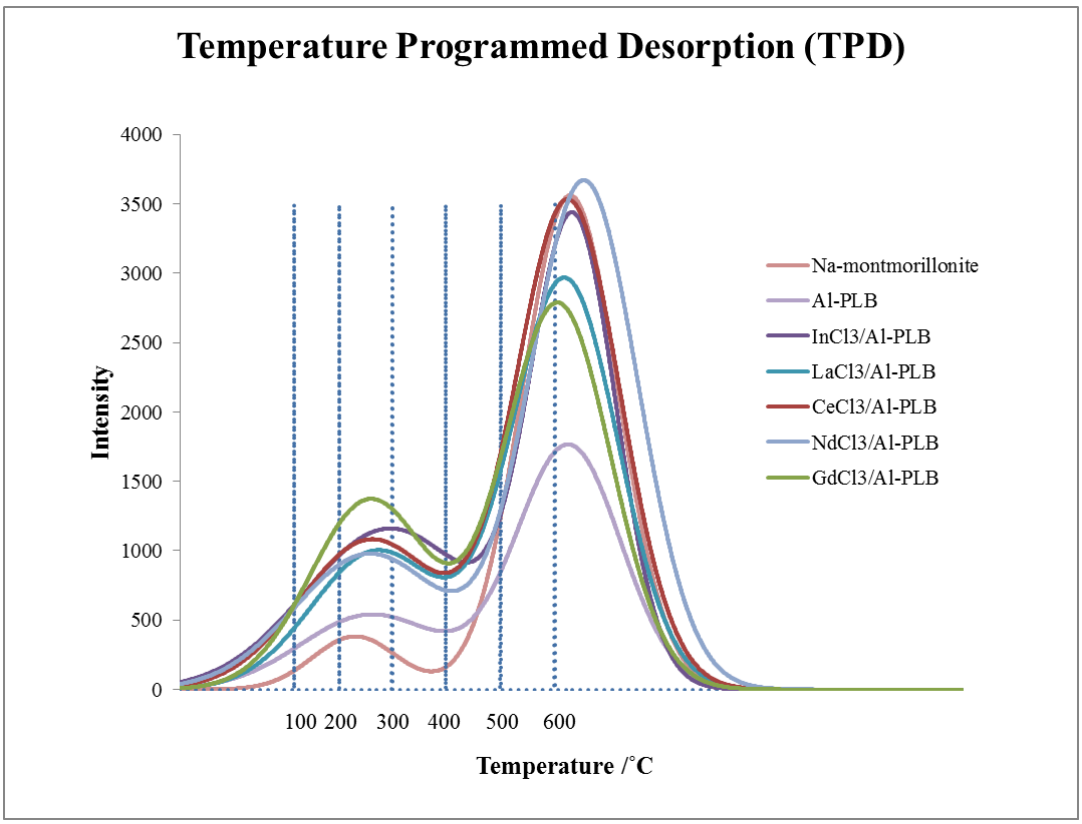

Figure 4.9 The acidity thermogram of derived bentonite case by NH_3-TPD

From the Figure 4.9, the acidity thermogram was shown two boundary of difference strengh of acidity. The first peak was around 100-400˚C, it was revealed to lower acid strength than another peak about 400-600˚C.

Table 4.1 was shown the breaking bond temperature of NH_3 coordination with bentonite species catalyst which weak bonding was represented on weak acid site and strong bonding was represented on strong acid site.

Table 4.1 Temperature zone of bentonite clays

Entry	Catalysts	Temperature (˚C)	
		Weak acid sites	**Strong acid sites**
1	Na-montmorillonite	230	529
2	Al-PLB	229	606
3	$InCl_3$/Al-PLB	300	525
4	$LaCl_3$/Al-PLB	275	594
5	$CeCl_3$/Al-PLB	261	604
6	$NdCl_3$/Al-PLB	259	602
7	$GdCl_3$/Al-PLB	264	609

Attractively, two distributions of thermal diagram of ammonia desorption presented high acidity by ammonia ungearing. The different site exhibition, strong and weak acidity, could be observed by thermogram around 600 and 240-300˚C, respectively. At weakly acidic site distribution, the acidity of montmorillonite was derived from hydroxyl framework of clay. At low temperature, the acidity was revealed unremarkably quantitative; meanwhile, strong acidity was detected as moderate amount. This was perhaps because it was mostly crystalline structure. The proposing of Al-polyoxocation [67] was presented to explain the structure of the precursor pillaring on Al-PLB in relation with strong acidic site. When impregnation metal (III) chloride on Al-PLB, was strongly coordinated with ammonia, which initiated to increasing of strong acidity sites in Figture 4.9, obviously. Weak acidity distribution was presented phenomenant of hydroxyl and hydrated coordination on the catalyst with ammonia which was bonded be weaker.

Table 4.2 shows the acidity of all catalysts derived from bentonite. The bentonite catalysts tested were Na-montmorillonite, Al-PLB, $InCl_3$/Al-PLB, $LaCl_3$/Al-PLB, $CeCl_3$/Al-PLB, $NdCl_3$/Al-PLB, and $GdCl_3$/Al-PLB.

Table 4.2 Total acidity of synthesized bentonite clays

Entry	Catalysts	Acidity (mmol/g)		Total amount of acidity (mmol/g)
		Weak acid sites	Strong acid sites	
1	Na-montmorillonite	0.71	0.32	1.03
2	Al-PLB	0.46	1.21	1.67
3	$InCl_3$/Al-PLB	0.34	1.52	1.86
4	$LaCl_3$/Al-PLB	0.90	1.58	2.48
5	$CeCl_3$/Al-PLB	0.77	2.51	3.28
6	$NdCl_3$/Al-PLB	0.81	2.86	3.67
7	$GdCl_3$/Al-PLB	0.88	1.25	2.13

Na-Montmorillonite was lower acidity than Al-pillared bentonite although both had more strong acid sites than weak acid sites. Considering the total amount of acidity, Al-pillared bentonite gave higher value than Na-montmorillonite as a result of aluminium polyoxocation. It resembles to perform as Lewis acid addition in spacing of clay layer.

Acidic character of pillared clays could be derived from either Brønsted or Lewis site. Weak and strong acid sites could be explained from desorption of ammonia from catalyst. Weak acid site was associated with the coordination of water with aluminium in pillars, whereas strong acid site was attributed from aluminium oxide in pillars.

Metal (III) chloride impregnated Al-PLB affected on the acidic character on the variation of metal impregnated. Table 4.2 displays that $NdCl_3$/Al-PLB possessed the highest acidity followed by $CeCl_3$/Al-PLB, $GdCl_3$/Al-PLB, $LaCl_3$/Al-PLB, and $InCl_3$/Al-PLB, respectively. These NH_3-TPD results were related by redox potential of all metals which were measured from reduction of M^{3+} to M^{2+}.

In Table 4.3 was compared acidity of various clay species which provided difference capacity exchange cation its turned into difference acidity.

Table 4.3 Comparison of total acidity on catalysts

Entry	Catalysts	Acidity (mmol/g)		Total amount of acidity (mmol/g)
		Weak acid sites	Strong acid sites	
1	Na-Montmorillonite	0.71	0.32	1.03
2	Li-TN	0.34	0.56	0.90
3	Al-PLB	0.46	1.21	1.67
4	Al-PLT500	0.46	0.53	0.99
5	$InCl_3$/Al-PLB	0.34	1.52	1.86
6	$InCl_3$/Al-PLT500	0.33	0.99	1.32

The comparison of the acidity of different clay is shown in Table 4.3. Li-TN revealed less acidity than Na-montmorillonite, while Al-PLT had higher acidity than Al-PLB. This was a result of increasing taeniolite cation exchange capacity, thus, taeniolite had higher capacity than montmorillonite. The increasing of exchange capacity of bentonite to taeniolite was 2.68 and 0.7-1.2, respectively.

The increasing of taeniolite cation exchange capacity was a point of increasing acidity because aluminium ions could be exchanged more than montmorillonite. The amount of Al-ions was confirmed by ICP.

$InCl_3$/Al-PLB was investigated. The amount of $InCl_3$ had no effect on the acidity of catalyst comparing with different raw clay. This was because all $InCl_3$ was applied to impregnate on clays, no loss of $InCl_3$ by washing method.

Figure 4.10 was presented acidity thermogram for comparing Li-TN, before calcination of Al-pillared taeniolite and various of calcination temperature of Al-pillared taeniolite.

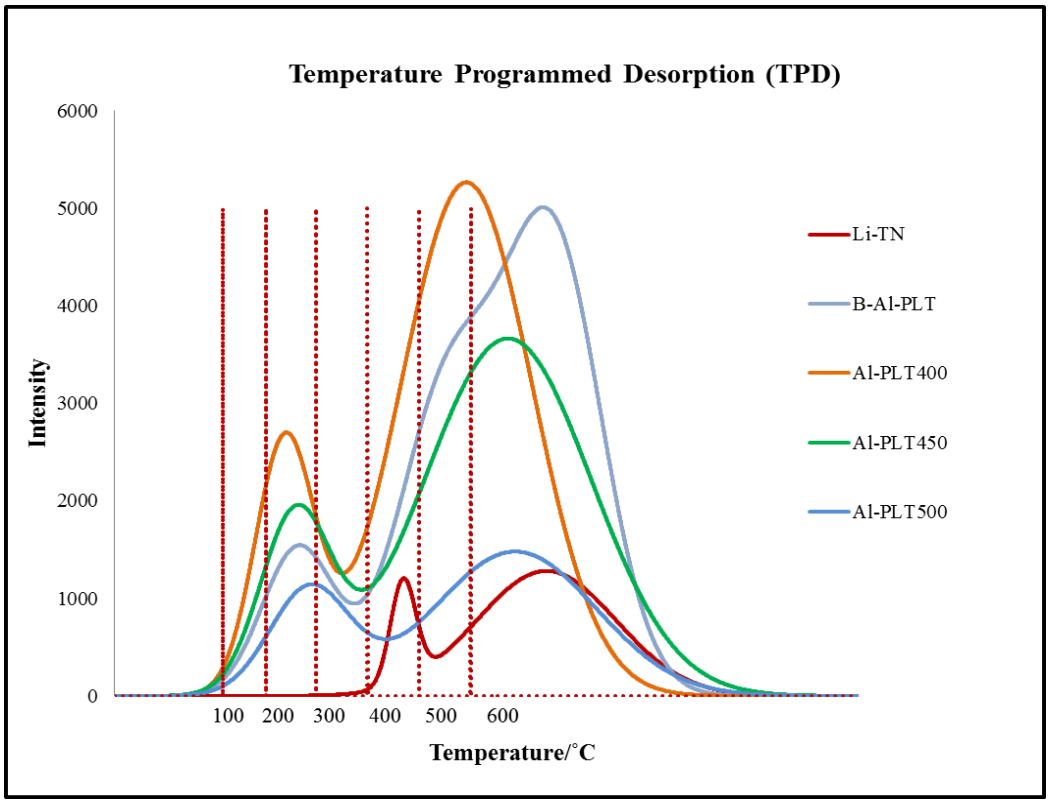

Figure 4.10 TPD profile of Li-TN, BAl-PLT and calcined at various temperatures

In Figure 4.11 was shown thermogram of $InCl_3$/BAl-PLT which was not calcined and presented effect of difference calcination temperature for synthesis catalysts.

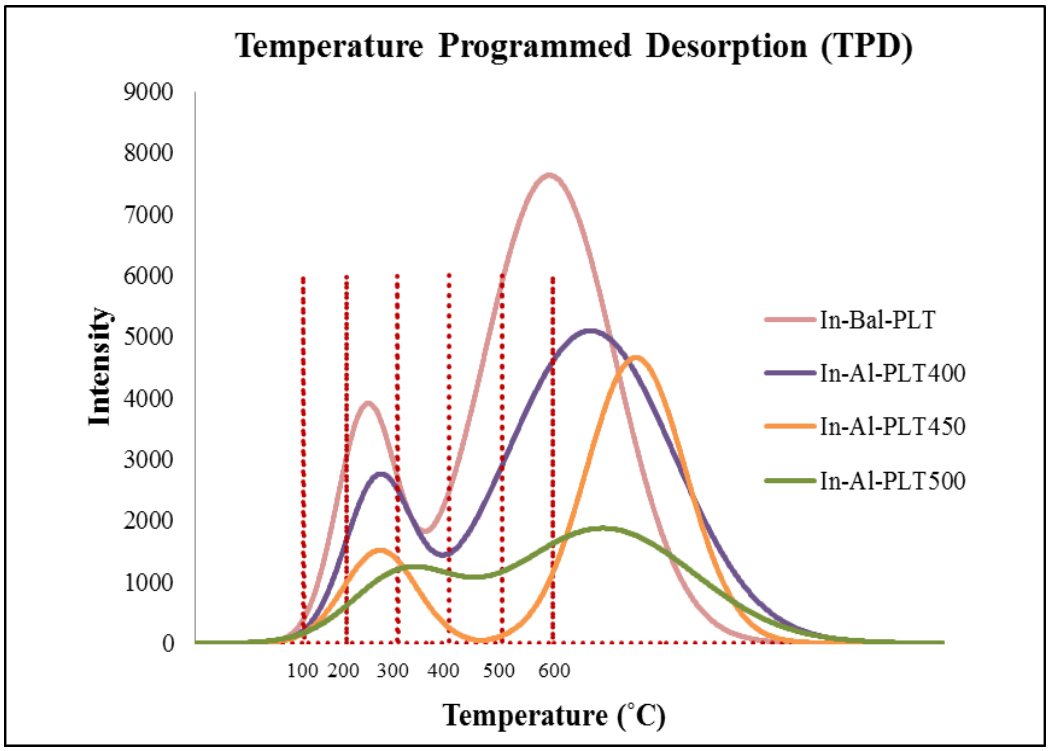

Figure 4.11 TPD profile of $InCl_3$/BAl-PLT calcined at various temperatures

Table 4.4 was shown the breaking bond temperature of NH_3 coordination with taeniolite species catalyst which weak bonding was represented on weak acid site and strong bonding was represented on strong acid sites.

Table 4.4 Temperature zone of different catalyst acidity based on taeniolite type of clay

Entry	Catalysts	Temperature (˚C)	
		Weak acid sites	**Strong acid sites**
1	Li-TN	471	597
2	BAl-PLT	267	600
Calcination at 400°C			
3	Al-PLT	265	601
4	$InCl_3$/Al-PLT	300	601
Calcination at 450°C			
5	Al-PLT	293	601
6	$InCl_3$/Al-PLT	331	599
Calcination at 500°C			
7	Al-PLT	312	603
8	$InCl_3$/Al-PLT	327	601

The diagram of temperature programmed desorption is shown in Figure 4.9 comparing with ammonia ungearing. The different site exhibition, strong and weak acidity were presented by thermogram around 600 and 260˚C, respectively. Deriving of two distributions, strongly acidic peak was prognosticated of Al-hydroxypolycation [69] and weakly acidic peak was predicted from leaking of proton coordinated structure [70]. Histograms of ammonia emitting revealed several cacination temperatures for the synthesis of Al-pillared taeniolite, escalation heated temperature contributed to higher strongly acidity site. Aluminium polyoxocations were complicated to lower oxidation number from dehydration of water and hydroxyl group which related to the reduction with electron donor species. These results are implied in Table 4.4.

Table 4.5 reveals the effective acidity of calcination temperature on catalyst of Li-TN, before calcination of Al-PLT, various calcination temperatures of Al-PLT and $InCl_3$/Al-PLT.

Table 4.5 Total acidity of Li-TN, Al-PLT using different calcination temperatures and $InCl_3$/ Al-PLT

Entry	Catalysts	Acidity (mmol/g)		Total amount of acidity (mmol/g)
		Weak acid sites	Strong acid sites	
1	Li-TN	0.34	1.12	1.46
2	BAl-PLT	0.75	1.53	2.28
Calcination at 400°C				
3	Al-PLT400	0.87	1.47	2.34
4	$InCl_3$/Al-PLT400	0.76	1.91	2.67
Calcination at 450°C				
5	Al-PLT450	0.79	1.22	2.01
6	$InCl_3$/Al-PLT450	0.48	1.65	2.13
Calcination at 500°C				
7	Al-PLT500	0.46	0.53	0.99
8	$InCl_3$/Al-PLT500	0.33	0.99	1.32

The acidity results of all catalysts based on taeniolite were examined by desorption of NH_3 (g) on TPD. The amount of acidity on strong crystalline Li-TN gave lower quantitative acidity; whereas, Al-PLT was better which was corresponding to theory of adding metal oxide. The calcination temperature is mainly cause for designing aluminium polyoxocation structure which it could created to various acidity. The augmentation of temperature at 500˚C was revealed the lowest amount of acidity; however, declined temperature to 450 and 400˚C was still provided higher acidity. In case of increasing acidity from impregnation of $InCl_3$, acidic character was presented to higher than Al-pillared taeniolite at all species.

4.4 Nitrogen adsorption-desorption (Brunauer-Ednmelt-Teller method, BET)

The general method using for determination of surface area of porous materials is BET specific surface area analysis. The BET specific surface area of raw bentonite, Al-PLB and metal (III) chloride/Al-PLB ($InCl_3$/Al-PLB, $LaCl_3$/Al-PLB, $CeCl_3$/Al-PLB, $NdCl_3$/Al-PLB, $GdCl_3$/Al-PLB) are exhibited in Table 4.6.

Table 4.6 BET specific surface area of Na-montmorillonite, Al-PLB and MCl_3/Al-PLB

Catalysts	BET specific surface area (m^2/g)
Na-montmorillonite	60.21
Al-PLB	145.70
$InCl_3$/Al-PLB	121.40
$LaCl_3$/Al-PLB	111.40
$CeCl_3$/Al-PLB	127.25
$NdCl_3$/Al-PLB	122.40
$GdCl_3$/Al-PLB	121.60

The nitrogen adsorption-desorption isotherms of Al-PLB displayed distorted reversible type IV isotherm as a result of aluminium pillaring calcined samples being added to clay layer structure (2-dimensional structure) which was then converted to mesoporous structure (3-dimensional structure). In Table 4.6, the specific surface area of intercalation of aluminium to montmorillonite was higher than montmorillonite. That was because Al-precursor between the layers of montmorillonite was designed to increase surface area of catalysts. Al-PLB had still higher surface area than metal (III) chloride/Al-PLB which was observed by poor metal such as $InCl_3$ and metals in lanthanide group ($LaCl_3$, $CeCl_3$, $NdCl_3$, $GdCl_3$). Since metal (III) chloride shielded the specific surface area, accordingly the surface area was decreased. The pore size distribution was classified to the range of 50 to 70 A° which was observed by BJH analysis. The pore size could be indicated as mesoporous material. Al-PLB had higher specific surface area than montmorillonite due to increasing of gap between clay layers. This result was related with the measurement of d_{001} basal spacing which was widen from 12.37 to 16.36 A°. Moreover, the 3 dimensional structure of Al-connection on the adjacent aluminosilicate layers was assumed to be a precursor between layers of montmorillonite, confirmed by XRD. The XRD results indicated that Al was not aggregated outside clay because specific surface area was not lower than montmorillonite, thus it was not a dense structure.

The pore size of metal (III) chloride/Al-PLB was characterized by BJH analysis which was in the range of 50 to 70 A° (mesoporous structure). Specific

surface area of metal (III) chloride/Al-PLB was lower than Al-PLB because metal (III) chloride could be deposited on the wall of Al-PLB pore and position in mesoporous structure as a result of decreasing specific surface area.

Table 4.7 was compared of BET specific surface area on difference clay which was calculated by nitrogen absorption-desorption.

Table 4.7 BET specific surface area of exchanged ion on clays, Al-pillared clays and $InCl_3$/Al-pillared clays

Catalysts	**BET specific surface area (m^2/g)**
Na-montmorillonite	60.21
Al-PLB	145.70
$InCl_3$ /Al-PLB	121.40
Li-TN	3.53
Al-PLT[a]	21.4
$InCl_3$ /Al-PLT[b]	17.7

[a] calcination at 500° [b] at 450°C

The pore size of taeniolite distribution could be classified to the range of 130 to 140 A° observed by BJH analysis. The pore size could be indicated as mesoporous materials as montmorillonite which had a range of 50 to 70 A°. Montmorillonite had higher specific surface area than taeniolite because montmorillonite had smaller pore size than taeniolite.

Table 4.8 exhibits the variation of calcination temperature of Al-PLT to investigate specific surface area at 400, 450 and 500°C.

Table 4.8 The BET specific surface area of Li-TN, Al-PLT and $InCl_3$/Al-PLT

Catalysts	BET specific surface area (m^2/g)
Li-TN	3.53
BAl-PLT	47.2
Calcination 400˚C	
Al-PLT400	71.1
$InCl_3$/Al-PLT400	64.0
Calcination 450˚C	
Al-PLT450	60.2
$InCl_3$/Al-PLT450	55.3
Calcination 500˚C	
Al-PLT500	21.4
$InCl_3$/Al-PLT500	17.7

The pore size of taeniolite distribution could be classified to the range of 130 to 140°A. The results of specific surface area were increased by decreasing calcination temperature.

Before calcinations, Al-PLT had higher specific surface area than Li-TN. That was because polyoxoaluminated complex formed in the adjacent aluminosilicate layers was likewise increased many small pores which were related with specific surface area. Furthermore, XRD results were applied to confirm the probability of adjustment taeniolite structure by increasing of teaniolite d_{001} spacing.

The calcination temperatures at 400 and 450°C gave higher specific surface area than uncalcined. This was because the intercalation of polyoxocation of aluminium became aluminium polyoxocation by calcination method in air. The structure was changed to many mesopores as a result of increasing specific surface area. The calcination temperature of 500°C was the lowest specific surface area because the structure of aluminium polyoxocation was adjusted by high temperature. The dehydration of aluminium polyoxocation species was a main cause to explain the decease of specific surface area.

4.5 Determination of aluminium contents

The aluminium content was analyzed by ICP-OES which was technique for confirming the aluminium amount was not various on different catalysts. The aluminium content of clay sample such as montmorillonite, taeniolite, Al-PLB, $InCl_3$/Al-PLB and lanthanide/Al-PLB were shown in Table 4.9.

Table 4.9 The aluminium contents in bentonite samples

Entry	Catalysts	Wt% of Al content[a]	Wt% of Al content in pillaring[a]
1	Na-montmorillonite	19.6	-
2	Al-PLB	24.5	4.9
3	$InCl_3$/ Al-PLB	24.1	4.5
4	$LaCl_3$/ Al-PLB	24.2	4.4
5	$CeCl_3$ / Al-PLB	23.8	4.1
6	$NdCl_3$ / Al-PLB	24.3	4.3
7	$GdCl_3$ / Al-PLB	24.2	4.4

[a] The aluminium content was analyzed by ICP.

In bentonite catalyst, they were revealed nearly amount of aluminium; therefore, different metals impregnated did not influence on the amount of aluminium.

Table 4.10 was compared aluminium contents in difference clay catalyst following by bentonite and taeniolite species.

Table 4.10 The aluminium contents in clays sample

Entry	Catalysts	Wt% of Al content[a]	Wt% of Al content in pillaring[a]
1	Na-montmorillonite	19.6	-
2	Li-TN	0.35	-
3	Al-PLB	24.5	4.90
4	Al-PLT	6.11	5.76

[a] The aluminium content was analyzed by ICP.

The aluminium content in different clays was investigated by ICP-OES as shown in Table 4.10. Teaniolite contained higher amount of aluminium content than bentonite which was related to cation exchange capacity.

Table 4.11 shows the percent weight of aluminium contents in Al-PLT which was observed the difference in calcination temperature.

Table 4.11 The aluminium contents in taeniolite sample

Entry	Catalysts	Wt% of Al content[a]	Wt% of Al content in pillaring
1	Li-TN	0.35	-
2	BAl-PLT	6.73	6.38
Calcination 400˚C			
3	Al-PLT400	6.22	5.87
Calcination 450˚C			
4	Al-PLT450	6.11	5.76
Calcination 500˚C			
5	Al-PLT500	6.11	5.76

[a] The aluminium content was analyzed by ICP.

The results investigated at 400, 450 and 450°C gave similar values around 6 wt%. Comparing these results with those before calcinations, the latter was found to have higher percentage weight than the former. Calcination at 500°C was too high for synthetic taeniolite clay catalyst and temperature at 400°C and 450°C were absolutely suitable for using in phenol alkylation.

4.6 Effect of MCl_3/Al-PLB and MCl_3/Al-PLT on phenol alkylation.

This research concentrates on the development of a new protocol for regioselective phenol alkylation. The reaction conditions were optimized using *p*-cresol as a chemical model. Generally, the alkylation of phenol could be taken place *via* two pathways: *O*- and *C*-alkylations.

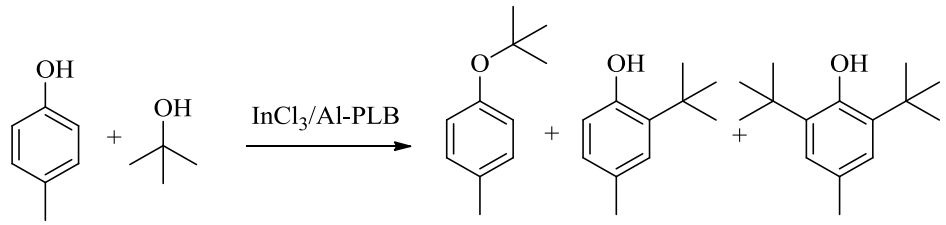

3a **3b** **3c**

p-*tert*-Butoxytoluene (**3a**) was verified as an *O*-alkylated product, while 2-*tert* butyl *p*-cresol and 2,6-di-*tert*-butyl *p*-cresol were *C*-alkylated products. All products could be identified by GC compared with authentic specimen synthesized. The authentic specimen **3a**, **3b** and **3c** were prepared from the reaction of *p*-cresol with *tert*-butanol as described in chapter II. After separation and purification, their identities were confirmed by ^{1}H NMR and GC-MS.

From previous reports [7], the product selectivity was proposed to stem from two main causes: i) reaction conditions including reaction time and temperature and ii) catalyst acidity. Lower acidic site with moderate reaction conditions was reported to influence *O*-alkylation; however, alternation to harder reaction condition with a designed catalyst possessing higher acid strength would turn the reaction into *C*-alkylation as shown in Scheme 4.1.

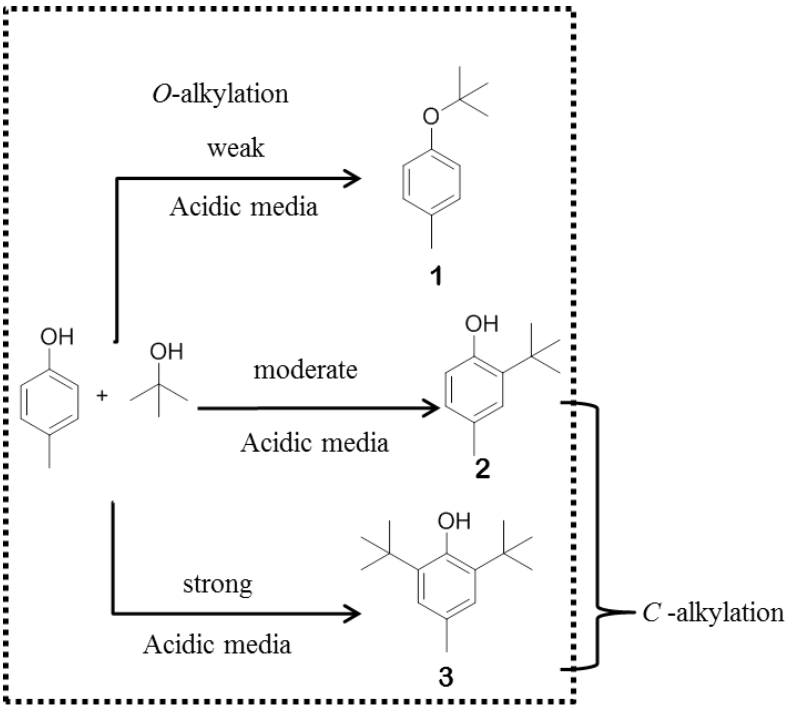

Scheme 4.1 Probability of *p*-cresol alkylation

4.6.1 The effect of Na-montmorillonite, Al-PLB and metal (III) chloride impregnated Al-PLB on *p*-cresol alkylation

Conditions for catalytic activity study were 5% mol catalyst of *p*-cresol at 150°C for 2 h. The results are presented in Table 4.12.

Table 4.12 Effects of Na-montmorillonite, Al-PLB catalysts and metal (III) chloride impregnated Al-PLB on *p*-cresol alkylation

Entry	Catalysts	S_{BET} (m^2/g)	Acidity(mmol/g)		% Recovery	% Yield			MB (%)
			Weak acid site	Strong acid site		3a	3b	3c	
1	None	-	-	-	100.0	-	-	-	100.0
2	Na-Montmorillonite	60.21	0.14	1.12	100.0	-	-	-	100.0
3	Al-PLB	145.70	0.46	1.21	55.8	10.2	34.0	-	100.0
4	$InCl_3$/Al-PLB	121.40	0.34	1.52	-	105.0	-	-	105.0
5	$LaCl_3$/Al-PLB	111.40	0.90	1.58	-	-	36.7	69.2	105.0
6	$CeCl_3$/Al-PLB	127.25	0.77	2.51	-	-	22.7	77.3	100.0
7	$NdCl_3$/Al-PLB	122.40	0.81	2.86	-	-	21.1	80.6	101.7
8	$GdCl_3$/Al-PLB	121.60	0.88	1.25	9.1	-	53.6	37.3	100.0

Reaction condition: *p*-cresol (1 mmol), *tert*-butanol (8 mmol), 5% mol catalyst of *p*-cresol at 150°C for 2 h.

Evidently, different types of clay catalysts including those with different metal (III) chlorides impregnated Al-PLB had a profound effect on the reaction efficiency and product selectivity. This trend was believed to ground from the acidity of catalysts. In entry 1, Na-montmorillonite was found to be inefficient for *p*-cresol alkylation. Bentonite catalysts were then investigated to increase the activity by adding aluminium polyoxocation. Aluminium pillaring agent was associated to layers of Na-montmorillonite, and alternated to aluminium polyoxocation interlayer of montmorillonite by high temperature. Al-PLB revealed higher activity than Na-montmorillonite. Na-montmorillonite was assigned as 2 dimensional layers; whereas, complexing with aluminium polyoxocation between layers turned the structure to be 3 dimensional layer; hence, increasing specific surface area [71]. Furthermore, the selectivity was also controlled by acidity which could be measured by ammonia desorption technique. The Al-PLB had higher acidity as a consequence it was selective to *C*-alkylation, yielding mono-substituted product (**3b**).

According to literatures, the impregnation of $InCl_3$ and lanthanide metals on Al-PLB has not been utilized as catalysts in phenol alkylation. Thus, this research was focused on its catalytic activity *p*-cresol alkylation. Indium (III) chloride and lanthanide (III) chloride were anticipated to possess high acidity according to redox potential previously report. The synthesis of catalysts using $InCl_3$ and lanthanide metal group ($LaCl_3$, $CeCl_3$, $GdCl_3$, $NdCl_3$), respectively, was experimented. Impregnation method was believed to increase catalyst acidity. This research investigated on the effect of metal (III) chloride on the catalyst acidity. The examination of acidity was described by redox potential as shown in Table 4.13. The redox potential was selected to append for classifying metal acidity which were increased following by In, Gd, La, Ce and Nd, respectively. An increasing in redox potential represented a good ability to reduction, thus displaying high acidity.

Table 4.13 Redox potential of metal (III) chloride [72]

	In	La	Ce	Nd	Gd
$Ln^{3+} + e \rightarrow Ln^{2+}$	-4.2	-3.1	-3.2	-2.6	-3.9

Considering all catalysts impregnated on Al-PLB, $InCl_3$/Al-PLB provided quantitative yield of *O*-alkylated product. On the contrary lanthanide metals impregnated Al-PLB revealed high acidity; accordingly yielding *C*-alkylated product. The amount of mono and di-substitued products had directly related to acidity. In view of metal lanthanide variation, neodymium (III) chloride could catalyze the formation of di-substituted product in the highest yield, while cerium (III), lanthanum (III), and gadolinium (III) chloride was decreased.

4.7 Optimum conditions for alkylation of *p*-cresol

Variable parameters including reaction time, reaction temperature and ratio of substrate to alkylating agent were explored for alkylation of *p*-cresol.

4.7.1 Effect of the reaction time on alkylation of *p*-cresol

The effects of reaction time on *p*-cresol alkylation using $InCl_3$/Al-PLB are presented in Table 4.14.

Table 4.14 The effect of reaction time on alkylation of *p*-cresol with *tert*-butanol using $InCl_3$-Al-PLB as catalyst.

Entry	Reaction time (h)	% *p*-Cresol (recovered)	% Yield of 3a	MB (%)
1	0.5	100.0	0.0	100.0
2	1	43.7	56.7	100.4
3	1.5	9.6	89.6	99.2
4	2	0.0	105.0	105.0

Reaction conditions: *p*-cresol (1 mmol), *tert*-butanol (8 mmol), 5% mol catalyst of *p*-cresol at 150°C

Table 4.14 clearly exhibited that the reaction was exclusively produced **3a**. Within 2 h, the quantitative yield of *O*-alkylated product was attained.

4.7.2 Effect of the reaction temperature on *p*-cresol alkylation

Table 4.15 shows the effect of reaction temperature which was another significant parameter to influence the production of alkylated product.

Table 4.15 The effect of reaction temperature on *p*-cresol alkylation with *tert*-butanol using $InCl_3$/Al-PLB as catalyst.

Entry	Reaction temperature (°C)	% *p*-Cresol (recovered)	% Yield of 3a	MB (%)
1	RT (30)	100.0	0.0	100.0
2	70	41.2	58.8	100.0
3	100	20.5	78.6	99.1
4	150	0.0	105.0	105.0
5	180	0.0	99.8	99.8

Reaction conditions: *p*-cresol (1 mmol), *tert*-butanol (8 mmol), 5% mol catalyst of *p*-cresol for 2 h.

The reaction temperature is a crucial parameter that needed to be evaluated. Using reaction temperatures at 150 and 180°C the quantitative yield of **3a** was obtained. The reaction produced exclusively *O*-alkylated product (entries 4-5). However, for further study, the reaction temperature at 150°C was selected.

4.7.3 Effect of mole ratio of substrate on alkylation of *p*-cresol

Table 4.16 shows the effect of mole ratio of *p*-cresol to *tert*-butanol on the production of alkylated product.

Table 4.16 The effect of mole ratio of substrate on *p*-cresol alkylation using $InCl_3$/Al-PLB as catalyst

Entry	Mole ratio *p*-cresol : *tert*-butanol	% *p*-Cresol (recovered)	% Yield of 3a	MB (%)
1	1:8	0.0	105.0	105.0
2	1:10	41.2	58.8	100.0
3	1:30	20.5	78.6	99.1

Reaction conditions: *p*-cresol (1 mmol), *tert*-butanol (8 mmol), 5% mol catalyst of *p*-cresol for 2 h.

From Table 4.15, the mole ratio of *p*-cresol to *tert*-butanol as 1: 8 provided the highest yield of the target product.

Henceforth, the optimized conditions for *p*-cresol alkylation can be summarized as: *p*-cresol 1 mmol, *tert*-butanol 8 mmol and $InCl_3$/Al-PLB 5% mol at 150°C for 2 h. Under the optimized condition, *O*-alkylated product was selectively produced *O*-alkylated product from the reaction of *p*-cresol with *tert*-butanol was 1-*tert*-butoxy-4-methylbenzene (**3a**). ^{1}H NMR spectrum revealed a noticeable singlet peak of *tert*-butyl alkylated on *p*-cresol at δ 1.32 ppm, doublet of doublet at δ 7.05 and 6.88 of the proton on *p*-cresol and at δ 2.31 for three methyl protons.

4.8 Variation of alkylating agent on *p*-cresol alkylation

The effects of alkylating agents on *p*-cresol alkylation are exhibited in Table 4.17. In order to prove which pathway the reaction undergoes, various alkylating agents were investigated. The alkylating agents tested were *n*-butanol, *iso*-propanol, *tert*-butanol, methyl-*tert*-butyl ether (MTBE), allyl alcohol, and 2-methyl-3-buten-2-ol.

4.8.1 Variation of alkylating agents

Various alkylating agents were selected to perform alkylation of *p*-cresol catalyzed by $InCl_3$/Al-PLB under optimized conditions. The variation of alkylating agents was carried out and the results are presented in Table 4.17.

Table 4.17 Variation of alkylating agent on *p*-cresol alkylation using $InCl_3$/Al-PLB as catalyst

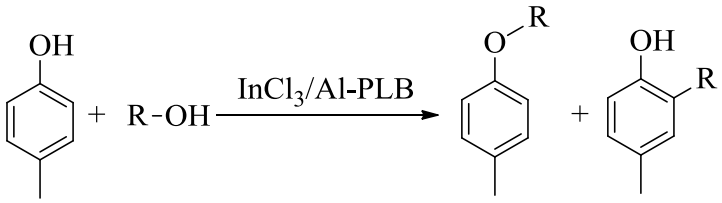

a **b**

(1) R = $-CH_2(CH_2)_2(CH_3)$

(2) R = $-CH(CH_3)_2$

(3) R = $-C(CH_3)_3$

(4) R = $-CH_2CH=CH_2$

(5) R = $-C(CH_3)_2CH=CH_2$

Entry	Alkylating agent	% *p*-Cresol (recovered)	% Yield	MB (%)
1	*n*-Butanol	42.3	**1a** (47.8)	90.1
2	*iso*-Propanol	21.8	**2a** (79.1)	100.9
3	*tert*-Butanol	0.0	**3a** (105.0)	105.0
4	MTBE	0.0	(100.0) **3a**	100.0
5	Allyl alcohol	52.3	**4a** (20.0)[a], **4b** (27.0)[a]	99.3
6	2-Methyl-3-buten-2-ol	-	**5a** (11.1)[a], **5b** (23.2)[a]	-

Reaction condition: *p*-cresol (1 mmol), alkylating agent (8 mmol), 5% mol catalyst of *p*-cresol at 150°C for 2 h.

[a] Isolated yield

Alkylating agents such as *tert*-butanol and MTBE would form tertiary carbocation intermediate. The highest stability of tertiary carbocation derived from *tert*-butanol and MTBE involved in this electrophilic aromatic substitution. Quantitative yield of *O*-alkylated products (entries 3-4) were achieved. With *iso*-propanol, the target molecules were attained in moderate yield, (entry 1). In the case of allylic reagent, higher yield of target products were obtained more than aliphatic species. Allyl alcohol was typically primary carbocation, while tertiary carbocation was observed by 2-methyl-3-buten-2-ol. 2-Methyl-3-buten-2-ol provided higher yield than allyl alcohol because of carbocation effect. For allylic alkylating agent, the alkylation was to accomplish only *O*-alkylated product. Since optimized conditions were conducted at high temperature resulting in occurring side reaction, Claisen rearrangement producing *ortho*-substituted alkylated product, *C*-alkylation.

The proposed mechanism of *p*-cresol alkylation with *tert*-butanol using $InCl_3$/Al-PLB as catalyst can be portrayed as shown in Scheme 4.2.

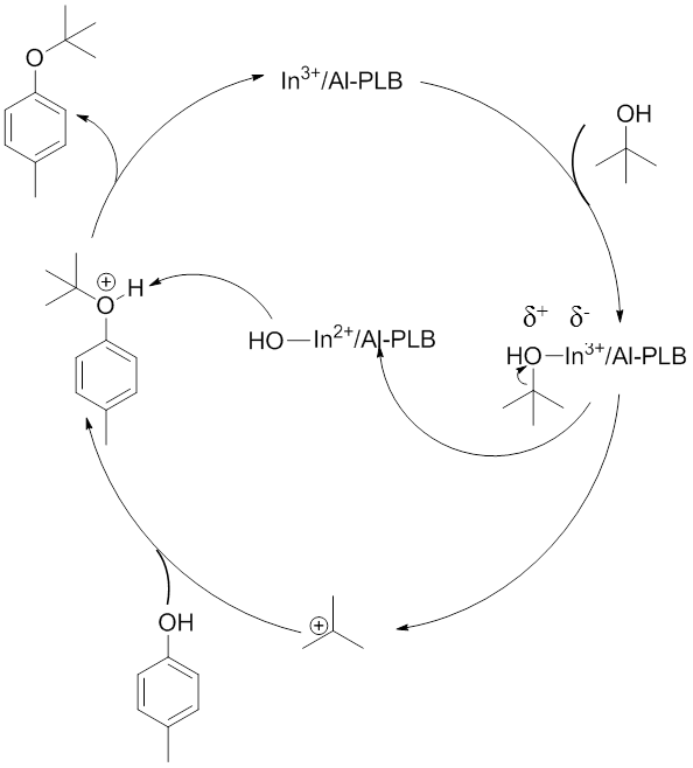

Scheme 4.2 Proposed mechanism of *p*-cresol alkylation with *tert*-butanol using $InCl_3$/Al-PLB as catalyst.

From Table 4.17, various alkylating agents could be employed to synthesize *O*-alkylated product in high yields. To compare this protocol with other previous reported methods, this present method provided exclusively *O*-alkylated product in excellent yield whereas most previous reports addressed the manipulation of alkylated product with nonspecific manner [73]. Additionally, this optimized conditions required shorter reaction time to complete the reactions comparing with many procedures [74-76].

4.8.2 The exploration of the scope of alkylation $InCl_3$/Al-PLB

4.8.2.1 Alkylation of *p*-cresol with *n*-butanol

Based on the results in Table 4.18, the lower amount of the desired product was mainly stemmed from a less stable intermediate, primary carbocation. Attempts to lift up the yield by altering reaction temperature and time were conducted and the results are presented in Table 4.18.

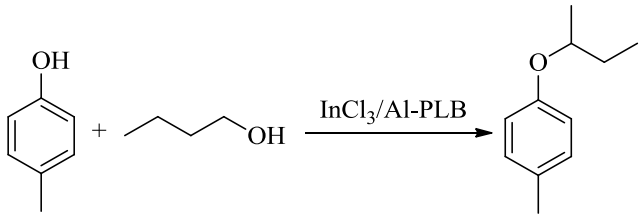

1a

Table 4.18 Alkylation of *p*-cresol with *n*-butanol using $InCl_3$/Al-PLB as catalyst

Entry	Reaction time (h)	Reaction Temperature (°C)	% *p*-Cresol (recovered)	% Yield of 1a	MB (%)
1	2	150	42.3	47.8	90.1
2	2	180	36.1	59.1	95.2
3	3	150	12.6	85.5	98.1
4	3	180	12.1	88.3	91.6

Reaction conditions: *p*-cresol (1 mmol), *n*-butanol (8 mmol), 5% mol catalyst of *p*-cresol.

To explore the effect of reaction temperature (entries 1 *vs* 2 and entries 3 *vs* 4), only slightly increased yield of **1a** was observed when reaction temperature was altered from 150 to 180°C. The reaction time of 3 h (entries 3-4) provided the highest yield. The optimized conditions of *p*-cresol alkylation with *n*-butanol were therefore at 180°C for 3 h. The product derived from alkylation of *p*-cresol with *n*-butanol was characterized as 1-(*sec*-butoxy)-4-methylbenzene **(1a).** This could be explained from the fact that the primary carbocation intermediate first generated was rearranged to form more stable secondary carbocation which then reacted with *p*-cresol to yield the product. The proposed mechanism was depicted in Scheme 4.3.

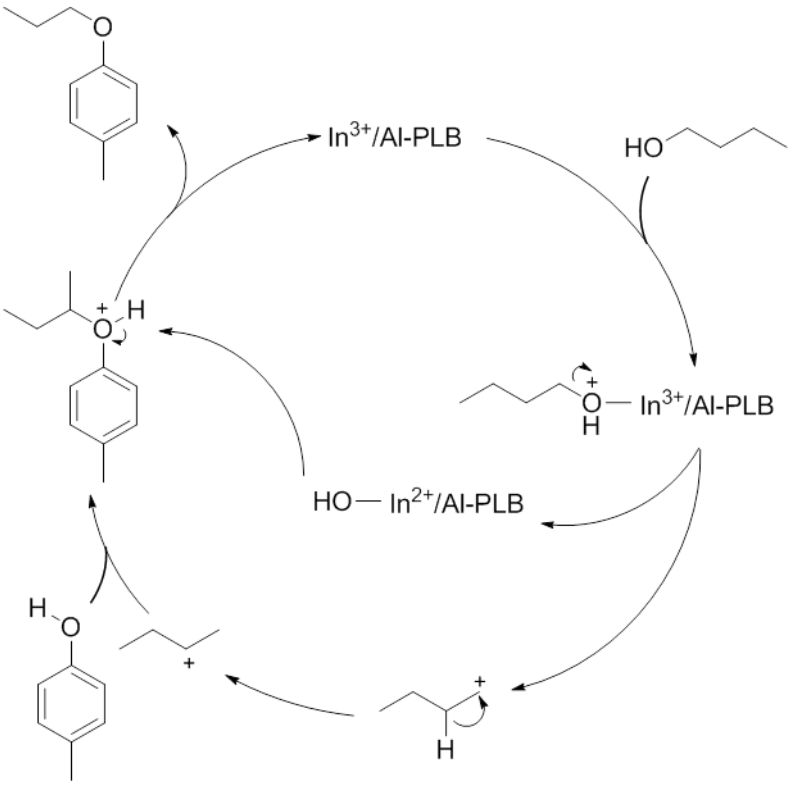

Scheme 4.3 Proposed catalytic mechanism of *p*-cresol alkylation with *n*-butanol using $InCl_3$/Al-PLB as catalyst.

The sole product as 1-(*sec*-butoxy)-4-methylbenzene **(1a)** was separated by silica gel column chromatography using hexane/EtOAc (9:1) as an eluent and was characterized its identity by ^{1}H NMR. This product was proved to be 1-(*sec*-butoxy)-4-methylbenzene **(1a)**. [77] The aromatic protons revealed as doublet at δ 7.11 (2H, *J* = 6.0 Hz) and δ 6.83 (2H, *J* = 6.0 Hz). The proton signal of -OC**H**$(CH_3)CH_2CH_3$ as

multiplet was detected at δ 4.20 (2H, J = 6.0 Hz). A singlet signal of Ar(C**H**$_3$)$_3$ at δ 2.32 (3H), a multiplet signal of -OCH(CH$_3$)C**H**$_2$CH$_3$ at δ 1.73(2H), a triplet signal of -O(CH$_2$)$_2$C**H**$_2$CH$_3$ at δ 1.41 (2H, J = 6.2 Hz), a doublet signal of -OCH(C**H**$_3$)CH$_2$CH$_3$ at δ 1.32 (2H, J = 6.0 Hz) and a triplet signal of -OCH(CH$_3$)CH$_2$C**H**$_3$ at δ 0.99 (3H, J = 6.2 Hz) were also visualized.

4.8.2.2 Alkylation of *p*-cresol with *iso*-propanol

The effects of reaction temperature and time on alkylation of *p*-cresol with *iso*-propanol are presented in Table 4.19.

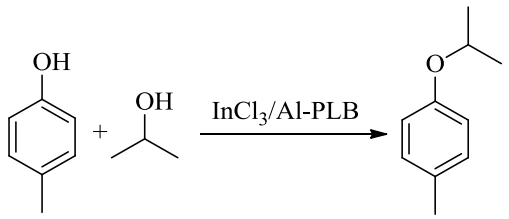

2a

Table 4.19 Alkylation of *p*-cresol with *iso*-propanol using InCl$_3$/Al-PLB as catalyst

Entry	Reaction time (h)	% *p*-Cresol (recovered)	% Yield of 2a	MB
1	2	21.8	79.1	100.9
2	2.5	4.2	93.3	97.5
3	3	4.1	94.5	98.6

Reaction condition: *p*-cresol (1 mmol), *iso*-propanol (8 mmol), 5% mol catalyst of *p*-cresol at 150°C.

Entries 2-3 revealed significantly increasing yield when the reaction time was increased. Thus, the reaction time of 2.5 h at 150°C was perfectly used for further examination.

The product as 1-*iso*-propoxy-4-methylbenzene (**2a**) was separated by silica gel column chromatography using hexane/EtOAc (9:1) as an eluent and was characterized by ^{1}H NMR. This product was identified as 1-*iso*-propoxy-4-

methylbenzene (**2a**). [78] The signals belonging to Ar**H** as doublet at δ 7.11 (2H, *J* = 6.2 Hz) and at δ 6.83 (2H, *J* = 6.2 Hz), -OC**H**$(CH_3)_2$ as multiplet at δ 3.97 (1H), Ar(C**H**$_3)_3$ as singlet at δ 2.32 (3H) and –OCH(C**H**$_3)_2$ as doublet at δ 1.42 (6H, *J* = 6.2 Hz) were observed.

4.8.2.3 Alkylation of *p*-cresol with allyl alcohol

The effect of reaction time on alkylation of *p*-cresol with allyl alcohol is presented in Table 4.20.

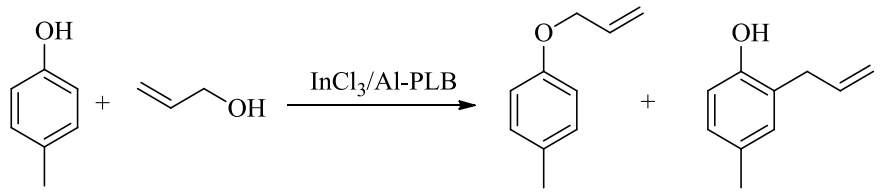

4a **4b**

Table 4.20 Alkylation of *p*-cresol with allyl alcohol using $InCl_3$/Al-PLB as catalyst

Entry	Reaction time (h)	% *p*-Cresol (recovered)	% Yield		MB (%)
			4a	4b	
1	2	52.7	20.0	27.0	99.7
2	3	4.5	21.2	70.1	98.3

Reaction condition: *p*-cresol (1 mmol), allyl alcohol (8 mmol), 5% mol catalyst of *p*-cresol.

Two products were visualized on TLC with the Rf values of 0.32 and 0.64 (hexane/EtOAc; 19 :1). The reaction mixture was then separated by silica gel column chromatrography employing hexane/EtOAc (9:1) as an eluent and characterized by ^{1}H NMR. The first product isolated was proved as 1-(allyloxy)-4-methylbenzene (**4a**). [79] To illustrate this, the signals belonging to Ar**H** as doublet at δ 7.01 (2H, *J* = 6.5 Hz) and at δ 6.78 (2H, *J* = 6.5 Hz), -OCH(C**H**$_2$CH$_2$) as multiplet at δ 5.85 (1H) and -OCH(CH$_2$C**H**$_2$) as doublet at δ 5.18 (2H, *J* = 6.0 Hz) and -OC**H**(CH$_2$CH$_2$) as doublet at δ 4.62 (1H, *J* = 6.0 Hz) were detected. In addition, the singlet signal of Ar(C**H**$_3)_3$ at δ 2.32 (3H) was visualized. 2-Allyl-4-methylphenol **(4b)** [80], the other isolated

product displayed the signal belonging to Ar**H** as doublet at δ 7.18 (1H, *J* = 6.6 Hz) and Ar**H** as double of doublet at δ 6.98 (2H, *J* = 6.6, 1.2 Hz), Ar**H** as doublet at δ 6.69 (1H, *J* = 6.6 Hz), -OC**H**$(CH_2)_2$ as multiplet at δ 6.18 (1H), -OCH(CHC**H**$_2$) as doublet at δ 5.05 (2H, *J* = 6.6 Hz), -OC**H**(CH_2CH_2) as doublet at δ 3.36 (2H, *J* = 6.3 Hz), ArC(C**H**$_3)_2$ as singlet at δ 2.31 (s, 3H).

The selectivity of *O*-alkylated production is the aim for this reaction. However, when the reaction was carried out at higher temperature, a rearranged product (**4a**) was taken place to form **4b**. The rearrangement is well known as Claisen rearrangement. The proposed mechanism was depicted in Scheme 4.4.

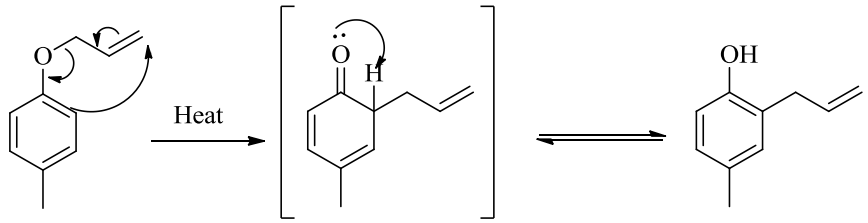

4a **4b**

Scheme 4.4 Claisen rearrangement of 1-(allyloxy)-4-methylbenzene (**4a**)

4.8.2.4 Alkylation of *p*-cresol with 2-methyl-3-buten-2-ol

The effect of reaction temperature and time on alkylation of *p*-cresol with 2-methyl-3-buten-2-ol are presented in Table 4.21.

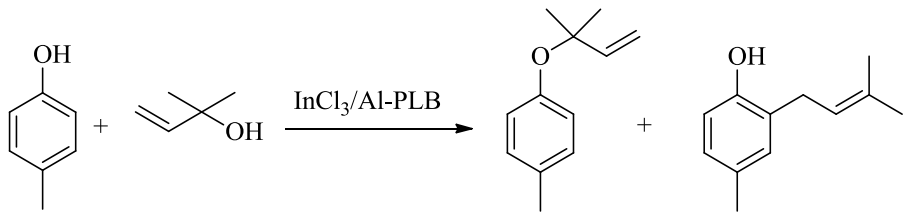

5a **5b**

Table 4.21 Alkylation of *p*-cresol with 2-methyl-3-buten-2-ol using $InCl_3$/Al-PLB as catalyst

Entry	Reaction time (h)	Temperature (°C)	% *p*-Cresol (recovered)	% Yield		MB (%)
				5a	5b	
1	1	150	6.2	-	90.4	96.6
2	2	150	-	11.1	23.2	-

Reaction condition: *p*-cresol (1 mmol), 2-methyl-3-buten-2-ol (8 mmol), 5% mol catalyst of *p*-cresol.

Table 4.21 discloses that the alkylation of *p*-cresol with 2-methyl-3-buten-2-ol could be carried out at 150°C using $InCl_3$/Al-PLB furnishing the target product 90.4% within 1 h (entry 1). This reaction was selective for the production of C-alkylation product **5b**. The formation of 5bwas believed to occur via Claisen rearrangement of 5a**.** In entry 2, the condition was too severe, thus many products were produced which could not identify.

The allyl group of **5a** could be rearranged to *ortho*-position of *p*-cresol by heating to reaction. The mechanism of this reaction was passed claisen rearrangement; therefor, entry **1** which using $InCl_3$/PLB (selected with *O*-alkylated product) was not occurred **5a**. The mechanism is shown in Scheme 4.5.

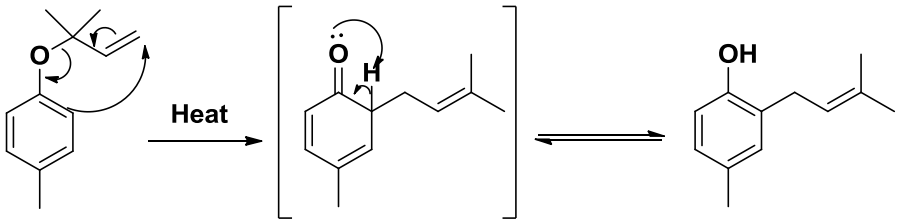

5a **5b**

Scheme 4.5 Claisen rearrangement mechanism of 1-methyl-4-(2-methylbut-3-en-2-yloxy) benzene

Two products could be separated by silica gel column chromatography employing hexane/EtOAc (9:1) as an eluent and characterized by ^1H NMR. The structure of the first product was elucidated as 1-(allyloxy)-4-methylbenzene (**5a**).

[80] The ^{1}H NMR spectrum revealed the signals belonging to Ar**H** as doublet at δ 7.01 (2H, *J* = 6.5 Hz) and Ar**H** as doublet at δ 6.78 (2H, *J* = 6.5 Hz), -OCH(C**H**$_2$CH$_2$) as multiplet at δ 5.85 (1H) and -OCH(CH$_2$C**H**$_2$) as doublet at δ 5.18 (2H, *J* = 6.0 Hz) and -OC**H**(CH$_2$CH$_2$) as doublet at δ 4.62 (1H, *J* = 6.0 Hz). In addition, the signal of Ar(C**H**$_3$)$_3$ as singlet at δ 2.32 (3H) was observed. The structure of 2-allyl-4-methylphenol **(5b)** [81] was characterized based on the observed signals belonging to Ar**H** as doublet at δ 7.15 (2H, *J* = 0.8 Hz), Ar**H** as double of doublet at δ 6.98 (1H, *J* = 6.2, 0.8 Hz), and Ar**H** as doublet at δ 6.71 (1H, *J* = 6.2 Hz), ArC(CH$_2$)C**H**=C(CH$_3$)$_2$) as triplet at δ 5.50 (1H, *J* = 6.0 Hz), ArC(C**H**$_2$)CH=C(CH$_3$)$_2$) as doublet at δ 3.41 (2H, *J* = 1.2 Hz), and Ar(C**H**$_3$)$_3$ as singlet at δ 2.32 (3H) and ArC(CH$_2$)CH=C(C**H**$_3$)$_2$ as singlet at δ 1.57 (s, 6H).

4.9 Alkylation of selected phenols using InCl$_3$/Al-PLB as catalyst

Selected phenols including thymol, 3-methoxyphenol, *p*-cumylphenol, 4-hydroxybiphenyl and 2-naphthol were employed in alkylation to observe the scope of this developed system. The results are collected as shown in Table 4.22.

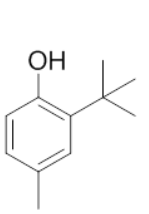

3a

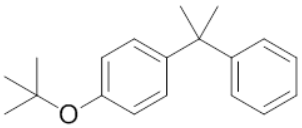

7a

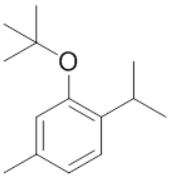

8a

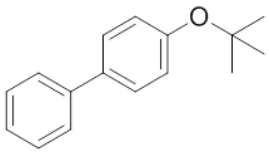

9a

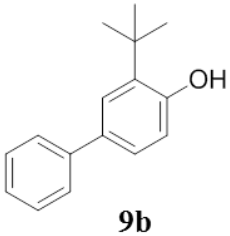

9b

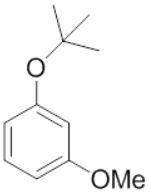

11a

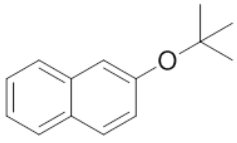

10a

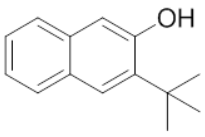

10b

Table 4.22 Alkyltion of selected phenols with *tert*-butanol using $InCl_3$/Al-PLB as catalyst

Entry	Phenols	% Phenols (recovered)	% Isolated yield (Base on substrate)	MB (%)
1	*p*-cresol	0.0	**3a** (105.0)[a]	105.0
2	Thymol	21.2	**8a** (75.8)	97.0
3	3-methoxyphenol	-	**11a** (45.3)	-
4	*p*-cumylphenol	74.3	**7a (**24.8)	100.9
5	4-hydroxybiphenyl	60.0	**9a** (31.1), **9b** (9.6)	101.0
6	2-naphthol	20.4	**10a** (45.3), **10b** (30.9**)**	96.6

Reaction condition: phenols (1 mmol), alkylating agent (8 mmol), 5% mol catalyst of phenols at 150°C for 2 h.

The substituents on phenol directly had a profound effect on acidity of the molecule. *p*-Cresol and thymol (entries 1-2) which are phenols bearing electron donating group selectively yielded *O*-alkylated product with good yield. The compound containing an electron withdrawing group (entry 3) provided less yield of target molecule; however, an excellent selectivity was still preserved. *p*-Cumylphenol was chosen to explore the effect of steric substituent on phenol structure. Under these particular conditions, *O*-alkylation was observed, nonetheless with poor yield. p*K*a values of selected phenols are collected in Table 4.23.

Table 4.23 p*K*a value of selected phenols

Entry	Substance	p*K*a
1	*p*-cresol	10.21
2	thymol	10.59
3	3-methoxyphenol	9.58
4	4-hydroxybiphenyl	9.82
5	*p*-cumylphenol	10.62
6	2-naphthol	9.57

Calculated using Advanced Chemistry Development (ACD/Labs) Software V11.02 (© 1994-2011 ACD/Labs)

The p*K*a values of substrate perhaps can be used to ascribe for the selectivity of phenol alkylation. *O*- and *C*-alkylations were induced by weak and strong acids, respectively.

4.9.1 Alkylation of thymol

The alkylation of thymol could be carried out at 150°C for 2 h to furnish 1-*tert*-butoxythymol (**8a**) 75.8% with excellent regioselectivity. An attempt to lift up the yield of target product was carried out such as in creasing temperature, the yield of the target product was not increased significantly.

The products were separated by silica gel column chromatrography using hexane/EtOAc (9:1) as an eluent and was characterized as 1-*tert*-butoxythymol (**8a**). ^{1}H NMR spectrum displayed the signal belonging to –C**H**Ar as double of doublet at δ 7.12 (1H, *J* = 6.4, 1.2 Hz). –C**H**Ar as doublet at δ 6.78 (1H, *J* = 6.4) and singlet at δ 6.64 (1H) and –O(C**H**$_3$)$_3$ as a singlet at δ 1.41 (9H).

4.9.2 Alkylation of 3-methoxyphenol

3-Methoxyphenol contained an electron withdrawing group at *meta* position. The alkylation of 3-methoxyphenol could be carried out at 100°C for 5 h to furnish 1-*tert*-butoxy-3-methoxybenzene (**11a**) with high yield and excellent regioselectivity. The variation of reaction condition was examined as presented in Table 4.24.

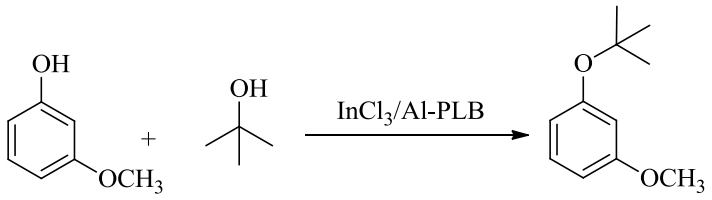

11a

Table 4.24 Alkylation of 3-methoxyphenol using $InCl_3$/Al-PLB as catalyst

Entry	Reaction temperature (°C)	Reaction time (h)	% 3-Methoxyphenol (recovered)	% Isolated yield		MB (%)
				11a	11b	
1	100	5	18.6	74.2	-	92.8
2	150	2	-	45.3	-	-

Reaction condition: 3-methoxyphenol (1 mmol), *tert*-butanol (8 mmol), 5% mol catalyst of 3-methoxyphenol.

The alkylation of 3-methoxyphenol under optimized condition was examined; nevertheless, low selectivity was observed because many products were detected Adjustment of condition by increasing reaction time to 5 h and decreasing temperature to 100˚C was elected. The activity was significantly increased; the yield of **11a**, 74.2% could be attained.

Two products were separated by silica gel column chromatography using hexane/EtOAc (4:1) as an eluent and characterized by ^{1}H NMR. The first product was 1-*tert*-butoxy-3-methoxybenzene (**11a**) [82] displaying the signal belonging to Ar**H** as triplet at δ 7.21 (5H, *J* = 6.4 Hz), Ar**H** as multiplet at δ 6.54 (3H), -OC**H**$_3$ as singlet at δ 3.81 (3H) and that of –O(C**H**$_3$)$_3$ as singlet at δ 1.41 (9H).

4.9.3 Alkylation of *p*-cumylphenol

Alkylation of *p*-cumylphenol was successfully performed using $InCl_3$/Al-PLB yielding two products. By the aids of ^{1}H NMR, 1-*tert*-butoxy-*p*-cumylphenol **(7a)** and 2-*tert*-butyl-4-cumylphenol (**7b**) were identified. The results are shown in Table 4.25.

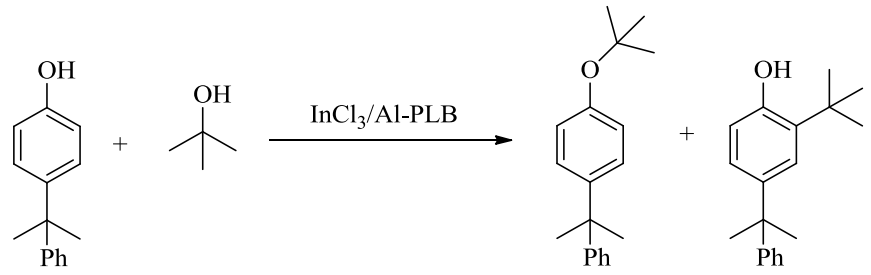

7a **7b**

Table 4.25 Alkylation of *p*-cumylphenol with *tert*-butanol using $InCl_3$/Al-PLB as catalyst

Entry	Reaction temperature (°C)	Reaction time (h)	% *p*-Cumylphenol (recovered)	% Isolated yield		MB (%)
				7a	7b	
1	80	10	100.0	-	-	100.0
2	120	4	66.7	31.6	-	98.3
3[a]	120	8	2.3	92.2	-	94.5
4	120	8	1.2	-	11.4	-
5	150	2	74.3	24.8	-	99.1
6	150	4	-	-	15.4	-

Reaction condition: *p*-cumylphenol (1 mmol), *tert*-butanol (8 mmol), 5% mol catalyst of *p*-cresol

[a] 2.5% mol catalyst of *p*-cumylphenol

None of product could be detected when the reaction was carried out at 80°C. Even using long time for 10 h (entry 1). Under optimized conditions, the reaction was conducted at 150°C for 2 h resulting less yield of product (entry 5). The reaction conditions were altered by using longer time for 4 h (entry 6) which gave up to yield of *C*-alkylated product (**7b**) at 15.4% and some products were not identified. Too many products observed as in entry 6 were brought to an adaptation of reaction conditions. Firstly, by decreasing reaction temperature to 120°C (entry 2), slightly increasing of percentage yield of **7a**. Increasing time to 8 h at 120°C gave many products which could not be identified. The results obtained from time adjustment gave higher yield of product; however, the reaction was still not selective. The

amount of catalyst was one of alternative factors for selectivity improvement. The result as presented in entry 3 at 120°C for 8 h using less amount of catalyst as 2.5% mole catalyst contributed to the highest yield and the best selectivity observed for *O*-alkylated product (**7a**). Consequently, the optimized conditions for alkylation of *p*-cumylphenol were at 120°C for 8 h using 2.5% mole catalyst.

Two products could be detected from the reaction mixture which was separated by silica gel column chromatography using hexane/EtOAc (4:1) and were characterized by ^{1}H NMR. The first product: 1-*tert*-butoxy-*4*-cumylphenol (**7a**) displayed the signals belonging to –C**H**Ar as multiplet at δ 7.18-7.35 (5H) and –C**H**Ar as doublet at δ 6.93 (2H, *J* = 6.4 Hz), doublet at δ 6.55 (2H, *J* = 6.4 Hz), the signal of Ar(C**H**$_3$)$_2$C as singlet at δ 1.71 (6H) and –O(C**H**$_3$)$_3$ as singlet at δ 1.41 (9H). The ^{1}H NMR spectrum of 2-*tert*-butyl-4-cumylphenol (**7b**) [83] showed the signal of –C**H**Ar as multiplet at δ 7.18-7.35 (5H), –C**H**Ar as double of doublet at δ 6.74 (1H, *J* = 6.4, 1.7 Hz), doublet at 7.09 (1H, *J* = 1.2 Hz) and doublet at 6.71 (1H, *J* = 6.0 Hz), the signal of Ar(CH_3)$_2$C as singlet at δ 1.71 (6H) and –O(CH_3)$_3$ as singlet at δ 1.41 (9H).

4.9.4 Alkylation of 4-hydroxybiphenyl

The alkylation of 4-hydroxybiphenyl could be carried out at 120°C for 3 h to furnish 4-*tert*-buthoxybiphenyl (**9a**) and 2-*tert*-buthyl-4-phenylphenol **(9b)** with excellent yield.

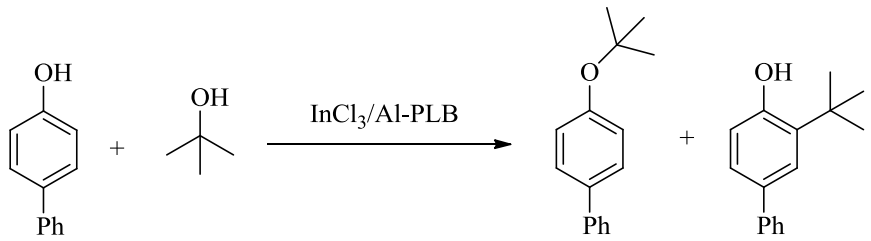

9a **9b**

Table 4.26 Alkylation of 4-hydroxybiphenyl using $InCl_3$/Al-PLB as catalyst

Entry	Reaction temperature (°C)	Reaction time (h)	% 4-Hydroxy biphenyl (recovered)	% Isolated yield		MB (%)
				9a	9b	
1	100	4	67.3	31.2	-	98.5
2	120	4	40.4	53.4	-	93.8
3	120	6	8.6	88.9	-	97.5
4	150	2	55.0	31.1	9.6	95.7
5	150	3	33.1	11.2	9.5	53.8

Reaction condition: 4-hydroxy biphenyl (1 mmol), *tert*-butanol (8 mmol), 5% mol catalyst of 4-hydroxy biphenyl.

Various conditions of 4-hydroxybiphenyl are presented in Table 4.21. Under the conditions for *p*-cresol model, there was no product observed from 4-hydroxy biphenyl. The next experiment was increasing reaction time to 3 h; the product was not obtained in high yield. In entry 1, the reaction temperature was at 100˚C for 4 hours was investigated. Even if, lower activity was observed, it still exhibited high selectivity. Nonetheless, when the reaction conditions were altered (entries 2-3), the highest yield of the target molecule could be attained at 120˚C for 6 hours.

Two products were separated by silica gel column chromatography using hexane/EtOAc 4: 1 and characterized by ^{1}H NMR spectroscopy. The products were characterized as 4-*tert*-butoxybiphenyl (**9a**) [84] displayed the signal belonging to –C**H**Ar as multiplet at δ 7.04-6.89 (5H) and –C**H**Ar as double of doublet at δ 6.74 (2H, *J* = 6.4, 1.21 Hz), –C**H**Ar as double of doublet at δ 6.12 (2H, *J* = 6.4, 1.21 Hz), the signal of –O(C**H**$_3$)$_3$ as singlet at δ 1.41 (9H). The ^{1}H NMR spectrum of 2-*tert*-buthyl-4-phenylphenol [85] (**9b**) showed the signal of proton aromatic belonging to –C**H**Ar as multiplet at δ 7.04-6.89 (5H), –C**H**Ar as double of doublet at δ 6.71 (1H, *J* = 6.4, 1.21 Hz) double at δ 6.42 (1H, *J* = 6.4 Hz), singlet at 6.06 (1H) and the signal of –O(C**H**$_3$)$_3$ as singlet at δ 1.41 (9H).

4.9.5 Alkylation of 2-naphthol

The alkylation of 2-naphthol could be performed by using $InCl_3$/Al-PLB. Two major products were obtained, and characterized as 2-*tert*-butoxynaphthalene **(10a)** and 3-*tert*-butyl-2-naphthol (**10b**). The reaction achieved the desired products in moderate yield. Various conditions of 2-naphthol are presented in Table 4.27.

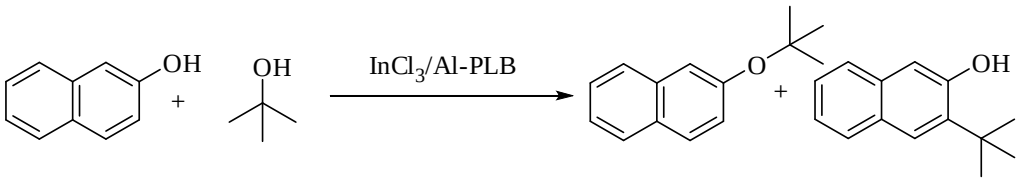

10a **10b**

Table 4.27 Alkylation of 2-naphthol using $InCl_3$/Al-PLB as catalyst

Entry	Reaction temperature (°C)	Reaction time (h)	% 2-Naphthol (recovered)	% Isolated yield		MB (%)
				10a	10b	
1	120	4	1.6	94.2	-	95.8
2	150	2	20.4	45.3	30.9	96.6

Reaction condition: 2-naphthol (1 mmol), *tert*-butanol (8 mmol), 5% mol catalyst of 2-naphthol.

Under optimized conditions, two products: both *C*- and *O*- alkylated products were observed. This implied that the conditions applied may be too harsh for this substrate. An attempt to increase the yield and selectivity of the reaction was conducted by increasing reaction time to 4 h and decreasing temperature to 120˚C. 94.2% of **10a** could be achieved

Two products were separated by silica gel column chromatography using hexane/EtOAc (4:1) and characterized by ^{1}H NMR spectroscopy. The first product was characterized as 2-*tert*-butoxynaphthalene **(10a)** [86] displaying the signal belonging to Ar**H** as multiplet at δ 7.72 (1H), Ar**H** as multiplet at δ 7.69 (1H) and Ar**H** as double of doublet at δ 7.56 (1H, J = 6.4, 1.2 Hz), Ar**H** as double of doublet at

δ 7.38 (1H, *J* = 6.4, 1.2 Hz), Ar**H** as multiplet at δ 7.34 (2H), Ar**H** as multiplet at δ 7.05 (1H), and –O(C**H**$_3$)$_3$ as singlet at δ 1.49 (9H). The ^{1}H NMR of 3-*tert*-butyl-2-naphthol (**10b**) [87] showed the signal of Ar**H** as multiplet at δ 7.64 (2H), Ar**H** as doublet at δ 7.32 (1H, *J* = 6.4 Hz), Ar**H** as multiplet at δ 7.25 (2H), Ar**H** as doublet at δ 6.95 (1H, *J* = 6.4 Hz) and ArC(C**H**$_3$)$_3$ as singlet at δ 1.45 (9H).

4.10 Comparative study on the efficiency of raw clays for *p*-cresol alkylation

This research focused on the utilization of two raw clays: bentonite and taeniolite. They were obtained from different sources. Bentonite was found as major clay in Thailand, whereas taeniolite was discovered in Japan. Both raw clays were smectite type which had T:O:T structure; nevertheless, they were different in metal basic structure and cation exchange capacity (CEC).

Henceforth, the different metal basic structures of bentonite as ($(Na,Ca)_{0.33}(Al,Mg)_2(Si_4O_{10})(OH)_2 \cdot nH_2O$) and taeniolite as ($Li[Mg_2Li)(Si_4O_{10})F_2]$) were impinged complication on aluminium polyoxocation structure which revealed different complex structure and oxidation number.

4.10.1 Effect of bentonite and taeniolite on alkylation of *p*-cresol

Table 4.28 exhibits the comparison of using different clays on *p*-cresol alkylation. The reaction was conducted under optimized conditions.

Table 4.28 Comparison of type of clays for the efficiency of *p*-cresol alkylation

Entry	Catalysts	S_{BET} (m^2/g)	Acidity (mmol/g)		% Recovery	% Yield			MB (%)
			Weak acidity sites	Strong acidity sites		3a	3b	3c	
1	Na-Montmorillonite	-	0.71	0.32	100.0	-	-	-	100.0
2	Li-TN	1.4	0.34	0.56	67.8	32.0	-	-	99.8
3	Al-PLB	145.7	0.46	1.21	55.8	10.2	34.0	-	100.0
4	Al-PLT500	17.7	0.46	0.53	46.2	53.7	-	-	99.9
5	$InCl_3$/Al-PLB	121.4	0.34	1.52	-	105.0	-	-	105.0
6	$InCl_3$/Al-PLT500	21.4	0.33	0.99	52.1	48.0	-	-	100.1

Reaction condition: *p*-cresol (1 mmol), *tert*-butanol (8 mmol), 5% mol catalyst of *p*-cresol at 150°C for 2 h.

Table 4.28, dissimilarity of bentonite and taeniolite was investigated. Na-montmorillonite exhibited higher activity than Li-TN. For Al-PLT, similar synthetic protocol with bentonite was performed. The collation of bentonite and taeniolite case was not in line with theoretically due to the fact that acidity was not the same trend with assumption that taeniolite increased acidity by escalating of capacity exchange cations (CEC). This comparison of different clay catalyst determinant was explained by calcination preparing of catalyst which influenced with complexity process on aluminium pillaring species as shown by XRD pattern in Figure 4.13.

4.11 Characterization and activity study of taeniolite

4.11.1Characterization

4.11.1.1 X-ray diffraction (XRD)

The effect of calcination temperature on synthesis Al-PLT

Al-PLT was synthesized by intercalation of Al-precursors between clay layers. Al-precursors were produced by high calcination temperature. Al-PLT contained high active site to catalyze organic reactions. In the aim of this case, Al-PLT and $InCl_3$/Al-PLT were examined the calcination temperature effective for taeniolite.

Figure 4.12 was compared d_{001} basal spacing on the XRD pattern of difference calcination temperature for synthesis Al-PLT and $InCl_3$/Al-PLT.

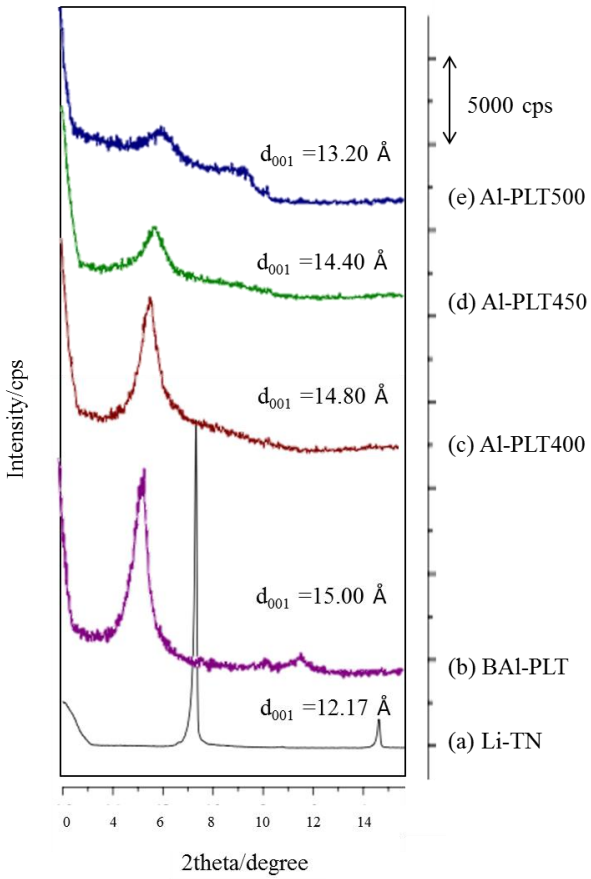

Figure 4.12 XRD pattern of various calcination temperatures in the synthesis of Al-PLT.

In Table 4.29, they were shown the different clearance space which was effected by heated treatment.

Table 4.29 The heated treatment effect on clearance space by X-ray powder diffraction (XRD)

Entry	Catalysts	2θ (dregree)	d_{001}(nm)	C.S.(nm) [a]
1	Li-TN	7.34	1.20	0.24
2	BAl-PLT	5.88	1.50	0.54
3	Al-PLT400	5.98	1.48	0.51
4	Al-PLT450	6.16	1.44	0.48
5	Al-PLT500	6.70	1.32	0.36

[a]C.S. = clearance space = d_{001}-thickness of silicate layer (0.96 nm)

The calcination temperature had a profound effect on the structure of clay catalyst as shown in Figure 4.12 by XRD pattern. When higher temperature was applied, clearance space decreased which brought about structure to Al-pillaring. The structure was changed to amorphous-like structure which was confirmed by decreasing intensity of XRD.

In Figure 4.13 was shown to confirm the protocol for synthesis of Al-PLT and $InCl_3$/Al-PLT.

The impregnation method by $InCl_3$

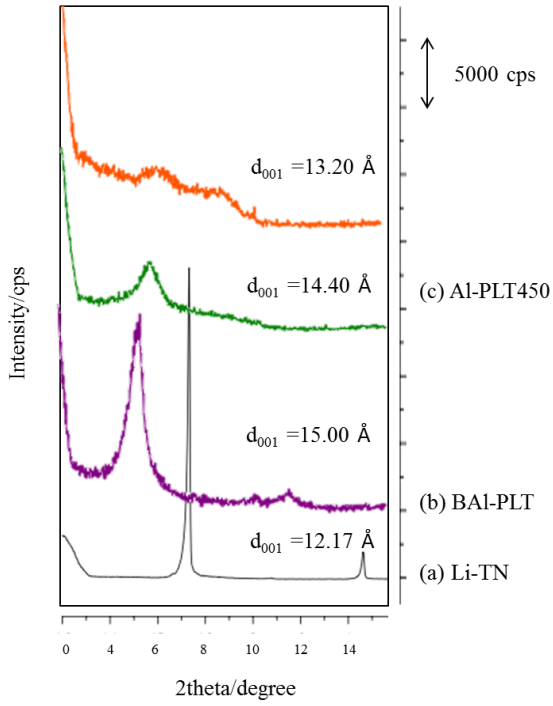

Figure 4.13 XRD pattern for follow synthesis method up to Al-PLT and $InCl_3$/Al-PLT

Figure 4.14 shows the comparison of XRD patterns of $InCl_3$/Al-PLT450, Al-PLT 450, and Li-TN.

In Table 4.30, it was investigated for affirmation structure of Al-PLT450 and $InCl_3$/Al-PLT450 impregnated catalyst.

Table 4.30 Investigated of clearance space by XRD

Entry	Catays ts	2θ (dregree)	d_{001} (nm)	C.S. (nm) [a]
1	Li-TN	7.34	1.20	0.24
2	Al-PLT450	6.16	1.44	0.48
3	$InCl_3$/Al-PLT450	6.70	1.32	0.36

[a]C.S. = clearance space = d_{001}-thickness of silicate layer (0.96 nm)

From XRD pattern, clearance space of $InCl_3$/Al-PLT was lower than that of Al-PLT because $InCl_3$/Al-PLT was re-calcined in impregnation method which mainly caused of dehydration and co-aggregation with Al-structure inside interlayers. The result of clearance space was shown in Table 4.30.

4.11.1.2 Multi nuclear solid-state NMR study of taeniolite (^{27}Al MAS NMR)

Magic angle spinning NMR of ^{27}Al was significant for characterization of atomic-level structural charge around aluminium. From earlier reports [88-89], heat-treated of catalyst was purposed that be mainly cause on the catalyst activity which derived from various aluminium coordinated. The structure of aluminium species was active site on catalyst. This supporting information was expected to clearly establish for selective alkylation. Firstly, unheated Al-pillared taeniolite (BAl-PLT) presented underlying peaks of remarkable six- and trivially four-coordinated ^{27}Al MAS NMR around 6.7 and 56.7 ppm, respectively. These significant peaks of BAl-PLT could be used to confirm aluminium structure resemble of polyoxoaluminated as reported by Wang [90]. Figure 4.14 was ^{27}Al-MAS NMR of BAl-PLT which shown the highly intensity of octrahedral species.

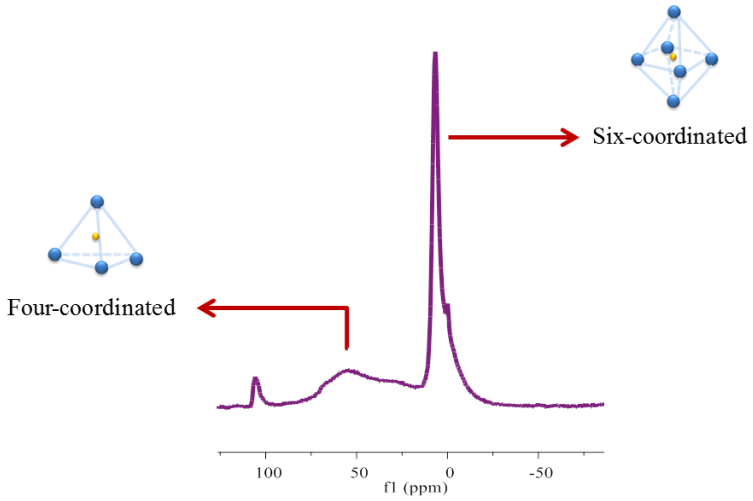

Figure 4.14 ^{27}Al-MAS NMR of BAl-PLT

The structure of unheated Al-PLT was proposed. This was correlated to six-coordination Al which was shown to deshield of chemical shift of dehydration of $[Al(H_2O)_6]^{3+}$ at 0 to 6.7 ppm and unheated Al-PLT revealed a broad and weak peak at 56.7 and 28.3 ppm for four and five coordinated, respectively. This result was related with those reported by Akitt [91] and Hutson [6].

From recently report, hydrolytic behavior of aluminum ions in solution was investigated. Generally, Al^{3+} had the same coordination number as water of 6 which had a chemical formula as $[Al(H_2O)_6]^{3+}$ at pH up to 3; nevertheless, when the pH of solution increased, $[Al(H_2O)_6]^{3+}$ was hydrolyzed as shown below:

$$[Al(OH_2)_6]^{3+} + nH_2O \longrightarrow [Al(OH)_n(H_2O)_{6-n}]^{(3-n)} + nH^+$$

Whereas, n was a molar ratio of hydrolysis which equilibrium on OH and Al ratio, it was preseted in preparing process catalyst. At neutral aluminium solution, the formations of aluminium polynuclear species was presented as polyoxocation as $[Al_{13}O_4(OH)_{24}(H_2O)_{12}]^{7+}$, as equated to Keggin structure (Figure 4.15).

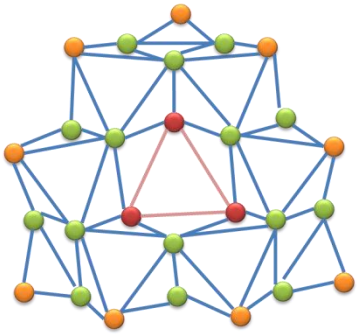

Figure 4.15 The Keggin Structure

The Keggin structure exhibited a ratio of six-coordination to four-coordination of 12. In this case, the structure was changed because aluminium pillars was intercalated into clay interlayers and was formatted the linkages as Si-O-Al(IV). The structure are presented to lower Al(VI)/Al(IV) than 12. Al_{13}-cluster was not stable at high temperature such as increasing more than 100˚C. Henceforth, increasing of temperature by calcination method could be adjusted the structure of aluminium coordinated.

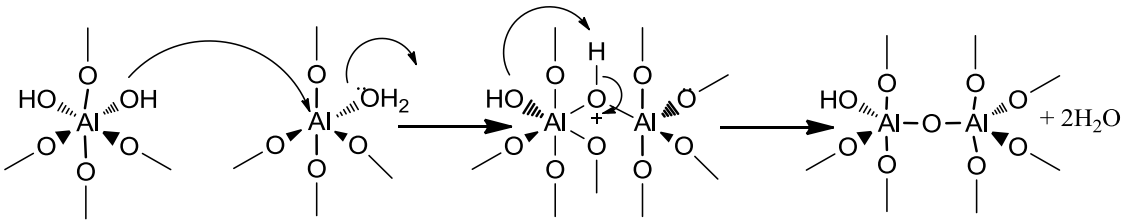

Scheme 4.6 Possibility of dehydration mechanism on aluminium polyoxocation

Secondly, observation of increasing temperature by calcination method was proposed at 400, 450 and 500˚C, which was conjectured to adjustment formation of Al-interlayers. When increasing temperature was applied, the intensity of six-coordinated Al was decreased, while four-coordinated Al was increased. Furthermore, a new peak was appeared around 30 ppm. According to a previous report from MacKenzie [92], a new peak was detected as five-coordinated Al around 31 to 41 ppm. [93] From literatures, five-coordinated Al was anticipated about alteration structure by eliminating of six-coordinated Al hydroxyl group. Figure 4.16 reveals the increasing of five-coordinated intensity by heat treatment. A water molecule from six-

coordinated $Al(Al(OH)_2)$ was released in order to generate a new form as five-coordinated which may act as a Lewis acid site. The increasing of temperature for calcinations was the most influence factor for the structure of polyoxocation. Following Keggin dehydrogenation-dehydroxylation, the oxidation number of aluminiumpolyoxocation was turned to lower number. ^{27}Al MAS NMR was chosen to confirm the structure of Al-PLT.

Finally, $InCl_3$/Al-PLT was re-calcinated at below temperature for synthesis pillaring species at 50˚C. Re-calcination effect initiated result as increasing temperature which trend to higher intensity of four-coordinated Al. From ^{27}Al MAS NMR resulting discussion, six-coordinated Al which acted as a Brønsted acid influenced to produce *C*-alkylated product and five-coordinated Al was presented like Lewis acid was displayed to generate *O*-alkylation.These results were confirmed on earlier another report [94].

Table 4.31 Chemical shifts of ^{27}Al MAS NMR spectra of unheated Al-PLT and $InCl_3$/Al-PLT and heated treatment temperature

Entry	**Catalysts**	**Heat-treatment temperature (˚C)**	**Chemical shift (ppm)**		
			$^{[4]}Al$	**$^{[5]}Al$**	**$^{[6]}Al$**
1	BAl-PLT	R.T.	56.7	28.3	6.7
2	Al-PLT400	400	53.0	26.5	4.0
3	$InCl_3$/Al-PLT400	350	57.7	32.9	5.0
4	Al-PLT450	450	58.5	33.8	4.3
5	$InCl_3$/Al-PLT450	400	58.7	36.1	4.2
6	Al-PLT500	500	63.6	32.7	5.1
7	$InCl_3$/Al-PLT500	450	60.8	33.1	4.5

a)$^{[4]}Al$, $^{[5]}Al$, $^{[6]}Al$ are six-, five-, and four-coordinated Al, respectively

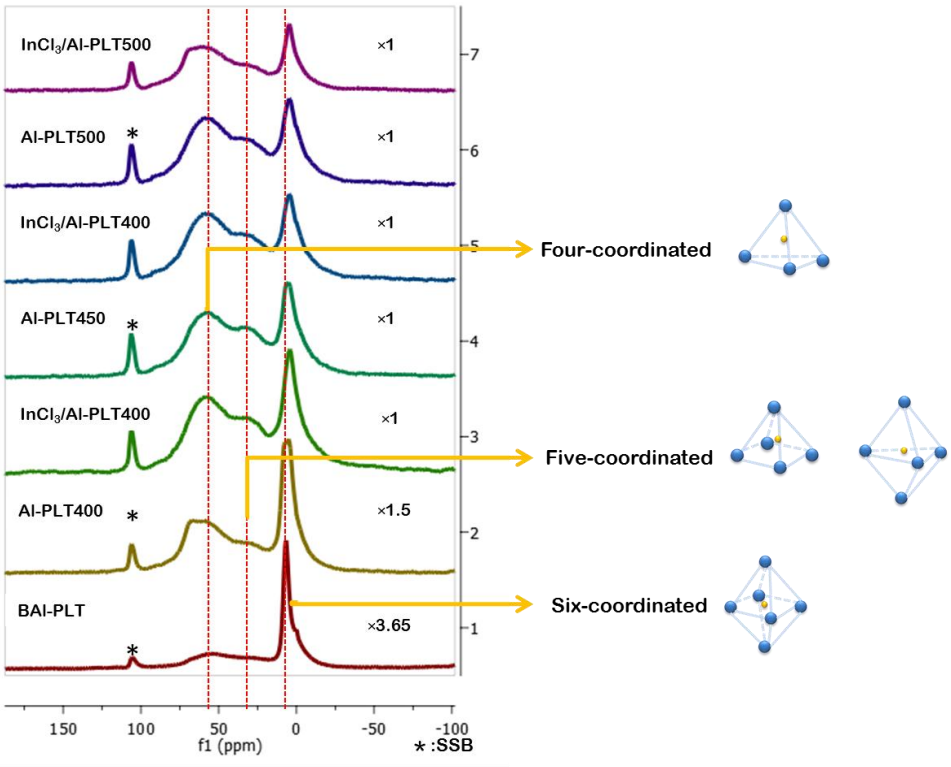

Figure 4.16 ^{27}Al MAS NMR spectra of Al-PLT unheated and heated at high temperature

Table 4.32 displays the activities of synthetic acid catalyst in alkylation of *p*-cresol.

Table 4.32 Variation of taeniolite clay catalysts using in alkylation of *p*-cresol

The catalytic activity of taeniolite species using in *p*-cresol alkylation are shown in Table 4.33.

Entry	Catalysts	S_{BET} (m^2/g)	Acidity (mmol/g)		% Recovery	% Yield			MB (%)
			Weak acidity sites	Strong acidity sites		3a	3b	3c	
1	Li-TN	1.4	0.34	0.56	67.8	32.0	-	-	99.8
2	BAl-PLT	47.2	0.75	1.53	19.2	-	70.9	8.7	98.8
	Calcination at 400°C								
3	Al-PLT400	21.4	0.87	1.47	8.0	-	81.2	11.0	100.2
4	$InCl_3$/Al-PLT400	64.0	0.76	1.91	6.1	-	82.3	11.5	99.9
	Calcination at 450°C								
5	Al-PLT450	60.2	0.44	1.5	-	-	96.6	-	96.6
6	$InCl_3$/Al-PLT450	55.3	0.48	1.65	4.6	-	93.2	-	97.8
	Calcination at 500°C								
7	Al-PLT500	17.7	0.46	0.53	46.2	53.7	-	-	99.9
8	$InCl_3$/Al-PLT500	21.4	0.33	0.99	52.1	48.0	-	-	100.1

Reaction condition: *p*-cresol (1 mmol), *tert*-butanol (8 mmol), 5% mol catalyst of *p*-cresol at 150°C for 2 h.

This exploration was emphasized on the optimization calcination temperature for synthesis clay catalysts, selected taeniolite as model main structure for adaptation as high quality catalyst. Li-TN was synthetic clay that it qualified acidity could be a little bit accelerated in alkylation of *p*-cresol because it is lower acidity and activity hence, Li-TN was applied to higher acidity by pillaring of aluminium polyoxocation that was calcined difference temperature. Al-PLT revealed higher activity than Li-TN because it had 2 dimensional layers which could complex with aluminium polyoxocation transform into 3 dimensional layers which was the cause of increasing specific surface area. The first of interesting remarked temperature at 500°C which reported recently. This point is too high temperature which it was decreased activity; still, shown highly selective of *O*-alkylated product, this result are associated with characterization supported. Although, this research was discovered cause of lower activity by decreasing calcination temperature to 450°C, that show higher activity to quantitative yield and selective to produce *C*-alkylated product. Moreover, decreasing calcination temperature to 400°C was obtained to high activity but lower selective only in mono-substitution of *C*-alkylated product, but still occurred some di-substitution product. Impregnation was the method to increase catalyst acidity which was directly related with the selectivity of *O*- *vs C*- alkylation. Whereas *O*-alkylation required lower acidic catalyst than *C*-alkylation, and Lewis acid property was involved with *O*-alkylation, was described in ^{27}Al MAS NMR section. Evidently, selectivity was controlled by acidity which were measured by ammonia desorption technique, and the effect of aluminium structure was illustrated various basic coordinated controlling on mechanism pathway of alkylation for highly selective. Since Al-PLT exhibited higher acidity, it was selective for *C*-alkylation. In summary, changing from heat-treated to unheated could increase acidity of catalyst which brought about to high yield and provided more *C*-alkylated product.

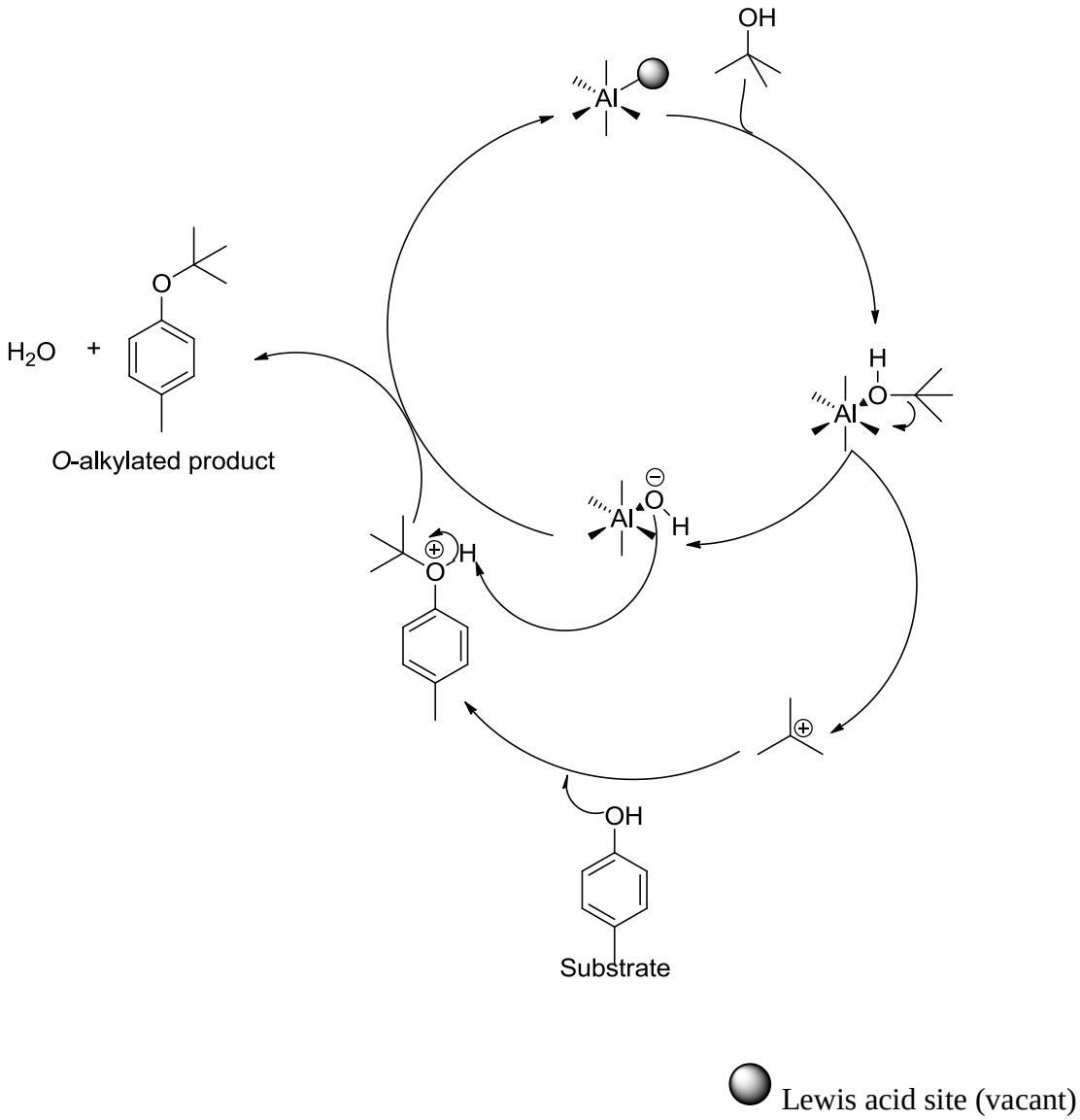

Scheme4.7 Plausible mechanism of electrophilic aromatic substitution to produce *O*-alkylated product

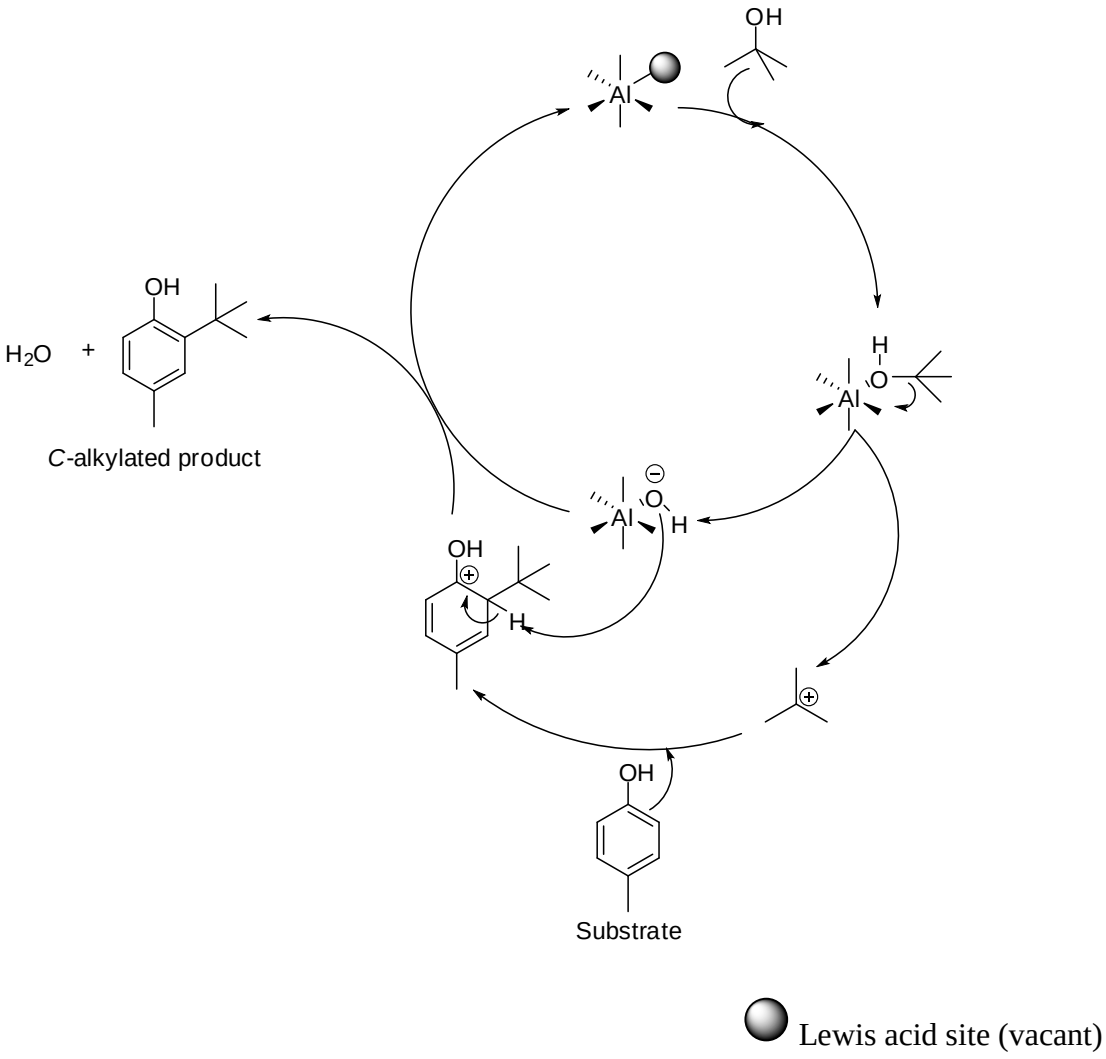

Scheme 4.8 Plausible mechanism of electrophilic aromatic substitution to produce *C*-alkylated product

4.11.2 The alkylation of selected phenols using Al-PLT450 as catalyst

Table 4.33 presents the scope of alkylation of selected phenols including thymol, *p*-cumylphenol, and 4-hydroxybiphenyl.

Table 4.33 Alkylation of selected phenols with *tert*-butanol using Al-PLT450 as catalyst

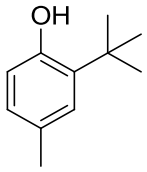

3b

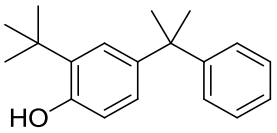

7b

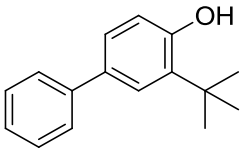

9b

Entry	Phenols	% Phenols (recovered)	% Isolated yield (Base on substrate)	MB
1	*p*-cresol	0.0	96.6 (**3b**)	96.6
2	thymol	94.8	trace	94.8
3	*p*-cumylphenol	14.3	80.1(**7b**)	94.4
4	4-hydroxybiphenyl	6.0	86.6 (**9b**)	95.6

Reaction condition: phenols (1 mmol), *tert*-butanol (8 mmol), 5% mol catalyst of phenols at 150°C for 2 h.

The effect of substituted on phenols was studied in alkylation with *tert*-butanol using Al-PLT which was calcined at 450°C as catalyst. The mono-alkyl (entry 1) and di-alkyl (entry 2) groups were representative electron donating group. Mono-alkylated group gave to quantitative yield of *C*-alkylated product, whereas, di-alkyl group provided trace amount of product. The steric effect of alkyl group on phenolic substrate was a basic necessity of lower yield in thymol. In entry 4 was representative with electron withdrawing group which was achieved to highly yield at 86.6%. In entry 3, *p*-cumylphenol gave moderate yield of *C*-alkylated product. Nonetheless, the

selectivity of all entries is excellent since the reaction produced mono-substitution of *C*-alkylated product.

4.12 Regenerated catalyst

4.12.1 The characterization of regenerated catalyst

The XRD patterns of $InCl_3$/Al-PLB and regenerated $InCl_3$/Al-PLB derived from alkylation of *p*-cresol are shown in Figure 4.18.

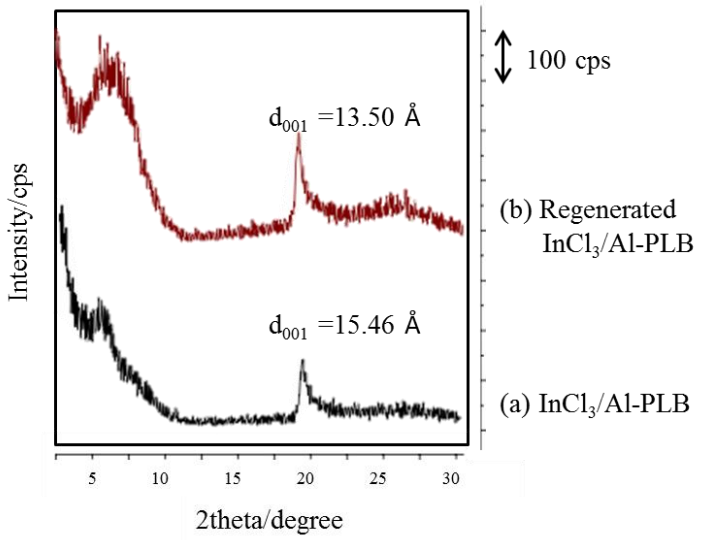

Figure 4.17 XRD patterns of (a) $InCl_3$/Al-PLB and (b) regenerated $InCl_3$/Al-PLB.

The stability of reused catalysts was crucial in heterogeneous catalyst system. The investigation of regenerated catalyst activity after alkylation was conducted following 3 steps: i) the solid catalyst was filtered out of the reaction mixture ii) washed with MeOH, and iii) calcined at 450°C for 5 h. The characterization by XRDwas carried out as presented in Figure 4.12.The patterns of regenerated $InCl_3$/Al-PLB and native one was similar. The fresh $InCl_3$/Al-PLB and regenerated one revealed 2θ in range of 6°-8° and showed the broad peak of 001. It was important that the structure of catalyst should conserve, not depending on the regeneration process. However, the d_{001} basal spacing achieved of regenerated catalyst was around 13.50 Å that was lower than fresh Al-pillared bentonite. The mainly cause is re-calcination processing and the local heat produced from decomposition of trapped organic species.

4.12.2 Nitrogen adsorption-desorption of regenerated catalyst

The nitrogen adsorption-desorption of $InCl_3$/Al-PLB and regenerated $InCl_3$/Al-PLB is collected in Table 4.34.

Table 4.34 The BET specific surface area of $InCl_3$/Al-PLB and regenerated $InCl_3$/Al-PLB after *p*-cresol alkylation

Entry	Catalysts	BET specific surface area (m^2/g)
1	$InCl_3$/Al-PLB	122.40
2	Regenerated $InCl_3$/Al-PLB #1	71.17

Table 4.34 revealed that the BET specific surface areas of $InCl_3$/Al-PLB and regenerated $InCl_3$/Al-PLB. The BET specific surface area of regenerated $InCl_3$/Al-PLB was significantly lower than that of $InCl_3$/Al-PLB. The main cause of change was two reasons: (i) high temperature of re-calcination at 450°C, still was not divested of all organic residues, which could be explained by blocking of pores catalyst, and (ii) Al-pillaring was turned structure into lower activity as tetrahedral and pentahedral coordinated.

4.12.3 Temperature programmed desorption of regenerated catalyst

The total acidity (mmol/g) of $InCl_3$/Al-PLB and regenerated $InCl_3$/Al-PLB for *p*-cresol alkylation is compared in Table 4.35.

Table 4.35 The acidity of $InCl_3$/Al-PLB and regenerated$InCl_3$/Al-PLB for phenol alkylation

Entry	Catalysts	Acidity (mmol/g)		Total acidity (mmol/g)
		Weak acid sites	Strong acid sites	
1	$InCl_3$/Al-PLB	0.34	1.52	1.86
2	regenerated $InCl_3$/Al-PLB #1	0.31	1.33	1.64

The lower acidity in Table 4.35 of $InCl_3$/Al-PLB was compared with regenerated $InCl_3$/Al-PLB could be explained by temperature programmed ammonia desorption. Cause of strong acidity decreasing was presented two points due to the remaining organic residues in catalyst pores, possibly the regenerated process at 450°C could not completely decompose the organic compounds which adsorbed on used catalyst and re-calcination effect was mainly cause of adjustment structure by dehydrated of aluminium precursor which could be decreasing of acidity.

4.12.4 Activity of regenerated $InCl_3$/Al-PLB in alkylation of *p*-cresol with *tert*-butanol

Currently, industrial appreciates heterogeneous catalyst because the catalytic efficiency of reused catalyst was the main cause for diminishing payment. Regenerated catalyst was used in alkylation of *p*-cresol with *tert*-butanol under optimized conditions. The results are presented in Table 4.36.

Table 4.36 The results of regenerated $InCl_3$/Al-PLB in alkylation of *p*-cresol with *tert*-butanol

Run	% Yield
1	quant
2	93
3	92
4	90
5	88

Reaction conditions: *p*-cresol (1 mmol), *tert*-butanol (8 mmol), 5% mol catalyst of *p*-cresol at 150°C for 2 h.

The regenerated $InCl_3$/Al-PLB exhibited lower activity than the original $InCl_3$/Al-PLB. This result was well corresponded to the collapse of d_{001} basal spacing which turned into lower BET surface area and acidity.

4.13 Regenerated of Al-PLT450

4.13.1 The characterization of regenerated catalyst

The XRD patterns of Al-PLT450 and regenerated Al-PLT450 from alkylation of phenols are shown in Figure 4.18.

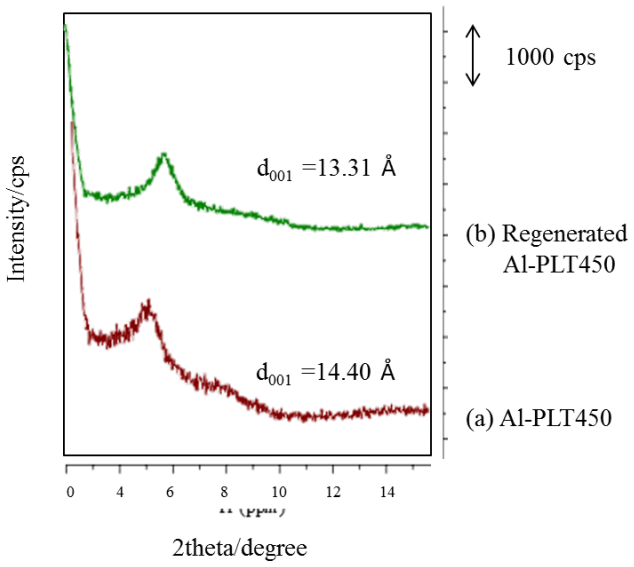

Figure 4.18 XRD patterns of (a) Al-PLT450 and (b) regenerated Al-PLT450.

The regenerated catalyst at 400°C with long time influenced on the structure of active site catalyst which turned activity to lower. From XRD characterization, intensity of d001 Al-PLT450 peak was decresed because structure of aluninium pillaring was adjusted to various species, and the d_{001} basal spacing of regenerated Al-PLT450 achieved around 13.31 Å that was lower than fresh Al-PLT450 which is the similarly cause of above-mentioned. The local heat produced from decomposition of trapped organic species.

4.13.2 Nitrogen adsorption-desorption of regenerated catalyst

The nitrogen adsorption-desorption of Al-PLT450 and regenerated Al-PLT450 are shown in Table 4.37.

Table 4.37 The BET specific surface area of Al-PLT450 and regenerated Al-PLT450 for *p*-cresol alkylation

Entry	Catalysts	BET specific surface area (m^2/g)
1	Al-PLT450	60.2
2	regenerated Al-PL450 #1	12.3

Table 4.37 shows the BET specific surface area of Al-PLT450 and regenerated Al-PLT450. The BET specific surface area of regenerated Al-PLT450 was lower than Al-PLT450. The main cause of change could be explained by two reasons: high temperature of re-calcination at 400°C for 5 h and Al-pillaring was turned structure into lower activity.

4.13.3 Temperature programmed desorption of regenerated catalyst

The total acidity (mmol/g) of Al-PLT450 and regenerated Al-PLT450 for *p*-cresol alkylation is compared in Table 4.38.

Table 4.38 The acidity of Al-PLT450 and regenerated Al-PLT450 for *p*-cresol alkylation

Entry	Samples	Acidity (mmol/g)		Total acidity (mmol/g)
		Weak acid sites	Strong acid sites	
1	Al-PLT450	0.44	1.50	1.94
2	Regenerated Al-PLT450 #1	0.35	0.99	1.34

The lower acidity in Table 4.38 of Al-PLT450 was compared with regenerated Al-PLT450. Decreasing of strong acidity was derived from two points: due to the remaining organic residues in catalyst pores, possibly the regenerated process at

400°C may not completely destroy or decompose organic compounds adsorbed on used catalyst and adjusted structure to tetrahedral coordinated could be decreasing of acidity.

4.13.4 Activity of regenerated Al-PLT450 using in alkylation of *p*-cresol with *tert*-butanol

Regenerated Al-PLT450 catalyst was reused in alkylation of *p*-cresol with *tert*-butanol under optimized conditions. The results are presented in Table 4.40.

Table 4.39 The results of regenerated Al-PLT450 using in alkylation of *p*-cresol with *tert*-butanol

Run	% Yield[a]
1	Quant
2	64
3	-

Reaction conditions: *p*-cresol (1 mmol), *tert*-butanol (8 mmol), 5% mol catalyst of *p*-cresol at 150°C for 2 h.

The regenerated Al-PLT450 obviously exhibited lower activity than the original Al-PLT450. This result was well corresponded to that of the collapse of d_{001} basal spacing, lower BET surface area and lower acidity.

CHAPTER V

CONCLUSION

The aim of research is observed selectively catalytic alkylation which catalytic study in bentonite section is investigated the suitable catalyst for highly selective of *O*-alkylation from various metal (III) impregnated on Al-pillared bentonite. Al-pillared bentonite was synthesized by intercalation of aluminium polyoxocation into clay layers and calcined at 500˚C. Furthermore, the impregnation method of metal (III) chloride ($InCl_3$, $LaCl_3$, $CeCl_3$, $NdCl_3$ and $GdCl_3$) was investigation for synthesis metal impregnated Al-pillared bentonite by using re-calcination method. The synthesis step of clay was characterized by XRD, N_2-adsorption-desorption, NH_3-TPD and ICP-OES technique. For catalytic in bentonite species, catalysts were presented highly reactivity following by $NdCl_3$/Al-PLB, $CeCl_3$/Al-PLB, $LaCl_3$/Al-PLB, $GdCl_3$/Al-PLB and $InCl_3$/Al-PLB, but in this case, the only $InCl_3$/Al-PLB was selective to produce *O*-alkylated product. At the optimized alkylation condition, $InCl_3$/Al-PLB was applied to various phenols and alkylating agent and the results were shown lower selectivity with *O*-alkylated product; nevertheless, we could also observed to be appropriated condition to highly yield and selective.

For the synthesis of taeniolite catalyst species, Al-pillared taeniolite was investigated calcination temperature which was followed by 400, 450, and 500ºC, respectively. The result was revealed high *C*-alkylation selective of Al-pillared taeniolite calcined at 450ºC (Al-PLT450). The heated treatment was mainly effect to adjustment structure of pillaring for designed to highly selective. Al-PLT 450 could be selective with other phenols

The reusability of $InCl_3$/PLB is presented many times to run for recover; on the other hand, Al-PLT450 could not work because highly re-calcination in processing recovery altered structure to lower reactivity.

Propose for the future work

This research concerns with development of reactivity and selectivity in catalytic system. The condition for synthesis catalyst is appreciated such as mole ratio OH/Al, rate for dropping to mixing pillaring agent, temperature for holding on miscellaneous because these affect mentioned, impinged to structure of pillaring. The structural of pillared is influenced on selectivity for using in organic reaction as alkylation and open epoxide ring.

REFERENCES

[1] Nishiyama, T., Sugimoto, T., and Andoh, Y. Antioxidant Activity of Phenols in Intramolecularly Cooperating Stabilizing Systems. Polymer Degradation and Stability. 74 (2001) : 189-193.

[2] Kajiyama, T., Ohkatsu, Y. Effect of *para*-Substituents of Phenolic Antioxidants. Polymer Degradation and Stability. 71 (2001) : 445-452.

[3] Klein, E., Lukes, V., and Cibulkova, Z. On the Energetic of Phenol Antioxidants Activity. Petroleum & Coal. 47 (2005) : 33-39.

[4] Znoiko, S.A., Maizlish, V.E., and Shaposhnikov, G.P. Nucleophilic Substitution in 4-Bromo-5-nitro-phthalodinitrile: VIII. Synthesis of 4-(Benzotriazol-1-yl)-5-[4-(1-methyl-1phenylethyl) phenoxy]phthalo-dinitrile and Phthalocyanines on Its Basis. Russian Journal of General Chemistry. *77* (2007) **:** 1551-1555.

[5] Yuan, P., *et al.* A combined study by XRD, FTIR, TG and HRTEM on the Structure of Delaminated Fe-intercalated/pillared clay. Journal of Colloid and Interface Science. 324 (2008) : 142-149.

[6] Hutson, N.D., Hoekstra, M.J., and Yang, R.T. Control of Microporosity of Al_2O_3-pillared clays: Effect of pH, Calcination Temperature and Clay Cation Exchange Capacity. Microporous and Mesoporous Materials. 28 (1999) : 447-459.

[7] Bodman, S.D., *et al*. Metal-ion pillared clays as Hydrocracking Catalysts (I): Catalyst Preparation and Assessment of Performance at Short Contact Times. Fuel. 81 (2002) : 449-459.

[8] Cativiela, C., Fraile, J. M., Garcia, J. I. Josh., Mayoral, A., and Pires, E. Effect of Clay Calcination on Clay-Catalysed Diels-Alder Reactions of Cyclopentadiene with Methyl and (-)-Menthyl Acrylates. Tetrahedron. 48 (1992) : 6467-6476.

[9] Balci, S., and Gökçay, E. Effects of Drying Methods and Calcination Temperatures on the Physical Properties of Iron Intercalated Clays. Materials Chemistry and Physics. 76 (2002) : 46-51.

[10] Choudhary, V. R., Jha, R., and Narkhede, V.S. In-Mg-hydrotalcite Anionic Clay as Catalyst or Catalyst Precursor for Friedel–Crafts type Benzylation

Reactions. Journal of Molecular Catalysis A-Chemical. 239 (2005) : 76-81.

[11] Yuan, P., He, H., Bergaya, F., Wu, D., Zhou, Q., and Zhu, J. Synthesis and Characterization of Delaminated Iron-pillared Clay with Meso–Microporous Structure. Microporous and Mesoporous Materials. 88 (2006) : 8-15.

[12] Mahfuzah Masalaeh, Catalytic Cracking of Polypro-pylene and Polyethylene using Zirconium/aluminium oxide-pillared Clay Master's Thesis, Department of Chemistry, Faculty of Science, Chulalongkorn University, 2008.

[13] Evans, W.J., Perspectives in Reductive Lanthanide Chemistry. Coordination Chemistry Reviews. 206-207 (2000) : 263-283.

[14] Valuerra, J. M., Zaldivar, O., Sanchez, M. A., Montoya, J.A., Navarrete, J., and Reyes, J.A. Selectivity to Cumene in the Alkylation of Benzene with *iso*-Propanol on a MCM-41/γ-Al_2O_3 Catalyst. Applied Catalysis A: General 166 (1998) : 387-392.

[15] Jun, S., and Ryoo, R. Aluminum Impregnation into Mesoporous Silica Molecular Sieves for Catalytic Application to Friedel–Crafts Alkylation. Journal Catalysis. 195 (2000) : 237-243.

[16] He, N., Bao, S., and Xu, Q. Fe-containing Mesoporous Molecular Sieves Materials: Very active Friedel–Crafts Alkylation Catalysts. Applied Catalysis A: General 169 (1998) : 29–36.

[17] Choudary, V.R., Jana, S.K., and Kiran, B.P. Highly Active and Moistureinsensitive Solid Catalysts—$GaCl_3$ and $InCl_3$ Supported on Montmorillonite-K10 and Si-MCM-41 for Benzylation of Benzene. Catalysis Letter. 64 (2) (2000) : 223–226.

[18] Okumura, K., Nishigaki, K., and Niwa, M. Prominent Catalytic Activity of Ga-containing MCM-41 in the Friedel-Crafts Alkylation. Microporous and Mesoporous Materials. 44 (2001) : 509–516.

[19] Hu, X., Foo, M.L., Chuah, G.K., and Jaenicke, S. Pore Size Engineering on MCM-41: Selectivity Tuning of Heterogenized $AlCl_3$ for the Synthesis of Linear Alkyl Benzenes. Journal Catalysis. 195 (2000) : 412–415.

[20] Shinde, A. B., Shrigadi, N. B., and Samant S. D. *tert*-Butylation of Phenols using *tert*-Butyl Alcohol in the Presence of $FeCl_3$-modified Montmorillonite K10. Applied Catalysis A: General 276 (2004) : 5-8.

[21] Perego, C., Amarilli, S., Carati, A., Flego, C., Pazzuconi, G., Rizzo, C., and Bellussi, G. Mesoporous Silica-Aluminas as Catalysts for the Alkylation of Aromatic Hydrocarbons with Olefins. Microporous and Mesoporous Materials. 27 (1999) : 345–354.

[22] Zhang, K., et al. Alkylation of Phenol with *tert*-Butyl Alcohol Catalyzed by Zeolite Hβ. Applied Catalysis A: General 166 (1998) : 89-95.

[23] Bal, R., and Sivasanker, S. Vapour Phase Selective *O*-alkylation of Phenol over Alkali loaded Silica. Applied Catalysis A: General. 246 (2003) : 373-382.

[24] Grabowska, H. Syper, L., and Zawadzki, M. Vapour Phase Alkylation of *ortho*-, *meta*- and *para*-Cresols with Isopropyl Alcohol in the Presence of Sol–Gel Prepared Alumina Catalyst. Applied Catalysis A: General 277 (2004) : 91-97.

[25] Sarish, S., Devassy B. M. and Halligudi, S.B, *tert*-Butylation of *p*-Cresol over WO_x/ZrO_2 Solid Acid Catalysts. Journal of Molecular Catalysis A-Chemical. 235 (2005) : 44-51.

[26] Devassy, B. M., Shanbhag, G.V., HalligudiSarish, S.B. Phenol *tert*-Butylation over Zirconia-Supported 12-Molybdophosphoric Acid Catalyst. Journal of Molecular Catalysis A-Chemical. 247 (2006) : 162-170.

[27] Bhatt, N., Patel, A. Liquid Phase Cyclohexylation of Phenol with Cyclohexene using 12-Tungstosilicicacid Supported onto Different Supports. Journal of Molecular Catalysis A-Chemical. 264 (2007) : 214-219.

[28] Reddy, B. M., Patil, M. K., Reddy, G. K., Reddy, B. T., Rao, K. N. Selective *tert*-Butylation of Phenol over Molybdate- and Tungstate-Promoted Zirconia Catalysts. Applied Catalysis A: General. 332 (2007) : 183-191.

[29] Kondamudia, K., Elavarasana, P., Dysonb, P. J., Upadhyayulaa, S. Alkylation of *p*-Cresol with *tert*-Butyl Alcohol using Benign Brønsted Acidic Ionic liquid Catalyst. Journal of Molecular Catalysis A-Chemical. 321 (2010) : 34-41.

[30] Wilson, K., Adams, D.J., Rothenberg, G. and Clark Solid, J.H., Comparative Study of Phenol Alkylation Mechanisms Using Homogeneous and Silica-Supported Boron trifluoride Catalysts. Journal of Molecular Catalysis A-Chemical. 159 (2000) : 309-314.

[31] Geatti, A., Lenarda, M., Storaro, L., Genzerla, R. and Perissinotto, M. Solid Acid Catalysts from Clays: Cumene Synthesis by Benzene Alkylation with Propene Catalyzed by Cation Exchanged Aluminium Pillared Clays. Journal of Molecular Catalysis A-Chemical. 121 (1997) : 111-118.

[32] Singh, V., Khurana, A., Kaur, I., Sapehiyia, V., Kad, G. L., and Singh, J. Microwave Assisted Facile Synthesis of Elvirol, Curcuphenol and Sesquichamaenol using Montmorillonite K10 Clay in Dry Media. Journal of Chemical Society. 1 (2002) : 1766-1768.

[33] Yadav, G. D. and Pathre, G. S., Novel Mesoporous Solid Superacids for Selective *C*-alkylation of *m*-Cresol with *tert*-Butanol. Microprorous and Mesoporous Materials. 89 (2006) : 16-24.

[34] Kurian, M. and Sugunan, S. *tert*-Butylation of Phenol Catalysed by Metal Exchanged Iron Pillared Montmorillonites. Catalysis Communication. *7* (2006) : 417-421.

[35] Nagendrappa, G. Organic Synthesis under Solvent Free-Conditions: An Environmentally Benign Procedure-I. Resonance. *7* (2002) : 59-68.

[36] Varma, R. S. Clay and Clay-Supported Reagents in Organic Synthesis. Tetrahedron 58 (2002) : 1235-1255.

[37] Motokura, K., Matsunaga, S., Miyaji, A., Sakamoto, Y., and Baba, T. Heterogeneous Allylsilation of Aromatic and Aliphatic Alkenes Catalyzed by Proton-Exchanged Montmorillonite. Organic Letter. 12 (2010) : 1508–1511.

[38] Choudhary, V.R., Mantri, K., and Jana, S.K. Selective Esterification of *tert*-Butanol by Acetic Acid Anhydride Over Clay Supported $InCl_3$, $GaCl_3$, $FeCl_3$ and $InCl_2$ Catalysts. Catalysis Communication. 2 (2001) : 57–61.

[39] Mitsudome, T., Nose, K., Mizugaki, T., Jitsukawa, K., and Kaneda, K. Reusable Montmorillonite-Entrapped Organocatalyst for Asymmetric Diels–Alder Reaction. Tetrahedron Letter. 49 (2008) : 5464–5466.

[40] Choudary, B. M., Sateesh, M., Kantam, M. L., Prasad, K. V. R. Acylation of Aromatic Ethers with Acid Anhydrides in the Presence of Cation-Exchanged Clays. Journal of Molecular Catalysis A-Chemical. 171 (1998) : 155-160.

[41] Bruce, W. D., and Hare, D. Inorganic materials, 2nd ed., New York, John Wiley& Sons, Inc., 1997.

[42] Shichi, T., and Takagi, K. Clay Minerals as Photochemical Reaction Fields. Journal Photochemistry and Photobiology C-Photochemistry Reviews. 1 (2000) : 113-130.

[43] Moore, D. M., and Reynolds, Jr. R. C. X-Ray Diffraction and the Identification and Analysis of Clay Minerals, New York, USA, Oxford University Press, 1989.

[44] Rajamathi, M., Thomas, G. S., and Kamath, P. V. The Many Ways of Making Anionic Clays. Process Indian Academic Science (Chemistry Science). 113 (2001) : 671-680.

[45] Lambert, J. F., and Poncelet, G. Acidity in Pillared Clay: Origin and Catalytic Manifestations. Topic in Catalysis. 4 (1997): 43-56.

[46] Novozhilov, A. I., Samoilovich, M. I., Anikin, I. N., and Sergeev-Bobr, A. A. Investigation of Structural Defects in the Crystals of Synthetic Mica (Fluorophlogopite and Taeniolite) by the EPR Method. All-Union Scientific-Research Institute of Mineral Raw Materials, Aleksandrov. Translated from Zhurnal Strukturnoi Khimii. 12 (1971) : 562-566.

[47] Varma, R. S. Clay and clay-supported Reagents in Organic Synthesis. Tetrahedron. 58 (2002) : 1235-1255.

[48] Schoonheydt, R. A., Pinnavaia, T., Lagaly, G., and Gangas, N. Pillared Clays and Pillared Layered Solids. Pure Applied Chemistry. 71 (1999) : 2367-2371.

[49] Vicente, M. A., et al. Preparation and Characterization of Vanadium Catalysts Supported over Alumina-pillared Clays. Catalytic Today 78 (2003) : 181-190.

[50] Gonzalez, F., Pesquera, C., Blanco, C., Benito, I., and Mendioroz, S. Synthesis and Characterization of Al-Ga Pillared Clays with High Thermal and Hydrothermal Stability. Inorganic Chemistry. 31 (1992) : 727.

[51] Piyada Sawangkam. Synthesis of Tangsten Containing MCM-41 Catalyst and Their Activity for Olefin Metathesis. Master's Thesis, Department of Chemistry, Faculty of Science, Chulalongkorn University, 2005.

[52] Basic operating principles of the sorptomatic. [online] Available from: http://saf.chem.ox.ac.uk./Instruments/BET/sorpoptprin. [2010.11.15].

[53] Analysis software user's manual, BELSORP, BEL JAPAN, INC. 57.

[54] Tago, T., Okubo, Y., Mukia, S. R., Tanaka, T., and Masuda, T. Simultaneous Characterization of Acidic and Basic Properties of Solid Catalysts by a New TPD Method and Their Correlation to Reaction Rates. Applied Catalysis A: General 290 (2005) : 54-64.

[55] Inductive coupled plasma atomic emission spectroscopy. [online] Available from: http://en.wikipedia.org/wiki/Inductive coupled plasma atomic emission spectroscopy. [2009.10.26].

[56] Manning, T. J., and Grow, R. W. Inductively coupled plasma-atomic emission spectrometry. The Chemical Educator. 2 (1997) : 1-19.

[57] Smith, M.E. Application of ^{27}A1 NMR Techniques to Structure Determination in Solids. Applied Magnetic Resonance. 4 (1993) : 1-64.

[58] De Boer, J. H. Constitution and Properties of Silica-Alumina-Catalysts. Faraday Society. 52 (1971) : 109-112.

[59] Tamele, M. W. Chemistry of the Surface and the Activity of Alumina-Silica Cracking Catalyst. Faraday Society. 8 (1950) : 270-279.

[60] MacKenziea, K.J.D., Temuujinb, J., and Okada, K. Thermal Decomposition of Mechanically Activated Gibbsite. Thermochimica Acta. 327 (1999) : 103-108.

[61] De Witte, B. M., Grobet, P. J., and Uytterhoeven, J. B. Pentacoordinated Aluminum in Noncalcined Amorphous Aluminosilicates, Prepared in Alkaline and Acid Medium. Journal Physical Chemistry. 99 (1995) : 6961-6965.

[62] Peeters, M.P.J., and Kentgens, A.P.M. A ^{27}A1 MAS, MQMAS and off-resonance nutation NMR Study of Aluminium Containing Silica-based Sol-Gel Materials. Solid State Nuclear Magnetic Resononance. 9 (1997) : 203-217.

[63] Cloos, P., Leonard, A. J., Moreau, J.P., Herbilion, A., and Fripiat, J.J. Structureral Organization in Amorphous Silico-aluminas. Clays & Clay Minerals. 17 (1969) : 279.

[64] Williams, M.F., Fonfé, B., Woltz, C., Jentys, A., van Veen, J.A.R., and Lercher, J.A. Hydrogenation of Tetralin on Silica-Alumina Supported Pt Catalysts I-Physicochemical Characterization of the Catalytic Materials. Journal Catalysis. 251 (2007) : 497.

[65] Kameshima, Y., Yoshizawa, A., Nakajima, A., and Okada, K. Solid acidities of SiO_2-TiO_2/montmorillonite composites synthesized under different pH conditions. Applied Clay Science. 46 (2009) : 181-184.

[66] Olejnik, S., Posner, A. M., and Quirk, J. P. Swelling of montmorillonite in polar organic liquids. Clays & Clay Mineral. 22 (1974) : 361-365.

[67] Wang, M., and Muhammed, M. Novel synthesis of Al_{13}-cluster based alumina. Nanostructured Materials. 11 (1999) : 1219-1229.

[68] Camilotia, A.M., Jahnb, S.L., Velascoa, N.D., Mouraa, L.F., and Cardosoa, D. Acidity of Beta Zeolite Determined by TPD of Ammonia and Ethylbenzene Disproportionation. Applied Catalysis A: General 182 (1999) : 107-113.

[69] Shin, Y.S., Oh, S.G., and Ha, B.H. Pore Structures and Acidities of Al-Pillared Montmorillonite. Korean Journal of Chemical Engineering. 20(1) (2003) : 77-82.

[70] Camilotia, A.M., Jahnb, S.L., Velascoa, N.D., Mouraa, L.F., and Cardosoa, D. Acidity of Beta Zeolite Determined by TPD of Ammonia and Ethylbenzene Disproportionation. Applied Catalysis A: General 182 (1999) : 107-113.

[71] Bhattacharyya, K. G., Talukdar, A. K., Das, P., and Sivasanker, S. Al-MCM-41 catalysed alkylation of phenol with methanol. Journal of Molecular Catalysis A-Chemical. 197 (2003) : 255–262.

[72] Evans, W.J., Perspectives in Reductive Lanthanide Chemistry. Coordination Chemical Reviews. 206-207 (2000) : 263-283.

[73] Elavarasan, P., Kondamudi, K., Upadhyayula, S. Kinetics of Phenol Alkylation with *tert*-Butyl Alcohol using Sulfonic Acid Functional Ionic Liquid Catalysts. Chemical Engineering Journal. 166 (2011) : 340-346.

[74] Shaohua, B., Nannan, Q., Jing, Z., and Jianguo, Y. Alkylation of *p*-Cresol with *tert*-Butanol Catalyzed by Novel Multiple-SO_3H Functioned Ionic Liquid. Chinese Journal of Chemical Engineering. 19(1) (2011) : 64-69.

[75] Devassy, B. M., Shanbhag, G.V., Lefebvre, F., and Halligudi, S.B. Alkylation of *p*-Cresol with *tert*-Butanol Catalyzed by Heteropoly Acid Supported on Zirconia Catalyst. Journal of Molecular Catalysis A-Chemical. 210 (2004) : 125–130.

[76] Liu, X., Liu, M., Guo, X., Zhou, J. SO_3H-Functionalized Ionic Liquids for Selective Alkylation of *m*-Cresol with *tert*-Butanol. Catalysis Communication. 9 (2008) : 1–7.

[77] Kinetics and Mechanisms of Nucleophilic Displacements with Heterocycles as Leaving Groups. Part 10.[1] Reactions of s-Alkyl Primary Amines with Pyryliums. Journal of the Chemical Society, Perkin Transaction 2. 9 (1983) : 1435-1441.

[78] Williams, F. J., Relles, H. M. Manello, J. S. and Donahue, P. E. Reactions of Phenoxides with Nitro-Substituted Phthalate Esters. Journal Organic Chemistry. 42 (1977)

[79] Paul, R., Ali, M.A., and Punniyamurthy, T. Copper-Catalyzed Hydroxylation of Aryl Halides with Tetrabutylammonium Hydroxide: Synthesis of

Substituted Phenols and Alkyl Aryl Ethers Synthesis. 24 (2010) : 4268–4272

[80] Aleksandrova, E. Possible Formation of Claisen Phenol in the Intermolecular Catalytic Rearrangement of 4-(1,1-dimethyl-2-propenoxy)toluene. Zhurnal Organicheskoi Khimii. 16 (1980) : 459.

[81] Julia, M., Nel, M., and Uguen, D. Organic synthesis with sulfones. XLI. Nucleophilic substitutions of allylic sulfones. Bulletin de la Societe Chimique de France. 3 (1987) : 487-492.

[82] Camps, F. Improved Procedure for Preparation of -Alkyl Aryl Ethers Synthesis-Stuttgart. 1982 (1982) : 186.

[83] Kuninobu, Y., Matsuki, T., and Takai, K. Rhenium-Catalyzed Regioselective Alkylation of Phenols. Journal of American Chemistry Society Communication. 131 (2009) : 9914-9915.

[84] Hanada, S., Yuasa, A., Kuroiwa, H. Motoyama, Y. and Nagashima, H. Hydrosilanes Are Not Always Reducing Agents for Carbonyl Compounds, II: Ruthenium-Catalyzed Deprotection of *tert*-Butyl Groups in Carbamates, Carbonates, Esters, and Ethers. European Journal of Organic Chemistry. 6 (2010), 1021–1025.

[85] Davis, B. R. Reactions of 4-hydroxycyclohexa-2,5-dienones under acidic conditions. (1982), 7: 1499.

[86] Mahammed, K.A., Murthy, K.P.S., and Raju, M.K. A Convenient Synthesis of *tert*-Butyl Ethers under Microwave condition Indian Journal Chemistry. 47B (2008) : 575-578.

[87] Gagea, B. C., Parvulescu, A. N., Parvulescu, V. I., Auroux, A., Grange, P., and Poncelet, G. Alkylation of Phenols and Naphthols on Silica-Immobilized Triflate Derivatives. Catalysis Letters. 91 (2003) : 141-144.

[88] Shin, Y.S., Oh, S.G. and Ha, B.H. Pore Structures and Acidities of Al-Pillared Montmorillonite. Korean Journal of Chemical Engineering. 20(1) (2003) : 77-82.

[89] Binitha, N.N., and Sugunan, S. Preparation, characterization and catalytic activity of titania pillared montmorillonite clays. Microporous and Mesoporous Materials. 93 (2006) : 82–89.

[90] Wang, M. and Muhammed, M. Novel Synthesis of Al_{13}-Cluster Based Aluminiuna Materials Nanostructure Materials. 11 (1999) : 1219–1229.

[91] Akitt, J.W. Multinuclear studies of aluminium compound Progress Nuclear Magnetic Resonance Spectroscopy. 21 (1989) : 1-149.

[92] MacKenziea, K.J.D., Temuujinb, J., Okadac, K. Thermal decomposition of mechanically activated gibbsite. Thermochimica Acta. 327 (1999) : 103-108.

[93] Smith, M.E. Application of ^{27}A1 NMR Techniques to Structure Determination in Solids. Applied Magnetic Resonance. 4 (1993) : 1-64

[94] Yadav, G. D., and Pathre, G. S. Chemoselective catalysis by sulphated zirconia in *O*-alkylation of guaiacol with cyclohexene Journal of Molecular Catalysis A-Chemical. 243 (2006) : 77–84.

Appendix

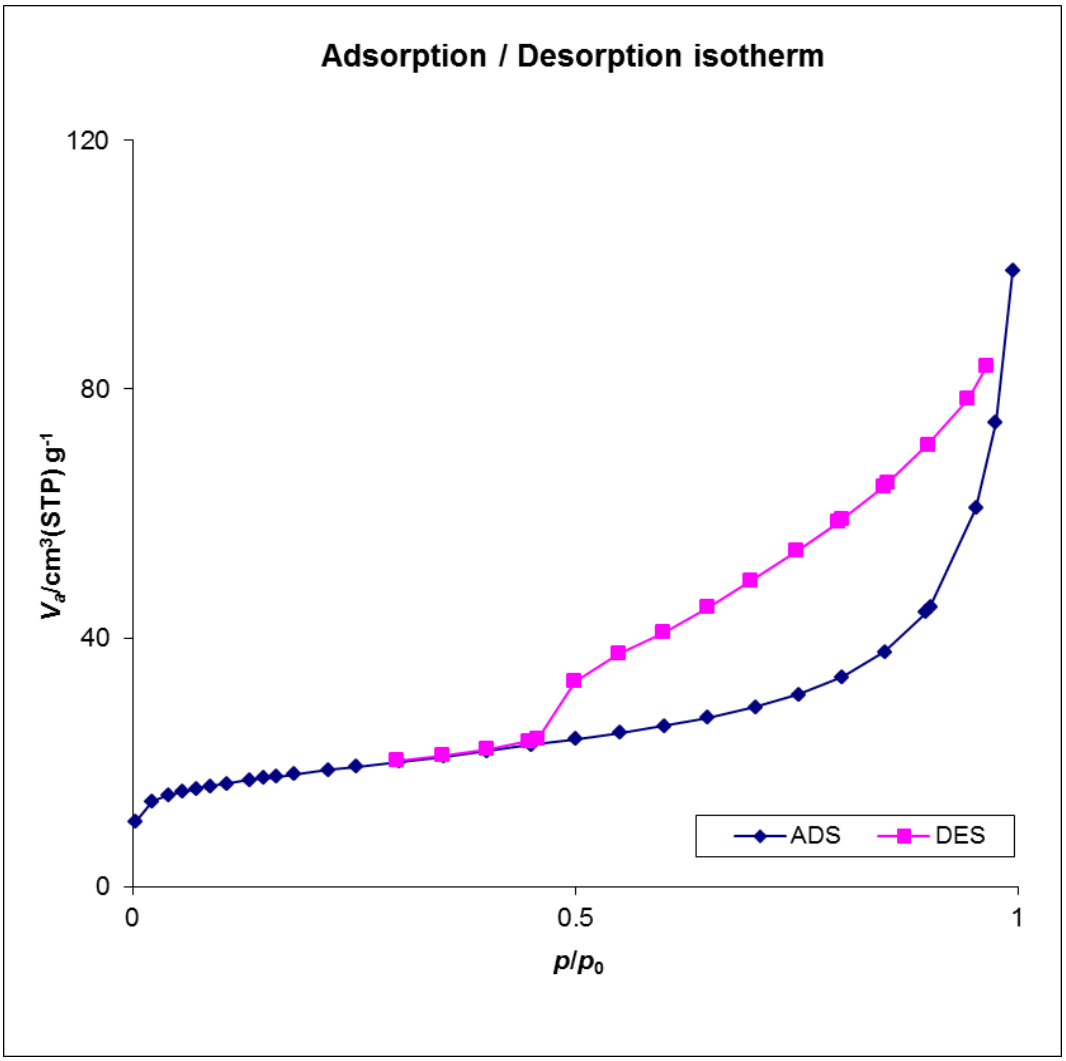

Figure A-1 N_2 adsorption-desorption isotherm of raw bentonite

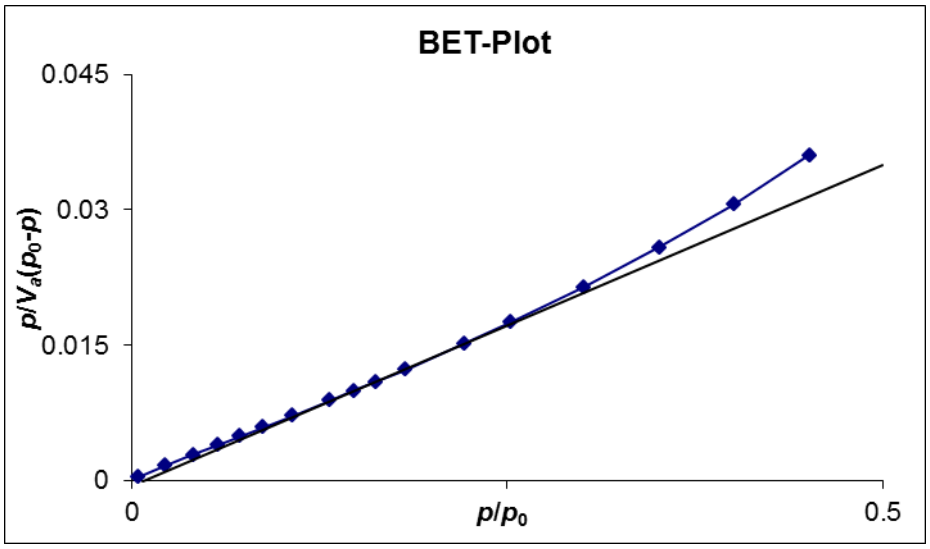

Figure A-2 BET plot of raw bentonite

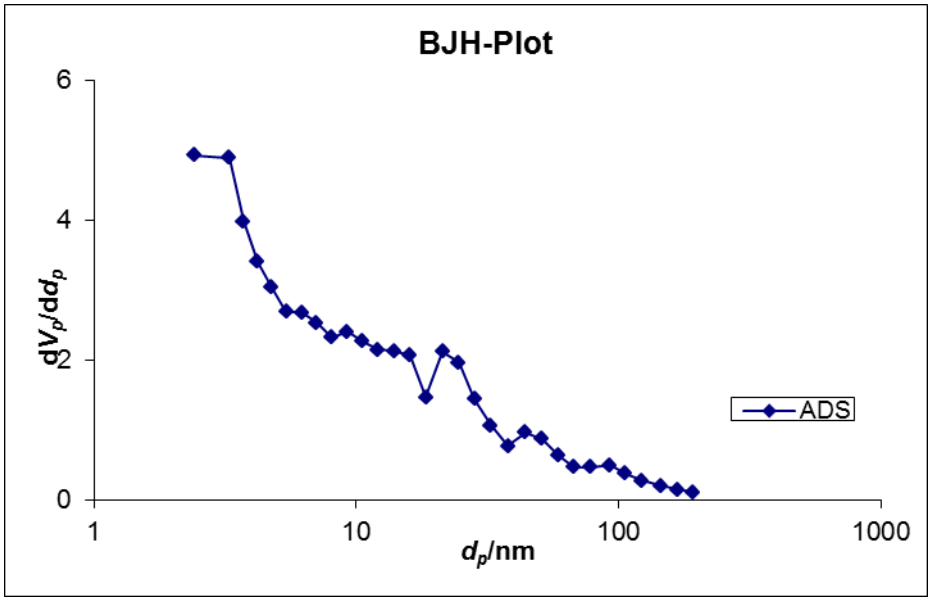

Figure A-3 BJH plot of raw bentonite

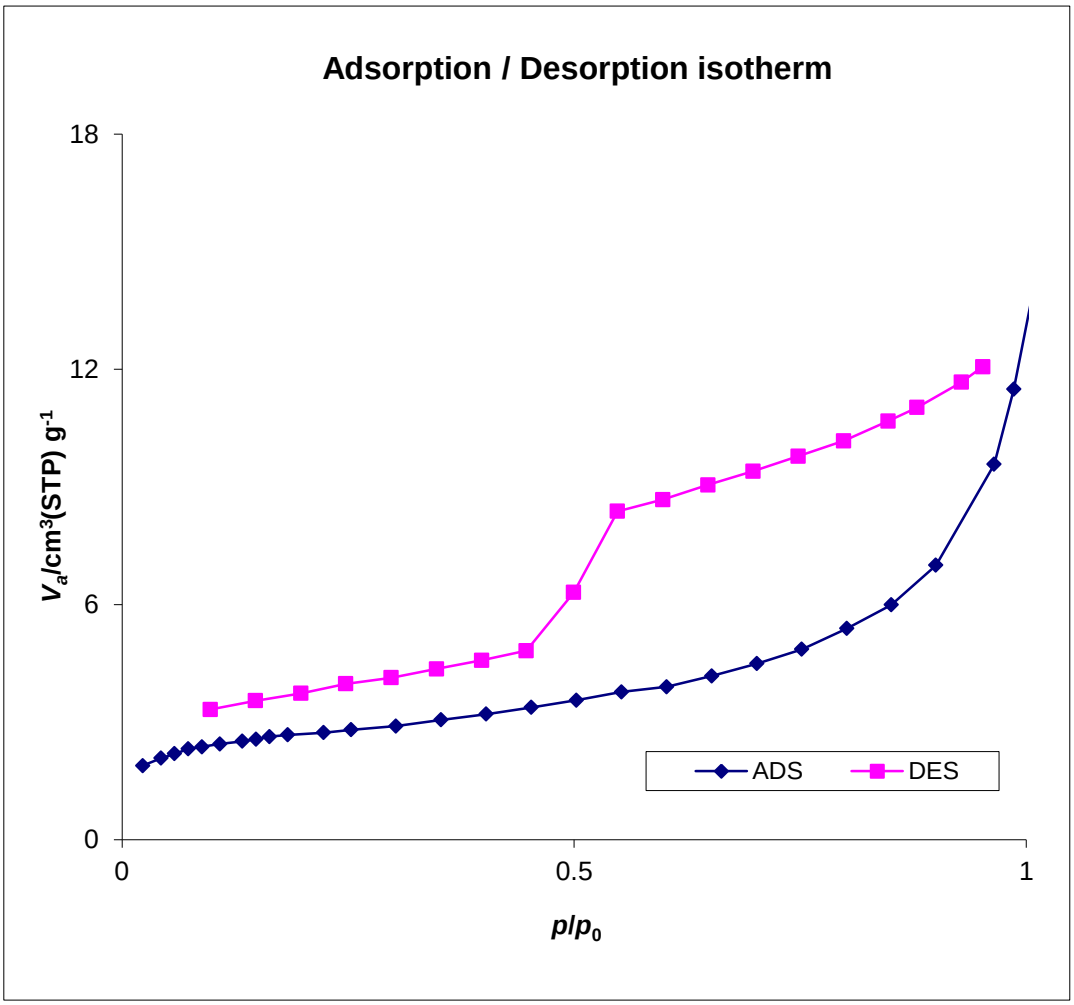

Figure A-4 N_2 adsorption-desorption isotherm of montmorillonite

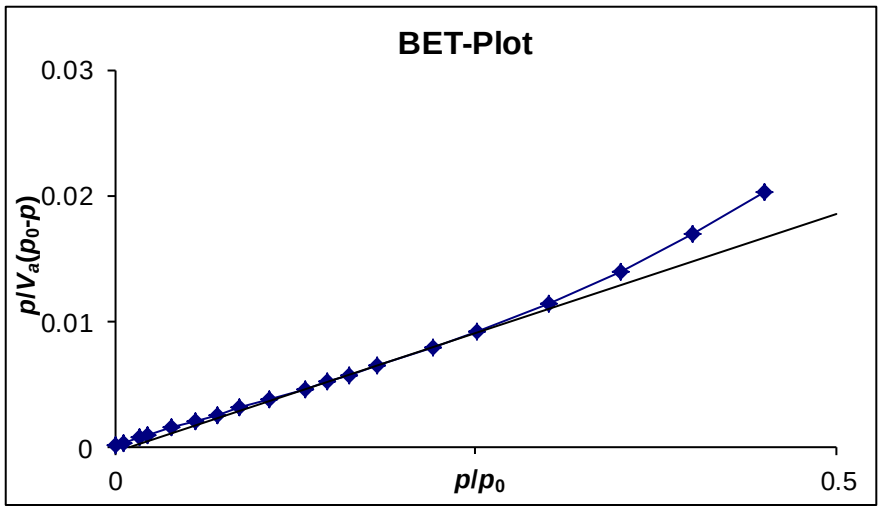

Figure A-5 N_2 adsorption-desorption isotherm of montmorillonite

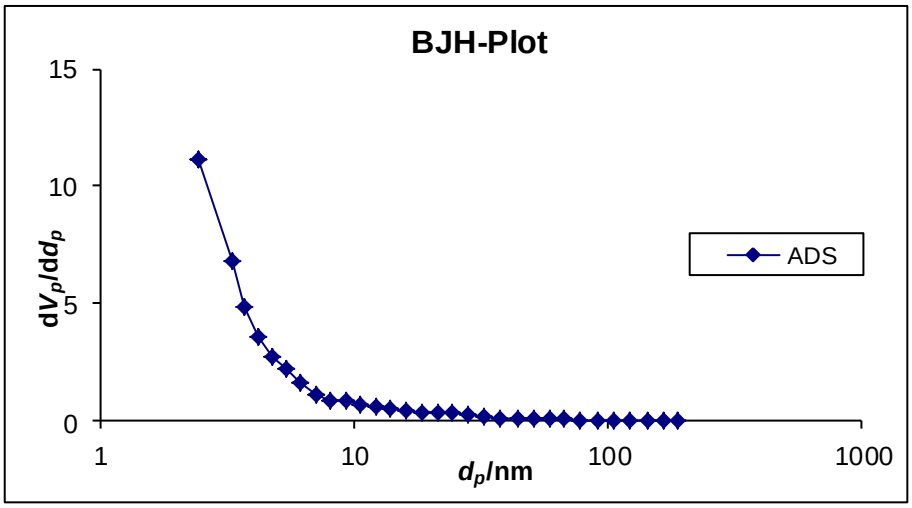

Figure A-6 BJH plot of montmorillonite

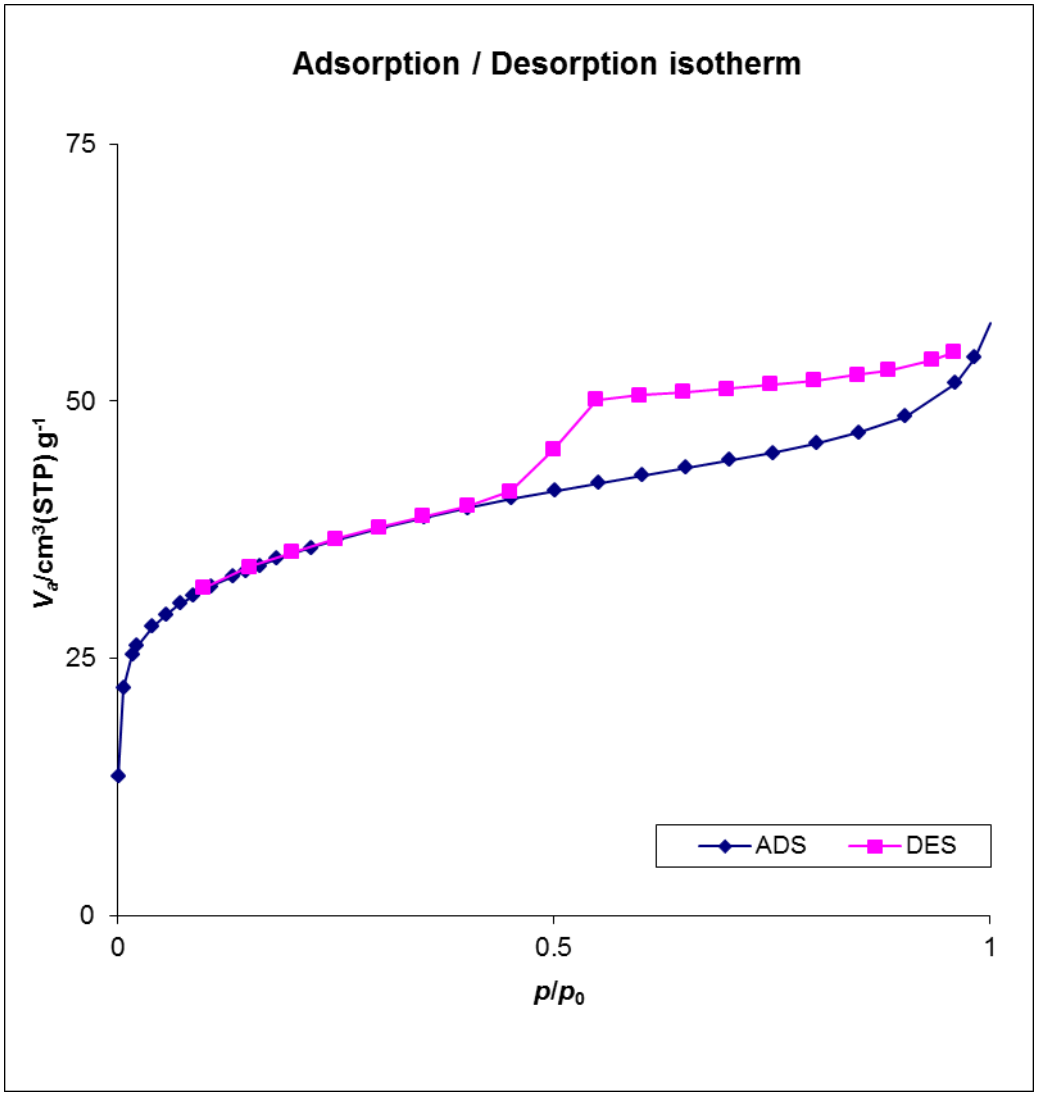

Figure A-7 N_2 adsorption-desorption isotherm of Na-montmorillonite

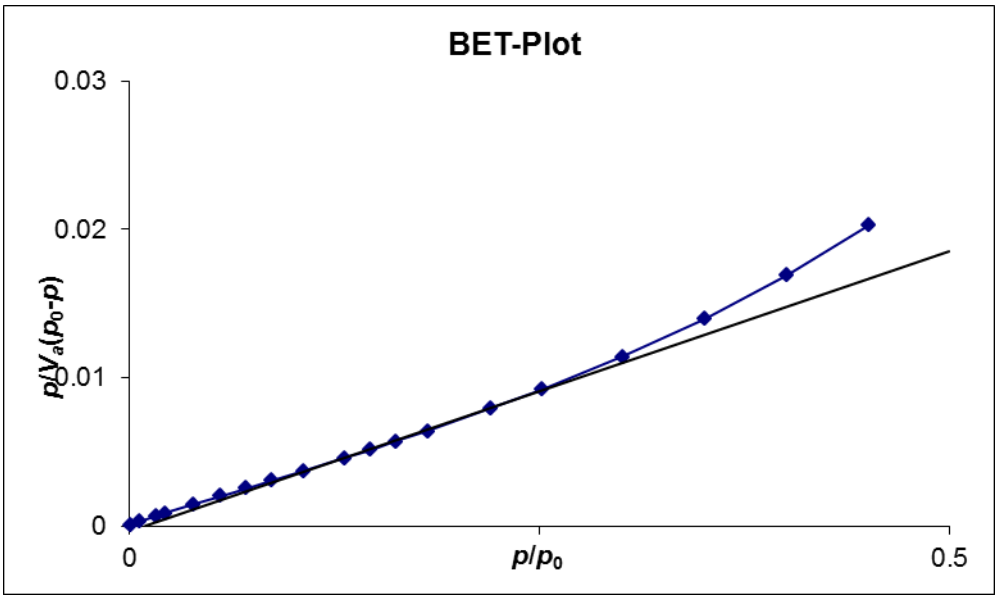

Figure A-8 BET plot of Na-montmorillonite

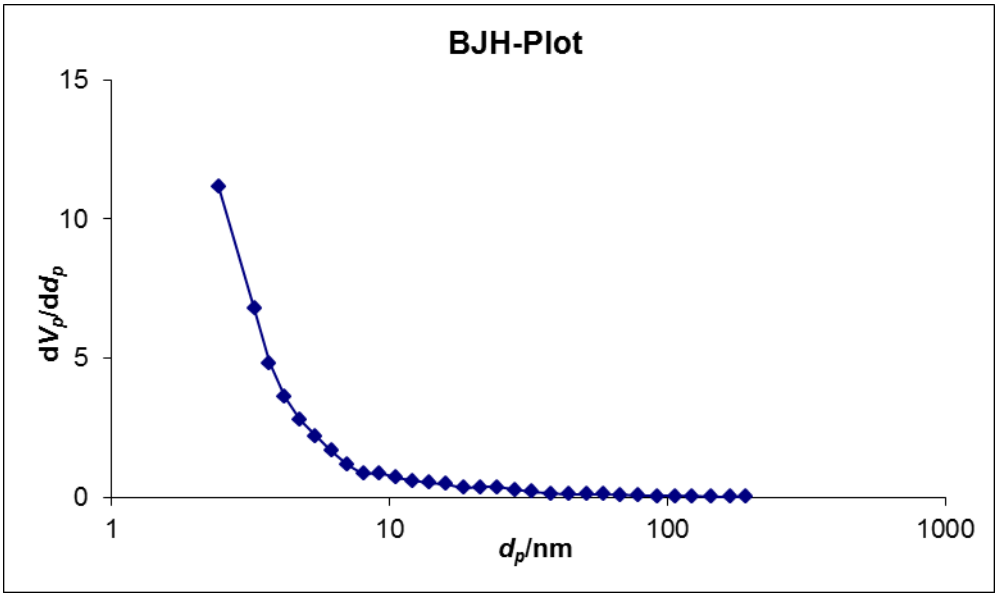

Figure A-9 BJH plot of Na-montmorillonite

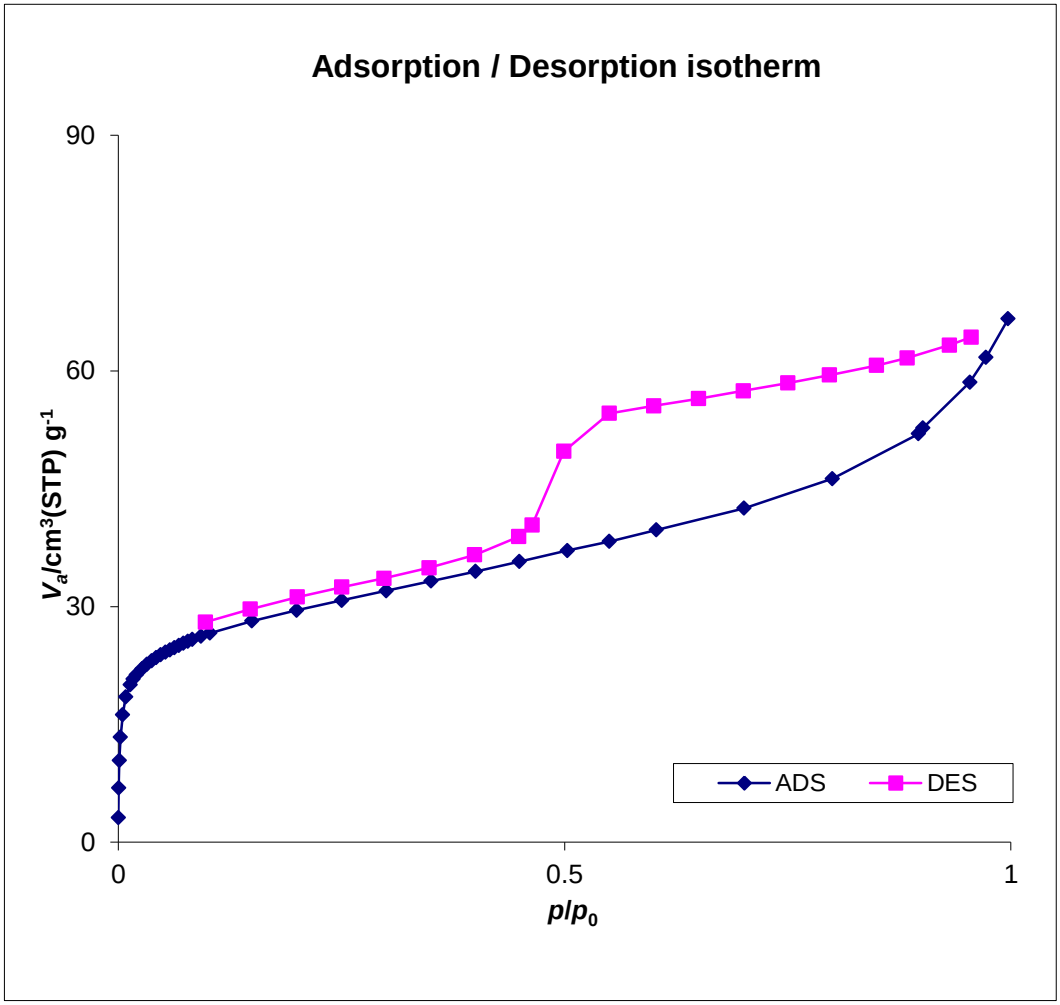

Figure A-10 N_2 adsorption-desorption isotherm of Al-PLB

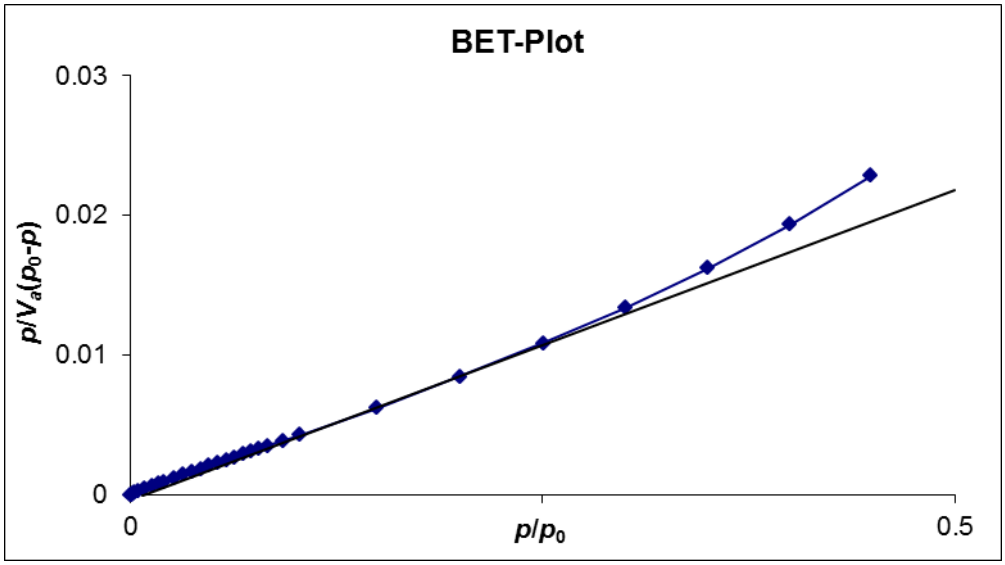

Figure A-11 N_2 adsorption-desorption isotherm of Al-PLB

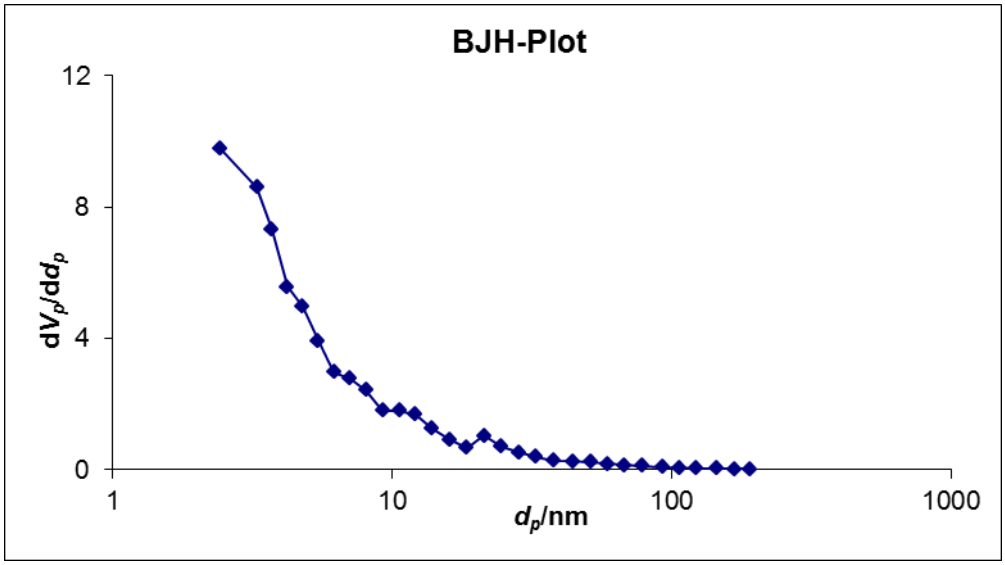

Figure A-12 N_2 adsorption-desorption isotherm of Al-PLB

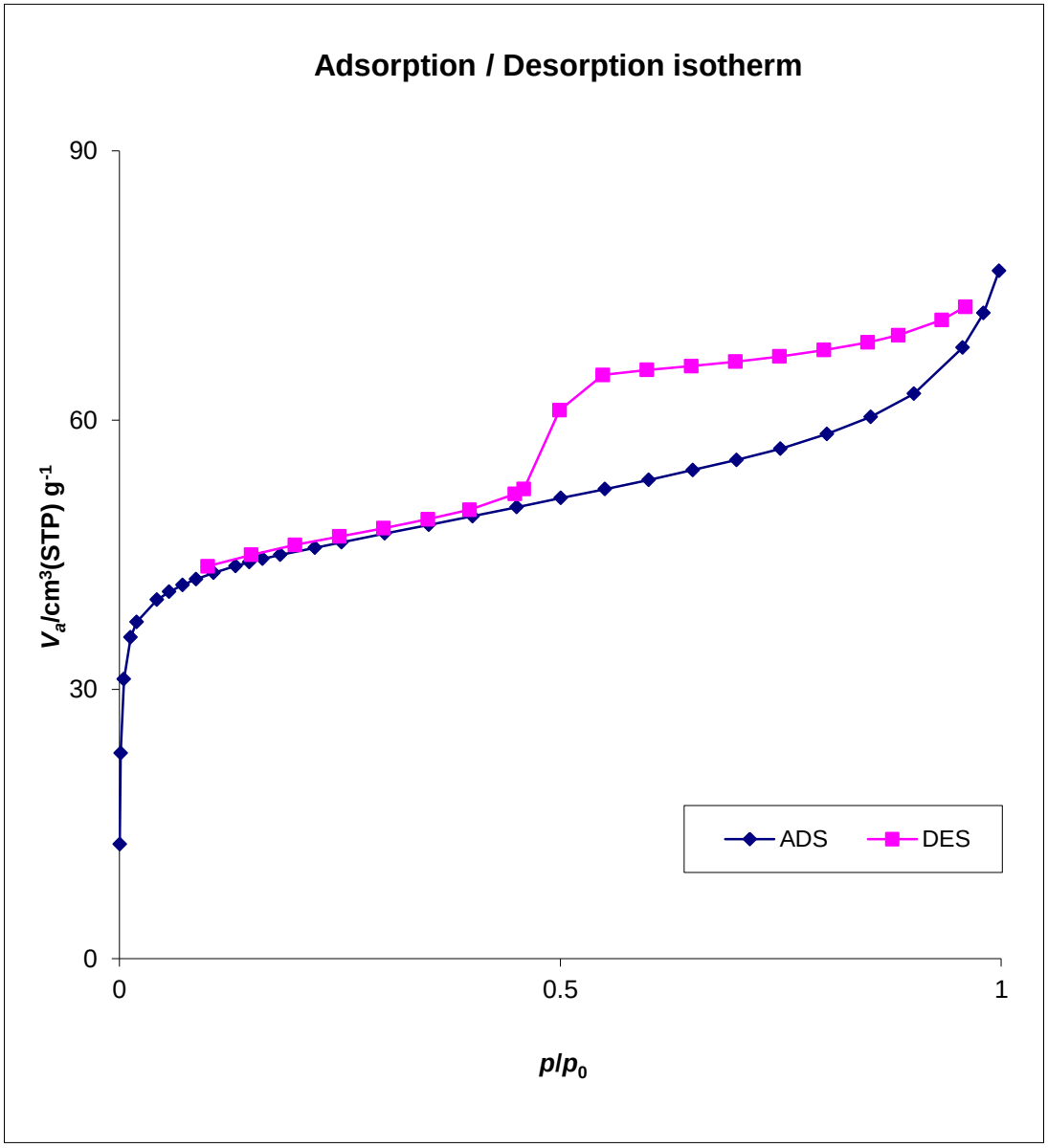

Figure A-13 N_2 adsorption-desorption isotherm of $InCl_3$/Al-PLB

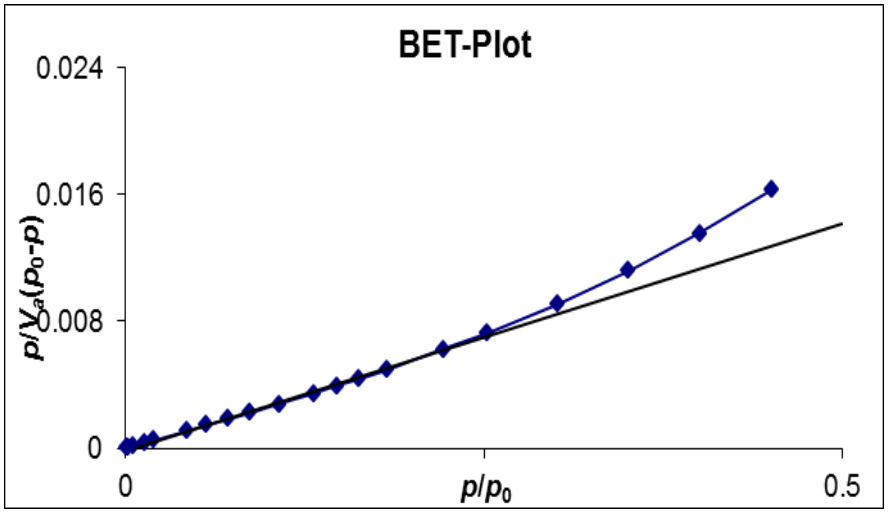

Figure A-14 N_2 adsorption-desorption isotherm of $InCl_3$/Al-PLB

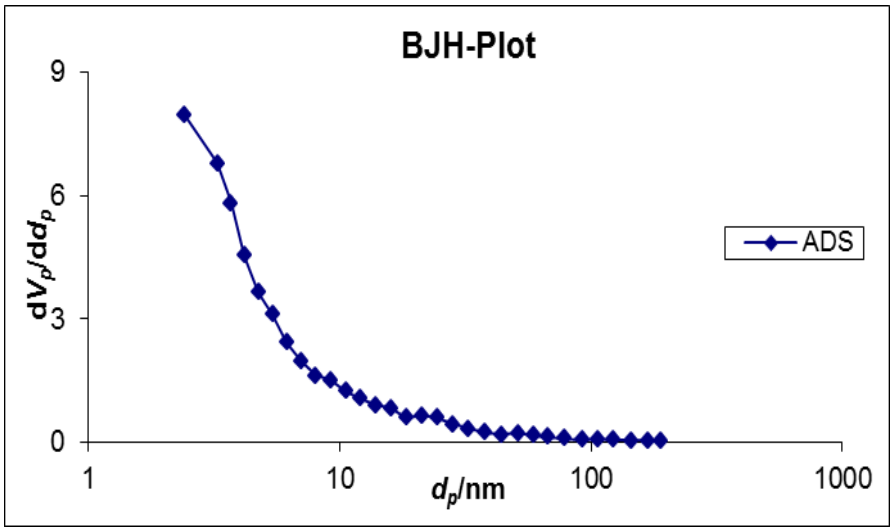

Figure A-15 N_2 adsorption-desorption isotherm of $InCl_3$/Al-PLB

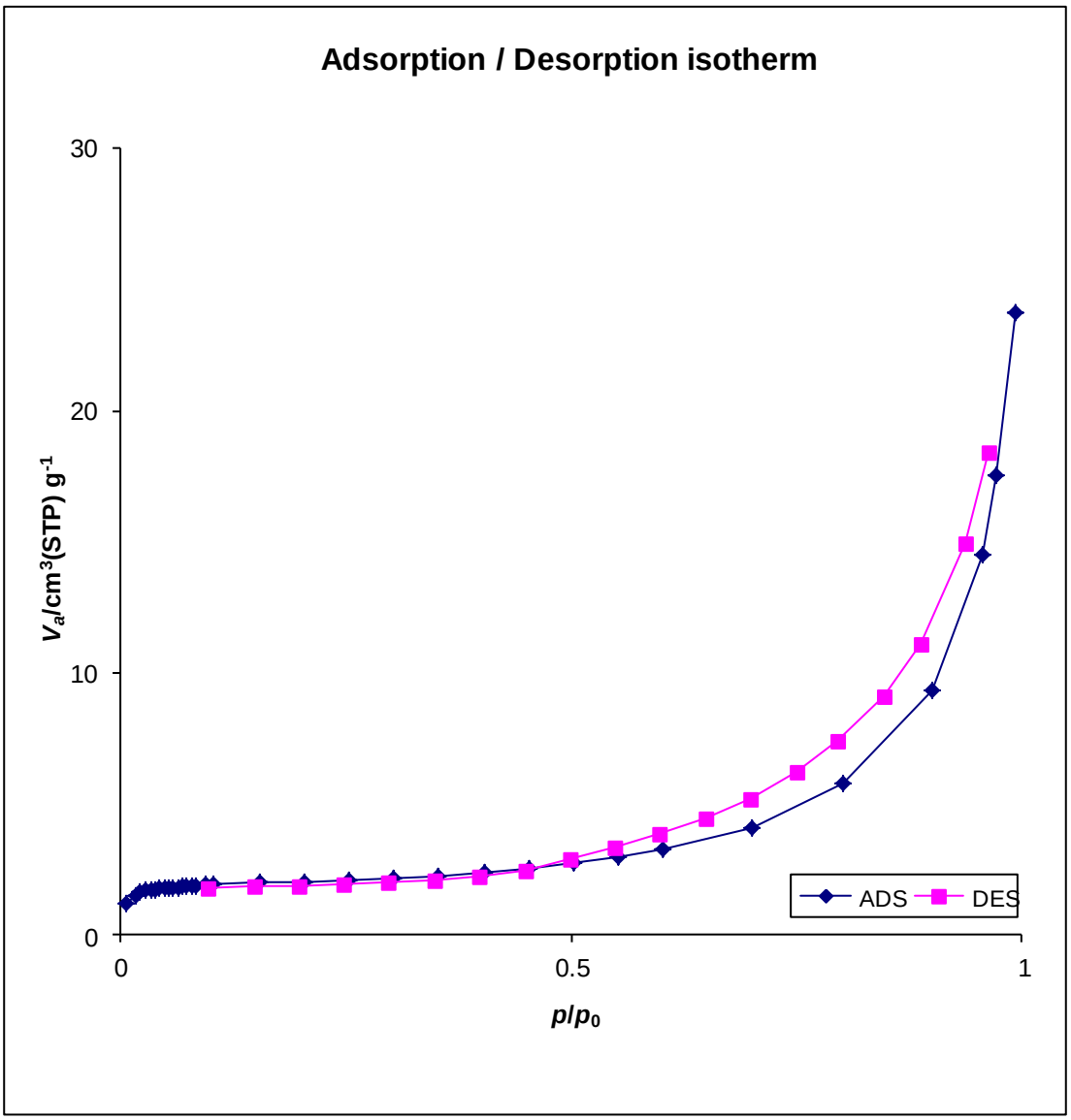

Figure A-16 N_2 adsorption-desorption isotherm of $LaCl_3$/Al-PLB

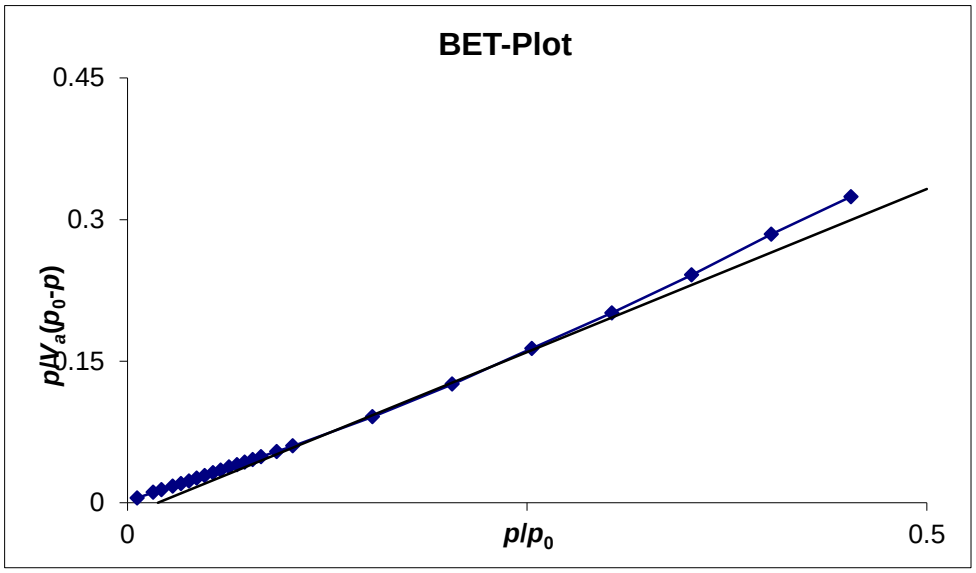

Figure A-17 BET plot of $LaCl_3$/Al-PLB

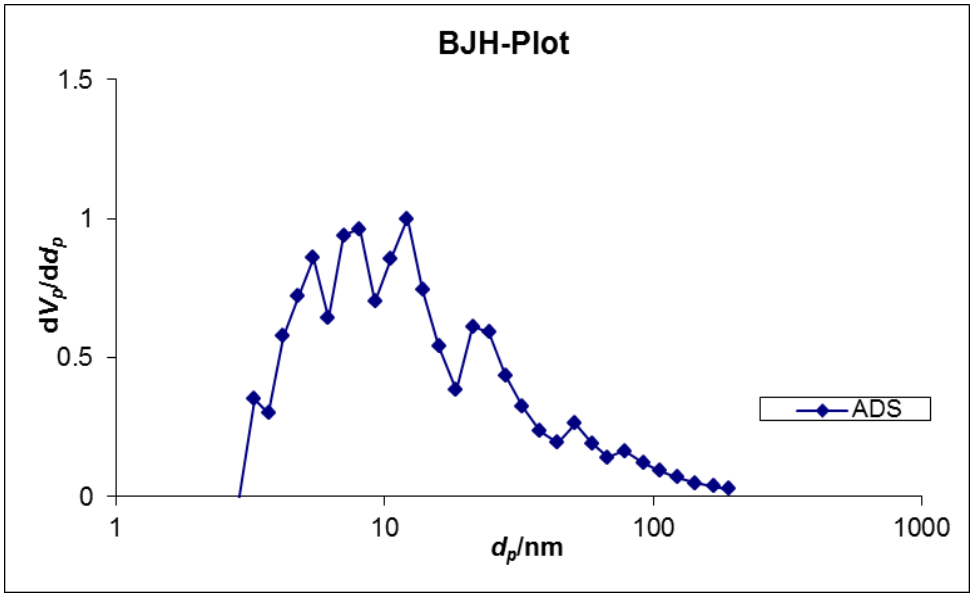

Figure A-18 BJH plot of $LaCl_3$/Al-PLB

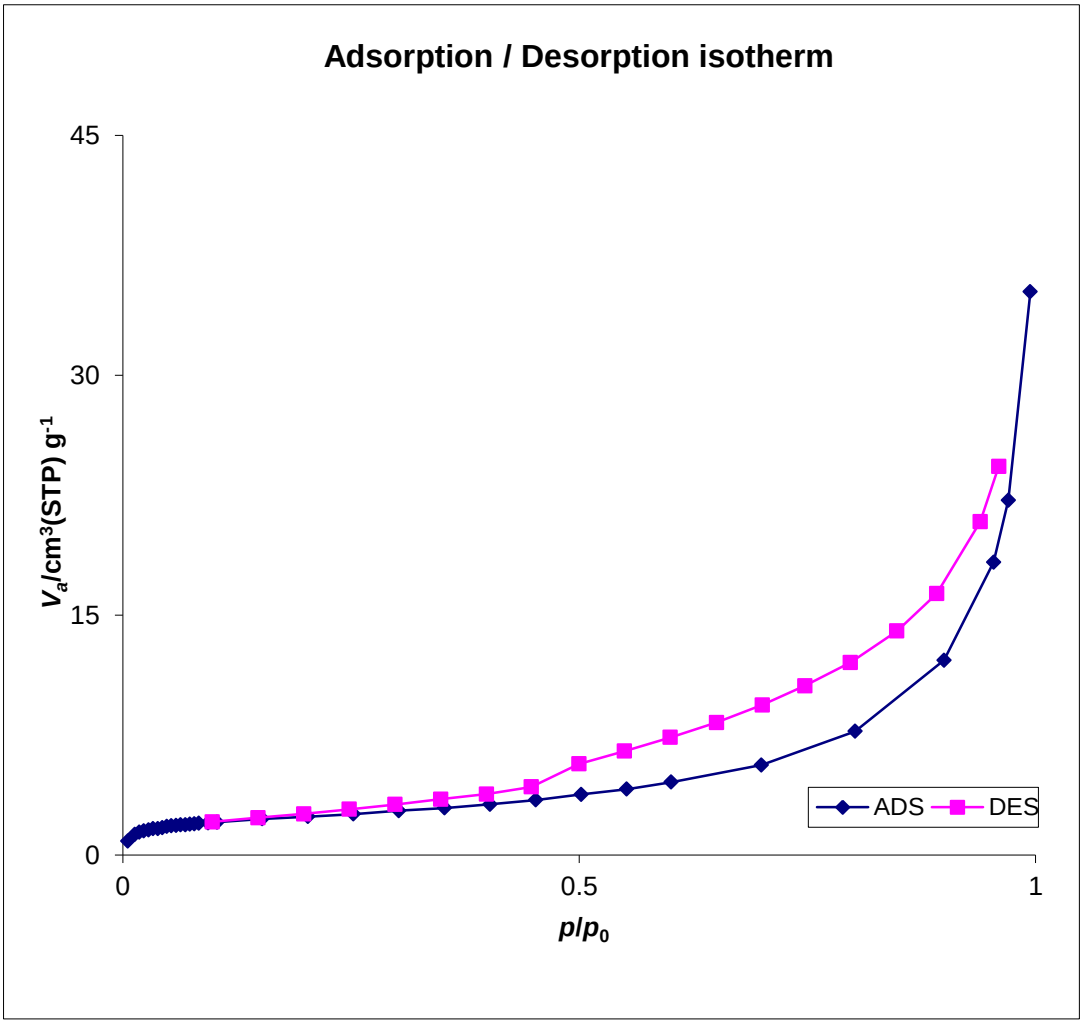

Figure A-19 N_2 adsorption-desorption isotherm of $CeCl_3$/Al-PLB

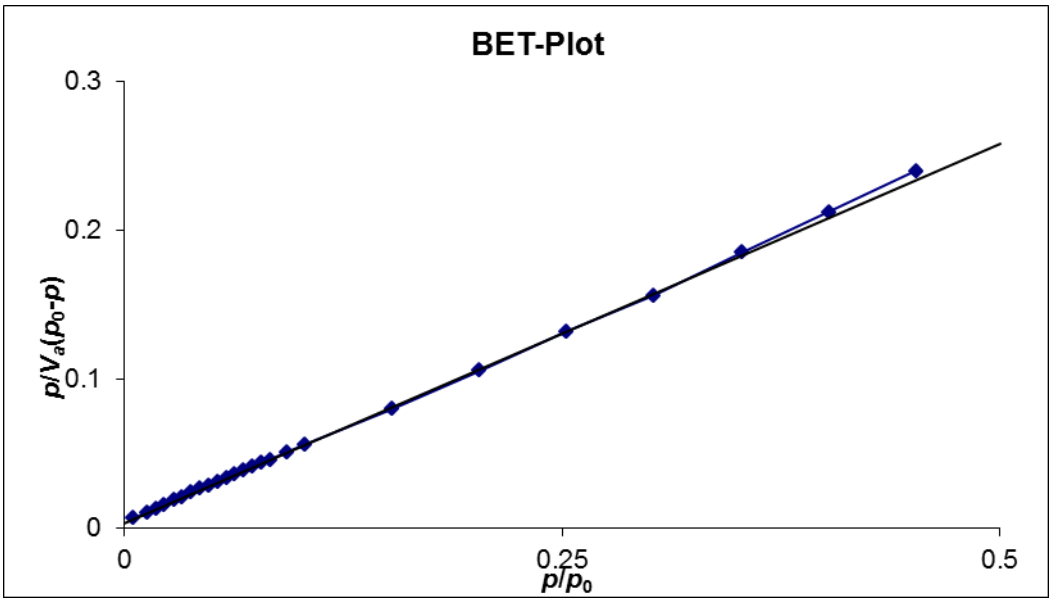

Figure A-20 BET plot of $CeCl_3$/Al-PLB

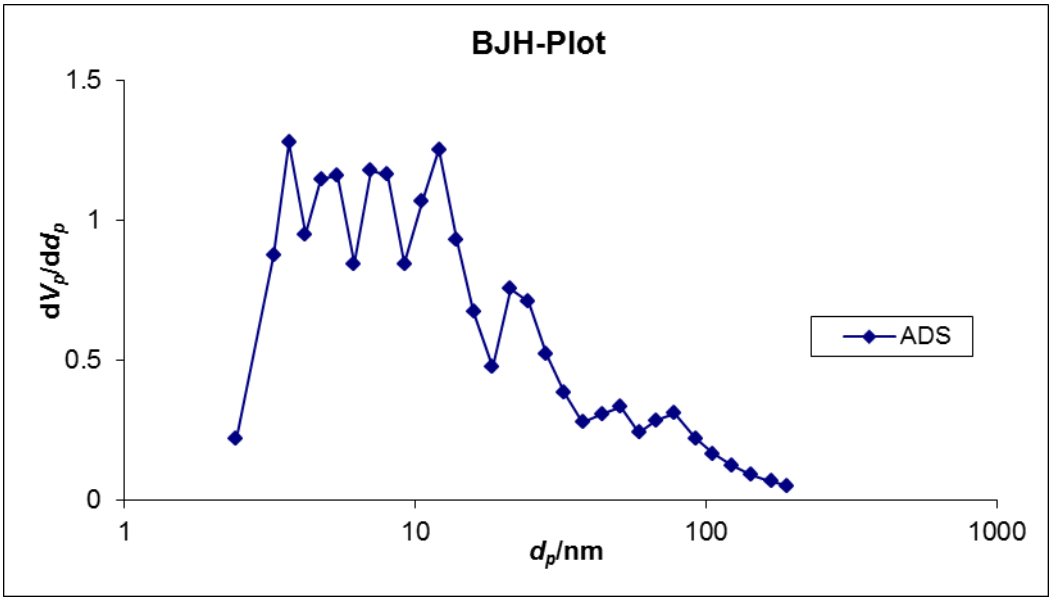

Figure A-21 BJH plot of $CeCl_3$/Al-PLB

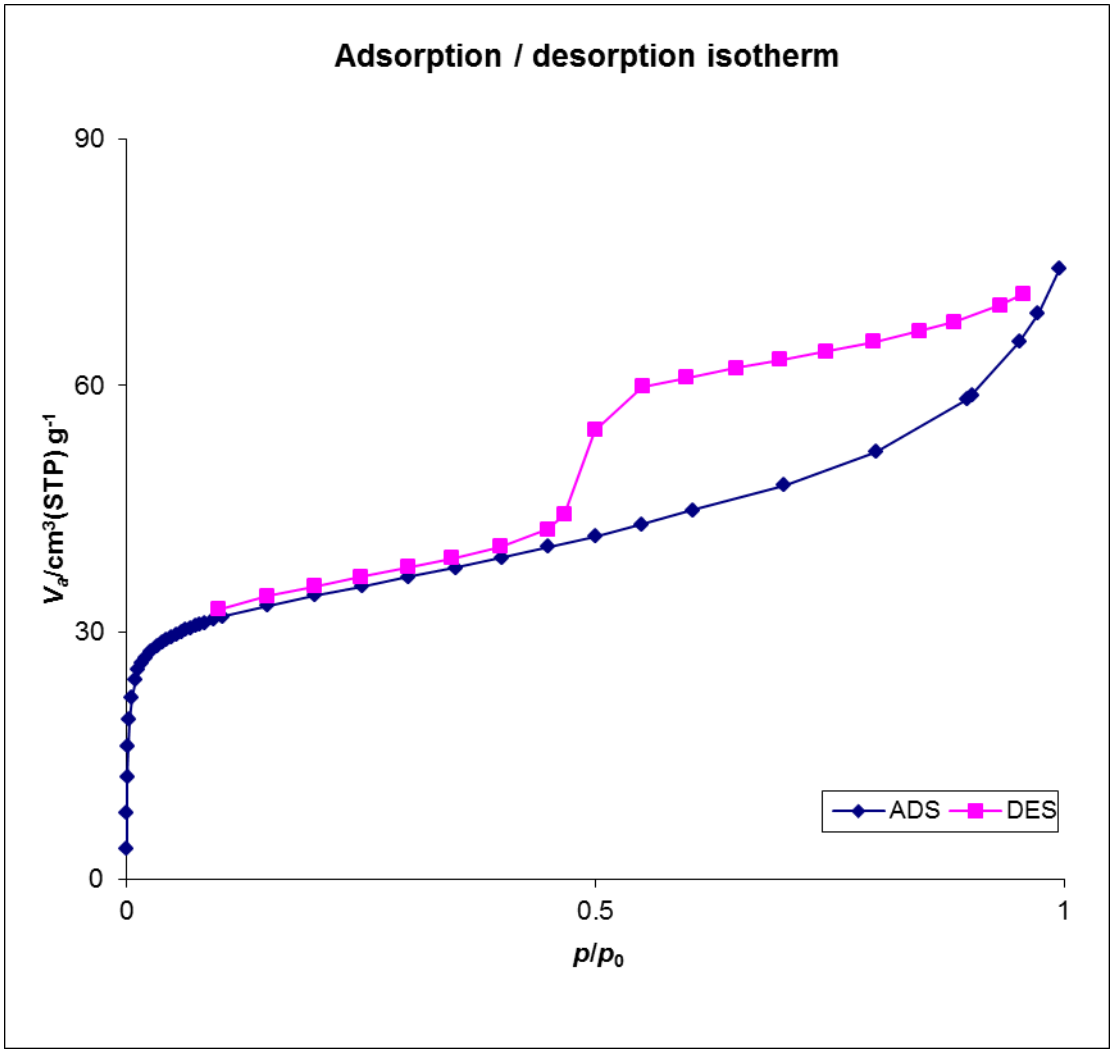

Figure A-22 N_2 adsorption-desorption isotherm of $NdCl_3$/Al-PLB

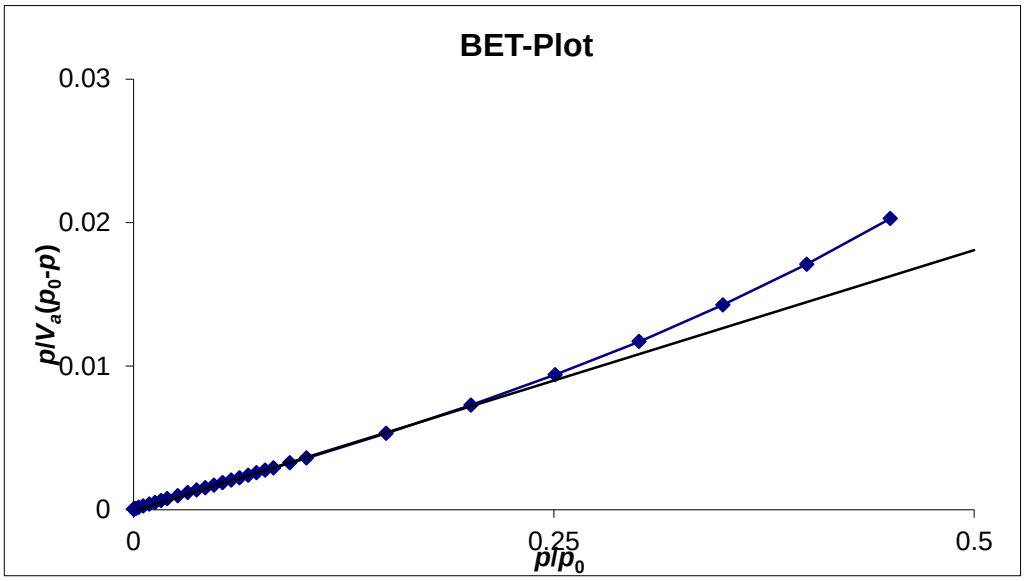

Figure A-23 BET plot of $NdCl_3$/Al-PLB

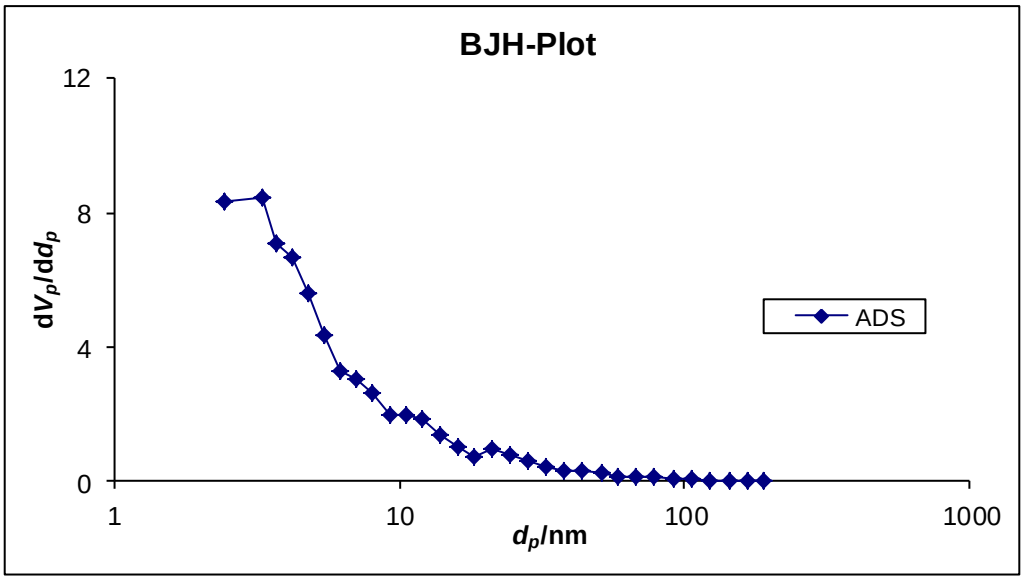

Figure A-24 BJH plot of $NdCl_3$/Al-PLB

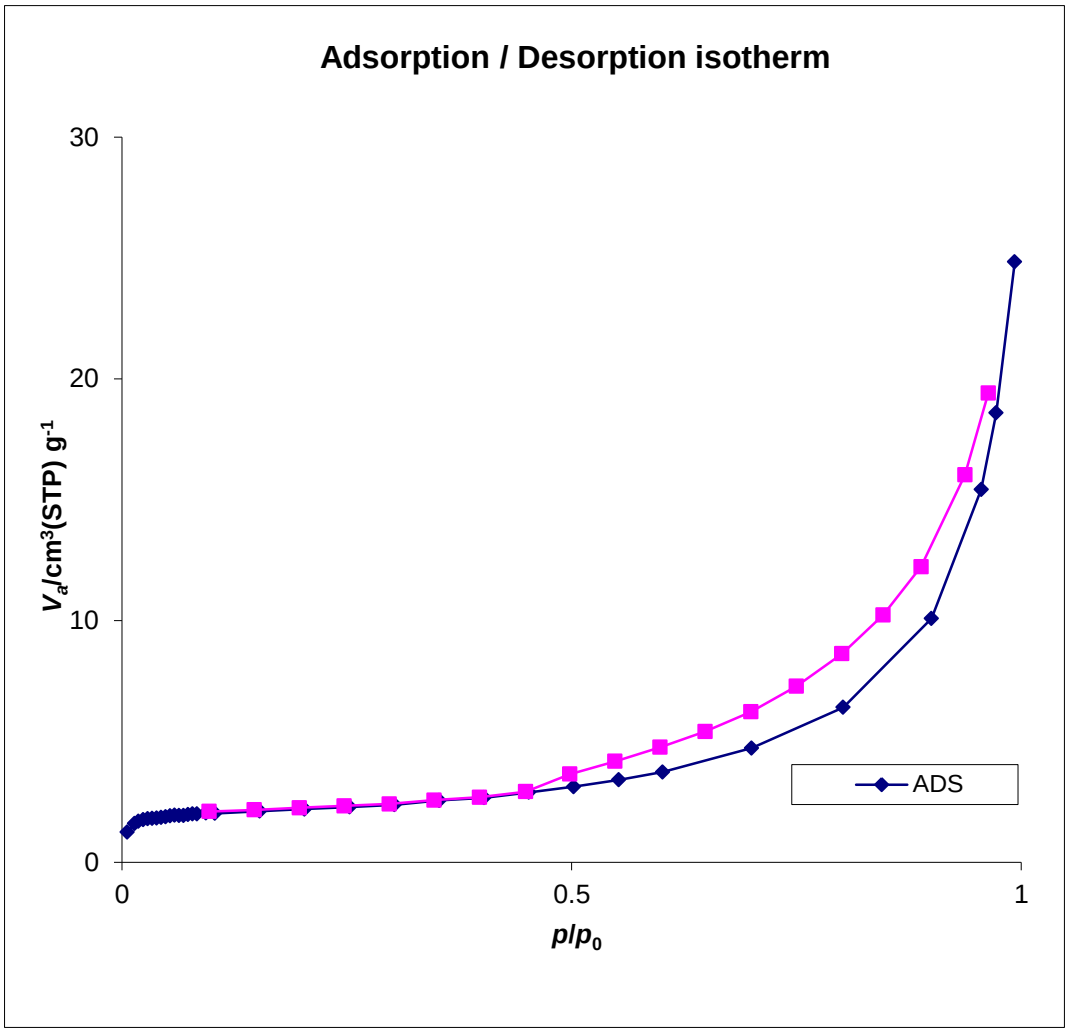

Figure A-25 N_2 adsorption-desorption isotherm of $GdCl_3$/Al-PLB

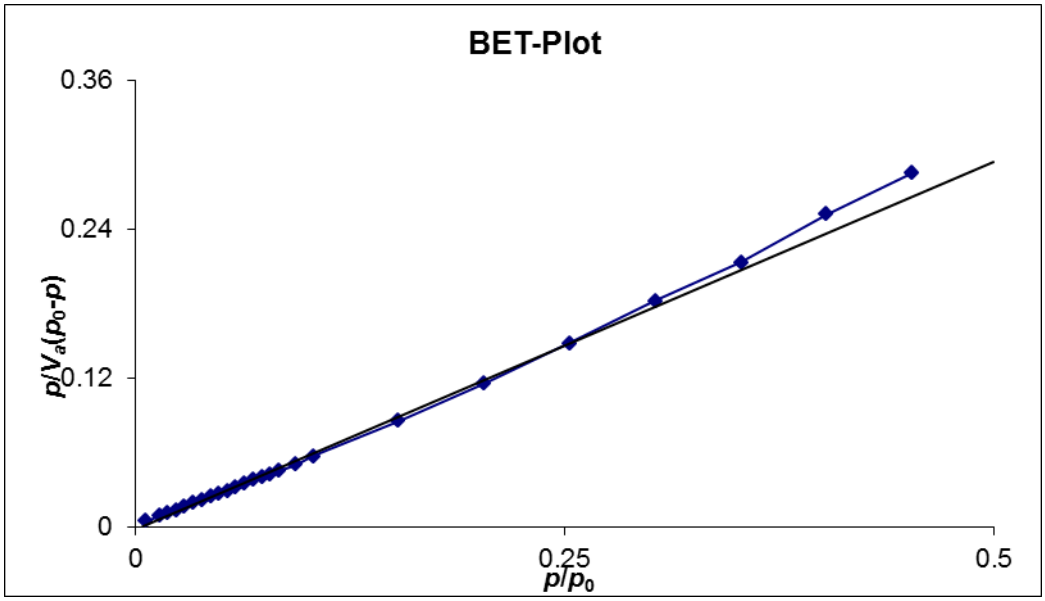

Figure A-26 BET plot of $GdCl_3$/Al-PLB

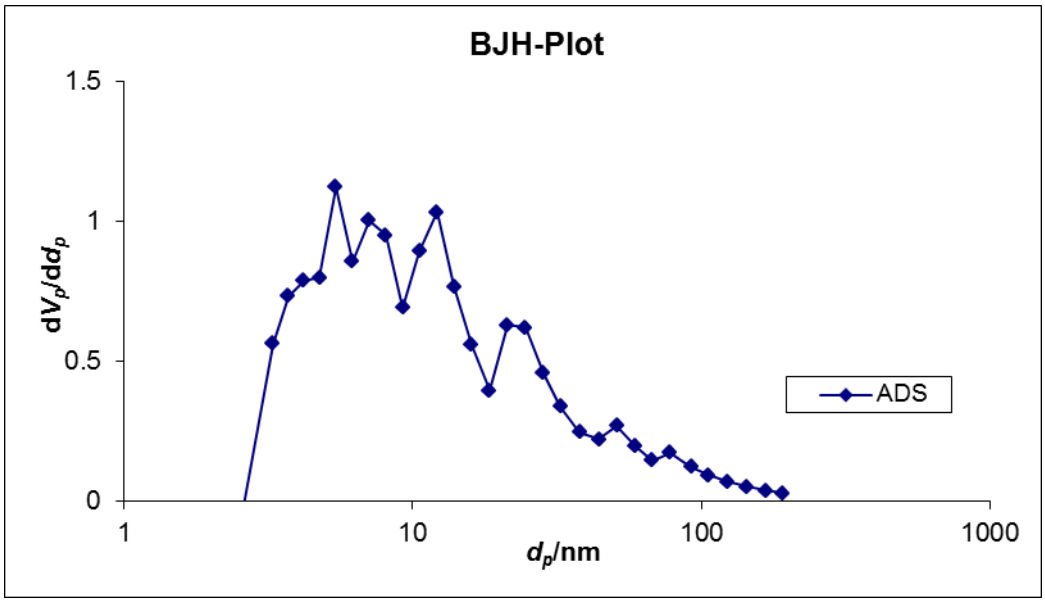

Figure A-27 BJH plot of $GdCl_3$/Al-PLB

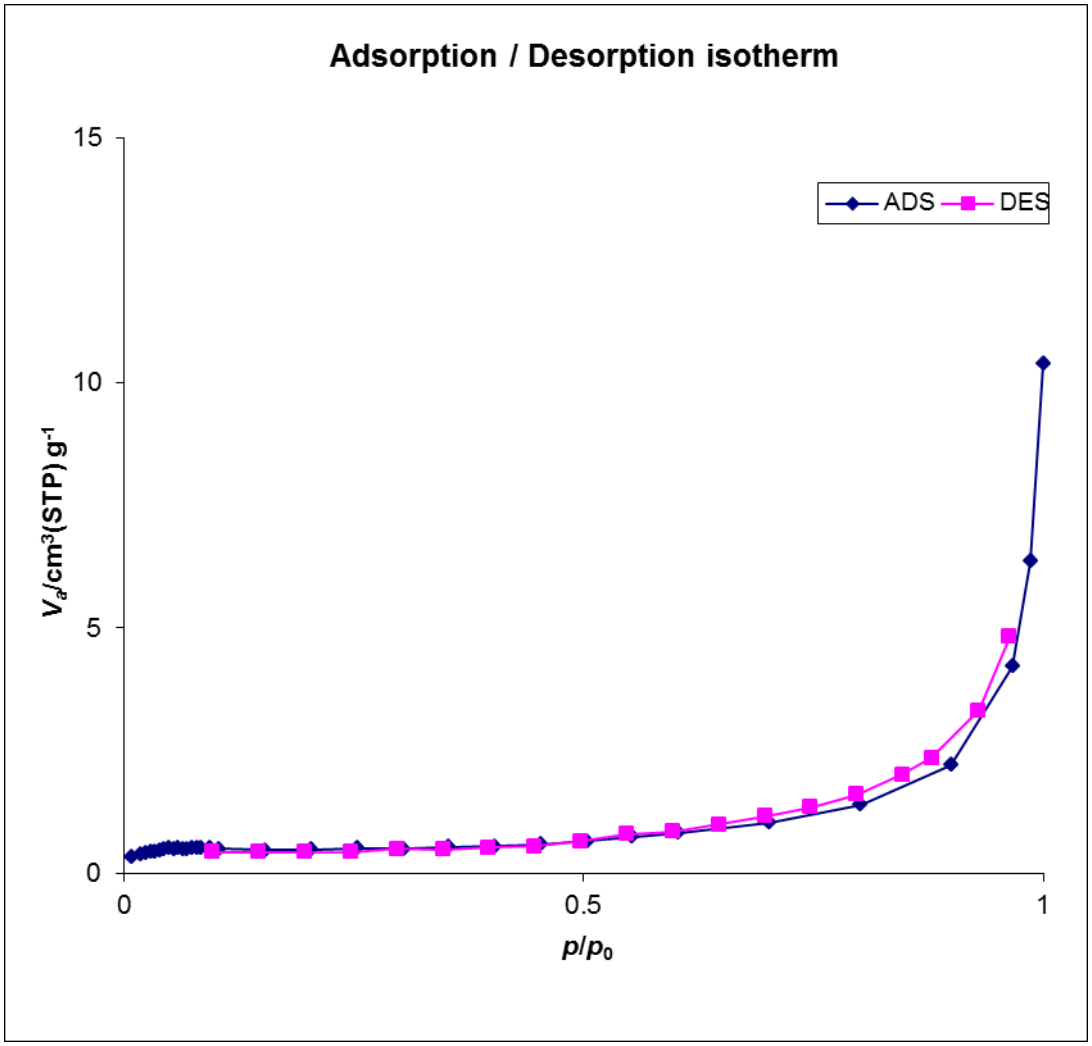

Figure A-28 N_2 adsorption-desorption isotherm of Li-TN

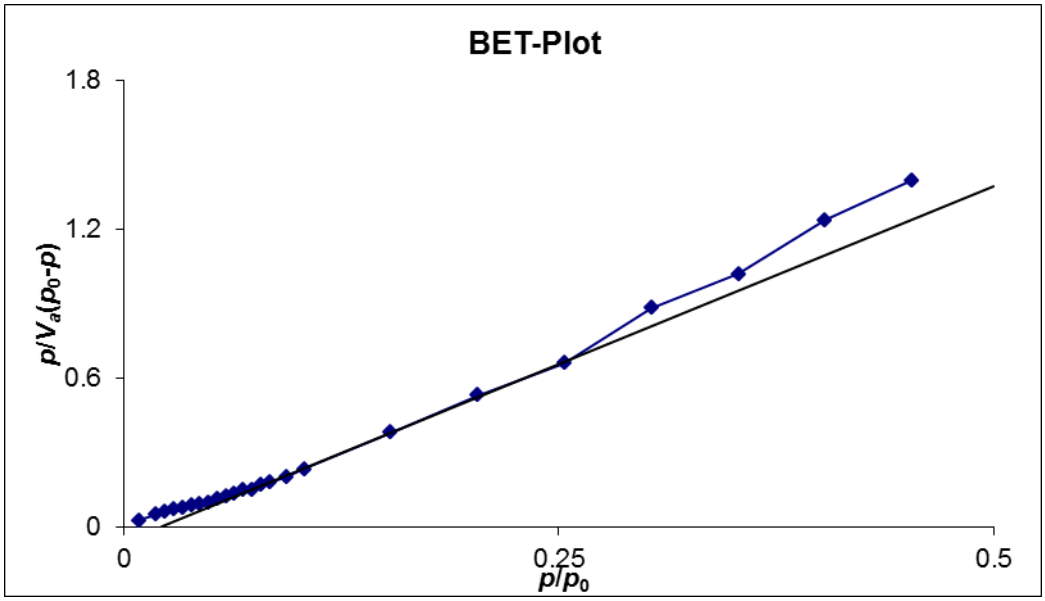

Figure A-29 BET plot of Li-TN

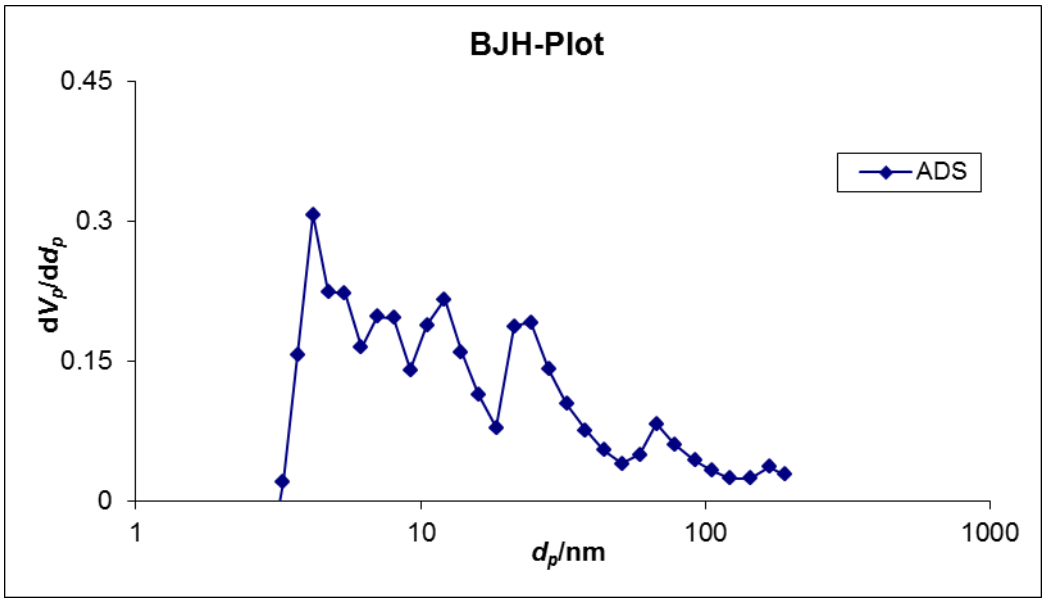

Figure A-30 BJH plot of Li-TN

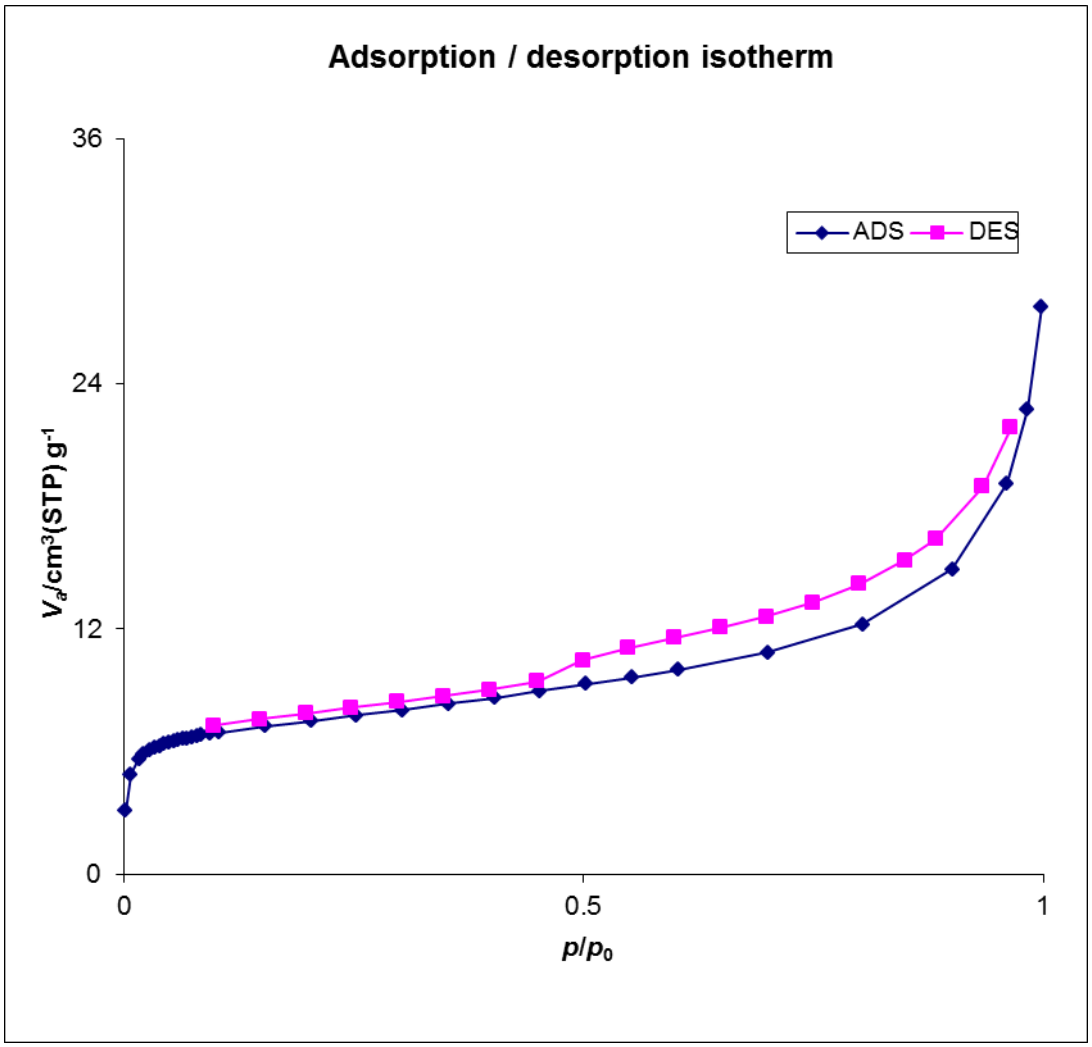

Figure A-31 N_2 adsorption-desorption isotherm of BAl-PLT

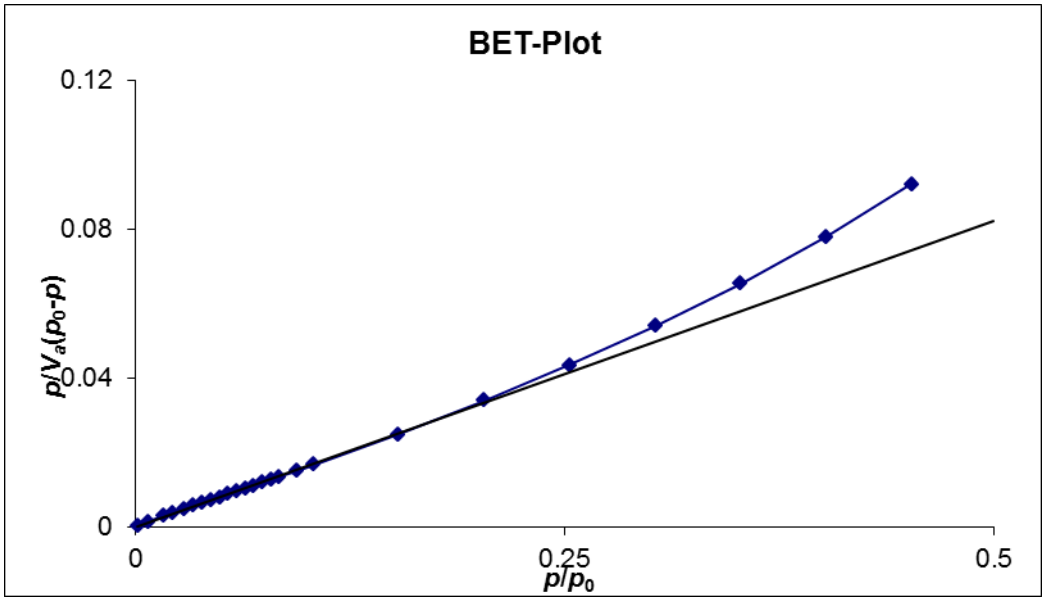

Figure A-32 BET plot of BAl-PLB

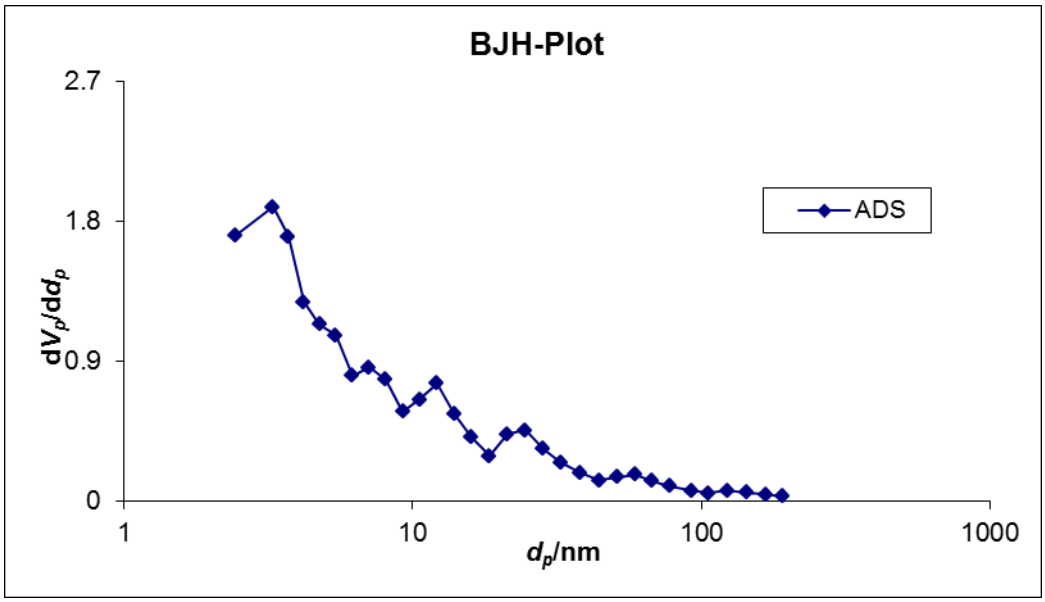

Figure A-33 BJH plot of BAl-PLB

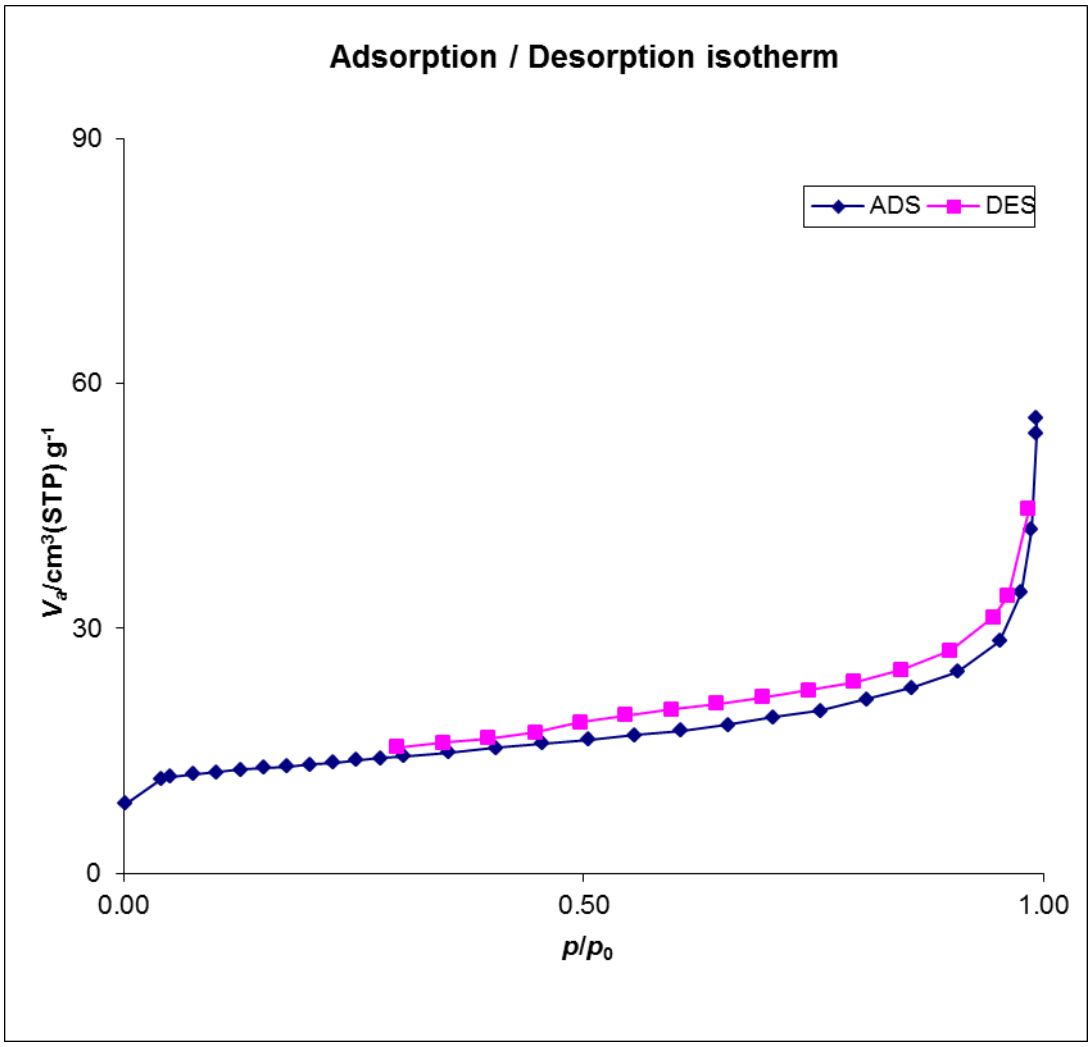

Figure A-34 N_2 adsorption-desorption isotherm of Al-PLT at 400°C

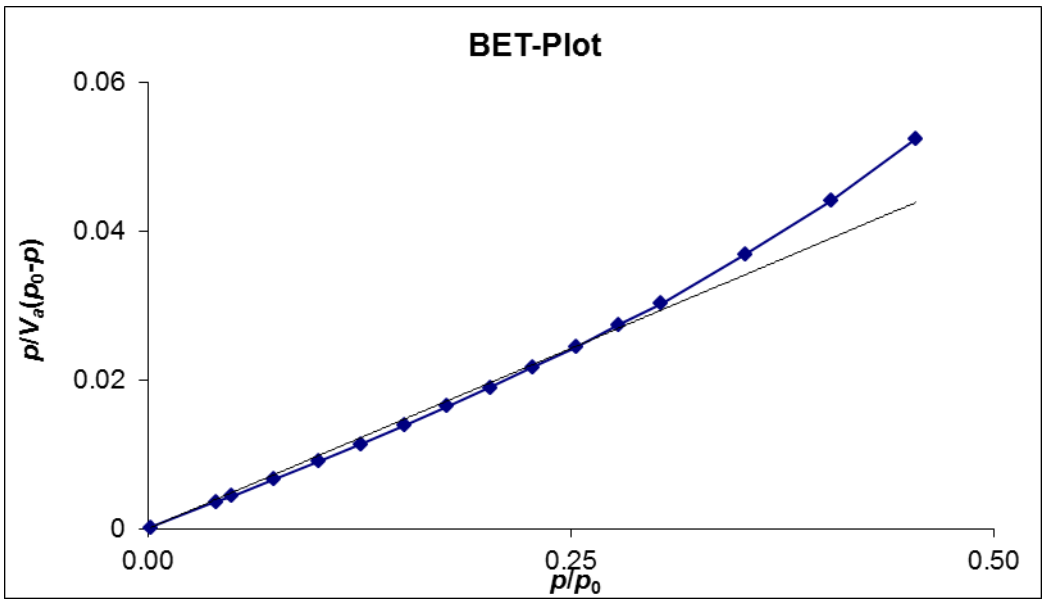

Figure A-35 BET plot of Al-PLT at 400°C

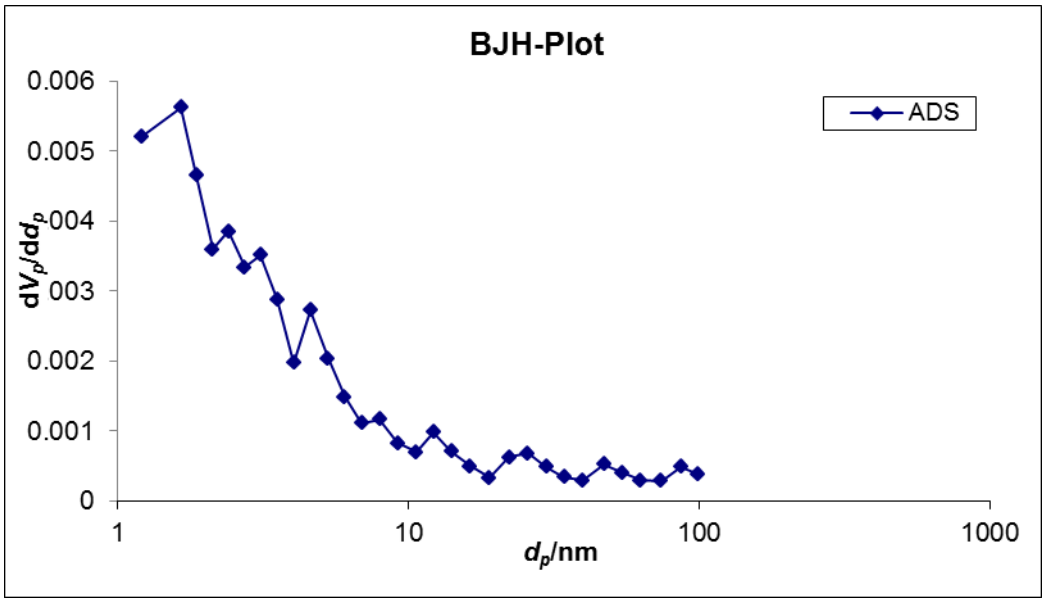

Figure A-36 BJH plot of Al-PLT at 400°C

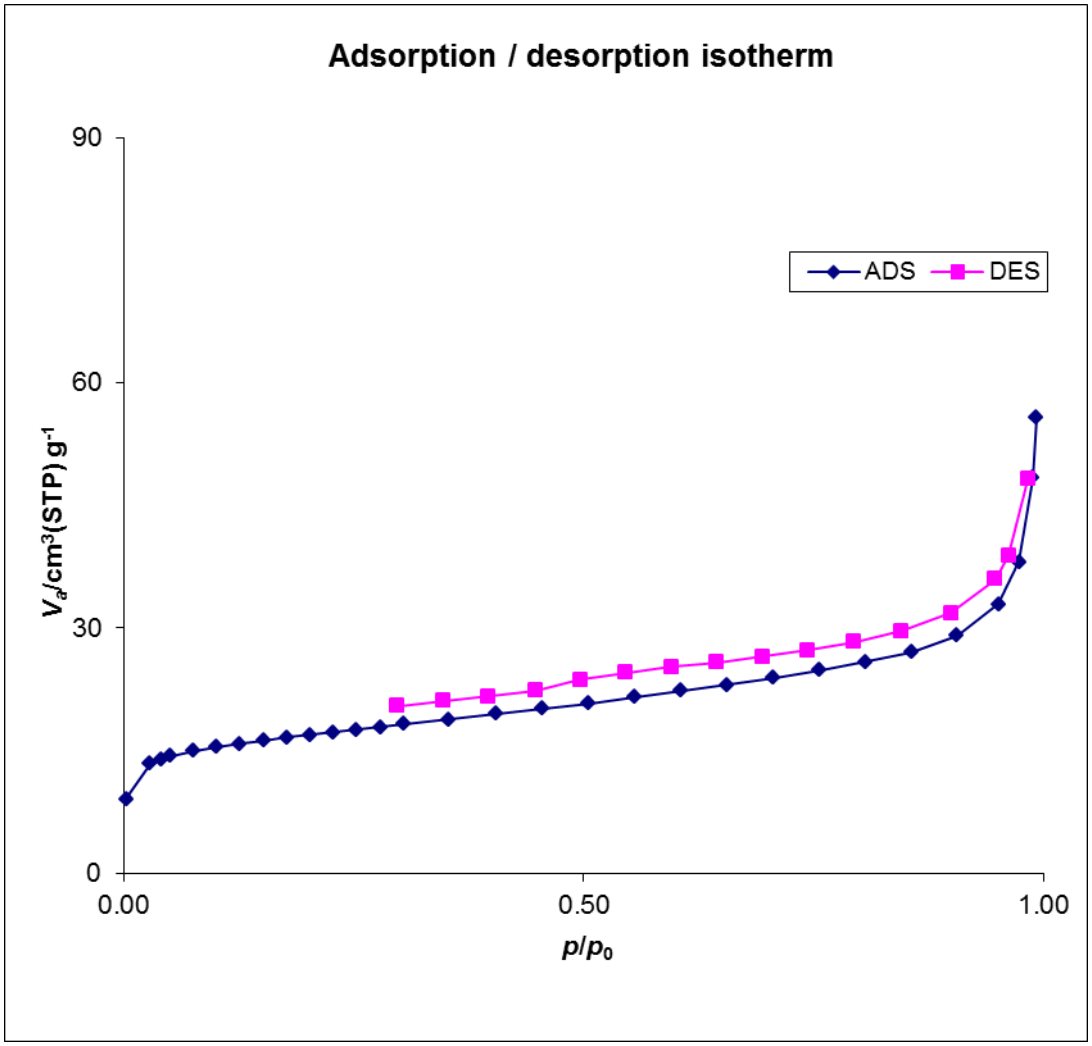

Figure A-37 N_2 adsorption-desorption isotherm of Al-PLT at 450°C

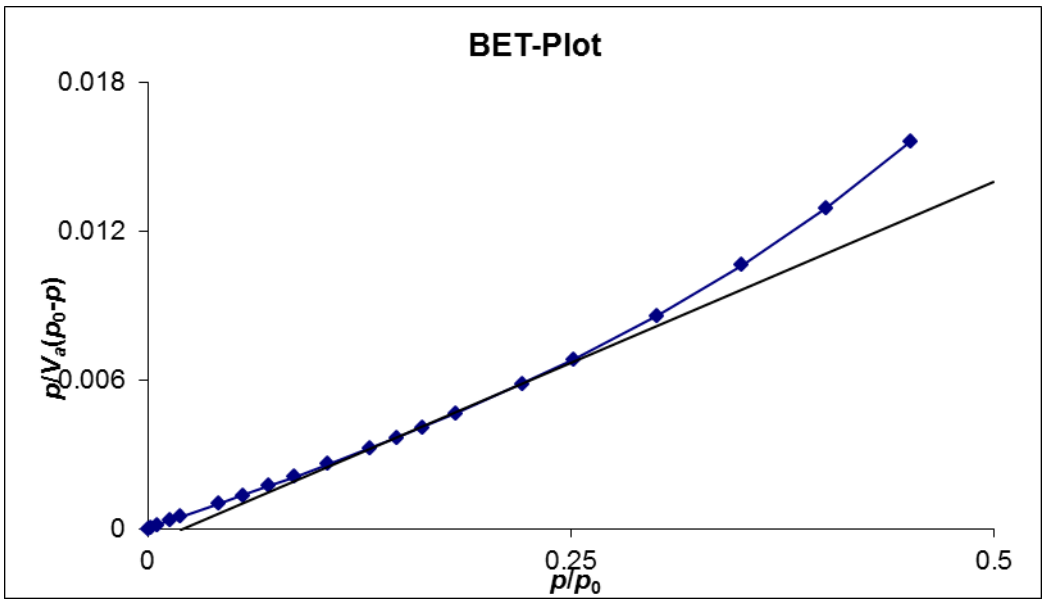

Figure A-38 BET plot of Al-PLT at 450°C

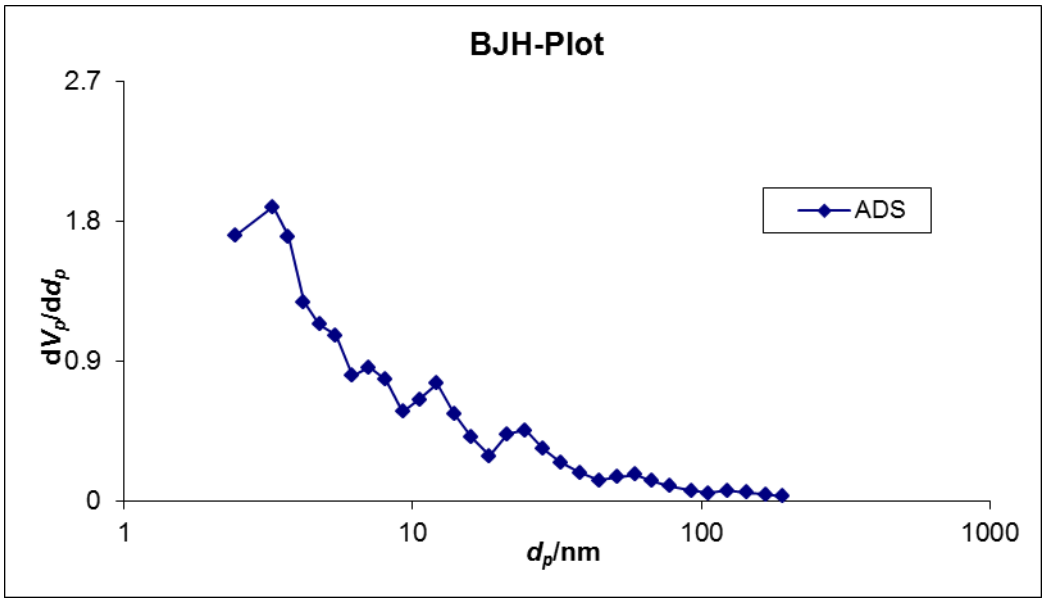

Figure A-39 BJH plot of Al-PLT at 450°C

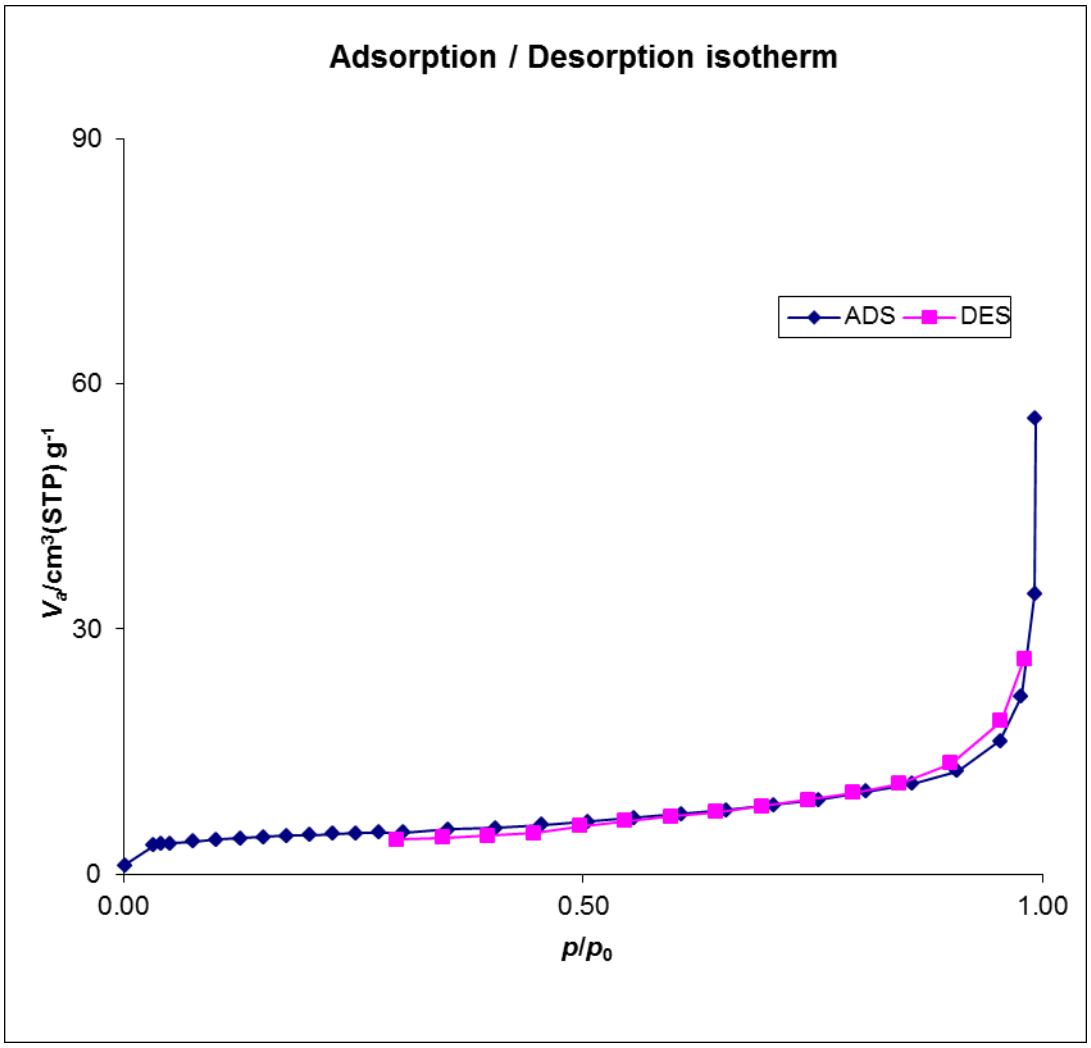

Figure A-40 N_2 adsorption-desorption isotherm of Al-PLT at 500°C

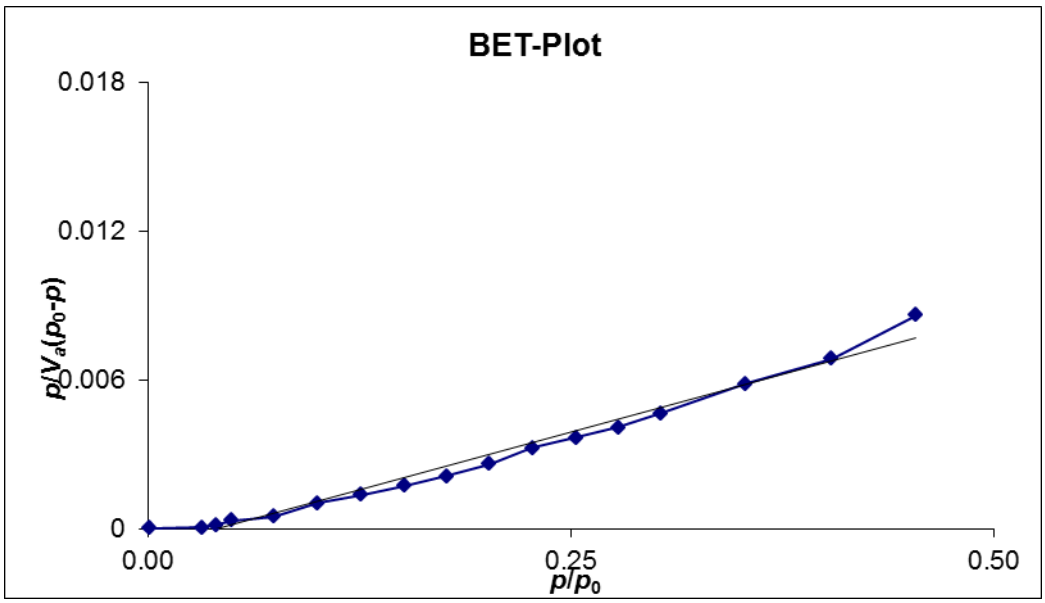

Figure A-41 BET plot of Al-PLT at 500°C

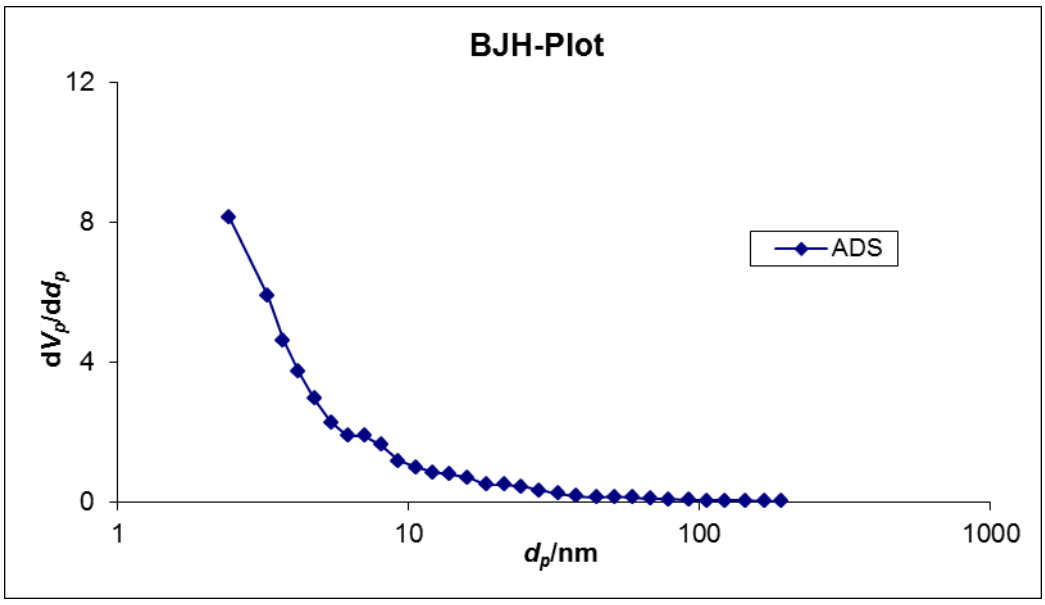

Figure A-42 BJH plot of Al-PLT at 500°C

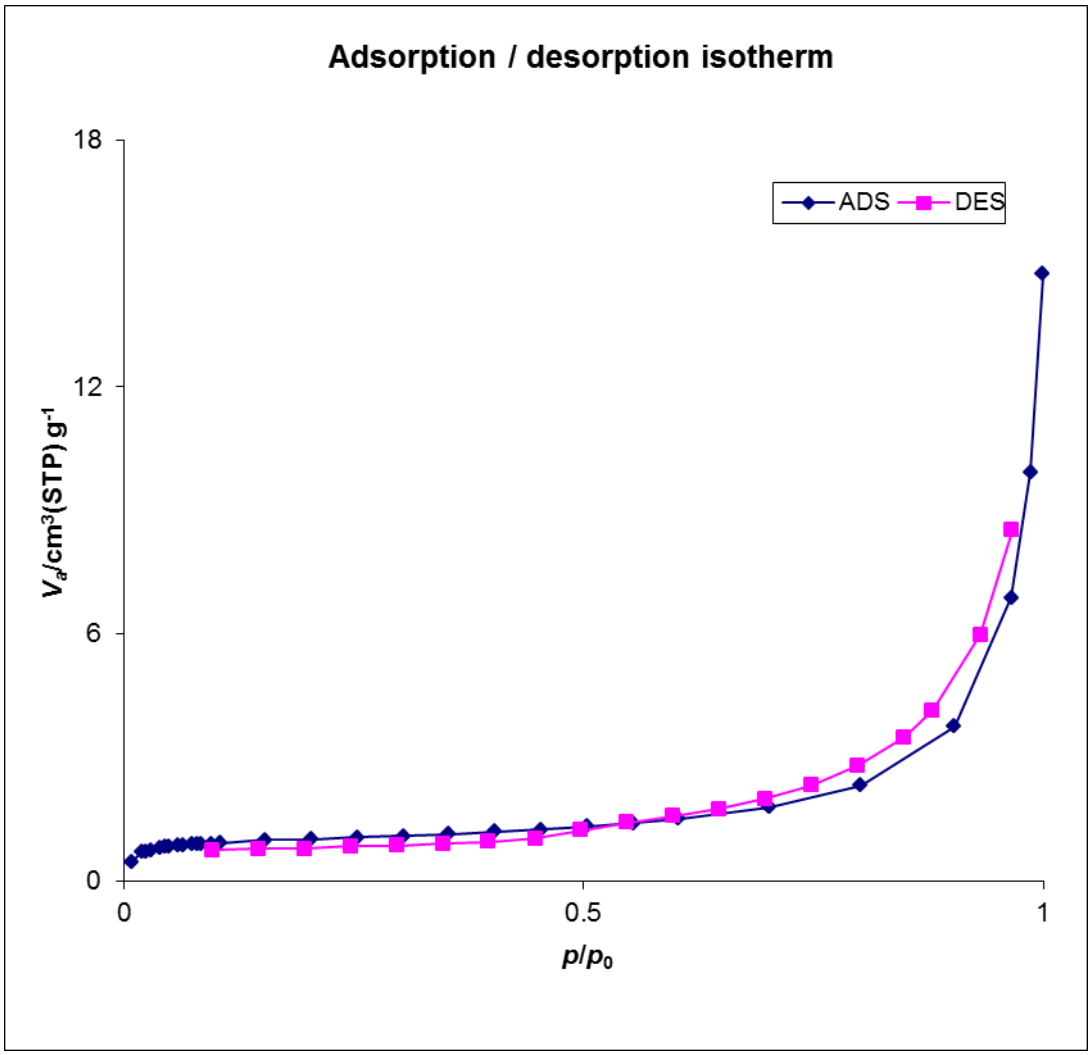

Figure A-43 N_2 adsorption-desorption isotherm of $InCl_3$/Al-PLT at 500°C

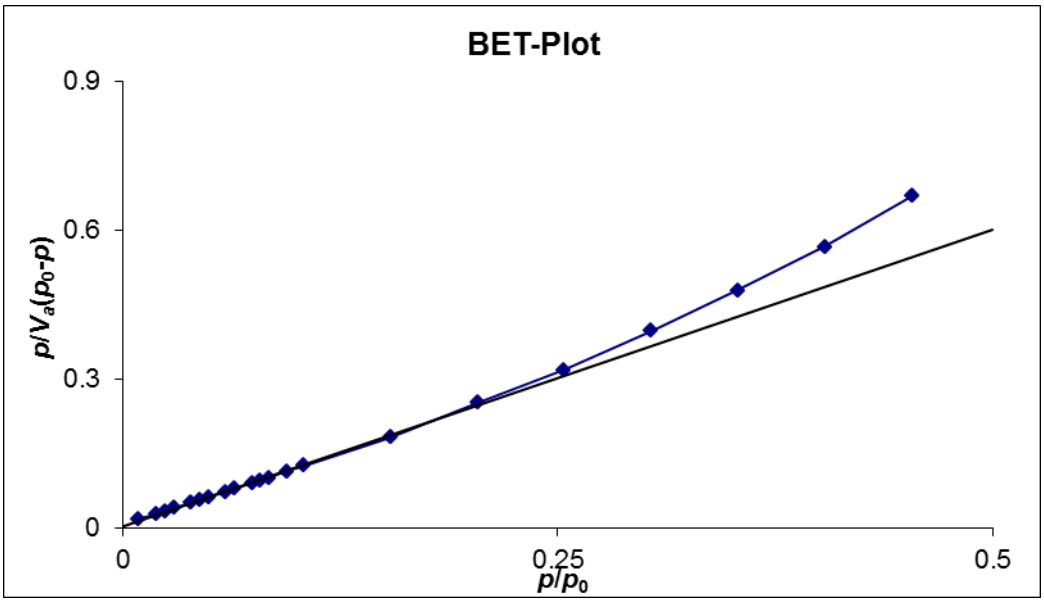

Figure A-44 BET plot of $InCl_3$/Al-PLT at 500°C

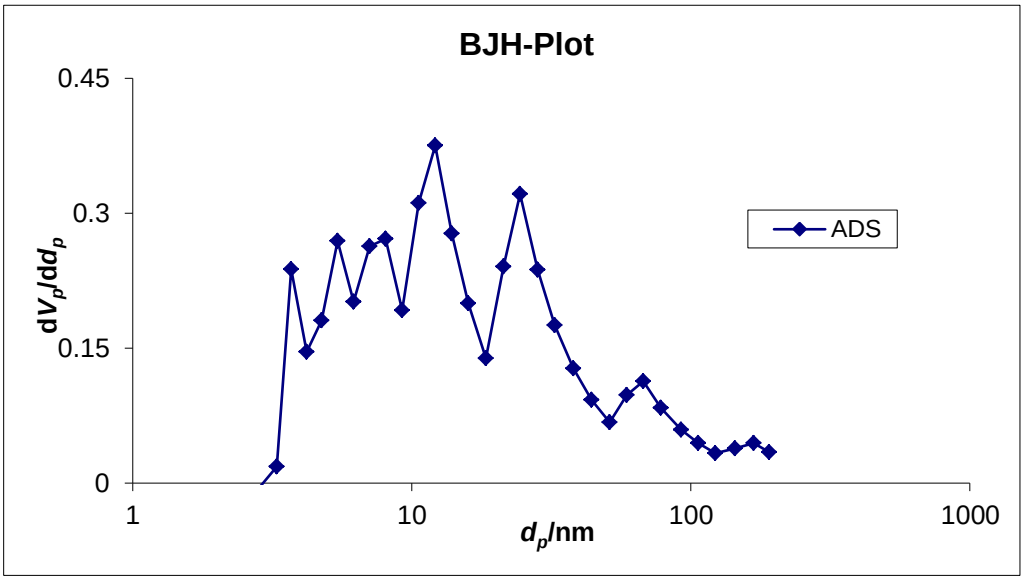

Figure A-45 BJH plot of $InCl_3$/Al-PLT at 500°C

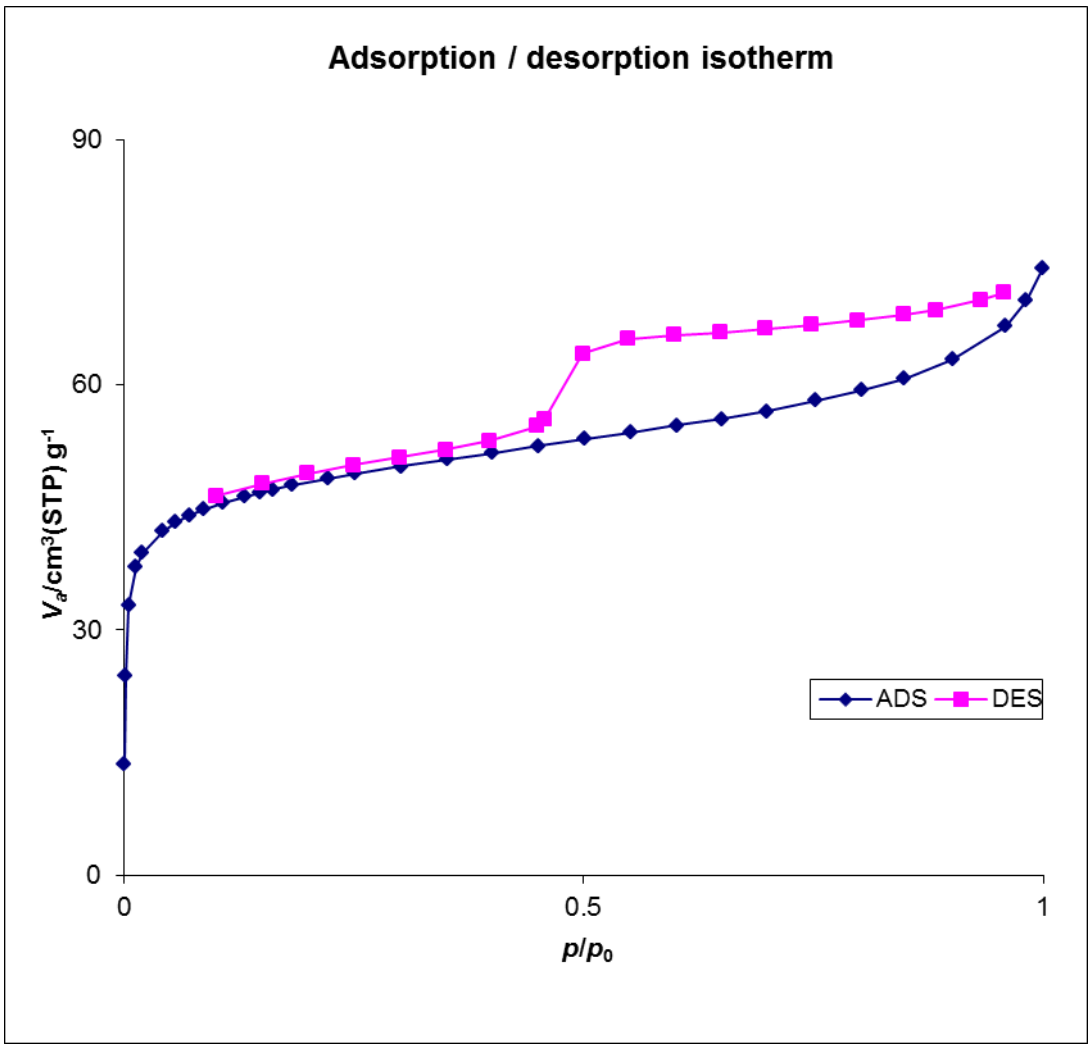

Figure A-46 N_2 adsorption-desorption isotherm of regenerated $InCl_3$/Al-PLB450

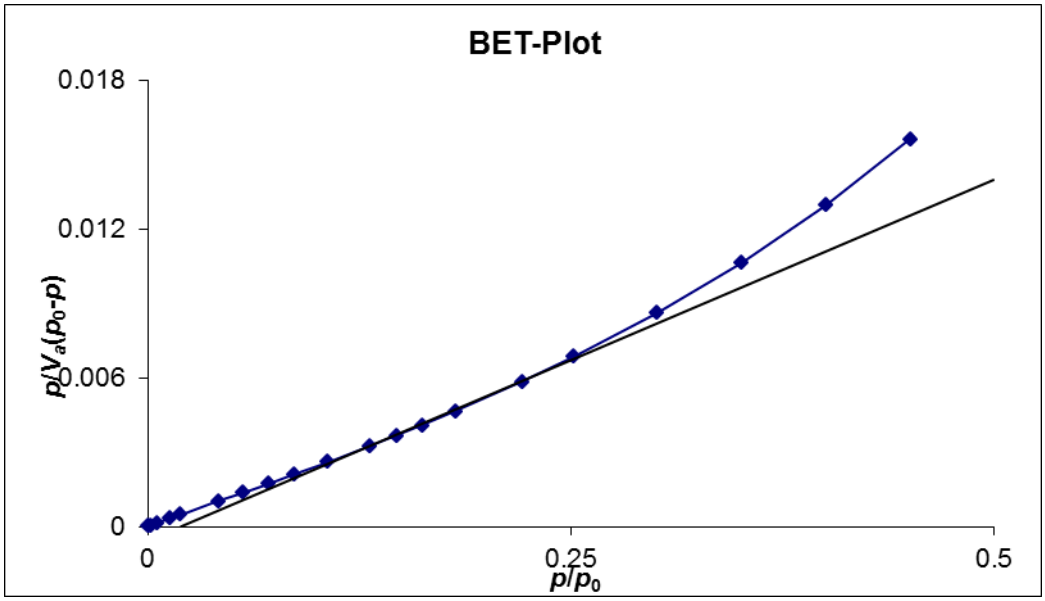

Figure A-47 BET plot of regenerated $InCl_3$/Al-PLB450

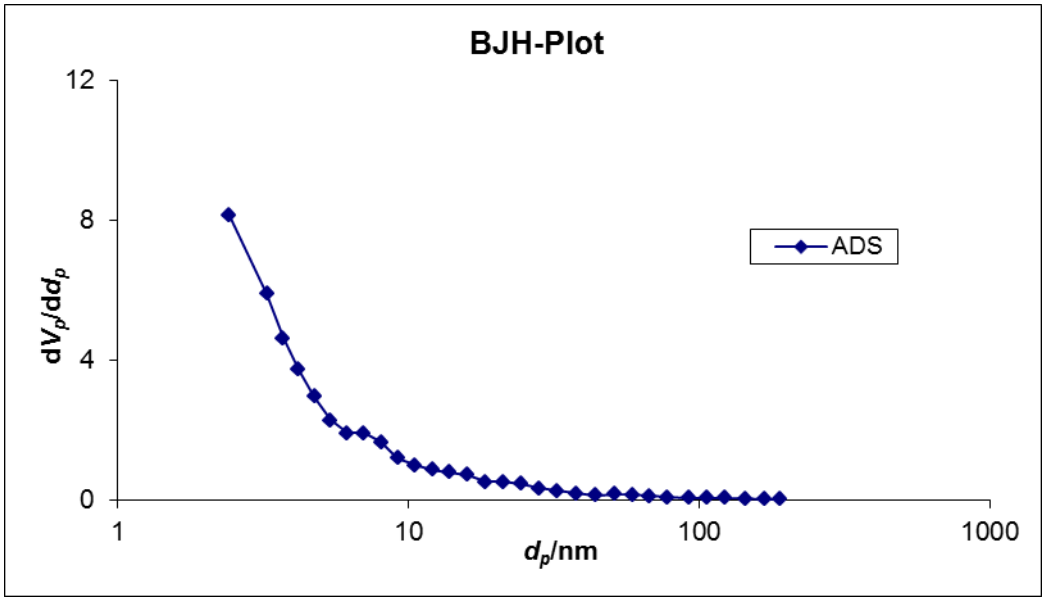

Figure A-48 BJH plot of regenerated $InCl_3$/Al-PLB450

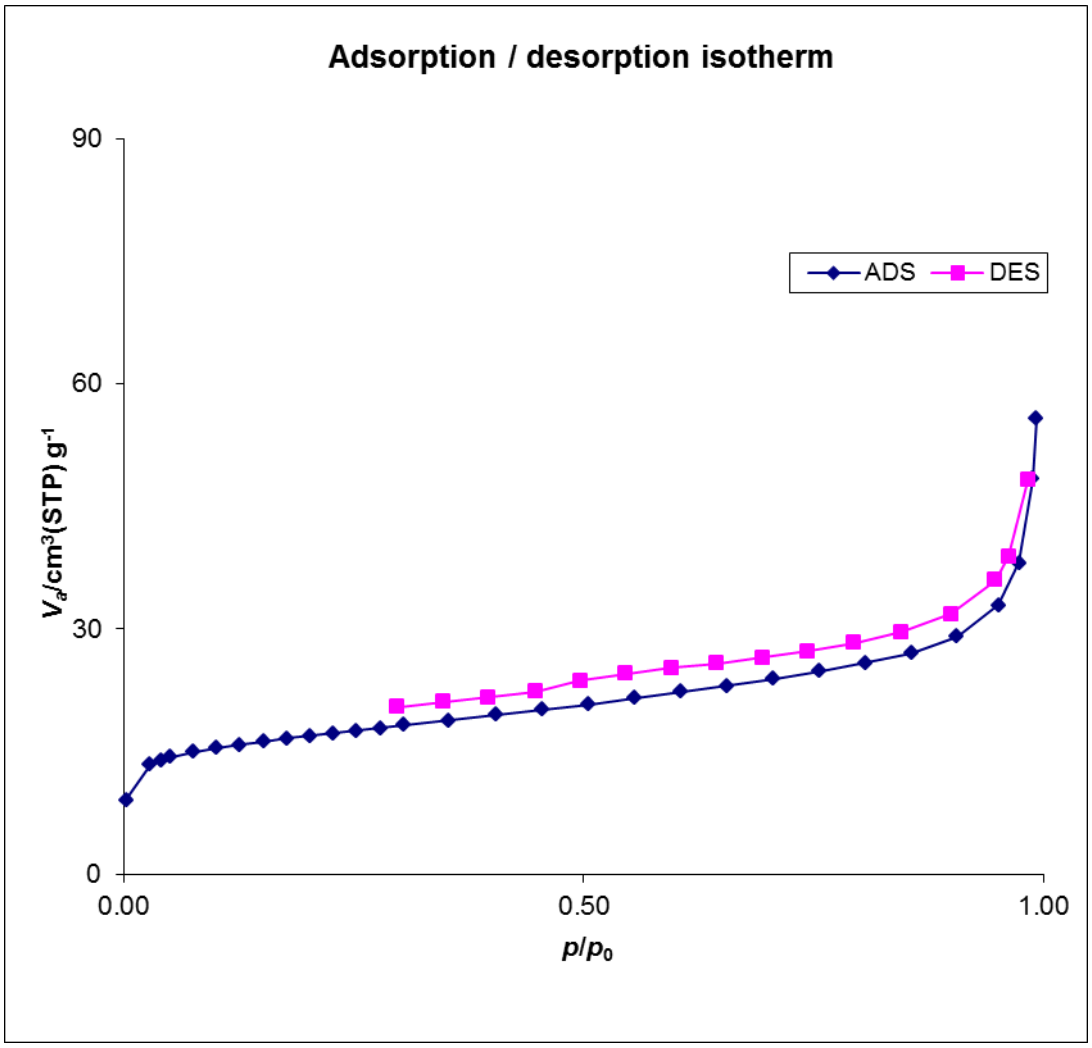

Figure A-49 N_2 adsorption-desorption isotherm of $InCl_3$/Al-PLB at 400°C

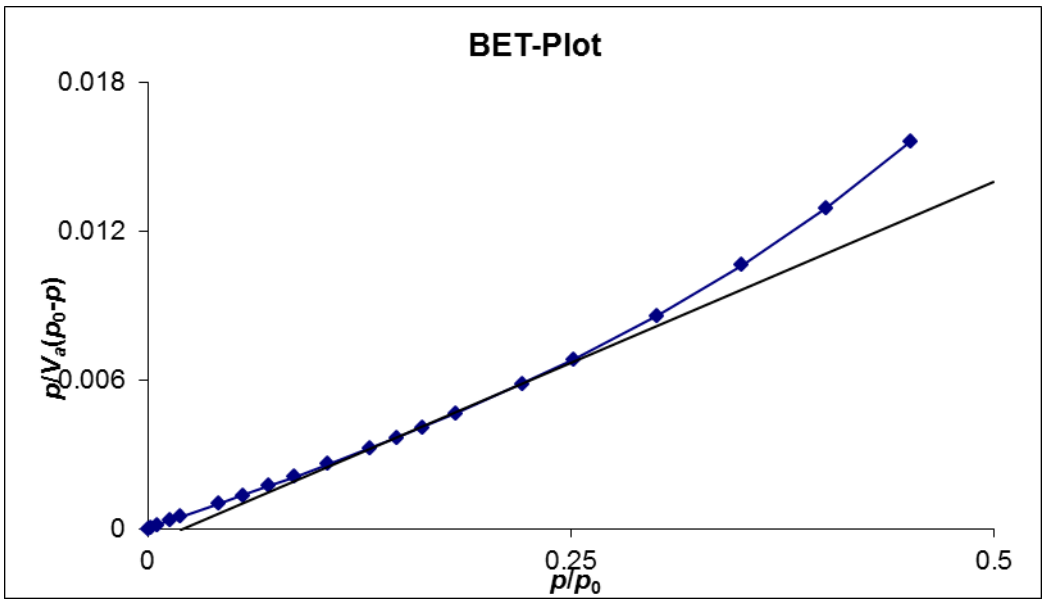

Figure A-50 BET plot of $InCl_3$/Al-PLB at 400°C

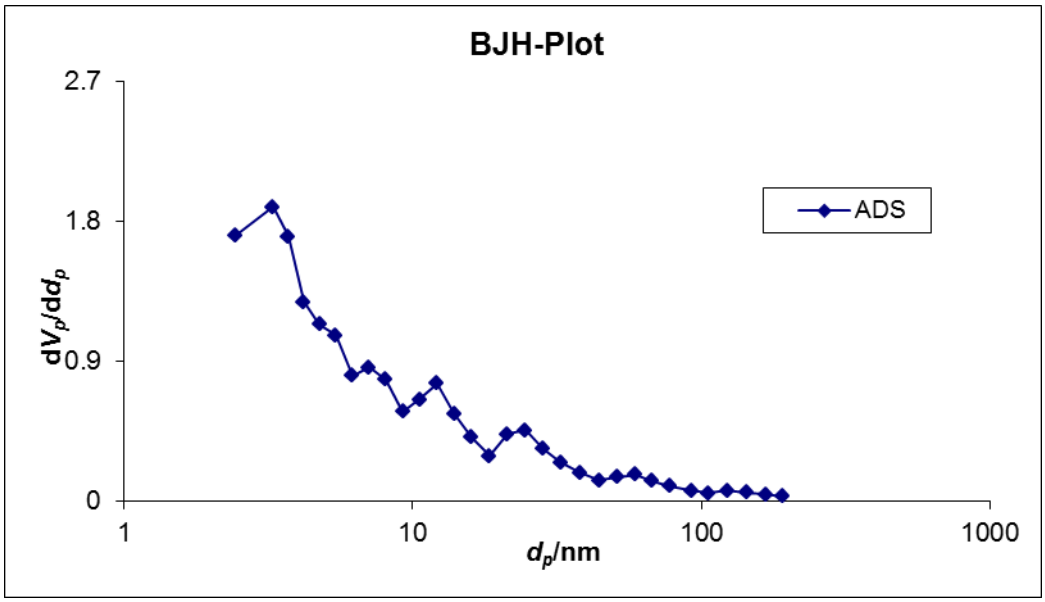

Figure A-51 BJH plot of $InCl_3$/Al-PLB at 400°C

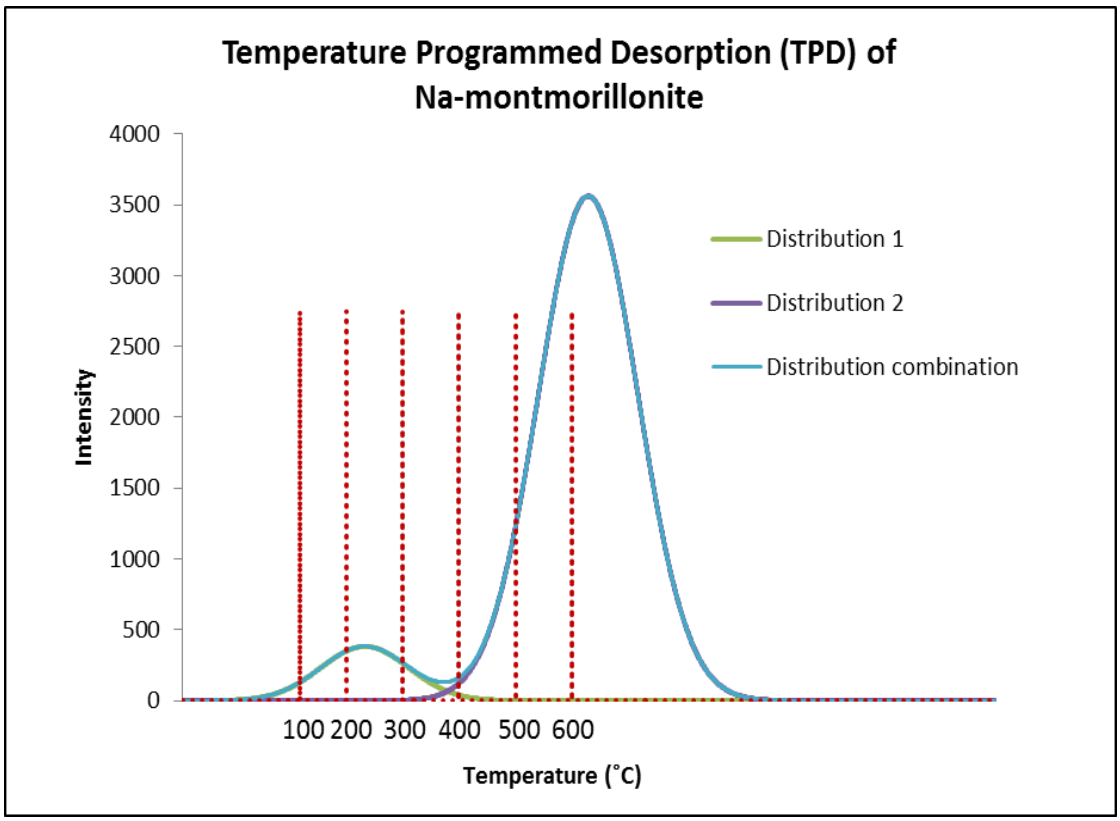

Figure A-52 Thermogram of Na-montmorillonite

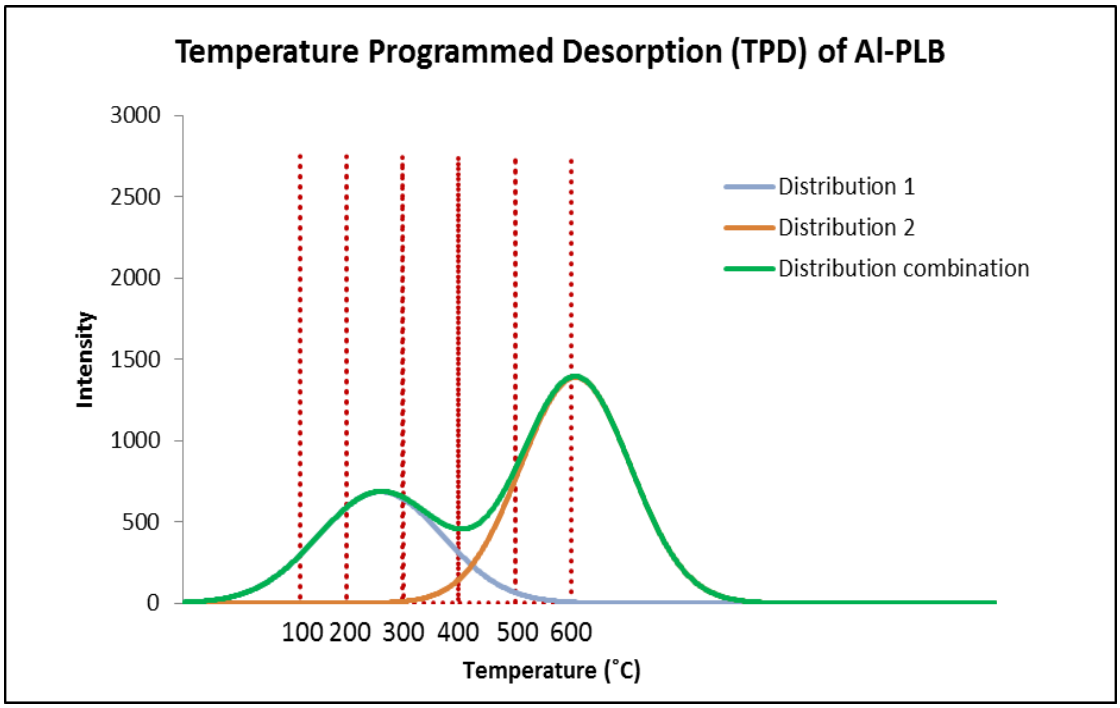

Figure A-53 Thermogram of Al-PLB

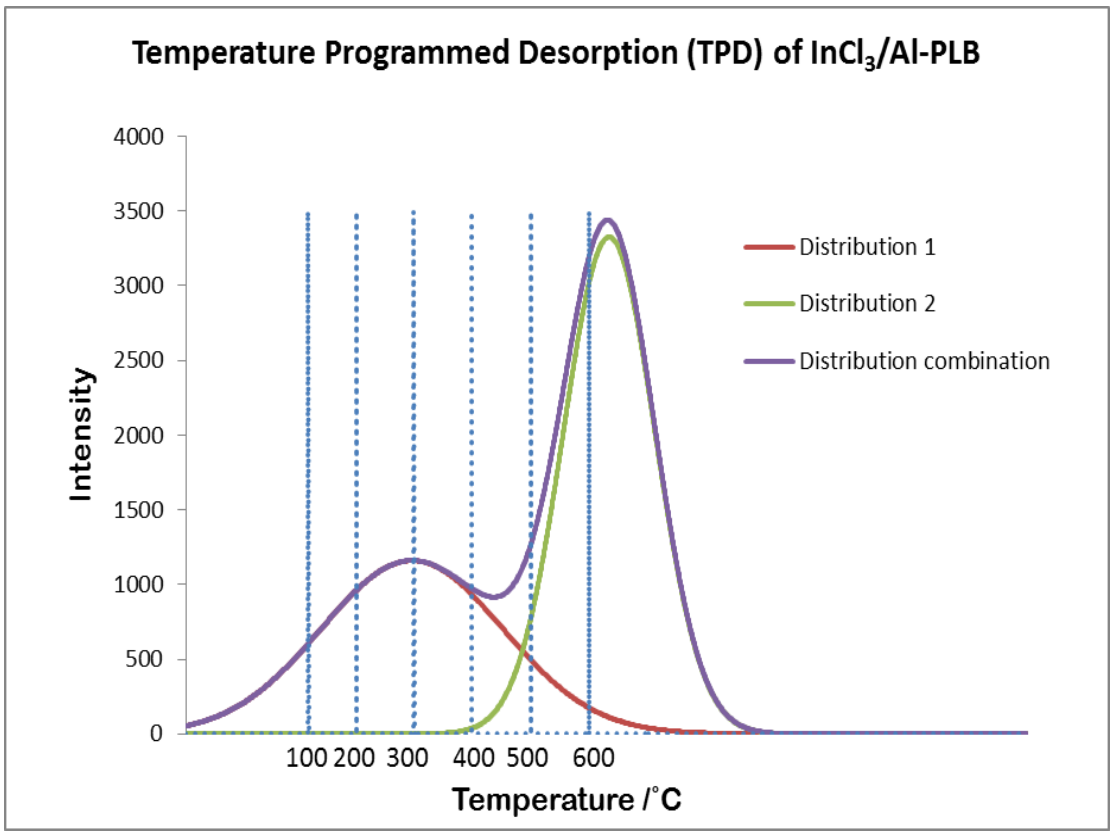

Figure A-54 Thermogram of $InCl_3$/Al-PLB

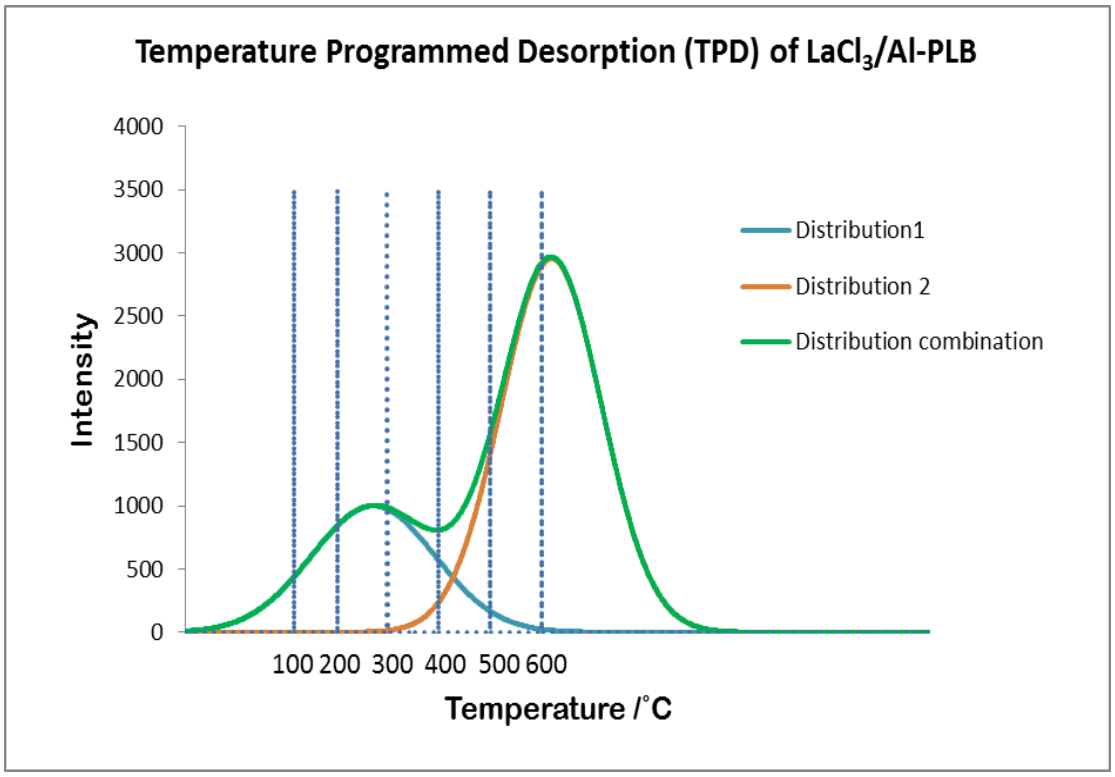

Figure A-55 Thermogram of $LaCl_3$/Al-PLB

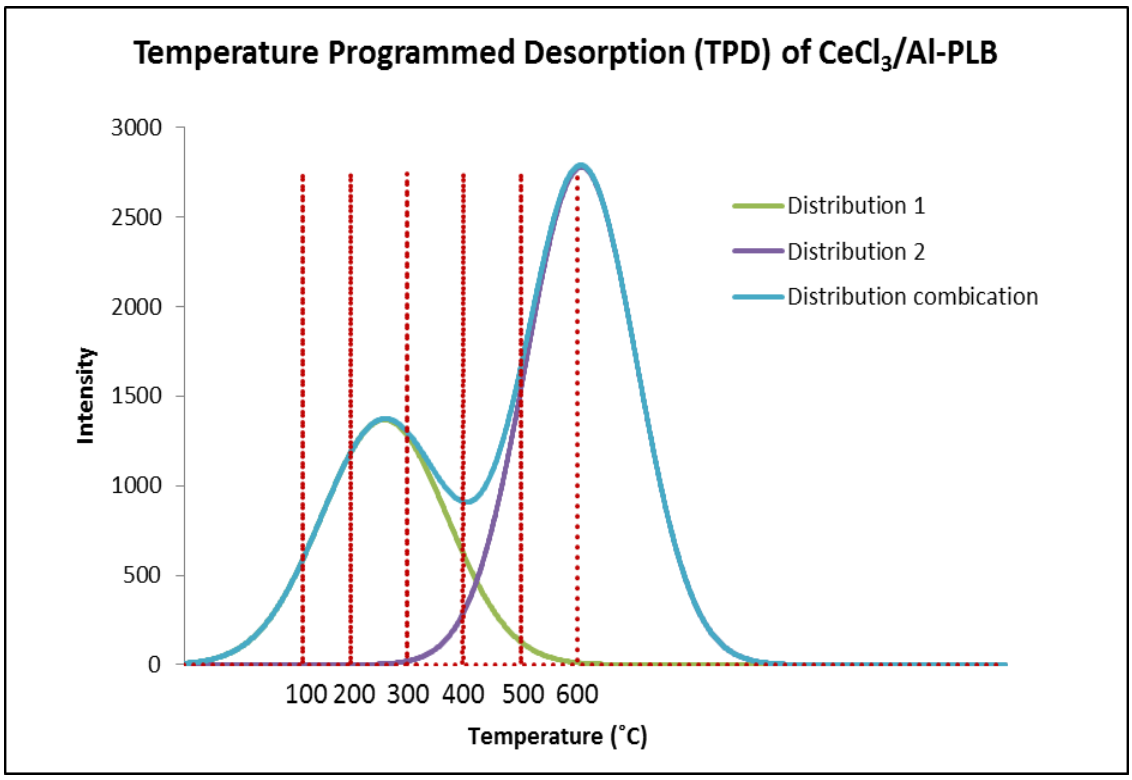

Figure A-56 Thermogram of $CeCl_3$/Al-PLB

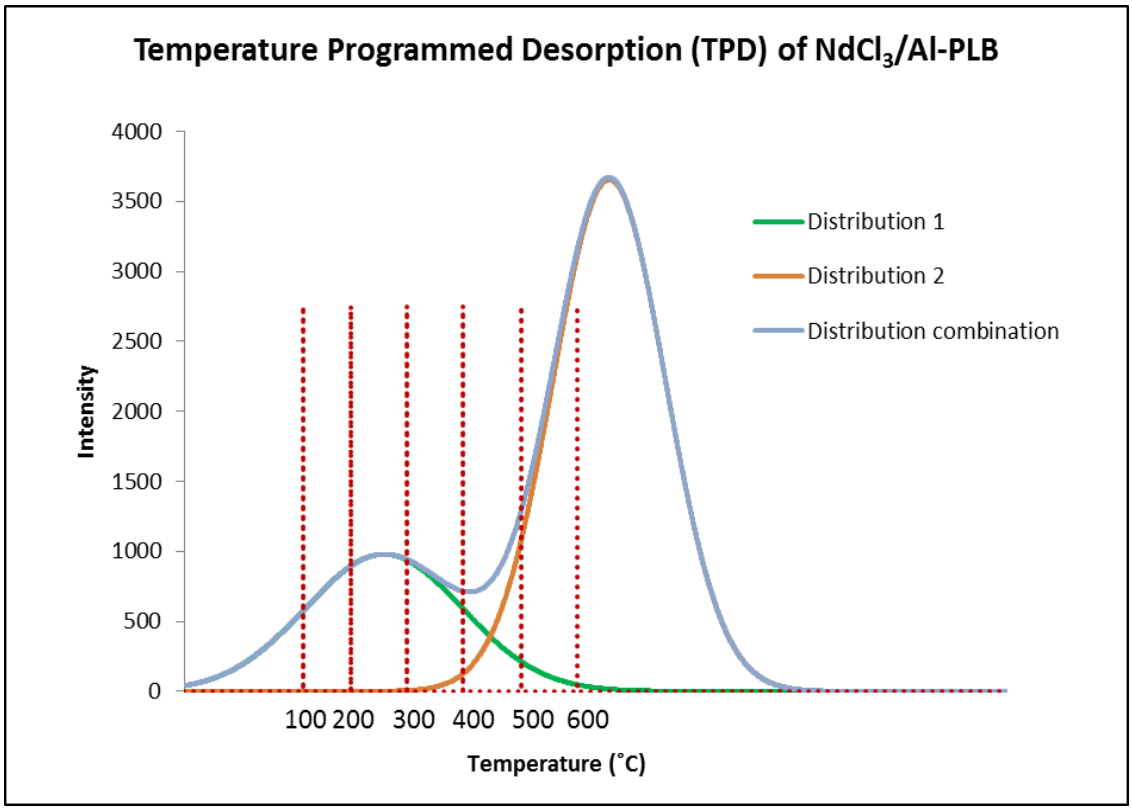

Figure A-57 Thermogram of $NdCl_3$/Al-PLB

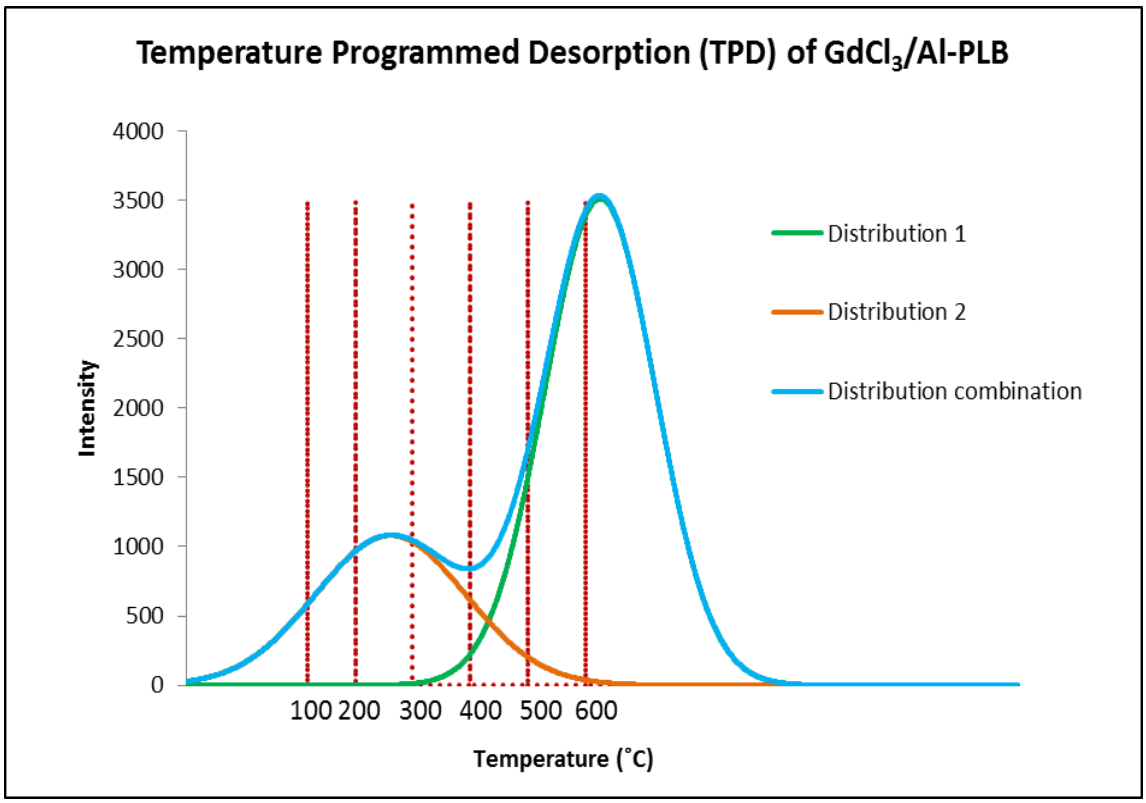

Figure A-58 Thermogram of $GdCl_3$/Al-PLB

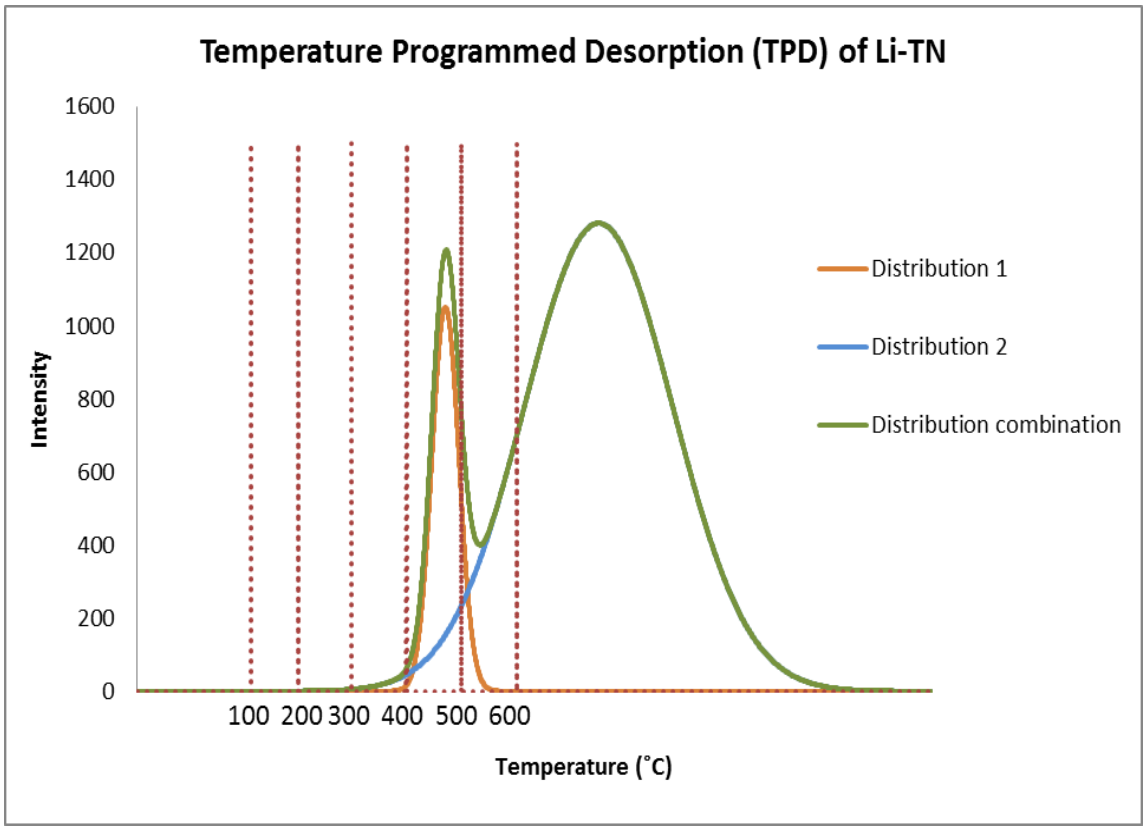

Figure A-59 Thermogram of Li-TN

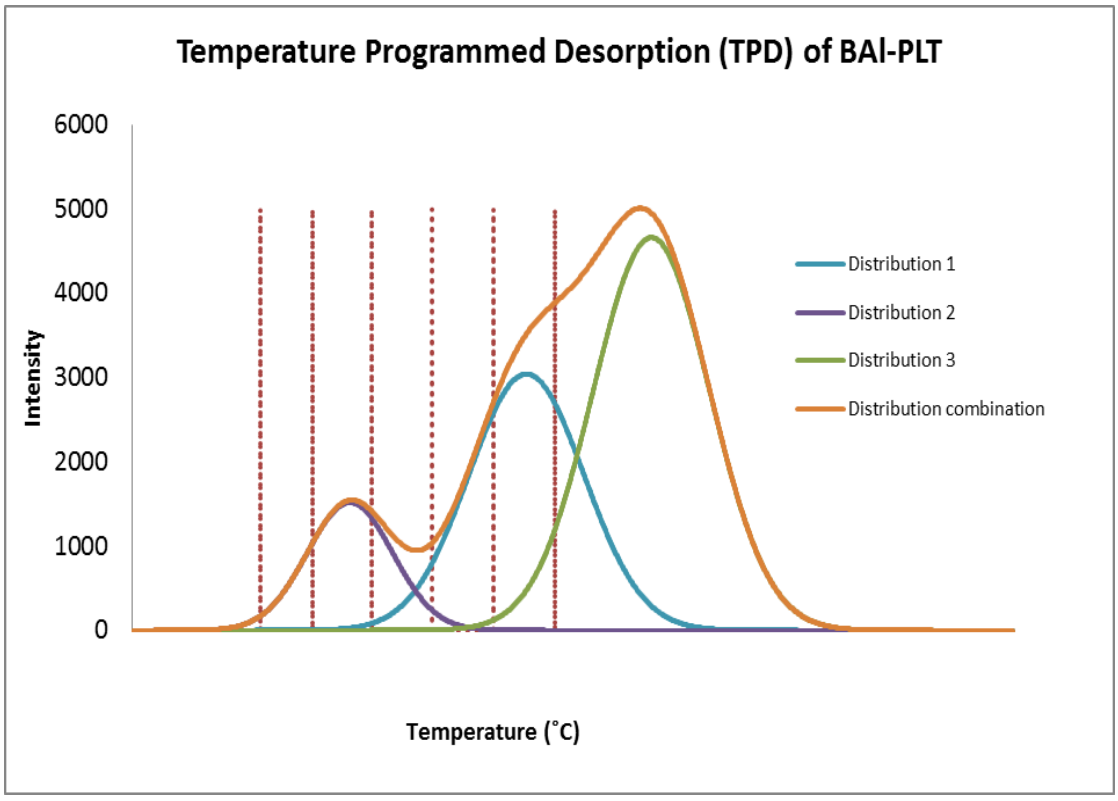

Figure A-60 Thermogram of BAl-PLT

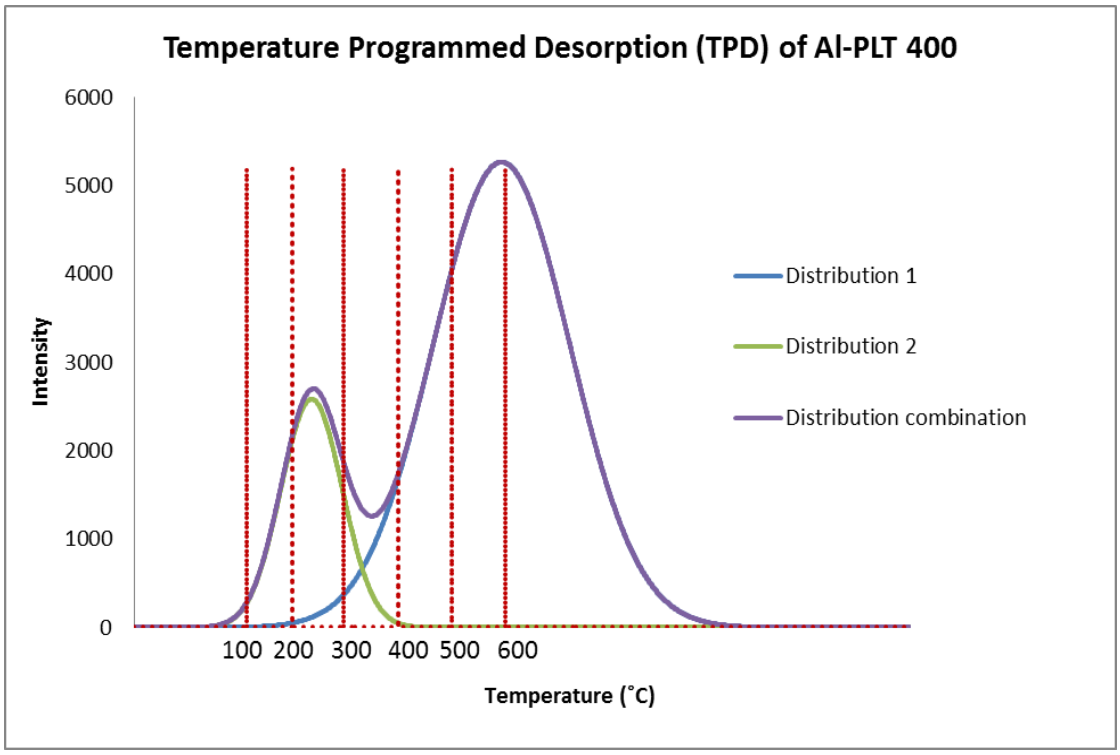

Figure A-61 Thermogram of Al-PLT400

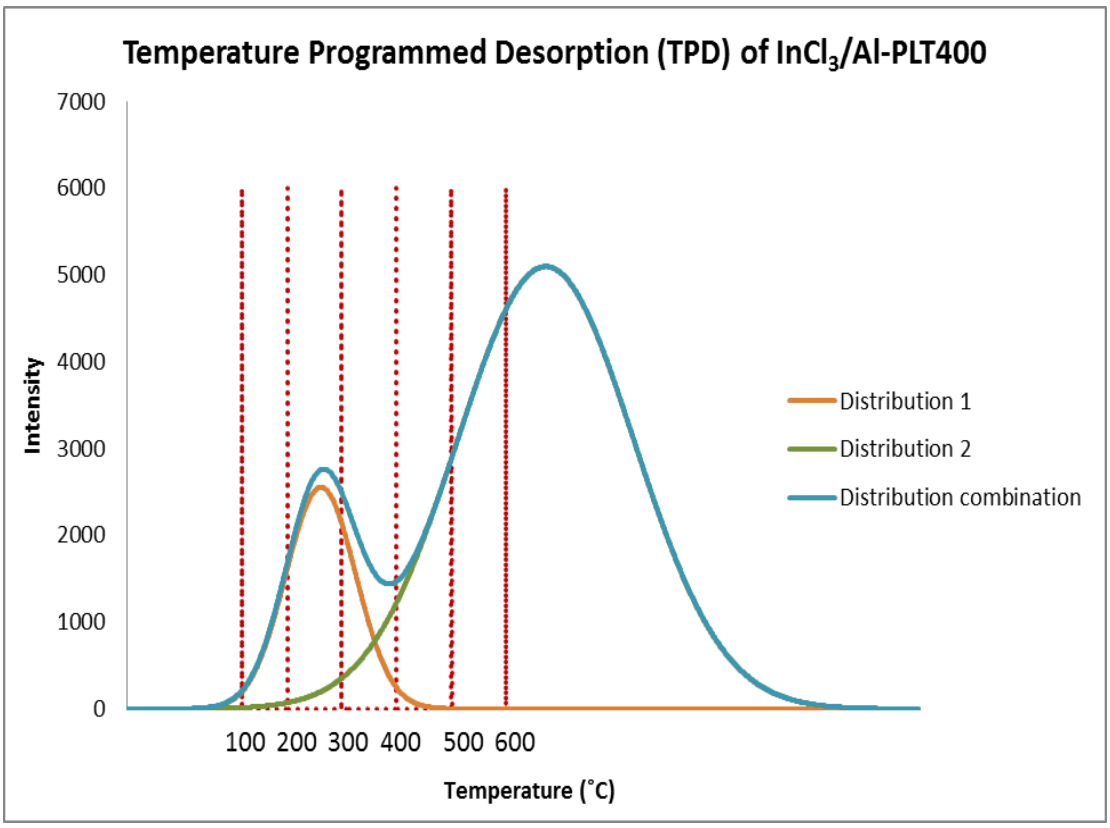

Figure A-62 Thermogram of $InCl_3$/Al-PLT400

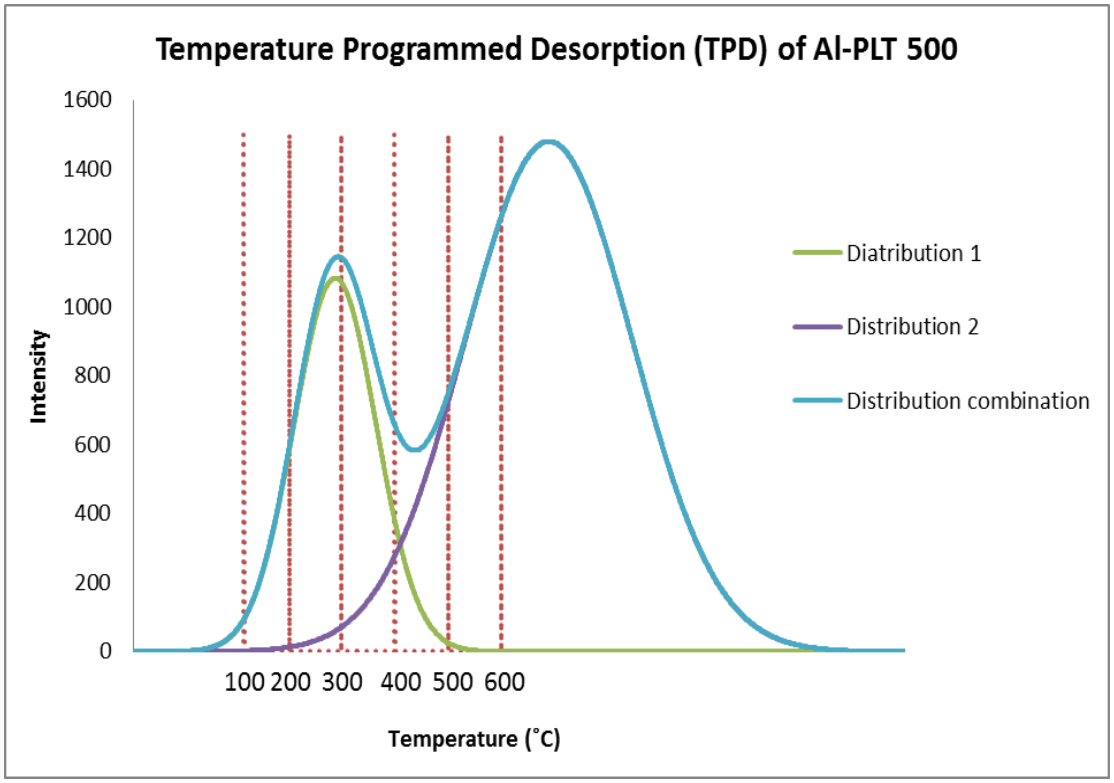

Figure A-63 Thermogram of Al-PLT500

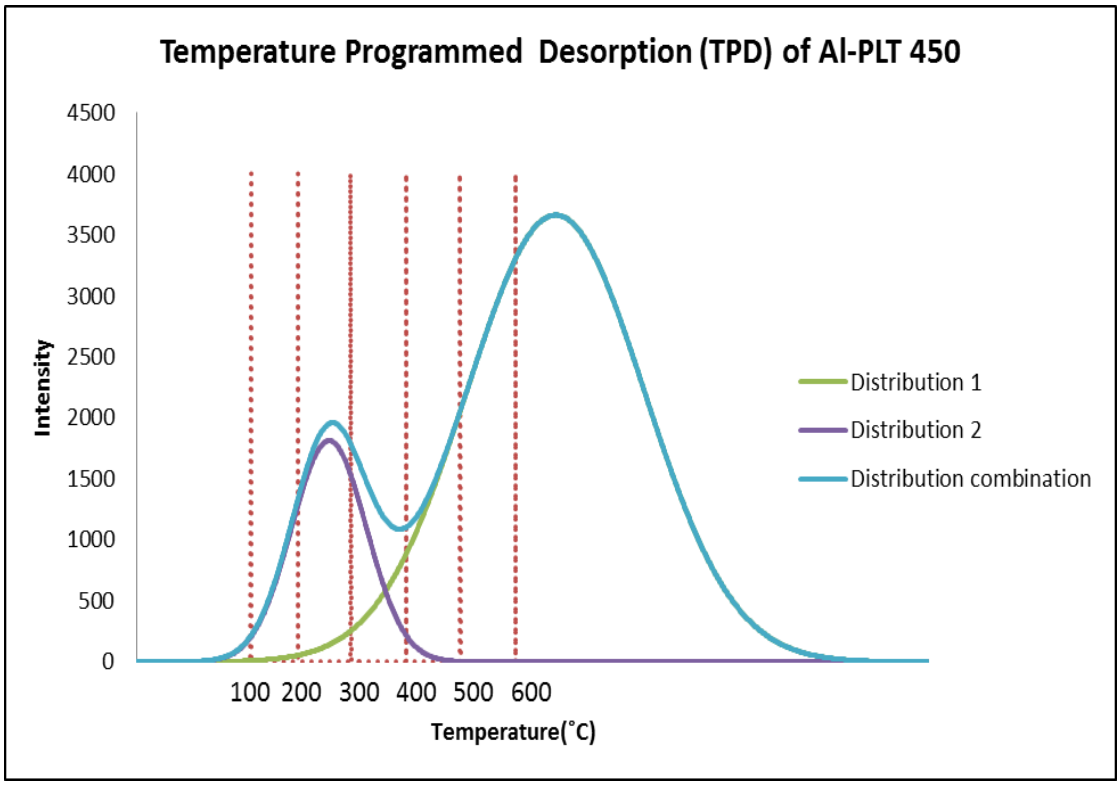

Figure A-64 Thermogram of Al-PLT450

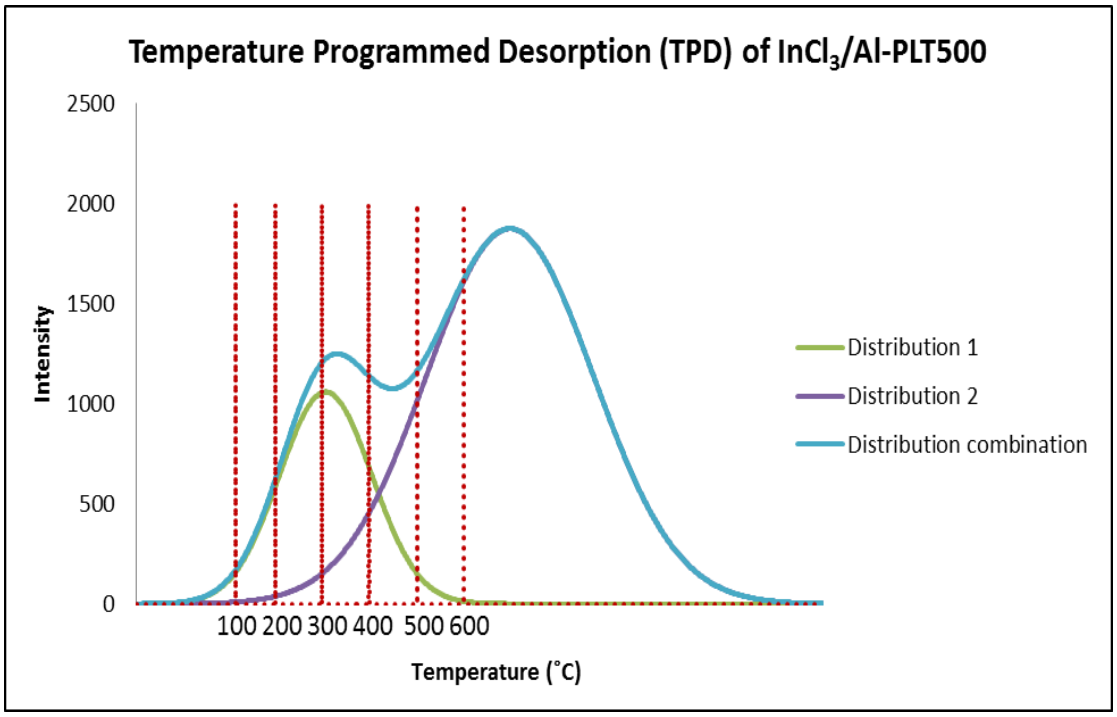

Figure A-65 Thermogram of $InCl_3$/Al-PLT500

VITA

Miss Patsarart Kaewbuarom was born on December 23, 1986 in Phitsanulok, Thailand. She graduated with Bachelor Degree of Science in Chemistry from Chulalongkorn University in 2008. Since then, she has been a graduate student studying Petrochemistry and Polymer Science at Chulalongkorn University. She was supported by research grant for this Master Degree's thesis from Center for Petroleum, Petrochemicals and Advanced Materials, Chulalongkorn University, Program in Petrochemistry and Polymer Science, Faculty of Science, Chulalongkorn University,

Her present address is 9/9 Phetkasem 54 Road., T. Bangduan, A. Phasricharoen, Bangkok, 10160, Thailand.